Optimization of Sustained Released based Drug Delivery system for Destruction of Cancer cells and causative agents for Typhoid and COVID -19 using nano carrier entrapped herbs

Thesis Submitted by

Pritha Pal

DOCTOR OF PHILOSOPHY (SCIENCE)

School of Materials Science & Nano Technology
Faculty of Interdisciplinary Studies, Law & Management
Jadavpur University
Kolkata-700032
India

2023

JADAVPUR UNIVERSITY
KOLKATA – 700032, INDIA

INDEX NO: D-7/ISLM/83-16 of 2016

1. TITLE OF THE THESIS:

Optimization of Sustained Released based Drug Delivery system for Destruction of Cancer cells and causative agents for Typhoid and COVID -19 using nano carrier entrapped herbs.

2. NAME, DESIGNATION & INSTITUTION OF SUPERVISORS:

Dr. Mahua Ghosh Chaudhuri
Associate Professor
School of Materials Science and Nanotechnology
Jadavpur University
Kolkata 32

Dr. Satadal Das
MD, DCP, Consulant Microbiologist
Peerless Hospital & B. K. Roy Research center
76, Satyen Roy Road, Kolkata-34

3. LIST OF PUBLICATION:

➢ Pritha Pal, Rajib Dey, Satadal Das, Mahua Ghosh Chaudhuri , Study of release kinetics of Diallyl Disulphide entrapped into mesoporous silica matrix & evaluation of antimicrobial activity of released drug, Nano Medicine Reseach Journal. 6(2):148-157, 2021, DOI: 10.22034/nmrj.2021.02.006

➢ Pritha Pal, Rajib Dey, Satadal Das, Mahua Ghosh Chaudhuri, Nanomaterials In Relation To Their Drug Delivery And Release Mechanisms: A Review Exemplified With Some Herbal Drugs , World Journal of Pharmaceutical Research, 7(9)1782-1804, 2018. DOI: 10.20959/wjpr20189-12234.

4. LIST OF PATENTS:
➢ **NIL**

5. LIST OF PRESENTATION IN NATIONAL /INTERNATIONAL:

➢ Pritha Pal, Sourav Adhikary, Raj Sohel Mullick, Rajib Dey, Mahua Ghosh Chaudhuri, Comparative study of kinetic behaviour for paracetamol, entrapped in morphologically different silica gel, 72th ATM,2018

➢ Pritha Pal, Subham Bose, Satadal Das, Mahua Ghosh Chaudhuri, Dye(Methylene Blue) Removal Using Mesoporous Rod Shaped Silica from Waste Water, ICONSAT 2020

STATEMENT OF ORIGINALITY

I, Pritha Pal, registered on 16th September, 2016 do hereby declare that this thesis entitled "Optimization of Sustained Released based Drug Delivery system for Destruction of Cancer cells and causative agents for Typhoid and COVID -19 using nano carrier entrapped herbs" contains literature survey and original research work done by the undersigned candidate as part of Doctoral studies.

All information in this thesis have been obtained and presented in accordance with existing academic rules and ethical conduct. I declare that, as required by these rules and conduct, I have fully cited and referred all materials and results that are not original to this work.

I also declare that I have checked this thesis as per the "Policy on Anti Plagiarism, Jadavpur University, 2019", and the level of similarity as checked by iThenticate software is 8%.
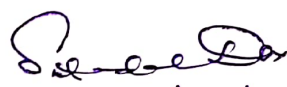
Signature of Candidate: *Pritha Pal*

Date: 03/05/2023   Registration no:- D-7/ISLM/83-16.

Certified by Supervisor(s):

(Signature with date, seal)

1. *Mahua Ghosh Chaudhuri*
   2/5/23

2. *[signature]*
   04/05/2023

   Dr. Satadal Das
   MBBS, MD, DCP, DBMS.

Dr. (Ms) Mahua Ghosh Chaudhuri
Associate Professor
School of Materials Science and Nano Technology
Jadavpur University
Kolkata-700 032, India

CERTIFICATE FROM THE SUPERVISORS

This is to certify that the thesis entitled "**Optimization of Sustained Released based Drug Delivery system for Destruction of Cancer cells and causative agents for Typhoid and COVID -19 using nano carrier entrapped herbs** " submitted by **Pritha Pal,** for the award of **PhD (FISLAM)** degree of Jadavpur University is absolutely based on her own work under the supervision of **Dr. Mahua Ghosh Chaudhuri** and **Dr. Satadal Das,** and that neither this thesis nor any part of the same has been submitted for any degree/diploma or any other academic award anywhere before.

Mahua Ghosh Chaudhuri
2/8/23

Satadal Das
04/05/2023

Dr. Mahua Ghosh Chaudhuri

Associate Professor

School of Materials Science and Nanotechnology

Jadavpur University

Kolkata 32

Dr. (Ms) Mahua Ghosh Chaudhuri
Associate Professor
School of Materials Science and Nano Technology
Jadavpur University
Kolkata-700 032, India

Dr. Satadal Das

MD, DCP, Consulant Microbiologist

Peerless Hospital &B. K. Roy Research center

76, Satyen Roy Road,

Kolkata-34

Dr. Satadal Das
MBBS, MD, DCP, DBMS.

Dedicated to my Family,

Husband & loving son

ACKNOWLEDGEMENT

I would like to take this opportunity to express my heartfelt gratitude to the people who supported me throughout this Ph.D. platform. I am privileged to have this opportunity to express my sincere appreciation for them. The completion of this thesis would have not been possible without the direction, assistance, and encouragement of many significant persons.

Firstly, I wish to convey my sincere gratitude to my father and mother for their love, encouragement, counsel, and support throughout my life.

I was captivated and daydreamed about adding "Doctor of Philosophy" as a greeting to my name when I was pursuing my masters in Microbiology with honours. This opportunity came into my life when I visited Jadavpur University for my master's project work under the guidance of Prof. Rajib Dey, Professor, Department of Metallurgical and Material Engineering, Jadavpur University.

I want to express my deepest gratitude to my supervisors, Dr. Mahua Ghosh Chaudhuri, Associate Professor, School of Materials Science & Nanotechnology, Jadavpur University and Dr. Satadal Das, MD, DCP, Consultant Microbiologist, Peerless Hospital & B. K. Roy Research Center for giving me the chance to work on this Ph.D. program at Jadavpur University. I also want to thank them for all their help and support with the experiments throughout my research as well as for their insightful criticism and advice. They have taught too many areas and subjects, sometimes more than science. I am very fortunate to spend lots of time with my supervisors during my Ph.D. tenure. I express my sincere gratitude to both of them - Madam and Sir for enriching me with their knowledge and support. Along with my adviser, I would like to express my gratitude to the distinguished doctorate committee members whose insightful comments aided the thesis excellence.

I am very much thankful to Prof. Dey for introducing me to Dr. Mahua Ghosh Chaudhuri & Dr. Satadal Das as well as his support and encouragement for my work.

I would like to thank Prof. M.K. Mitra, Dr. G.C. Das, Dr. S. Mukherjee, Dr. C.K. Ghosh, Dr. S. Sarkar for their intellectual and moral support.

Contents

6. Synthesis and characterization of nano clay carrier entrapped with Aloin & DADS and its applications.

List of figures

List of tables

CHAPTER 1

Introduction and Literature survey

1.1 Introduction:

Nanotechnology is a very systematic multidisciplinary area of science where the main business deals with some specific materials whose chemical and physical properties can be modulated at the nanoscale level (1–100 nm) by applying engineering, chemical science, and the ideas of development.[1] Nanobiotechnology is the convergence topic of interest of engineering and molecular biology. To investigate biological and chemical analysis with better sensitivity and specificity and a higher rate of recognition, these multifunctional nano biotechnology tools are very useful.[2] For the last few decades, engineers have been working on the invention of efficient higher-density electronic chips. These devices have reached feature sizes as small as 20 nm using deep UV-lithography. On the other hand, molecular biologists are also functioning in the field of molecular as well as cellular dimensions for many years. The dimensions size ranges started from several nanometers (DNA molecules, viruses) to various micrometers (cells).[3]

1.2 Nanomaterial:

Nanomaterials are defined as materials having particle sizes of less than 100 nm at least in one dimension. It has a larger specific surface area means a larger area-to-volume ratio. The surface area of any nanoparticle is inversely proportional to the diameter of the particles. Owing to their huge surface area nanomaterials can be used to hold drugs/ herbal values which can be released in a controlled manner to treat different diseases.

Additionally, nanoparticles also can migrate within a physiological system in the human body and are capable of crossing the heart, lung, gut, and brain barrier. This may lead to unexpected and unusual results.

Different classes of nanomaterials that can hold drugs/ herbal values are –

A. Zero dimensional / cluster material

B. 1D nanomaterial

C. 2D nanomaterial

D. 3D nanomaterial

A. ZERO DIMENTIONAL NANOMATERIAL

Zero dimensional nanomaterials have less than 100 nm diameter denoted by nanoparticles, nanoclusters or nanocrystals. All dimensions (x,y,z) are in nanoscale. These nanoparticles may

be semicrystalline or amorphous or single 0D nanostructures crystal having dimensions larger than 10 nm. For amorphous material, the term nanocluster will be appropriate showing narrow size distribution. These nanoparticles contain the following characteristics-

a. Uniform size dispersion also called monosize.

b. indistinguishable chemical property and crystal nature. Be metallic, ceramic, or polymeric.

c. Identical size and morphology.

d. Having dispersion property (i.e.no agglomeration occurs).

Presently, different variety of physical and chemical methods has been developed to fabricate 0D NMSs with well-controlled dimensions.[4]

B. ONE DIMENSIONAL NANOMATERIALS

1D nanomaterials are nanotubes, nanorods, nanofibers, and nanowires. Two dimensions (x,y) of this nanomaterial are at the nanoscale andthe other dimension (z) is micron-scale or larger. One dimensional nanomaterial exhibitsthe following features:

a. These materials may be crystalline or amorphous

b. Crystalline also in poly or single state

c. These materials can be individual materials or embedded within an additional medium.

d. Metallic, ceramic, or polymeric in nature.[4]

C. TWO DIMENSIONAL NANOMATERIALS

In 2D nanomaterials, two dimensions are not confined to the nanometer range and one dimension is in thenanoscale range. These nanomaterials are recently widely used in material research for their many low-dimensional features. Besides this 2D nanomaterial with specific geometries reveal some size-dependent exclusive characteristics and are also used as building blocks for nanodevices. Two-dimensional nanomaterials include nanofilms,nanolayers, and nanocoatings. The following are the features of 2D nanomaterials:

a. These materials may be amorphous or crystalline

b. These 2D structures are exploited as single or multilayered structures.

c. These nanofilms, layers, and coatings all are integrated with any surrounding matrix.

d. May be metallic, ceramic, or polymeric.

D. THREE DIMENSIONAL NANOMATERIALS:

The 3D materials are those where diameters do not confine in the nanoscale range. All three diameters are above the 100 nm range i.e., in macroscale called bulk nonmaterial. These 3D-nanomaterials are composed of nanocrystals arranged in numerous forms and in different orientations. Due to the large surface area and much absorption capacity nanomaterials are getting importance in the research field and applications. 3D nanomaterials with greater porosity are a unique combination to transport molecules or drugs. 3D nanomaterials include the structures like nanocones, nanoballs (dendritic structures), nanocoils, nanopillers, and nanoflowers.[4]

0D

Cluster materials

These are zero dimensional, amorphous nanomaterials with large surface areas. Amorphous silica synthesized by sol-gel route is a good example of cluster material. Silica gel is bioactive and completely biodegradable with no undesirable effects on the adjacent body tissue or any organ. They also have osteoconductive properties and can get attached to bones.[5] due to their porous structure and large surface area, they can hold drugs, proteins, peptides etc.[6,7]

1D

Nanotube or nanowire

Carbon nanotubes (CNT) are an example of 1D nanomaterial. The attractive properties of CNTs which make them a good drug carrier, high aspect ratio, high stability and length in the micron size with high mechanical strength, and some extraordinary surface properties like selectivity. [8,9]

CNTs are of two types [10]

• SWNTs- Single-walled carbon nanotubes made up of a single sheet of graphene.

• MWNTs- Multiple-walled carbon nanotubes made up of several tubes in concentric cylinders of single-walled carbon nanotubes.

The most attractive thing is the presence of a benzene ring which makes it easier for loading drugs that already contain a benzene ring in their molecules eg; epirubicin (EPI), doxorubicin (DOX) etc.[11]

2D

Compared with other nanomaterials ultrathin 2D nanomaterials particularly single-layer nanosheets enable undeniable electronic properties.[12] The atomic thickness of 2D materials exploits features like Mechanical litheness and optical transparency. These features allow them to fabricate highly flexible and transparent electronic devices. Ultrathin thickness and large cross-section provide them high specific surface area which helps them easily in surface active applications.[12-14] 2D nanosheet, and nanolayer structures have a high specific surface area so, they contribute to building functional composites as building blocks.[15-19]

3D

Organic nanomaterials like dendrimers are well-branched, nanoscale-sized, spherical polymeric macromolecules with many arms emanating from an inner core.[20,21] The central void space is mainly useful for the encapsulation of metals, tiny drug molecules, or imaging moieties. Besides this, the void space also facilitates the controlled release of drug molecules. In current decades dendrimers have been exposed as very promising carriers in gene delivery to magnetic resonance imaging for the development of vaccines, antibacterials, antivirals, and anticancer therapeutics.[22-25] Several polymers are successfully used for sustained and controlled drug delivery at specific target sites which therefore enhance the healing effect plus reduce the side effects.[26]

Quantum dots

Metallic nanomaterials such as Quantum dots are 2-20 normally nanometer-sized crystals [27] but some literature says that it should be firmly below 10 nm[28,29] The diameter of QDs depends on the material used. Usually, QD means a whole system where the quantum captivity effect happens. The nature of QDs may be metallic (e.g. Cobalt, Nickel, Platinum, Gold etc)[30] or predominantly based on semiconductor materials. In addition, some research says a metalloid QD can also be done such as silicon QD.[31] QDs have some extraordinarily attractive

properties because of their quantum captivity nature. In the application field especially in biological systems solubilization of QDs is important. With the help of hydrophobic inorganic solvents, water-insoluble QDs can be made easily but solubilization in water requires surface modification.[32]

According to many research cytotoxicity of QDs in in-vitro as well as in vivo studies is a major viable issue for its application. It affects cell growth by damaging DNA and disturbs normal cell activity with short-term (acute) and long term toxicity.[32-36] The level of cytotoxicity depends on several parameters. It includes the size of the QDs, the dosage of QDs, coating bioactivity, capping materials, surface chemistry alteration, and processing parameters.[37-39]

Different outer surface modified polymeric nanoparticles and block copolymers can augment the interface significantly among the nanoparticles and the biological atmosphere as a result more cellular uptake, more advantageous bio distribution level, and a longer half life occur.[40]

In general, the detrimental effects of nanoparticles come from various aspects. Usually, the combination of surface properties like high surface area and intrinsic toxicity of the surface may be a reason for harmfulness.[41] Nanoparticles below 100 nm diameter potentially be more deadly for lung tissue (gateway of entry), contrary to conventional particles of big size. The nanoparticles can relocate from their deposition site and also change their protein structure which helps them to run away from normal phagocytic cell defenses. As a result, an inflammatory and immunological response is triggered by these nanoparticles as well as normal tissue activity may be affected.[42]

1.3 Nanoconjugate:

Here, Tang et al (2015) report a scalable process of fabricating drug-silica conjugated nanoparticles, termed drug-silica nanoconjugates (drug-NCs), which hold monodisperse size distributions and the most advantageous particle sizes are expected as small as 20 nm. It is found that 20-nm NCs are superior to their 50-nm and 200-nm NC analogues by 2–5 and 10–20 folds, respectively, with regard to tumor accumulation and penetration, and cellular internalization.[43]

1.4 Types of Drugs:

Drug is a chemical compound, synthetic or natural (usually excluding any nutrients, water, or oxygen), that - by its chemical nature – it can alter bio molecule's structure or working when administered in the body and absorbed.

In daily life people are accustomed to different types of drugs to heal different diseases or physical problems.

Drugs may be categorized into 3 groups:

1. Allopathic drug

2. Homeopathic drug

3. Herbal drug.

Use of allopathic drug :

Allopathic drugs are not always used in a conventional way. There are varieties of drugs that are medicated in sustained release dosage form and results are in a positive range.

Theophyllinesis a sustained release drug for Asthma.

Procardia XL is a sustained release for High blood pressure.

Floxuridine, Mitomycin, and Cis-platinare all sustained releases for cancer treatment.

The allopathic drug is preferred during surgery for their advantageous effect to eliminate damaged portions from the body. Allopathic drugs are prescribed due to their instant relief action which is why it is used widely in our medicinal world. In accidental cases, these medicines are very useful to keep the body in perfect condition.[44]

Use of homeopathic drug :

Easiness of administration of a drug.

One of the main advantages is the high acceptability among children.

Extensively used for its much fewer side effects.

Herbal drug

Herbs are medicinal plants that have therapeutic agents (also called phytomedicinals) that can be used for controlling different diseases. These herbs can be administered as the whole plant or plant parts or as plant extraction in solvents.[45]

1.5 Importance of Herbal Medicines:

Medicinal plant metabolites and other natural materials may keep away from the side effects of synthetic drugs because they accumulate within the living cells which seems like our own system.[45,46]

In addition,Ayurvedic medicine aims to integrate and balance the body and mind. This balance is believed to lead to happiness and health, and to help prevent illness.

Herbal value :

India is the leading country where the production of medicinal plants is in huge quantity. That is why it is named the "Botanical garden of the World".[47] Medicinal plants have high natural therapeutic values against a variety of diseases. And it also supplies raw materials and high quality food for livelihood. A significant amount of work have already been done on these plants for the treatment of different diseases like cancer and many plant products have also been marketed as anticancer drugs, depending on their traditional uses and scientific reports (i.e., They are termed as medicinal plants).[47] Because of this reason in both developing and developed countries demand for medical plants is increasing day by day in human welfare.[48]

It is to be expected that dietary constituents, such as garlic, ginger, soya, curcumin, onion, tomatoes, cruciferous vegetables, chilies, and green tea, play an important role in protection from cancers. These nutritional agents are thought to suppress the transformative, hyperproliferative, and inflammatory processes that initiate carcinogenesis. These nutritional constituents have been classified as chemopreventive agents, and it has been studied broadly about their ability to delay the onset of carcinogenesis. As the source of this chemopreventive is from natural sources, they are considered pharmacologically not hazardous.[49]

In recent times the whole world is interested in herbal medicine or phytomedicines because of their repairing and strengthening ability for physical systems (especially the immune system, which can then properly fight foreign invaders). Herbal medicine also aids to demolish offending pathogens without lethal side effects.[50] As per World Health Organization (WHO), almost 80% of the world population is now applying medicinal plants to cure human disease.[51]

1.6 Nanophytochemicals:

Nanophytochemicals are simply the preparation of activephytoconstituents which is the heart of the herbal drugs or standardized extracts using different solvents. The utilization of nanophytomedicine improves the usefulness and bioavailability of administered drugs. They also reduce the side effects and toxicity of administered drugs.

The combination of nanotechnology with traditional herbal medicine occurs as a very constructive device in designing the future i.e., herbal medicine with an enhanced bioavailability profile and less toxicity.[52]

1.6.1Aloe vera: One of the about 420 species of Aloe plants, Aloe barbadensis Miller, sometimes known as Aloe vera, is a well-known dietary supplement and herbal medicine. Aloes contain green fleshy leaves coated in a thick cuticle, an inner clear pulp known as aloe vera gel, and pericyclic tubules along the outside margin of the leaf pulp that store and transport aloe vera latex. The Aloe vera plant leaf's main characteristic is its high water content, which ranges from 99.0% to 99.5%. However, it is reported that the remaining 0.5%–1.0% of the plant leaf contains over 75 potentially bioactive chemicals, including phenolic compounds like aloin [53]. The most widely distributed species of aloe, is Aloe vera. Leaf pulp processing is a significant matter in global industry. It has been used to make gel-containing health drinks and beverages and as a source of functional foods in other food products in the food industry. It has been used to make creams, lotions, soaps, shampoos, facial cleansers, and other products in the cosmetics and toiletry industry as a base material. Aloe has been utilized in the production of tablets and capsules as well as topical products like ointments and gel preparations in the pharmaceutical industry [54]. The ability to increase the bioavailability of co-administered vitamins in human subjects is one of the important pharmaceutical properties that have recently been discovered for both the whole leaf extract and the A. vera gel [55]. A. vera gel can be used to effectively deliver drugs that are difficult to absorb through the oral route of administration due to its ability to improve absorption. Additionally, directly compressible matrix-type tablets were successfully made with the dried powder obtained from A. vera gel. These matrix-type tablets showed potential for use as an excipient in modified release dosage forms by slowly releasing a model compound over an extended period of time [56].

The external layers contain a variety of pharmacologically active components includinganthraquinones, chromones, polysaccharides, and enzymes. Among them,anthraquinones and chromones are responsible for anti-cancer activity, anti-inflammatory, and evacuation.[57] It has also been reported that some elements are also present like Al, B, Ba, Ca, Fe, Mg, Na, P, Si etc. in *Aloe vera* gel.[57-59]

Next, the outer protective layer of the leaves consists, of derivatives of hydroxyanthracene, anthraquinone, and glycosides aloin A and B from 15% - 40% is reported by different investigations.[60-62] The other active principles of *Aloe* include hydroxyanthrone, aloe-emodin-anthrone 10-C-glucoside, and chrones.

It has been already reported that the middle layer of the leaf consists of yellow latex which contains anthraquinones and glycosides. The parenchymatous fleshy tissue contains proteins, lipids, amino acids, vitamins, enzymes, inorganic compounds, and small organic compounds in addition to the different carbohydrates. There is some evidence of chemotaxonomic variation in the polysaccharide composition [63] 16-different polysaccharides, 12 major polypeptides (molwt 15 - 77 kD), and various glycoproteins (29 kD in leaf gel).[64,65]

The innermost parenchymal layer of leaf gel contains almost 99% water, with glucomannans, lipids, sterols, amino acids, and vitamins.[65,66] The other potentially active ingredients include vitamins, enzymes, minerals, sugars, lignin, saponins, salicylic acids, and amino acids.[67-70] It also has several groups of monosaccharides and polysaccharides; numerous inorganic ingredients, vitamins B1, B2, B6, and C; niacinamide and choline, enzymes (acid and alkaline phosphatase, amylase, lactate dehydrogenase, lipase) and organic compounds (aloin, barbaloin, and emodin) as described by Hayes et al.[71] The most important functionally active component of *Aloe vera* is a long chain of acetylated mannose.[59,72,73]

Aloe vera juice helps our body to heal itself from cancer and also from the damaged tissues caused by chemotherapy and also radiotherapy because these destroy healthy immune cells which are essential for recovery. *Aloe vera* emodin, an anthraquinone, has the capability to suppress or inhibit the expansion of malignant cancer cells making it have antineoplastic properties.[74] Using a rat model, it can be suggested that the antimicrobial especially antibacterial effect of the *Aloe vera* gel *in vivo* could enhance the wound healing property by eliminating the bacteria that cause inflammation.[75] Powdered *Aloe vera* gel is used to prevent progressive dermal ischemia resulting from any type of injuries like burns, frostbite, electrical injury, and intra-arterial drug abuse. In vivo analysis of these injuries demonstrates that this gel acts as an inhibitor of thromboxane A2, a moderator of progressive tissue damage. [69]

1.6.2 Garlic (*Allium sativum*) :

Early investigation about garlic reported that \vegetable tissue of Allium sp is usually odor free and volatile odor principles in garlic oils were only generated during tissue damage and preparation which means the source of this volatile component was some non-volatile precursor compound. The first stable component of Allium is allin [(+)-*S*-allyl-L-cysteine sulfoxide (ACSO)] identified by Stroll et al 1948.[76] Allin is the key sulfur compound that is responsible for the majority of the odorous volatile compounds produced from any cut or crushed garlic.[77]

The sulfur compounds are responsible for not only garlic's pungent odor but also for its medicinal effects. The odor is formed from volatile compounds (allicin) by the action of the enzyme allinase on a non-volatile compounds (allin). The enzyme is heat sensitive, which is responsible for the drastic fall in odor intensity found in cooked garlic with similar physiological effects.[78]

Garlic has curative properties because of these organosulfur compounds, which are responsible for the typical odor and flavor of garlic.[79] The antibacterial activity of garlic is mainly attributed to thiosulfinates (e.g.,allicin).[79] Allicin mainly interrupts RNA synthesis and lipid production in a bacterial system. If RNA production is not carried out properly or in less amount then protein synthesis will be severely affected. If proteins cannot be produced then the growth and development of the organism will not occur as they are essential for all parts of cell structure. Besides this, synthesis of other biomolecules is also partially inhibited e.g., DNA and protein, though RNA is the main target of allicin action.[80]

Early studies reported that garlic extraction has shown effectiveness especially slows down the growth and development of both Gram-positive and Gram-negative bacteria, acid-fast bacteria such as *Klabsiella*, *Staphylococcus*, *E. coli*, *Micrococcus*, *Pseudomonas*, *Salmonella*, *Enterobacter*and *Helicobacter pylori*.[81,82]

This antibacterial property is mainly due to the structural organization of organisms so, they are vulnerable to garlic constituents[83], particularly Staphylococcus aureus, which contains only 2% lipid in their membrane[84] so that the permeability of allicin and other garlic components may be affected by the lipid content of the membranes. Therefore these phenomena may support the cell wall destruction and damage of genetic materials of Staphylococcus aureusstrongly.[85] Another example is about the inhibition property of garlic which showed that E. coli was inhibited more than 10 times greater than that seen in Lactobacillus caseifor the same garlic dose.[86] This also may be the differing compositions of bacterial cell membranes and their permeability to allicin.[87] Allicin itself is very unstable and decomposes rapidly reported by Brodnitz et al. 1971. [88] Also, upon reduction of allicin to diallyl disulfide, the antibacterial activity is greatly reduced.[89]

The first description of this molecule's in vivo anticancer action dates back to 1958.[90] A study on the in vitro anticancer activity of pure allicin on various cancer cell lines was carried out in 2001.[91] Allicin was recently discovered to be an anticancer agent that is present in aqueous

garlic extracts. The activity was assessed using an MTT cell viability assay on the colon cancer cell line CT26.WT from Musmusculus. The volatility of this molecule at moderate temperatures is one of its drawbacks.[92] In biological fluids, under light sources, and in the dark Dialyl disulfide is a tiny chemical that is the primary by-product of allicin breakdown (DADS). This means that it is yet another chemical that is frequently found in garlic extracts. DADS is more stable than allicin and retains many of its pharmacological properties. By causing cell proliferation and apoptosis to be inhibited and cell cycle progression to be arrested at the G0/G1 or G2/M phase, this small chemical exerts antiproliferative effects.[93] Moreover, DADS causes human A549 lung cancer cells to undergo time- and dose-dependent cell cycle arrest at the G2/M phase and apoptosis. The bioactive chemicals that provide garlic its biological effects have been identified as OSCs. Several OSCs were found to be lacking from intact garlic but present in cooked or processed garlic products. It is evident that GSAC, which is hydrolyzed and transformed into alliin during storage, is the main OSC found in intact garlic. [94] Bioactive DADS and DATS are not present in intact garlic. They are the byproduct of allicin's breakdown, which is facilitated by the enzyme alliinase, which is generated during the crushing or chopping of garlic.[95]

1.7 Types of Administration Routes for Drugs:

Route of administration is the way of drug delivery into the body to treat various diseases or disorders. Among different routes, the selection of the administration pathway depends upon the drug and patient-related factors like the condition of the patient (unconscious, vomiting, diarrhoea), age of the patient, emergency /routine use or sometimes the Patient's/doctor's choice. The various route of administration is given as follows-

In a conventional release system the drug /medicine is administered in the above mentioned pathways where the drug is released at once in the human body most of the time these are not targeted also.

Oral route

The oral drugs swelled after placing them in the mouth. Some advantages of the oral route are mainly painless, cheap, and can be self-administered. Absorption of the drug takes place along the whole length of the gastrointestinal tract.

The disadvantages are primarily the first pass effect means that initially drugs are absorbed in the mouth and then transported to the liver passing through the portal in vain. Sometimes irritation of the gastric mucosa results in nausea and vomiting. In some cases, only a part of the drug is absorbed and the acidic pH of the gastrointestinal tract along with gastric juice causes the destruction of the drug.

Intravascular Route

In an intravascular route system, the absorption process is bypassed. Here the drug is injected directly into the blood.

The advantages of this route are quite pain-free and shows quick action. This system is very beneficial for the specific, precise, and almost immediate onset of any emergency condition. Besides in this way, unconscious patients will be treated.

Some disadvantages are having pain at the site of injection, and a greater risk of undesirable effects. There is a risk of embolism because of the high concentration of the drug attained quickly.[96]

1.8 Types of Drug Release Mechanisms

☐ Conventional release

☐ Controlled release

☐ Sustained release

In the modern era, the expansion of new drug delivery systems creates more attention because the effective cost is very high to develop a new drug molecule instead. The principle objectives of sustained drug delivery over conventional delivery are to make sure about the safety and improvement of the efficiency of the drug with improved patient compliance. So the use of these dosage forms is increasing in the treatment of acute and chronic diseases. Because they can keep up the concentration of drug in plasma above the minimum effective concentration and below the minimum toxic level for an extended period of time.[97]

Sustained release drug delivery :

Generally in SR formulations, the first step is the dissolution of a drug into the matrix, which in turn swells into a gel, allowing the drug to exit through the gel's outer surface.

Some considerations of formulations of sustained release formulations:

• The active chemical compound will sustain on its own if this has a long half-life (over 6 hours).

• The pharmacological activity of this compound should be related to blood level otherwise time releasing has no purpose.

• If active transport is needed to absorb the active compound then the development of a time release product may be difficult.

If the pharmaceutically active compound has a short half-life, a huge amount of drug will be needed to sustain a long-lasting effective dose. So, a broad therapeutic window is essential to avoid toxicity, otherwise, the risk is unwarranted and a recommendation of another mode of administration would be required.[98]

Why sustained release over conventional release?

There are many more limitations of oral conventional dosage formulations [99]

1. Patient compliance is poor. Have a chance of missing the dose of a drug with a short half-life. So, here frequent administration is required.

2. In the case of a narrow therapeutic index drug the necessary drug concentration may lead to under-medication or over-medication.

3. A typical peak-valley plasma concentration time profile is obtained which makes the attainment of steady-state conditions impossible.[100]

There are some advantages of a sustained release drug delivery system over the conventional dosage form:

1. Reduction of dosing frequency

2. Dose reduction

3. Improved patient compliance.

5. Maintain a constant level of drug concentration in blood plasma.

6. Toxicity level reduction due to overdose. Reduced fluctuations of peak valley concentration.

7. Night-time dosing can be avoided.[101]

From the above discussion, it is clear that drug administration through nanocarriers in general is much superior to the conventional routes of drug delivery in combating diseases.

As an example, mesoporous silica material can draw attention as a matrix or carrier of any drug because silica gel is a very appropriate nanomaterial. In particular cases for example oral drug delivery, silica is a perfect material because of its suitable characteristics for working properly in the gastrointestinal tract at very low pH conditions (pH 1-3) and consequently silica is able to protect the loaded drug molecules from the changes in pH as well as degradative enzymes and bile salts.[102,103]

1.9 Drug Release/Delivery from Nanoconjugate:

Drug release or drug delivery from any matrices is implicated with many processes including erosion, diffusion, and leaching or dissolution.[104-105] In some cases more than one mechanisms are jointly responsible for the release of a drug; this may be attributed to the involvement of both diffusion and dissolution controlled processes.[106] In a modified drug delivery system (for example sustained or controlled release system) the diffusion process predominates because the encapsulated drug is distributed in a homogenous way in the polymeric matrix (capsules/tablets).

Zero-order kinetics, first order kinetics, the Higuchi model, and the Hixson-Crowell models are widely used to describe the dissolution kinetics of drugs from any solid matrices. Weibull model, Baker-Lonsdale model, Korsmeyer-Peppas, and Ritger-Peppas model and Hopfenberg model are involved to interpret the drug release mechanism [104-106].

Sustained release of drugs from nanostructured materials like silica and clay :

In this work, it is shown that a lot of work has been carried out on different nanostructured materials and the entrapment of herbal drugs inside those materials. At the present time sustained release is adopted over conventional releases for curing of different diseases. So, various studies have been carried out to get the sustained release mechanism for entrapped chemical / herbal drugs from nanostructured material in body fluids.

Chakrabarty et al. (2011) studied the release kinetics of Nanocarrier entrapped herbal values. Amdrographis paniculata has antimicrobial, anti-fungal etc. properties. It remains active in its antimicrobial state when it is entrapped in Nanocarrier like silica gel. They have shown the MIC values of the herbal extract Escherichia coli and Staphylococcus aureus successfully.[107]

In their paper, Chakrabarty et al. (2011) examined especially the antimicrobial activity of the released herbal extract from silica gel nanomaterial. The herbs Ocimum sanctum and Terminalia chebula were absorbed and adsorbed into the nanopore of silica gel matrix to make nanomaterial entrapped herbs. MIC values signify that herbal properties remain unchanged in the entrapped condition.[108] The drug release kinetics was also observed in different pH (SBF-7.4 & HCL-1.2) in the liquid liquid kinetics model.[109]

Xue et al (2015) fruitfully synthesized drug-loaded nanoclay material by using the electrospinning membranes technique. This technique is now very much used in polymer-like clay fiber processing in the field of tissue engineering with drug release applications, in vitro antimicrobial applications and to study the sustained release mechanism of loaded drugs.[110]

At present, polymeric systems especially polymer clay nanocomposite are significantly used as drug carriers. Actually, for sustained or controlled drug delivery, these systems are suitable kits very much. [111]

1.10 Selected diseases:

1. 10.1: Microbial disease:

As microbial disease typhoid fever is chosen.

A Gram-negative bacterium called *Salmonella typhi* is the source of typhoid fever. The *Salmonella* serotype paratyphi A causes an illness that is strikingly similar but frequently less severe. The ratio of *S. typhi* caused illness to *S. paratyphi* caused illness in the majority of the nations where these diseases have been investigated is approximately 10:1. Humans are the disease's only natural host and reservoir.[112] The majority of cases of typhoid respond well to antibiotic treatment. However, the emergence of multi-drug-resistant strains has made treatment extremely difficult, and typhoid fever cases treated with ineffective medications can result in death.[113] Typhoid Salmonellae have developed and spread multidrug resistance against traditional antityphoid medications (Ampicillin, Chloramphenicol, and Trimethoprim-

Sulfamethoxazole), particularly in South and Southeast Asia, over the past two decades. The preferred antibiotic for the treatment of typhoid fever is now fluoroquinolones. Since they have been in use for more than 18 years, fluoroquinolones, particularly ciprofloxacin, have remained a key tool in the fight against typhoid infections. In India, typhoid is a serious endemic health issue for kids.[114] According to WHO data, the global burden of typhoid fever is estimated to be 17–22 million cases with 0.2–0.6 million fatalities annually. By consuming feces contaminated food or water, the virus is spread. Where there is a high population served by contaminated water supplies, the incidence is highest. Typically, the incubation period lasts 8 to 14 days, however it can last anywhere from 3 to 2 months. Infected individuals who harbour *S. typhi* in their gall bladders develop into chronic carriers in about 2-5% of cases. The disease's propagation is significantly aided by chronic carriers. Numerous gentle and abnormal diseases happen and back slides are normal. Patients contaminated with HIV are at an essentially expanded hazard of extreme illness because of *S. typhi* and *S. paratyphi.*[115]

1.10.2: Viral disease:

As viral disease Covid-19 disease is chosen.

Coronavirus disease 2019 (COVID-19), caused by severe acute respiratory syndrome coronavirus 2 (SARS-CoV-2), was first reported in December 2019 and the number of countries affected increased rapidly, and recently WHO has declared it as a pandemic. Most of the patients with COVID-19 are asymptomatic or have mild to severe respiratory disease. However, deaths with multiorgan and systemic manifestations, such as sepsis, septic shock and multiorgan dysfunction syndromes (MODS) were also observed. Laboratory studies have shown that SARS-CoV-2 is cytopathic and may have caused the initial damage to the lungs as demonstrated by pathological examination. Along with virus replication, the host's immune responses are activated, which should eliminate the virus and treat patients. However, why some of the patients developed more severe disease, such as MODS, is not yet known. It is hypothesized that cytokine storm plays an important role in the pathogenesis of severe cases of COVID-19. [116,117] Cytokine storms can trigger multiple infectious or non-infectious diseases and cause severe damage to multiple organs. The immune system recognizes pathogen infection, which consists of two types of responses: the innate immune response that recognizes pathogen-associated molecular patterns (PAMPs) and the antigen-specific adaptive immune response. Both

responses involve multiple activated immune cells that play a key role in establishing the cytokine milieu. [118,119] However, exaggerated, over synthesized cytokines cause an acute, severe systemic inflammatory response called a "cytokine storm." Several experimental studies and clinical trials have shown that the cytokine storm is directly correlated with tissue damage and negative prognosis in severe lung disease. To date, the cytokine profile of COVID-19 patients with different disease severities is not clear. The signs of COVID-19, or coronavirus illness 2019, include sore throat, fever, coughing, and exhaustion, which are all signs of the regular flu. Some instances of these symptoms include along with vomiting and diarrhea. More than 5 million deaths have been documented worldwide as a result of this pandemic sickness, which has afflicted some 260 million individuals. Statistics showed that males are more likely than females to contract COVID-19 infection, and older adults (>55 years) with or without co-morbid conditions had the greatest infection fatality ratios. It is now known that COVID-19 causes cellular immune insufficiency, coagulation activation, cardiac injury, hepatic injury, renal dysfunction, and multiorgan failure in addition to the typical flu-like and respiratory distress symptoms. Early in 2020, Europe, Italy, and Spain were all negatively impacted. Beginning in the middle of February 2020, an epidemic peak quickly turned into a pandemic that affected the entire world. According to reports, quite a few infected people had a variety of symptoms, while some exhibited no signs at all. Severe respiratory illness like acute respiratory distress with interstitial pneumonia predominated in some patient subgroups by a significant margin. Patients in these hospitalized situations with respiratory failing states needed early and ongoing mechanical ventilation. The majority of the planet has already been impacted by COVID-19's second wave. In comparison to the initial wave, the situation in India has gotten far worse. India began reporting 10–20 new cases per day in February, and that number has since increased exponentially to 300–400 cases per day. [120]

The spike glycoprotein is present in numerous copies on the surface of corona viruses. The term "corona" was given to this family of viruses because of its distinctive crown-like shape (which in Latin means crown). Hence, the structures of the virus that are most exposed are spike proteins. The S1 and S2 subunits combine to form the trimetric fusion protein known as the spike protein. The receptor binding domain (RBD), which recognizes and interacts with host cells, is found in the S1 unit. Both a "up" and a "down" conformation are possible for the RBD. [121] As was previously demonstrated for SARS-Cov-1, in the SARS-Cov-2 the RBD has high affinity for

eukaryotic cell invasion in the "up" conformation Human angiotensin converting enzyme 2 (ACE2). Prefusion trimer destabilisation occurs in response to receptor engagement, which is then followed by a proteolytic cleavage between units S1 and S2 (e.g., by the transmembrane serine protease TMPRSS2).[122] Cell invasion and structural changes result from this point. The critical role of the spike protein makes it one of many possible SARS-CoV-2 therapeutic targets and makes it a vulnerable and significant target for viral neutralization.[123] The direct competition for the ACE2 binding site, the steric obstruction of ACE2 binding from nearby binding sites, or the suppression of structural rearrangements required for fusion are all potential neutralisation mechanisms.[124]

1.10.3: Neoplastic disease:

As neoplastic disease hepatocellular carcinoma is chosen.

One of the leading causes of death for people globally is cancer. Nowadays, radiation, clinical surgery, and chemotherapy are the main methods used to treat cancer.[125] Chemotherapy has a substantial cytotoxic effect on normal healthy tissues in addition to its limited ability to effectively treat tumours, which leads to the unsuccessful eradication of all cancer cells. In patients receiving radiotherapy, severe physiological problems might also occur.[126-128] Cancer still poses a serious threat to people's health despite the fact that many different ways have been explored in its treatment.

Hepatocellular carcinoma (HCC) is a giant and highly metastatic cancer worldwide. Hepatocellular carcinoma (HCC) is the most destructive and aggressive form of liver tumor. The incidence of HCC continues to increase rapidly and is third with more than 600,000 deaths per year. HCC has a strong tendency to invade the liver vasculature. More efforts should be made to explore new treatment strategies for HCC. Primary liver cancer is one of the most common causes of cancer death.[129] Hepatocellular carcinoma (HCC) is a common cancer with a high incidence and a 5-year survival rate in HCC of less than 20%. Approximately 75-85% of patients with primary liver cancer are hepatocellular carcinoma (HCC).[130] The incidence of liver cancer in Asian countries, especially East and Southeast Asia, remains the highest in the world. Today, surgical resection, orthotopic liver transplantation and local ablative therapies are considered potentially curative in patients with early-stage HCC. Sorafenib is the only chemotherapy drug approved by the US Food and Drug Administration for first-line treatment in

advanced HCC and remains the only drug approved for the systemic treatment of patients with metastatic HCC. However, despite advances in tumor therapy, effective systemic therapy for advanced HCC has not been established. Liver cancer 5-year survival after systemic therapy remains low and severe side effects limit the clinical use of chemotherapy in advanced HCC. [131] In conclusion, new, effective therapeutic agents with low toxicity are urgently needed.

As a result, scientists are searching for novel and more efficient therapeutic approaches, such as combination therapy, immunotherapy, and gene/RNA interference therapy.[132] Attention has been drawn more to multipurpose therapeutic agents as a result of the rapid advancement of nanoscience and technology. Multitargeted treatments may make it easier to diagnose and treat cancer in its preclinical stages. As therapeutic carriers, several different nanomaterials have been created during the past few years, including inorganic mesoporous silicon, [133] quantum dots, [134] metal nanoparticles, [135] organic micelles, [136] liposomes, [137] polymersomes, [138] and dendrimers.[139] However, the majority of the disadvantages of these nanocarriers include low biocompatibility, cytotoxicity, and a limited capacity for drug loading. Non-toxic, biocompatible, and biodegradable drug excipients with a high capacity to load drugs are considered safe and effective.[140] In order to achieve an excellent therapeutic index, the release of therapeutic agents from various carriers needs to be effectively controlled. As a result, a lot of work has been done to create multifunctional systems that can be used for diagnostic or therapeutic purposes as well as effective cancer treatment.[141]

In this literature review, different types of nanomaterial which are important in biotechnology to be used as drug delivery systems are discussed. The importance of herbal drugs and the possibility of entrapment of the drugs within the nonporous system have been discussed. The study of release kinetics to get the sustained release kinetic model of those entrapped drugs in the body fluids is elaborated.

This study aims to investigate the importance and effectivity of herbal medicine against S. typhi bacteria as well as over hepatocellular carcinoma disease. Besides this which cytokines were involved in the cytokine storm of COVID-19 and which cytokines were involved in the diagnosis and treatment of COVID-19 are also investigated here.

References :

1. B.Y. Kim, J.T Rutka, W.C. Chan, Nanomedicine. N Engl, J Med. 2010; 363: 2434–2443.

2. P. Fortina, L.J. Kricka, S. Surrey, P. Grodzinski, Nanobiotechnology: the promise and reality of new approaches to molecular Recognition, TRENDS in Biotechnology. 2005; 23: 4.

3. G.M. Whitesides, The —right‖ size in nanobiotechnology, Nat.Biotechnol. 2003; 18: 760–763.

4. J.N. Tiwari, R.N. Tiwari, K.S. Kim, Zero-dimensional, one-dimensional, two-dimensional and three-dimensional nanostructured materials for advanced electrochemical energy devices, Progress in Materials Science, 2012; 57: 724–803.

5. R. Shula, D. Paul, Nano structure control of important xerogels for the control release of biomolecules. NATO science series II: Mathematics, physics chemistry., 2003; 171: 59-74.

6. M. Hartmann, Ordered Mesoporous Materials for Bioadsorption and Biocatalysis, Chem. Mater., 2005; 17: 4577–4593.

7. J. Safari, Z. Zarnegar, Advanced drug delivery systems: Nanotechnology of health design A review, Journal of Saudi Chemical Society., 2014; 18: 85–99.

8. R. Hirlekar, M. Yamagar, H. Garse, M. Vij, V. Kadam, Carbon Nanotubes And Its Applications: A Review, Asian Journal of Pharmaceutical and Clinical Research. 2009; 2: 4.

9. P.M. Ajayan, O.Z. Zhou, Applications of Carbon Nanotubes, Topics Appl. Phys. 2001; 80: 391–425.

10. S. Iijima, Helical Microtubules of Graphaite Carbon, Nature., 1991; 354: 56-58.

11. S. Wei, A. Paul, Y. Mai, Carbon Nanotubes for Use in Medicine: Potentials and Limitations, LaetitiaRodes and SatyaPrakash., 2015.

12. A.K. Geim, K. S. Novoselov, The Rise of Graphene. Nat. Mater. 2007; 6: 183– 191.

13. X. Huang, X. Y. Qi, F. Boey, H. Zhang, Graphene-Based Composites Chem. Soc. Rev., 2012; 41: 666– 686.

14. C. L.Tan, X. Huang, H. Zhang, Synthesis and Applications of Graphene-Based Noble Metal Nanostructures Mater.Today., 2013; 16: 29– 36.

15. X. Huang, C.L. Tan, C. L. Z.Y. Yin, H. Zhang, 25th Anniversary Article: Hybrid Nanostructures Based on Two-Dimensional Nanomaterials. Adv. Mater., DOI: 10.1002/adma.201304964, 2014**;** 26: 2185-2204.

16. X. Y. Qi; C. L. Tan, J. Wei, H. Zhang, Synthesis of Graphene-Conjugated Polymer Nanocomposites for Electronic Device Applications Nanoscale. M, DOI: 10.1039/c2nr33145d, 2013; 5: 1440– 1451.

17. T. Kuilla, S. Bhadra, D. Yao, N.H. Kim, S. Bose, J.H. Lee, Recent Advances in Graphene Based Polymer Composites Prog. Polym. Sci., DOI: 10.1016/j.progpolymsci.2010.07.005, 2010; 35: 1350– 1375.

18. C.L. Tan, H. Zhang, Two-Dimensional Transition Metal DichalcogenideNanosheet-Based Composites. Chem. Soc. Rev. DOI: 10.1039/C4CS00182F, 2015; 44: 2713– 2731.

19. X. Huang, B. Zheng, Z. D. Liu, C.L. Tan, J.Q. Liu, B. Chen, H. Li, J.Z. Chen, X. Zhang, Z. X. Fan, Coating Two-Dimensional Nanomaterials with Metal-Organic Frameworks. ACS Nano, DOI: 10.1021/nn503834u, 2014; 8: 8695–8701.

20. J.M.J. Fréchet, D. Tomalia,(Eds.) Dendrimers and Other Dendritic Polymers, John Wiley & Sons., 2001.

21. G.R. Newkome, C.N. Moorefield, F. Vogtle, Dendrimers and Dendrons: Concepts, Syntheses, Applications, Wiley-VCH 2001.

22. F. Aulenta, W. Hayer, S. Rannard, Dendrimers: a new class of nanoscopic containers and delivery devices, Eur. Polym. J. 2003; 39: 1741–1771.

23. S.E. Stiriba, H. Frey, R. Haag, Dendritic polymers in biomedical applications: from potential to clinical use in diagnostics and therapy. Angew.Chem. Int. Ed. Engl. 2002; 41: 1329–1334.

24. A.K. Patri, I. J. Majoros, J.R Baker, Dendritic polymer macromolecular carriers for drug delivery,Curr. Opin. Chem. Biol., 2002; 6: 466–471.

25. U. Boas, P.M.H. Heegaard, Dendrimers in drug research, Chem. Soc. Rev., 2003; 33: 43–63

26. J. Nicolas, S. Mura, D. Brambilla, N. Mackiewicz, P. Couvreur, Design, functionalization strategies and biomedical applications of targeted biodegradable/biocompatible polymer-based nanocarriers for drug delivery, Chem. Soc. Rev., 2013; 42: 1147–1235.

27. P. Kluson, M. Drobek, H. Bartkova, I. Budil, Welcome in the Nanoworld, Chem. Listy, 2007; 101: 262-272.

28. A. Ferancova, J. Labuda, (Ed) DNA Biosensors based on nanostrucutred materials, In Nanostrucutred Materials in Electrochemistry, Eftekhari, A. Wiley-VCH: Weinheim, Germany, 2008; 409-434.

29. V. Kral, J. Sotola, P. Neuwirth, Z. Kejik, K. Zaruba, P. Martasek, Nanomedicine – Current status and perspectives: A big potential or just a catchword?, Chem. Listy., 2006; 100: 4-9.

30. M.A. Ghanem, P.N. Bartlett, P. de Groot, A. Zhukov, A double templatedelectrodeposition method for the fabrication of arrays of metal nanodots, Electrochem.Commun., 2004; 6: 447-453.

31. K. Fujioka, M. Hiruoka, K. Sato, N. Manabe, R. Miyasaka, S. Hanada, A. Hoshino, R.D. Tilley, Y. Manome, K. Hirakuri, K. Yamamoto, Luminescent passive-oxidized silicon quantum dots as biological staining labels and their cytotoxicity effects at high concentration,Nanotechnology., 2008; 19: 7.

32. T. Jamiesona, R. Bakhshia, D. Petrovaa, R. Pococka, Mo Imanib, A.M. Seifalian. Biological applications of quantum dots, Biomaterials., 2007; 28: 4717–4732.

33. M.A. Walling, J.A. Novak, J.R.E. Shepard, Quantum dots for live cell and in vivo imaging, Int.J. Mol. Sci., 2009; 10: 441-491.

34. X.H. Gao, S.R. Dave, Quantum dots for cancer molecular imaging, In Bio-Applications of Nanoparticles; Springer-Verlag Berlin: Berlin., 2007; 620: 57-73.

35. X.H. Gao, L.L. Yang, J.A. Petros, F.F. Marshal, J.W. Simons, S.M. Nie, In vivo molecular and cellular imaging with quantum dots, Curr. Opin.Biotechnol., 2005; 16: 63-72.

36. H.C. Li, Q.F. Zhou, W. Liu, B. Yan, Y. Zhao, G.B. Jiang, Progress in the toxicological researches for quantum dots, Sci. China Ser. B., 2008; 51: 393-400.

37. J. Lovric, H.S. Bazzi, Y. Cuie, G.R. A. Fortin, F.M. Winnik, D. Maysinger, Differences in subcellular distribution and toxicity of green and red emitting CdTe quantum dots, J Mol Med., 2005; 83: 377–85.

38. A. Shiohara, A. Hoshino, K. Hanaki, K. Suzuki, K.Yamamoto, On the cyto-toxicity caused by quantum dots, MicrobiolImmunol., 2004; 48: 669–75.

39. R. Hardman, A toxicologic review of quantum dots: toxicity depends on physicochemical and environmental factors, Environ Health Perspect., 2006; 114: 165–72.

40. X. You,Y. Kang, G. Hollett, X. Chen, W.Zhao, Z. Gu, J. Wu, Polymeric nanoparticles for colon cancer therapy: overview and perspectives, Journal of Materials Chemistry B. 4: 7779—7792.

41. K. Kostarelos, Rational design and engineering of delivery systems for therapeutics: biomedical exercises in colloid and surface science, Adv. Colloid Interface Sci., 2003; 106: 147–168.

42. K. Donaldson, V. Stone, C.L. Tran, W. Kreyling, P.J. Borm, Nanotoxicology, Occup Environ M. 61 (2004) 727-728.

43. L. Tang, T.M. Fan, L.B. Borst, J. Cheng, Synthesis and Biological Response of Size-Specific, Monodisperse Drug-Silica Nanoconjugates, ACS Nano., 2012; 6(5): 3954–3966.

44. M.A. Kalam, M. Humayun, N. Parvez, S. Yadav, A. Garg, S. Amin, Y. Sultana, A. Ali, Continental J Pharm Sci. 2007; 1: 30 - 35.

45. V.H.L. Lee, Controlled Drug Delivery Fundamentals and Applications: Introduction, Marcel Dekker, (2nd ed) INC, New York. 1987; 29.

46. D.M. Brahmankar, S.B. Jaiswal, Biopharmaceutics and Pharmacokinetics: Pharmacokinetics, 2nd ed. VallabhPrakashan, Delhi., 2009; 399-401.

47. M. Umadevi, K.P. Sampath Kumar, D. Bhowmik, S. Duraivel, Traditionally Used Anticancer Herbs In India, Journal of Medicinal Plants Studies., 2013; 1(3): 56-74.

48. U. Spandana, S.L. Ali, T. Nirmala, M.Santhi, S.D. SipaiBabu, A Review on Tinosporacordifolia, International Journal of Current Pharmaceutical Review and Research., 2013; 4(2): 61-68.

49. B.B. Aggarwal, H. Ichikawa, P. Garodia, P. Weerasinghe, G.G. Sethi, D.I. Bhatt, K.M. Pandey, S. Shishodia, G.M. Nair, From traditional Ayurvedic medicine to modern medicine: identification of therapeutic targets for suppression of inflammation and cancer, Expert Opin. Ther.Targets., 2006; 10(1): 87-118.

50. N.H.M. Yunos, H. Hamdan, L.S. Ling, Piperine Loaded Silica Xerogel as NANO-Enabled Drug Delivery system,World applied Sciences Journal 9 (Special Issue of Nanotechnology)., 2010; 06-16.

51. J. Serrentino, How Natural Remedies Work. Point Robert, Vancouver, Harley and Marks Publishers., 1991; 20-22.

52. A.N. Sahu., nanotechnology in herbal medicine and cosmetics. Int. J. Res. Ayurveda pharm., 2013; 4(3).

53. M. Lee , J. Liao, W. Huang , F.Jiang , Y. Jheng , Y. Jin , Ya-Shih Tseng, Aloin-induced cell growth arrest, cell apoptosis, and autophagy in human non-small cell lung cancer cells, Biomarkers and Genomic Medicine. 2014; 6: 144-149.

54. K. Eshun, Q. He, Aloe vera: A valuable ingredient for the food, pharmaceutical and cosmetic industries – A review. *Crit. Rev. Food Sci. Nutr.* 2004, *44,* 91-96.

55. J.A Vinson, H. Al Kharrat, L. Andreoli, Effect of *Aloe vera* preparations on the human bioavailability of vitamins C and E. *Phytomedicine* 2005, *12*, 760-765.

56. G.K Jani, D.P. Shah, V. C Jain, M.J Patel, D.A. Vithalan, Evaluating mucilage from *Aloe Barbadensis* Miller as a pharmaceutical excipient for sustained-release matrix tablets. *Pharm. Technol.* 2007, *31*, 90-98.

57. S.W. Choi, B.W. Son, Y.S. Son, Y.I. Park, S.K. Lee and M.H. Chung, The Wound-Healing Effect of a Gly- coprotein Fraction Isolated from Aloe vera, British Jour- nal of Dermatology., 2001; 145(4): 535-545.

58. T. Yamaguchi, H. Takamura, T. Matoba and J. Terao, HPLC Method for Evaluation of the Free Radical- Scavenging Activity of Foods by Using 1,1-Diphenyl-2- Picrylhydrazyl, Bioscience, Biotechnology and Biochem- istry., 1998; 62(6): 1201-1204.

59. A. Femenia, E. S. Sanchez, S. Simal and C. Rossello, Compositional Features of Polysaccharides from Aloe vera (Aloe barbadensis Miller) Plant Tissues, Carbohy- drate Polymers., 1999; 39(2): 109-117.

60. D. Saccu, P. Bogoni and G. Procida, Aloe Exudate: Cha- racterization by Reversed Phase HPLC and Headspace GC-MS, Journal of Agricultural and Food Chemistry., 2001; 4910: 4526-4530.

61. P.R. Bradley, British Herbal Compendium, British Herbal Medicine Association. Bournemouth. 1992.

62. J. Bruneton, Pharmacognosy, Phytochemistry, Medicinal Plants, England, Intercept, Hampshire., 1995; 434- 436.

63. Y. Ni, I. R. Tizard, Analytical Methodology: The Gel-Analysis of Aloe Pulp and Its Derivatives, In: T. Reynolds, Ed., Aloes the Genus Aloe, CRC Press, Boca Raton., 2004; 111-126.

64. Anonymous, Cosmetic Ingredient Review Expert Panel, Final Report on the Safety Assessment of Aloe andon-gensis Extract, Aloe andongensis Leaf Juice, Aloe arbor-escens Leaf Extract, Aloe arborescens Leaf Juice, Aloe arborescens Leaf Protoplasts, Aloe barbadensis Flower Extract, Aloe barbadensis Leaf, Aloe barbadensis Leaf Extract, Aloe barbadensis Leaf Juice, Aloe barbadensis Leaf Polysaccharides, Aloe barbadensis Leaf Water, Aloe ferox Leaf Extract, Aloe ferox Leaf Juice, and Aloe ferox Leaf Juice Extract, International Journal of Toxicology., 2007; 26(2): 1-50.

65. T. Reynolds and A. C. Dweck, Aloe vera Leaf Gel: A Review Update, Journal of Ethnopharmacology., 1999; 68(1-3): 3-37.

66. J.P. Brown, A Review of the Genetic Effects of Natu- rally Occurring Flavonoids, Anthraquinones and Related Compounds, Mutation Research., 1980; 75(3): 243-277.

67. B.K. Vogler and E. Ernst, Aloe vera: A Systematic Re- view of Its Clinical Effectiveness, The British Journal of General Practice., 1999; 49(447): 823-828.

68. J. Townsend, Aloe vera. The UK Reference Guide to Complimentary Medicine, Chartwell House Publishing, London., 1998.

69. P. Antherton, Aloe vera: Magic or Medicine? Nursing Standard., 1998; 12(41): 49-54.

70. M.S. Shelton, Aloe vera, Its Chemical and Therapeutic Properties, International Journal of Dermatology., 1991; 30(10): 679-683.

71. S.M. Hayes, Lichen Planus: Report of Successful Treat- ment with Aloe vera, General Dentistry., 1999; 47(3): 268-272.

72. A. Djeraba and P. Quere, In Vivo Macrophage Activation in Chickens with Acemannan, a Complex Carbohydrate Extracted from Aloe vera, International Journal of Immunopharmacology., 2000; 22(5): 365-372.

73. J.K. Lee, M.K. Lee, Y.P. Yun, Y. Kim, J.S. Kim, Y.S. Kim, K. Kim, S.S. Han and C. K. Lee, AcemannanPu- rified from Aloe vera Induces Phenotypic and Functional Maturation of Immature Dendritic Cells, International of Immunopharmacology., 2001; 1(7): 1275- 1284.

74. R.H. Thomson, Naturally Occurring Quinines, 2nd Edition, Academy Press, London., 1971.

75. J.P. Heggers, A. Kucukcelibi, C. J. Stabenou, F. Ko, L.D. Broemeling, M.C. Robson, W.D. Winters, Wound Healing Effects of Aloe Gel and Other Topical Antibacte- rial Agents in Rat Skin, Phytotherapy Research., 1995; 9(6): 455-457.

76. A. Stoll and E. Seebeck, Alliin, the pure mother substance of garlic oil, Experentia., 1947; 3: 114–115.

77. H.P. Koch, L.D. Lawson, Garlic-The Science and Therapeutic Application of Allium sativum L. and Related Species Williams, Wilkins, 2nd ed. Baltimore., 1996; 135-21.

78. S. Durairaj, S. Srinivasan, P. Lakshmanaperumalsamy, In vitro Antibacterial Activity and Stability of Garlic Extract at Different pH and Temperature, Electronic Journal of Biology., 2009; 5(1): 5-10.

79. J.C. Harris · S.L. Cottrell S. Plummer D. Lloyd. Antimicrobial properties of Allium sativum (garlic).ApplMicrobiolBiotechnol., 2001; 57: 282–286.

80. R.S. Feldberg, In vitro mechanism of inhibition of bacterial growth by allicin. Antimicrob.Agent.Chemother., 1988; 32: 1763-1768.

81. S.M. Tsao, M.C. Yin, In vitro antimicrobial activity of four diallylsulphides occurring naturally in garlic and Chinese leek oil, J. Med. Microbiol., 2001; 50: 646-649.

82. S. Durairaj, S. Srinivasan, P. Lakshmanaperumalsamy, In vitro Antibacterial Activity and Stability of Garlic Extract at Different pH and Temperature, Electronic Journal of Biology., 2009; 5(1): 5-10.

83. Z. Tyneka, Z. Gos, The fungistatic activity of garlic (A. sativum) in vitro. Ann. Univ. M ariae C urrieSkoldowaska Sect D. Med., 1975; 30: 5-13.

84. M.R.J. Salton, The bacterial Cell Wall. Elsevier, Amsterdam, The Netherlands, 1964.

85. D. Deresse. Antibacterial Effect of Garlic (Allium sativum) on *Staphylococcuaureus*: An in vitro Study. Asian Journal of Medical Sciences.. 2010; 2(2): 62-65.

86. D.A. Skyrme, The antimicrobial activity of Allium sativum. PhD Thesis, Cardiff University., 1997.

87. T. Miron, A. Rabinkov, D. Mirelman, H. Wilchek, L. Weiner, The mode of action of allicin: its ready permeability through phospholipid membranes may contribute to its biological activity. BiochemBiophysActa., 2000; 1463: 20–30.

88. M.H. Brodnitz, J.V. Pascale, L.V. Derslice, Flavour components of garlic extract. J Agric Food Chem., 1971; 19: 273–275.

89. H.D. Reuter, P. Koch, D.L. Lawson, Therapeutic effects and applications of garlic and its preparations., 1996.

90.15.A. S. Weisberger and J. Pensky, Cancer Res., 1958, 18, 1301.

91.16 .K. Hirsch, M. Danilenko and J. Giat, Nutr. Cancer, 2000, 38, 245.

92.18.H. Fujisawa, K. Suma, K. Origuchi, H. Kumagai, T. Seki and T. Ariga, J. Agric. Food Chem., 2008, 56, 4229.

9324.L. Yi and Q. Su, Food Chem. Toxicol., 2013, 57, 362..

94.126. H. Amagase, J. Nutr., 2006, 136, 716S–725S

95.7.B. Iberl, G. Winkler and K. Knobloch, Planta Med., 1990, 56, 202–211.

96. P. Verma, A.S. Thakur, K. Deshmukh, Dr. A.K. Jha, S. Verma, Routes of Drug Administration, International Journal of Pharmaceutical Studies and Research., 2010; 1(1): 54-59.

97. 87.S. Jawla , A.K. Gupta, R. Singla, V. Gupta, General awareness and relative popularity of allopathic, ayurvedic and homeopathic systems. Journal of Chemical and Pharmaceutical Research., 2009; 1(1): 105-112.

98. J. Alberts, Herbal and Synthetic Drugs: A Comparison; Pharmacist, Pharm. D., Ph.D.

99. B. Maiti, B.P. Nagori, R. Singh, P. Kumar, N. Upadhyay, Recent Trends In Herbal Drugs: A Review. International Journal of Drug Research and Technology., 2011; 1(1): 17-25.

100. M. Lahlou, The Success of Natural Products in Drug Discovery , Pharmacology & Pharmacy., 2013; 4: 17-31

101. B. Patwardhan, A. D. B. Vaidya and M. Chorghade, Ay- urveda and Natural Products Drug Discovery,‖ Current Science., 2004; 86(6): 789-799.

102. H. Jaganathan, B. Godin, Biocompatibility assessment of Sibasednano- and micro-particles, Adv. Drug Delivery Rev., 2012; 64: 1800−1819.

103. M.K. Rai, S.D. Deshmukh, A.P. Ingle, and A.K. Gade, Silver nanoparticles: the powerful nanoweapon against multidrug-resistant bacteria, J. Appl. Microbiol., 2012; 112: 841.

104. M.S. Wani, M.H. Dehghan. "Controlled release system-A review." Pharmaceutical Reviews, 2008; 6.1: 41-46.

105. E. Ernst, Is homeopathy a clinically valuable approach?, Trends in Pharmacological Sciences., 2005; 26(11): 547-8.

106. S.M. Sagar, Homeopathy: Does a teaspoon of honey help the medicine go down?, Current oncology., 2007; 14(4): 126–7.

107. S. Chakraborty, S. Biswas, R. Dey, M.K. Mitra, S Das, Sustained Release of Silica Gel Entrapped Methanol Extract of Andrographispaniculata and Its Retention of Antimicrobial Property, Int. J. Novel Drug Deliv. Tech. 2011; 1(3)

108. S. Chakraborty, J.S. Manna, S. Das, M.K. Mitra, R. Dey, Sustained release of silica gel entrapped herbal values and their antimicrobial activity, Asian Journal of Pharmaceutical and Clinical Research., 2011; 4(2): 5962.

109. S. Chakraborty, M.K. Mitra, M. G. Chaudhuri, B. Sa, S. Das, R. Dey, Study of the Release Mechanism of Terminaliachebula Extract from Nanoporous Silica Gel, ApplBiochemBiotechnol., 2012; 168: 2043–2056.

110. J. Xue, Y. Niu, M. Gong, R. Shi, D. Chen, L. Zhang, Y. Lvov, Electrospun Microfiber Membranes Embedded with Drug-Loaded Clay Nanotubes for Sustained Antimicrobial Protection, ACS nano, 2015; 9(2): 1600–1612.

111. M. Jafarbeglou M. Abdouss, A. M. Shoushtari, M. Jafarbeglou, Clay nanocomposites as engineered drug delivery Systems, RSC Advances., 2016; 6: 50002–50016.

112. E. Mweu and M. English. Typhoid fever in children in Africa. Trop Med Int Health. 2008;13(4): 532–40.

113. S. Wang, N. Mamedova, N. A. Kotov, W. Chen and J. Studer, Nano Lett., 2002, 2, 817–822.

114. C M. Parry, T T. Hien, G. Dougan, N J. White, J J. Farrar. Typhoid fever. N Engl J Med.2002; 34:1770–*82*.

115. S. K. Pandey, P. Rishi, C. R. Suri and A. C. Vinayaka, Anodic stripping voltammetry of anti-Vi antibody functionalized CdTe quantum dots for the specific monitoring of Salmonella enterica serovar Typhi, RSC Adv., 2015, 5, 88234.

116. X. Yang, Y.Yu, J. Xu, et al. Clinical course and outcomes of critically ill patients with SARS-CoV-2 pneumonia in Wuhan, China: a single-centered, retrospective, observational study. Lancet Respir Med. 2020 Feb 24. doi:10.1016/s2213-2600(20)30079-5.

117. Z. Xu, L. Shi, Y. Wang, et al. Pathological findings of COVID-19 associated with acute respiratory distress syndrome. Lancet Respir Med. 2020 Feb 18. doi:10.1016/s2213 2600(20)30076-x.

118. L. Ferrero-Miliani, O H. Nielsen, P.S Andersen, et al. Chronic inflammation: importance of NOD2 and NALP3 in interleukin-1beta generation. Clin Exp Immunol. 2007 Feb; 147(2):227–235. doi:10.1111/j. 1365-2249.2006.03261.x.

119. O. Takeuchi, S. Akira, Innate immunity to virus infection. Immunol Rev. 2009 Jan; 227(1):75–86. doi:10. 1111/j.1600-065X.2008.00737.x.

120. H. Han, Q. Ma, C. Li, R. Liu, L. Zhao, W. Wang, P. Zhang, X. Liu, G. Gao, F. Liu, Y. Jiang, X. Cheng, C. Z. & Y. Xia, Profiling serum cytokines in COVID-19 patients reveals IL-6 and IL-10 are disease severity Predictors, Emerging Microbes & Infections , 2020, 9 ; 1123-1130.

121. R. Henderson, R. J. Edwards, K. Mansouri, K. Janowska, V. Stalls, S. M. C. Gobeil, M. Kopp, D. Li, R. Parks, A. L. Hsu, M. J. Borgnia, B. F. Haynes and P. Acharya, Nat. Struct. Mol.

Biol., 2020, 27, 925–933, DOI: 10.1038/s41594-020-0479-4.

122. M. Hoffmann, H. Kleine-Weber, S. Schroeder, N. Krüger, T. Herrler, S. Erichsen, T. S. Schiergens, G. Herrler, N. H. Wu, A. Nitsche, M. A. Müller, C. Drosten and S. Pöhlmann, Cell, 2020, 181, 271–280.e8.

123. T. Noy-Porat, E. Makdasi, R. Alcalay, A. Mechaly, Y. Levy, A. Bercovich-Kinori, A. Zauberman, H. Tamir, Y. Yahalom- Ronen, M. Israeli, E. Epstein, H. Achdout, S. Melamed, T. Chitlaru, S. Weiss, E. Peretz, O. Rosen, N. Paran, S. Yitzhaki, S. C. Shapira, T. Israely, O. Mazor and R. Rosenfeld, Nat. Commun., 2020, 11, 1–7.

124. S. Pomplun, Targeting the SARS-CoV-2-spike protein: from antibodies to miniproteins and peptides, RSC Med. Chem., 2021, 12, 197–202.

125. S. Tran, P.-J. DeGiovanni, B. Piel and P. Rai, Clin. Transl. Med., 2017, 6, 44.

126. J. Tang, R. Zhang, M. Guo, L. Shao, Y. Liu, Y. Zhao, S. Zhang, Y. Wu and C. Chen, Biomaterials, 2018, 167,205–215.

127. S. Tohme, R. L. Simmons and A. Tsung, Cancer Res., 2017,77, 1548–1552.

128. H. H. Chen and M. T. Kuo, Oncotarget, 2017, 8, 62742.

129. R. Sun, R. Zhai, C. Ma, W. Miao, Combination of Aloin and Metformin Enhances Antitumor Effects by Inhibiting Growth and Invasion and Inducing Apoptosis and Autophagy in Hepatocellular Carcinoma via the PI3K/AKT/mTORPathway, Cancer Medicine. 2020; 9:1141-1151.

130. N. Taura, et al., Relationship of a-fetoprotein levels and development of hepatocellular carcinoma in hepatitis C patients with liver cirrhosis, Exp. Ther. Med., 2012, 4(6), 972–976.

131. J. Liu, H. Bao, H. Wang, Q. Luo, J. Zuo, Z. Liu, S. Qiu, X. Sun, and X. Liu, Synthesis of xanthone derivatives and antihepatocellular carcinoma potency evaluation: induced apoptosis, RSC Adv., 2019, 9; 40781–40791

132. R. S. Riley, C. H. June, R. Langer and M. J. Mitchell, Nat. Rev. Drug Discovery, 2019, 18, 175–196.

133. A. Watermann and J. Brieger, Nanomaterials, 2017, 7, 189.

134. K. J. McHugh, L. Jing, A. M. Behrens, S. Jayawardena, W. Tang, M. Gao, R. Langer and A. Jaklenec, Adv. Mater.,2018, 30, 1706356.

135. A. Sharma, A. K. Goyal and G. Rath, J. Drug Targeting, 2018, 26, 617–632.

136. S. Palazzolo, S. Bayda, M. Hadla, I. Caligiuri, G. Corona, G. Toffoli and F. Rizzolio, Curr. Med. Chem., 2018, 25, 4224–4268.

137. L. Belfiore, D. N. Saunders, M. Ranson, K. J. Thurecht, G. Storm and K. L. Vine, J. Controlled Release, 2018, 277, 1–13.

138 F. Oroojalian, M. Babaei, S. M. Taghdisi, K. Abnous, M. Ramezani and M. Alibolandi, J. Controlled Release,2018, 288, 45–61.

139. L. Palmerston Mendes, J. Pan and V. P. Torchilin, Molecules, 2017, 22, 1401.

140. L. He, Y. Liu, J. Lau, W. Fan, Q. Li, C. Zhang, P. Huang and X. Chen, Nanomedicine, 2019, 14, 1343–1365.

141. M. Falsafi, A. Sh. Saljooghi, K. Abnous, S. M. Taghdisi, M. Ramezani, M. Alibolandi, Smart metal organic frameworks: focus on cancer treatment, Biomater. Sci., 2021, 9, 1503–1529.

CHAPTER 2

Statement of the problem

From the ancient ages herbs are used for their medicinal values to cure diseases. At present, herbal medicines are gaining popularity because of their less side effect compared to chemical drugs [1,2] and low price. Phytochemicals present in herbal drugs are found to be highly effective in controlling different diseases like bacterial, viral infections or even cancer.

Sustained released drugs in our body fluid can maintain a constant level of medicine in our body for a long period of time. This helps to reduce the dosing frequency and improves patient's compliance.

In this thesis, two herbs *Aloe vera* and garlic (*Allium sativum*) are chosen because of their high medicinal values and ease of availability. [3,4] Phytochemicals present in these herbs are found to be very effective in controlling different bacterial, viral and neoplastic disease.[5]

To get sustain release of the above mentioned drugs, two types of porous substrates – silica nanoparticles and nano clay are synthesized and modified. The herb extracts are released in two media – SBF & SGF to estimate the efficacy of the herbs in controlling the diseases.

The objective of this research work is-

1. To synthesize silica nanoparticles with different morphology (irregular and sphere shaped) and nano clay as porous substrate to encapsulate herbal extract and release then in SBF & SGF.
2. To characterize the nanocarriers with XRD, BET, FESEM and TEM to confirm the phases, estimate the area of the porous substrate and to observe the morphology of the substrate.
3. To extract the herbs and entrap the herbal extracts with in the nanocarriers.
4. To confirm the presence of herbal phytochemicals in the carrier.
5. To study the release kinetics of their herbal extracts from silica nanocarriers and nanoclay in both SBF & SGF medium.
6. Optimization of the process parameters for the synthesis of silica nano carriers based of the cumulative release of both the drugs in SBF and GIF.

7. Finally, in the application part, the efficacy of sustained released herbal extracts of Aloevera and garlic (Allium sativum) are studied for the treatment of typhoid (bacterial disease), Covid-19 (viral disease) and liver cancer (neoplastic disease).

References:

1.B.B. Aggarwal, H. Ichikawa, P. Garodia, P. Weerasinghe, G.G. Sethi, D.I. Bhatt, K.M. Pandey, S. Shishodia, G.M. Nair, From traditional Ayurvedic medicine to modern medicine: identification of therapeutic targets for suppression of inflammation and cancer, Expert Opin. Ther.Targets., 2006; 10(1): 87-118.

2. N.H.M. Yunos, H. Hamdan, L.S. Ling, Piperine Loaded Silica Xerogel as NANO-Enabled Drug Delivery system,World applied Sciences Journal 9 (Special Issue of Nanotechnology)., 2010; 06-16.

3. M. Lee , J. Liao, W. Huang , F.Jiang , Y. Jheng , Y. Jin , Ya-Shih Tseng, Aloin-induced cell growth arrest, cell apoptosis, and autophagy in human non-small cell lung cancer cells, Biomarkers and Genomic Medicine. 2014; 6: 144-149.

4.76. A. Stoll and E. Seebeck, Alliin, the pure mother substance of garlic oil, Experentia., 1947; 3: 114–115.

5. M. Umadevi, K.P. Sampath Kumar, D. Bhowmik, S. Duraivel, Traditionally Used Anticancer Herbs In India, Journal of Medicinal Plants Studies., 2013; 1(3): 56-74.

CHAPTER 3

Methodology

3.1 Introduction:

In the present research work two different nanostructured drug carriers are used. One of them is silica nanoparticles and another one is nanoclay. By changing the catalysts (acid or base catalyst) of the sol gel process and the ratio of water, alcohol and TEOS, silica nanoparticles of different morphology with different porosity are synthesized. Alluminosilicate clay is modified with Na to make it suitable for drug encapsulation and drug release study. Selected herbal drugs are encapsulated within nanocarriers during chemical synthesis of carriers. Drugs are chosen based upon their effectiveness and availability to our continent. Selected drugs are *Aloevera* and *Allium sativum* or garlic. Aloin and Diallyl disulphide (DADS) are the most active and stable compounds of *Aloevera* and *Allium sativum* respectively. Here another important subject is sustained release behavior study of drugs. Encapsulated drugs are released in different pH medium namely simulated body fluid (SBF) and simulated gastric fluid (SGF) for different selected time period. Released drugs as samples are analyzed through UV- Vis spectrophotometer and the data is recorded. The release behavior study is done through kinetic modeling using the spectrophotometric datas. Released drugs are subjected for the applications such as antimicrobial assay, antiviral andanticancer assay. For antimicrobial activity *Salmonella typhi* bacteria, for antiviral study deltaSARS‑CoV‑2 Spike proteinand for anticancer activity HepG2 cell line of hepatocellular carcinomaare chosen and execute all the applications successfully.

This chapter describes the overall methodology to fulfill above mentioned objectives.

The schematic presentation of overall process is as follows:
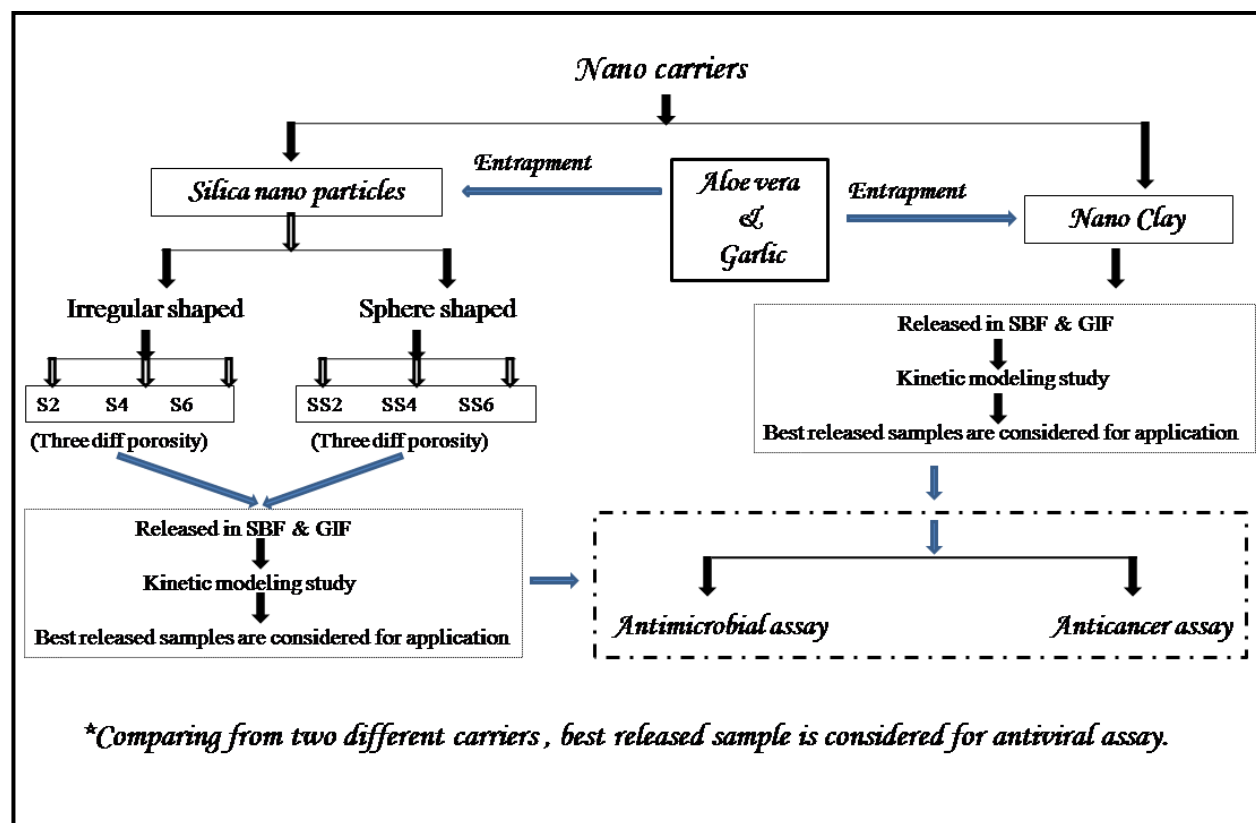
Fig 3.1: Flowchart of overall project work

3.2 Synthesis of nano carriers:

> **Synthesis of silica nano carriers:**

Mesoporous silica particles are synthesized through a very traditional, well-established Stober method by the sol gel process. In this process tetraethyl orthosilicate (TEOS) is used as analkoxide precursor, Ethyl alcohol (EtOH) as co-solvent, hydrochloric acid (HCl) as the acid catalyst, ammonia solution (NH$_4$OH) as a basic catalyst, cetyltrimethylammonium bromide (CTAB) as surfactant and de-ionized water. The chemical reactions are mainly hydrolysis which

can be either base or acid catalyzed and condensation which formsthree dimensionalnetworkwith siloxane (Si-O-Si) bonds.

Two different types of mesoporous silica are synthesized using acid and base catalysts. Acid catalyzed silica particles are irregularly shaped and base catalyzed silica particles when CTAB is added are sphere shaped. By altering the chemical ratio different pore containing materials are also synthesized.

> **Nanoclay:**

Clay is purchased from himedia lab. This clay is modified with Na, and used as a carrier for drug delivery.

3.3 Characterization of synthesized and modified nanocarriers:

Synthesized silica nanoparticles and modified nanoclay are characterized through different characterization tools.

Surface properties (surface area, pore diameter, pore volume) of the synthesized silica& clay nanoparticles are examined through N_2 adsorption desorption isotherm at 77.350 K on a mechanical pore diameter, surface area analyzer (Quantachrome Novawin, version 11.03). Surface area is measured through BET (Brunauer- Emmett- Teller) analysis method. Before experiment, the samples are degassed under a vacuum at 100 ˚C for 2 hours. Particle size, morphology, and porous nature of silica & clay particles are analysed by Scanning electron microscope (SEM, ZEISS), field-emission scanning electron microscopy (FESEM, ZEISS) equipped with an energy-dispersive X-ray spectrometer (EDX) and transmission electron microscope (TEM, JEOL-2010) Before analysis, the samples are coated with platinum for 120 s using an automatic magnetron sputter coater (Auto sputter coater) in case of SEM & FESEM.

X-ray diffraction (XRD) patterns are analyzed with Rigaku, Ultima IV, Japan. The phases of the silica and clay nanocarrier samples are analyzed through this.

Fourier transform infrared spectra (FTIR Schimadzu, Model: prestige 22) of the silica and clay with and without encapsulated drug are obtainedin the range 4000–400 cm^{-1}. FTIR study helps to confirm the encapsulation of drugs in the nanomaterial.

3.4 Selection of herbs:

Herbs are medicinal plants that have therapeutic agents (also called phytomedicinals) that can be used for controlling different diseases. These herbs can be administered as the whole plant or plant parts or as plant extraction in solvents. [1]

Aloe vera: Aloin is ananthraquinone compound extracted from aloe, which has the physiological functions of diarrhea, depigmentation, tyrosinase inhibition, free radical scavenging, and antibacterial activity.[2] Aloin is also a natural organic compound, which has anti-inflammatory, bactericidal, antiviral, and other effects.[3] Aloin is the main antibacterial active componentof aloe [4] and can inhibit the growth of several fungi and bacteria.[5] The crude extractof aloe is different from general antibiotics. It can not only effectively inhibit microbialproliferation but also effectively kill resistant bacteria induced by antibiotics. [6]

Allium sativum: *Allium sativum* (garlic) has curative properties because of someorganosulfurcompounds, which are responsible for the typical odor and flavor of garlic.[7] The antibacterial activity of garlic is mainly attributed to thiosulfinates (e.g.,allicin).[7] Allicin mainly interrupts RNA synthesis and lipid production in a bacterial systems. If RNA production is not carried out properly or produced in less amount then protein synthesis will be severely affected. If proteins are not produced in adequate quantity then growth and development of the organism will not occur as they are essential for all parts of cell structure. Besides this, synthesis of other biomolecules is also partially inhibited e.g., DNA and protein, though RNA is the main target of allicin action. [8] Diallyl disulphide is one of the stable compounds derived from allicin which is extremely active in antibacterial and anticancer activity. This compound is also used to enhance immunologically active cells in our body which further can protect our body from other infections.

Extraction of herbs:

Extraction of phytochemicals from selected herbs *Aloe vera* and garlic, ethanol is used as extracting solvent. At first, the herbs are immersed in ethanol and then ground with a morter pesters followed by filtration with Whatman filter paper 4. Collect the supernatant and store it at -20˚ C for further analysis.

Entrapment of herbs within nanocarriers:

➢ Entrapment of herbs within silica nanocarrier: Entrapment of herbs within silica nanocarriers is done through in situ process to maintain the homogeneity of a drug within the carriers. Herbs are entrapped within the carriers through different hydrogen bonding. There is no chemical bonding formed between the phytochemicals (an actual active component of herb) and carriers. That is why pH changes can release the phytochemicals from the carriers.

➢ Entrapment of herbs within nanoclay: Herbs are entrapped within nano clay through three different processes– grinding, melting & dispersion.
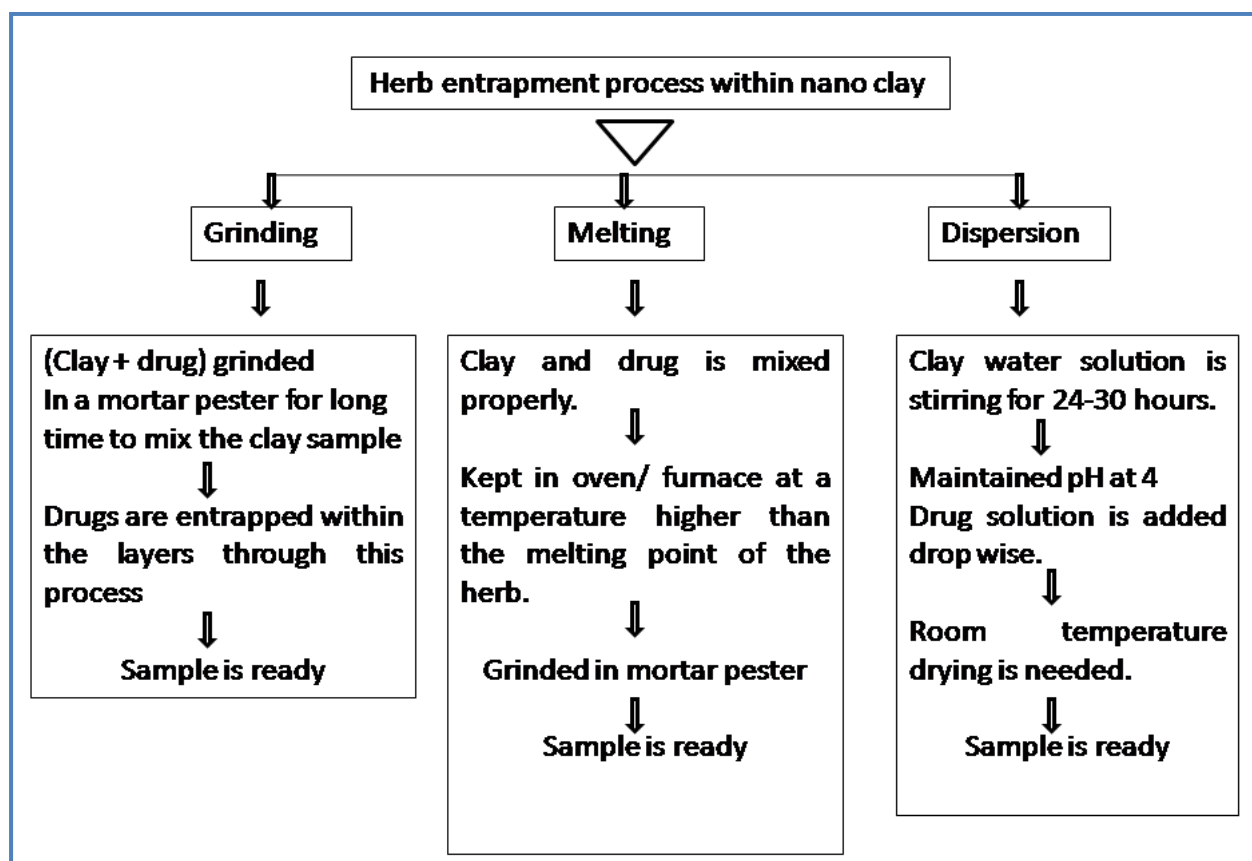
Fig 3.2: The schematic representation of the drug entrapment processes within nanoclay carrier.

➢ Characterization: X-ray diffraction (XRD) patterns were analyzed with Rigaku, Ultima IV, Japan. The phases of the silica and clay samples with herbal values entrapped drugs are analyzed. Fourier transform infrared spectra (FTIR Schimadzu, Model: prestige 22) of the silica and clay with an encapsulated drug was obtained in the range 4000–400 cm-1 to identify the presence of drugs within the nanocarriers.

3.5 Release of drug and kinetics study:

➢ In the case of in vivo drug delivery, the drug is exposed to different body fluids containing different pH. For example; orally given drugs are exposed to stomach juice of acidic pH. If there is intravenously applied drugs are present, they are exposed to the blood which is slightly basic. Here in vitro, drug release study is mimicked at 37° C in two different mediums namely simulated body fluid (SBF; pH -7.4) which is nothing but the ionic solution of different acidic and basic salts, close to the human blood plasma and simulated gastrointestinal fluid (SGF; pH-1.2) is simply 0.1(N) HCl to observe the release behavior of the drug as well as how the drug is released from their respective matrix. Drug-loaded silica-based matrixes are immersed within both SBF and SGF solutions for drug release. For both burst and sustained release, each time 3 ml aliquot is taken from the beaker at the predetermined time intervals and the same amount of fresh fluid is poured into the respective beaker to maintain the volume as well as concentration. The predetermined time means for burst release 0 - 6 hours' time duration is studied where the sample is taken at 15 mins time interval upto 1 hour like 15 mins, 30 mins, 45 mins and 1 hour, then the sample is taken at 30 mins time interval from1 to 6 hours like 1.30 hours, 2 hours, 2.5 hours etc. In the case of sustained released samples aliquots are taken at 24 hours upto 168 hours like 24 hours, 48 hours, 96 hours, and so on. The collected samples are analyzed through UV-Vis spectrophotometer at selected $\lambda_{max.}$The concentrations of collected samples are determined from the calibration curve of each drug which is already plotted with known drug concentration through UV-Vis spectrophotometer. The in vitro dissolution data obtained from UV-Vis spectrophotometer is used to study liquid liquid kinetic modeling.

➤ Characterization: At the required time interval released herbs (*Aloe vera* and garlic) from silica matrix and clay samples were collected and analysed by UV −Vis spectroscopy (Perkin Elmer, Lambda 35 UV-VIS spectrophotometer).

3.6 Applications of released drugs:

➤ **Antimicrobial study:** Antimicrobial study is performed through several well-established processes like minimum inhibitory concentration study (MIC), zone of inhibition (ZOI), Colony forming unit (CFU) study, and growth curve analysis study.

According to the Clinical Laboratory Standards Institute (CLSI) guidelines agar well diffusion method is applied to test the antimicrobial activity of any drug. Drug silica conjugate is introduced into SBF and SGF solution and sonicated for 1-2 hours in order to release the drug from the matrix. After that, the solutions are centrifuged and the supernatant is used as a drug sample in agar plates, which is already, contained *S. typhi* microorganism. The agar plates are then incubated at 37 ˚C overnight. After incubation, the zone of inhibition is measured and documented. All the experiments are done three times.

➤ **MIC study:**Minimum inhibitory concentration of any antimicrobial means the lowest concentration of it that can inhibit the visible growth of bacteria. This is inversely proportional to the growth of thebacteria. Microbial growth or the presence of living microbes could be examined through an optical densitymeasurement. 96 ELISA flat-bottomed plates are considered to do the experiment.

Antimicrobial assay (MIC) is done in the Micronaut system (Merlin, Germany), and data is collected through Multiskan EX (Thermo, Finland) spectrophotometer system.

➤ **ZOI study:**The Zone of inhibition study is the same as the disk diffusion method. A disk of any antimicrobial is placed on the top of the nutrient agar plate which is already inoculated with microorganisms. After 24 hours of incubation, a zone is observed over the disk where no growth of microorganism is seen. This circle is measured and considered the zone of inhibition. After getting the MIC value of any antimicrobial over a specific microorganism, the ZOI study is done with four different concentrations such as MIC, ½ MIC, 2MIC, and 4MIC.

- **CFU study:** The colony-forming unit is one of the estimation processes of viable cells of microorganisms which are competent to binary fission for multiplication. This study is done on a nutrient agar plate under controlled conditions with 24 hours of incubation. After getting the MIC value of any antimicrobial over a specific microorganism, the CFU count is done with four different concentrations such as MIC, ½ MIC, 2MIC and 4MIC.

3.6.2Anticaner study: Hepatocellular carcinoma (HepG2) cell lines were maintained at laboratories. The cell culture medium was Dulbecco's modified Eagle's medium supplemented with 10% fetal bovine serum, 100 IU/mL penicillin and 100 μg/mL streptomycin. The cells were cultured at 37ºC under a humidified atmosphere containing 5% CO_2. [9] Here, different in vitro studies are done to observe the effectivity of selected drugs over the cell line. MTT assay analysis is based on the spectrophotometric method and MB staining assay analysis is based on the microscopic method.

- **MTT assay:** At first cancer cells are plated into 12 well tissue culture plates with required nutrients for proper growth and incubated for 24 hours for attachment. After 72 hours of incubation with the drug the well plates are examined through a microscope and active cells are treated with 3-(4,5-dimethylthiazol-2-yl)-2,5 diphenyltetrazolium bromide (MTT) reagent. Nutrient media and drug mixture is kept as negative control and live cancer cell is kept as positive control.

- **Methylene blue staining assay:** This assay is done for direct, automated cell counting methods for grown cells within any culture plates over other traditional methods. This is applicable to any phytochemicals, natural products, bioactive molecules etc. Cancer cells are seeded and allowed for 24 hours of incubation with drugs. After incubation cells are fixed with formal saline followed by staining with methylene blue for 30 minutes. PBS wash is done after 30 minutes of staining. Microscopic analysis is done before and after PBS wash for cell viability study. 24 hours incubated cell culture plate is considered a control.

3.6.3 Antiviral study: A virus always attacks susceptibleprokaryotic or eukaryotic tissues and controls their DNA during their lifecycle. For the last 1-2 years SARS-CoV-2 creates a pandemic situation and claimed million people's lives worldwide. For any viral propagation egg models are preferable and established. Generally 13-14 day embryonated chicken eggs are used as the host system. Here, the efficacy of the selected drugs on Delta SARS-CoV-2 spike RBD protein is analyzed in embryonated chicken eggs. The process is as follows-egg candling, preparation of viral inoculum, virus inoculation, incubation of eggs and harvesting. [10]

- ➤ **Egg inoculation and candling:** 13th-day-old pathogen-free fertilized chicken eggs are collected from Government StatePoultry Farm, Kolkata, India. Upon arrival, the surface of the eggs is cleansed with water and sterilized with 70% ethanol, 3.5 % iodine, and 1.5% sodium iodide to reduce the risk of contamination.After sterilization, all eggs are candled and incubated in 60-70% humidity at room temperature and rotated three times a day. A tiny hole was drilled in the shell of each egg on the sterilized air space carefully.

- ➤ **Virus inoculums preparation:** 100 μg Delta SARS-CoV- 2 spike protein RBD antigen was dissolved in 10 ml phosphate buffer saline (PBS). Pipetting was done to dissolve it properly and make a homogeneous mixture.

- ➤ **Virus inoculation and incubation:** On next the day the eggs are divided into a set of three according to the sample's name and marked with a marker. To each set of eggs, 100 μl of samples (drugs) are injected with a sterilized needle through the tiny whole except the control. During inoculation, needle should insert carefully to avoid any fracture of the inner embryo. Then seal the hole with glue or a paper sticker. Then all the injected eggs were incubated at 38° C at almost 70% humidity for 48 hours.

- ➤ **Egg harvesting:** The harvesting procedure of eggs was starting with exposure at 2-8° C for almost 2- 3 hours to kill the embryo. After proper chilling, the egg shells were broken with sterile scissors and forceps very carefully. Disrupt the chorioallantoic membrane, tilt the egg slightly, and collect 5-10 ml of slightly yellowish allantoic fluidswith a pipette and transfer to the respective sterile vial and stored it at -80° C for further experimental analysis.

References:

1. V.H.L. Lee, Controlled Drug Delivery Fundamentals and Applications: Introduction, Marcel Dekker, (2nd ed) INC, New York. 1987; 29.

2. K. Mahajan, S. Kumar, Z. Naqvi, T. E. Mungure, A. E.A. Bekhit, Functionalization of carrageenan based edible film using Aloevera for improved lipid oxidative and microbial stability of frozen dairy products. Food Biosci. 2021; 43, 101336.

3. M. A. Lone, D. Malviya, P. Mishra, A. Dubey, R. C. Saxena, Antiinflammatory and antimicrobial activity of anthraquinoneisolated from Aloe vera (Liliaceae). ASIAN J. Chem. 2009; 21, 1807–1811.

4. B. Tian, Y. J. Hua, X. Q. Ma, G. L. Wang, Relationship between antibacterial activity of aloe and its anthaquinone compounds. ZhongguoZhong Yao ZaZhi2003; 28, 1034–1037.

5. A. Oumer, D. Bisrat, A. Mazumder, K. Asres, A new antimicrobial anthrone from the leaf latex of aloe trichosantha. Nat. Prod. Commun. 2014; 9, 949–952.

6. T. Reynolds, A. C. Dweck, Aloevera leaf gel: A review update. J. Ethnopharmacol. 1999; 68, 3–37.

7. J.C. Harris, S.L. Cottrell, S. Plummer, D. Lloyd, Antimicrobial properties of Allium sativum (garlic). ApplMicrobiolBiotechnol. 2001; 57: 282–286.

8. R.S. Feldberg, In vitro mechanism of inhibition of bacterial growth by allicin. Antimicrob. Agent. Chemother. 1988; 32: 1763-1768.

9. D. Chatterjee, B. Singh, A. K. Pradhan, K. Paira and S. Das, Diluted lycopodium induced cell death and clinical improvement in hepatocellular carcinoma, Clinical oncology and research. 2022; 5(3): 2-8.

10. S. Das, D. Chatterjee, K. Paira, P. Goswami , S. Ghosh, D. Chaudhuri, R. Chakravarty, P. Agarwal, S.Bhajanka., Ultra diluted Delta SARS-CoV-2 Spike protein enhances interferon gamma expression and control cytokine milieu. DOI: 10.13140/RG.2.2.11773.08162, 2021; 1-12.

CHAPTER 4

Release kinetic study of Aloevera from SiO$_2$nanocarrier and its application

4.1 Introduction:

In the field of multidisciplinary science, nanotechnology investigates the invention and use of structures with a dimension of less than 100 nm. [1] Due to their small size, high surface area, and ability to pass through epithelial and endothelial barriers, nanomaterials have been used as carriers for controlled drug release, increasing drug permeability without altering its pharmacological properties. [2] These nanosystems are able to make contact with the action site with significant drug amount, which increases their specific retention time and reduces side effects. [3] Additionally, nanoparticles' tunable morphology, size, surface charges, and pores make them good carriers with low toxicity, excellent biocompatibility and biodegradability, and efficient biodistribution and elimination. Improving diagnosis, decreasing side effects, and increasing drug efficacy all rely on effective drug delivery. Mesoporous silica nanoparticles are thought to be a very promising option for delivering drugs, particularly those that are insoluble in water. These nanoparticles are reservoirs for storing hydrophobic drugs due to their large surface areas and pores. Besides this, their shape and size can be altered to meet specific requirements. [4] Silica nanoparticles are proposed as alternative drug delivery carriers due to their non-toxicity and biocompatibility because they can be broken down into their basic silanol units and removed from the body. [5] There are three steps in the dissolution of amorphous silica in aqueous media: i) hydration, in which water is adsorbed into the framework of siloxane; ii) hydrolysis, in which siloxane is hydrolyzed into silanols; and iii) ion exchange processes, in which nucleophilic attack of OH results in the leaching of silicic acid. In aqueous media, silica hydrolyzes at the molecular level to produce the same nontoxic products as silica nanoparticles. These products diffuse through the blood or lymphatic system and are eventually eliminated in the urine. [6]

In this chapter SiO_2 nanocarriers are synthesized by the sol-gel method and characterized. The active component of *Aloe vera* is Aloin, entrapped in the nanocarrier and a detail kinetic study of the release of aloin in SBF & SGF is carried out. The efficacy of released aloin as an antibacterial, antiviral, anticancer treatment is also evaluated.

4.2 Methodology:

The sol-gel process involves the manufacture of inorganic matrices through the formation of acolloidal suspension (sol) and the gelation of the sol to form a wet gel, which, after spontaneous drying, forms a dry gel known as xerogel. In this process, water and metallic alkoxysilanes are used, such as tetraethoxysilane (TEOS). TEOS is used as a silica precursor. TEOS hydrolyses in water in presence of alcohol forming silicon hydroxide. The hydrolysis reaction which could be acid or base catalyzed, replaces alkoxide groups by hydroxyl groups.

Hydrolysis reaction $\equiv$ Si-OR + H$_2$O $\rightarrow$ $\equiv$ Si-OH+ ROH

Alcohol condensation $\equiv$ Si-OH + RO-Si$\equiv$ $\rightarrow$ $\equiv$Si-O-Si $\equiv$ + ROH

Water condensation $\equiv$ Si-OH + HO-Si$\equiv$ $\rightarrow$ $\equiv$Si-O-Si$\equiv$ + H2O

In the case of a condensation reaction siloxane bonds are formed.[7]

As mentioned earlier two different types of porous silica nanomaterials using acid and base catalysts are synthesized. The detailed procedure of acid catalyzed irregular shaped silica nanoparticles and base catalyzed sphere-shaped silica nanoparticles is given here.

4.2.1 Synthesis of irregular shaped silica nanoparticles:

First of all TEOS and EtOH are taken in a beaker and put under stirring. In another beaker, EtOH and deionized water are stirred for 10 minutes. The solution of the first beaker is added dropwise to the deionized water solution under continuous stirring for up to 25-30 minutes at room temperature. After complete addition, the entire solution is further stirred for upto 2 hours then kept for gelation and aging followed by oven drying at 70-80˚C. By altering the molar ratio of ethanol three different pores containing irregularshaped silica particles with different porosity are obtained. The entire process is schematically shown in Fig 4.1 and the sample names with the different molar ratios of the precursors are given in table 4.1.
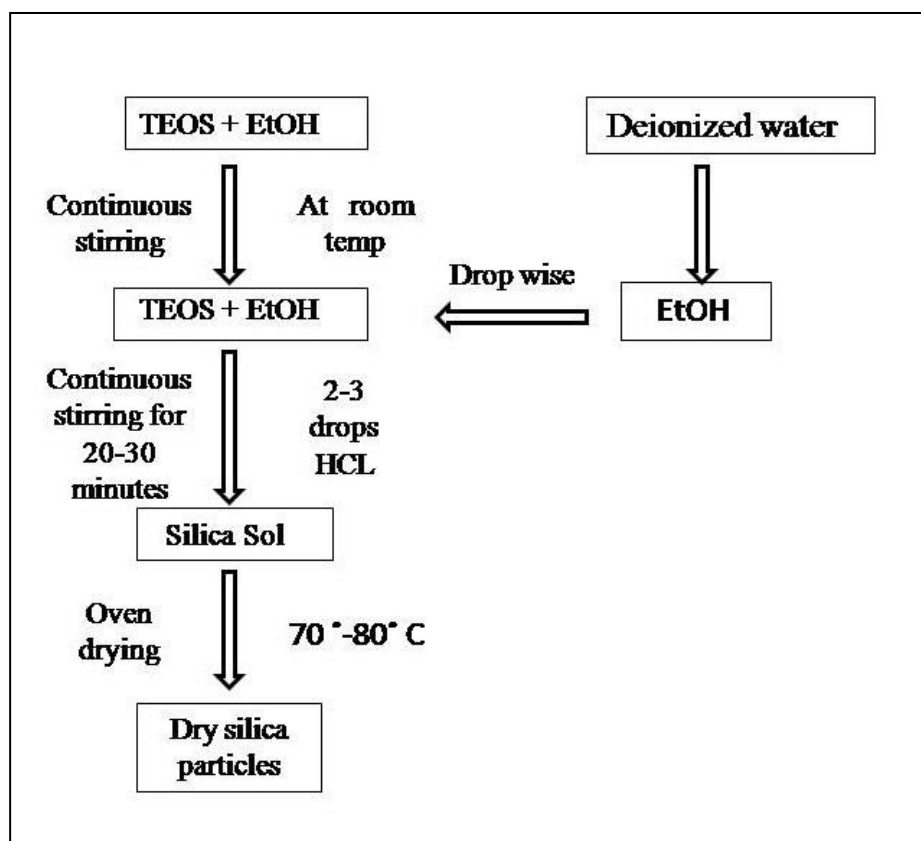
Fig 4.1: Flowchart of synthesis procedure of irregular shaped silica nanoparticles

Table 4.1: Molar ratio of the precursors for different acid catalyzed silica gel samples

Sample no	Sample Name	Raw materials ratio			Catalyst
		TEOS	Ethanol	DI water	
1	S2	11.5	5	1	HCL
2	S4	11.5	10	1	
3	S6	11.5	15	1	

4.2.2 Synthesis of sphere-shaped silica nanoparticles:

For sphere-shaped silica, first, a solution is prepared with EtOH, DI H_2O and NH_4OH with continuous stirring. Then CTAB is added to this solution at stirring condition. AfterwardTEOS is added dropwise to the solution at room temperature under stirring conditions. After some timewhite precipitation occurs. The precipitated material is filtered and washed with deionized water followed by room temperature drying and calcination at 550°C for 4 hours. By changing the ethanol ratio three different spheres are procured having different sizes and pores. The details are shown in flowchart 4.2 and the sample name with different molar ratio is given in table 4.2.
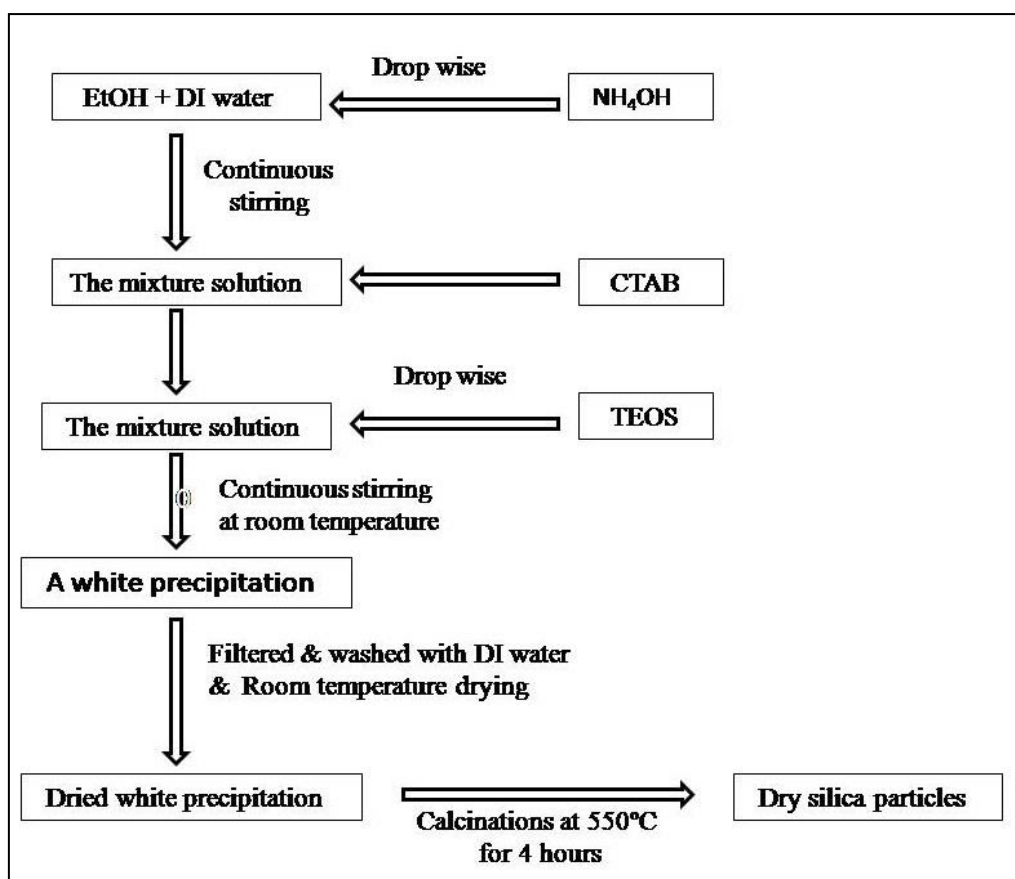
Fig 4.2: Flowchart of synthesis procedure of sphere shaped silica nanoparticles

Table 4.2: Molar ratio of the precursors for different base catalyzed silica gel samples

Sample no	Sample Name	Raw materials ratio			Catalyst
		TEOS	Ethanol	DI water	
1	SS2	11.5	5	1	$NH_4 OH$
2	SS4	11.5	10	1	
3	SS6	11.5	15	1	

4.3 Characterization of synthesized silica nanoparticles:

Synthesized silica nanomaterials are characterized with FTIR, XRD, SEM, and BET characterization tools as discussed in chapter 3 (section : 3.3 characterization).

4.4 Results and discussions:

4.4.1 FTIR analysis: Fig 4.3 & 4.4 represent FTIR spectra of irregular and sphere shaped silica.
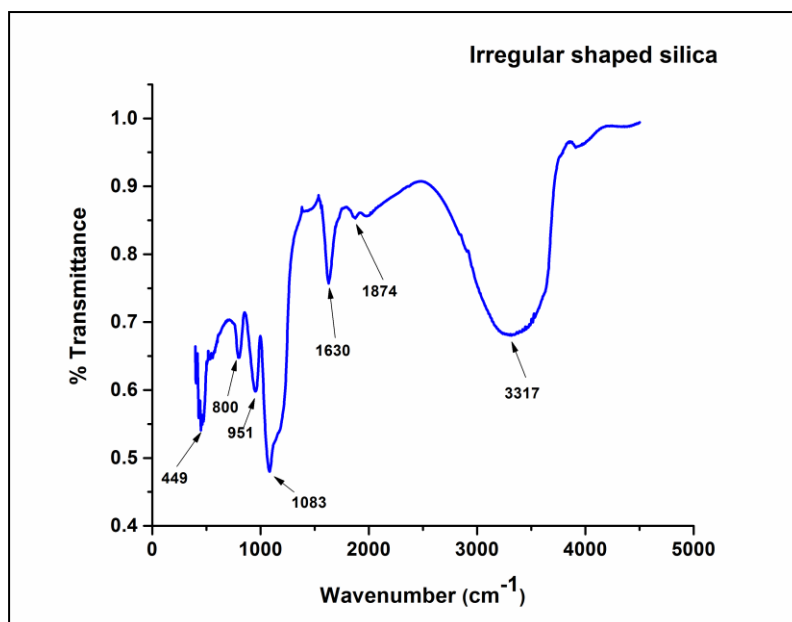
Fig 4.3: FTIR spectrum of irregular shaped silica particles
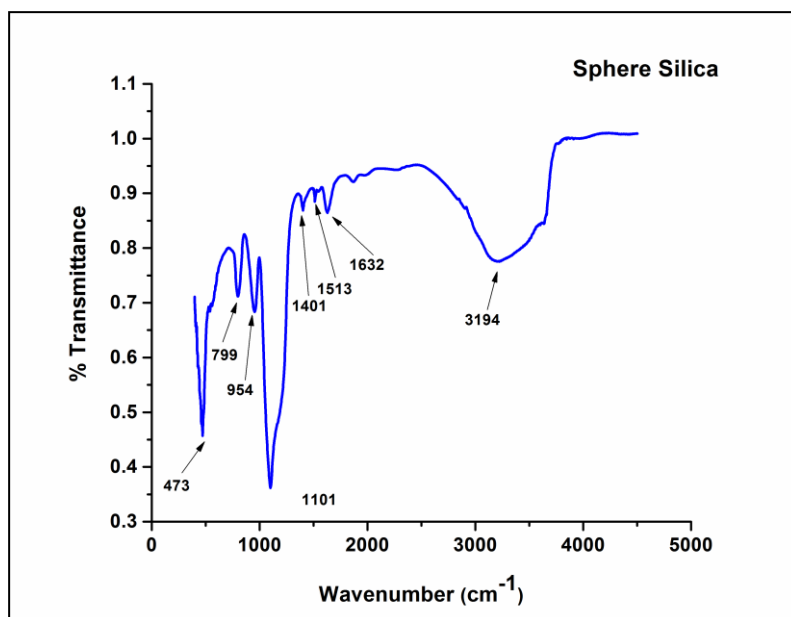
Fig4.4: FTIR spectrum of sphere shaped silica particles

Above Figures represent the FTIR spectra of irregular shaped silica gel and sphere silica gel within the range 400-4000 cm⁻¹. The frequency near 460 cm⁻¹ and 800 cm⁻¹ i.e., 449 cm⁻¹ & 800 cm⁻¹ (for Fig. 4.3) and 473 cm⁻¹ & 799 cm⁻¹ (for Fig. 4.4) are observed for out of plane bending of Si-O-Si bond and the stretching vibration of Si-O bond respectively.[8]

In the 900-1300 cm⁻¹ interval, an almost complete overlap of the Si-alkoxy compounds with the siloxane bands is realized. The presence of a very broad strong peak at 1083 cm⁻¹ can be assigned as the stretching of C-O bond of TEOS and ethanol both (intense in Fig. 4.3). [9]

A strong absorption band between 3300 and 3500 cm⁻¹ assigned to O–H stretching in H-bonded is observed in both clustered and sphere silica for molecularly adsorbed water. Also, this band can be cross-checked through the 1630 cm⁻¹band due to the scissor bending vibration of molecular water. [10]

4.4.2 XRD analysis:

Fig 4.5 & 4.6 are the XRD patterns of irregular silica nanoparticles and spherical silica nanoparticles. In both plots a hump between 15°-30° is observed. This hump indicates the amorphous nature of synthesized silica particles which is nontoxic to the human body and can be chosen as a biocompatible drug carrier.
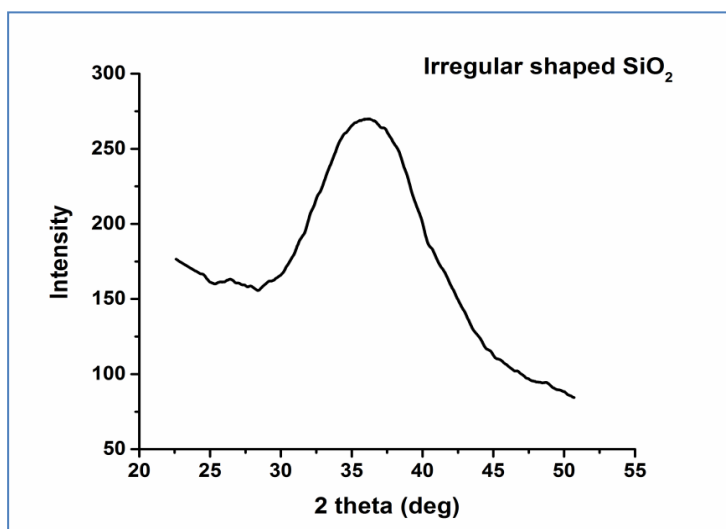
Fig 4.5: XRD graph of irregular shaped silica particles
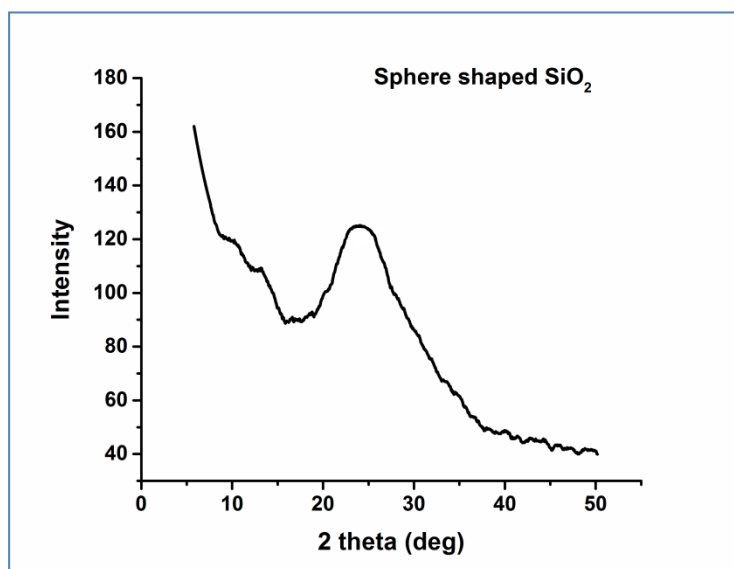
Fig 4.6: XRD graph of sphere shaped silica particles

4.4.3 BET analysis:

It is observed that surface area of SiO_2 nanoparticles increases with increase in alcohol ratio in the acid catalyzed sample. Maximum surface area is available when TEOS: Water: ethyl alcohol is 1: 1: 6 (sample S6). However, in case of base catalyzed silica nanoparticle maximum surface area is achieved when TEOS: Water: ethyl alcohol is 1: 1: 2 i.e. at lowest alcohol content for the sample SS2.   If the surface area of the carrier is increased more drug adsorption is possible and the sample will be better for drug delivery purpose.

Table 4.3: BET data of different samples of synthesized silica particles

Sl no	Sample name		Surface area(m^2/g)
1	Irregular shaped silica	S2	118.850
2		S4	422.700
3		S6	442.600
4	Sphere shaped silica	SS2	540.035
5		SS4	227.214
6		SS6	128.677

4.4.4 Microscopic analysis:

Scanning electron microscopic photograph shows the morphology of the synthesized silica particles. It shows the difference in structures influenced by acid and base catalysts. SEM image (Fig 4.7) is the image of acid catalyst silica that does not give any particular shape but rather some irregular uneven nanoparticles which are mainly clumped together.
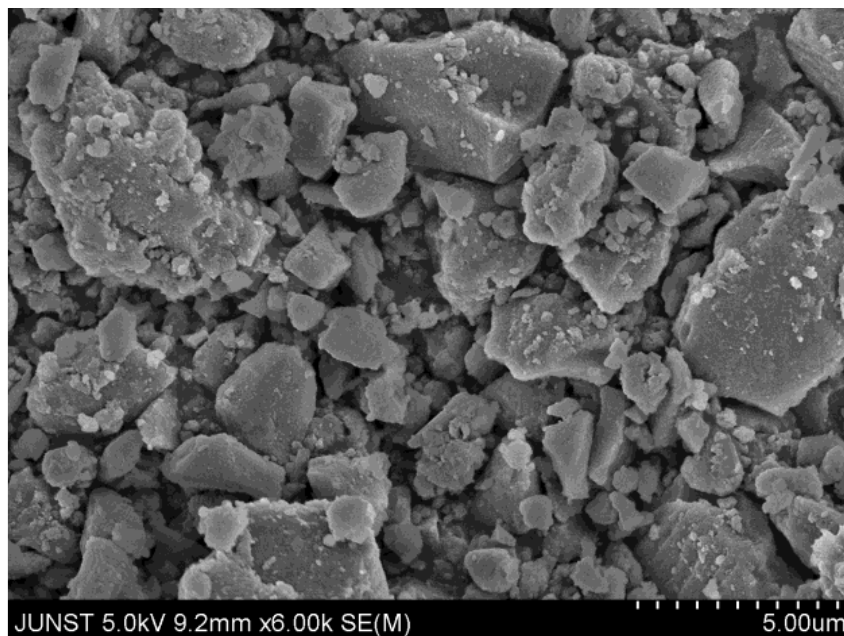
Fig 4.7: Scanning electron microphotograph of irregular shaped silica
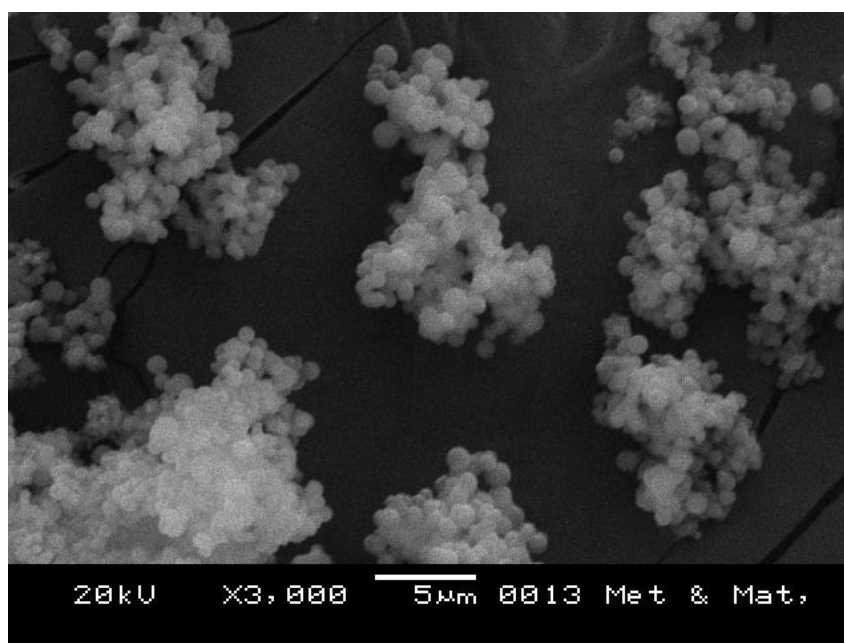
Fig 4.8: Scanning electron microphotograph of sphere shaped silica

The base catalyst gives a spherical shape (Fig 4.8) of silica particlesthat are micron-sized, confirmed by SEM analysis. Fig 4.7 is the SEM image of acid catalysed silica nanoparticles where uneven, irregular shaped silica particles are observed.

To get a more accurate structure of silica nanoparticles highest magnified microscopic analysis is carried out. SEM &FESEM pictures can clearly distinguish the size difference of the three different sphere-shaped silica particles with their actual sizes. However, there are no specific size differences for a different sample observed in irregular shaped silica. Fig 4.10 shows the FESEM images of different sizes of sphere SiO_2 synthesized by sol-gel method with CTAB surfactant. Three sets of sphere samples exhibit smooth external surfaces of each namely SS2, SS4 & SS6 having their average diameter of 25-40 nm (fig 4.10 A, B) 60-75 nm (fig 4.10 C, D) &110- 140 nm (fig 4.10 E, F) respectively. Here, the morphology changes occur due to base catalyst and surfactant CTAB and size changes occur because of ethanol percentage changes. Due to agglomeration of the nano particles in case of irregular shaped silica nano particles, the size difference of the particles with precursor ratio is not clearly visible.
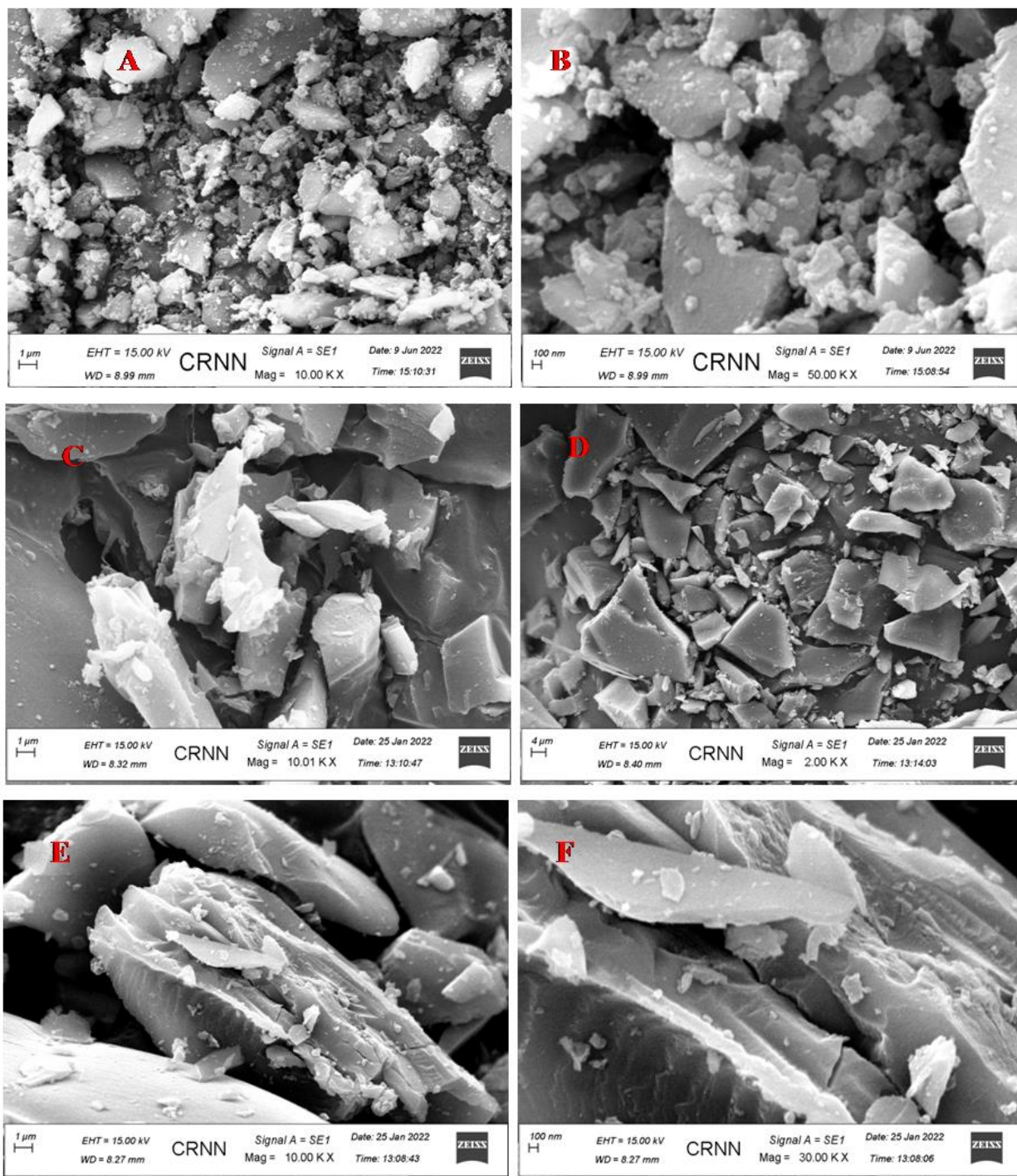
Fig 4.9: Microscopic view of irregular shaped silica nano particles of three different samples S2 (A&B), S4 (C&D, S6 (E&F)
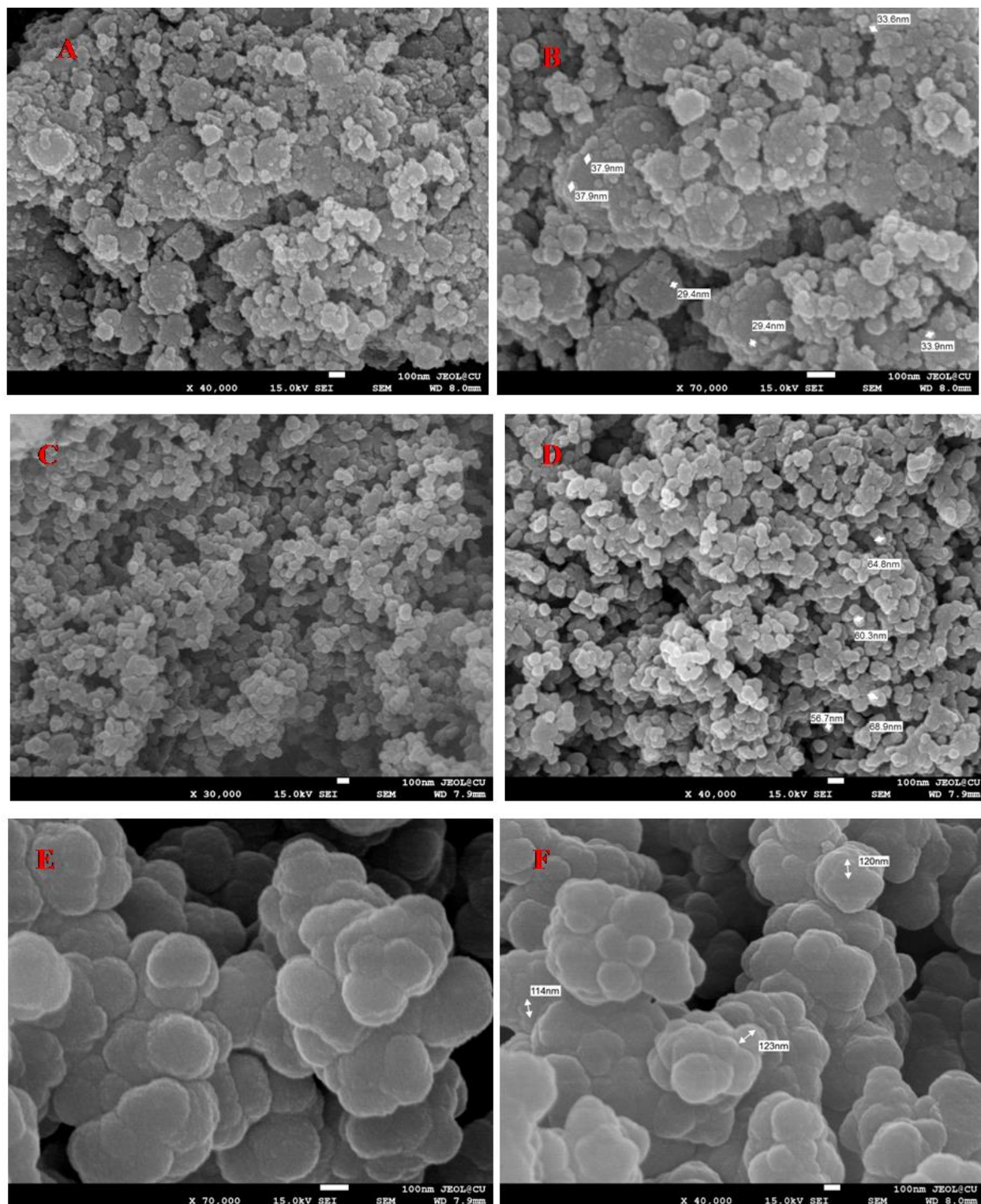
Fig 4.10: Microscopic view of different size containing sphere shaped silica nano particles, SS2 (A&B), SS4 (C&D), SS6 (E&F)

From the above results & discussion it can be inferred that amorphous silica nanoparticles of irregular & spherical morphology are successfully synthesized by sol-gel process and are confirmed by FTIR, XRD, SEM & FESEM.

4.5 Drug loading determination:

Aloin powder (5 mg) is dispersed in 2% methanol solution with continuous stirring where 2 mg silica particles are added and this mixture is stirred for at least 24 hours at 37 ˚C at 250 rpm. The concentration of a drug is calculated through a UV-Vis spectrophotometer at 298 nm. The loading percentage of a drug within any silica matrix or vehicle is determined through this equation (1)

$$\text{Drug loading \% (Actual)} = \frac{Amount\,of\,drug\,in\,nanoparticles}{Amount\,of\,nanoparticles} \times 100 \qquad (1)$$

Drug loading within the delivering carrier is an important parameter to evaluate the therapeutic efficacy of the particular drug delivery because it determines the administered formulation.

Encapsulation efficiency is determined through equation (2)

$$\text{Encapsulation efficiency (\%)} = \frac{Drug\,loading\,\%\,(Actual)}{Drug\,loading\,\%\,(Theoritical)} \times 100 \qquad (2)[11]$$

Table 4.4: Sample name with drug loading and encapsulation efficiency

Sl no	Sample name	Drug loading (%)	Encapsulation efficiency (%)
1	AS2 (Aloin entrapped irregular shaped S2 SiO₂)	0.34	76.63
2	AS4 (Aloin entrapped irregular shaped S4 SiO₂)	0.346	79.89
3	AS6 (Aloin entrapped irregular shaped S6 SiO₂)	0.361	81.58
4	ASS2 (Aloin entrapped sphere shaped SS2 SiO₂)	0.7	92.01
5	ASS4 (Aloin entrapped sphere shaped SS4 SiO₂)	0.55	96.98
6	ASS6 (Aloin entrapped sphere shaped SS6 SiO₂)	0.53	90.53

4.6 Characterization of drug entrapped silica nano particles:

4.6.1 FTIR analysis:
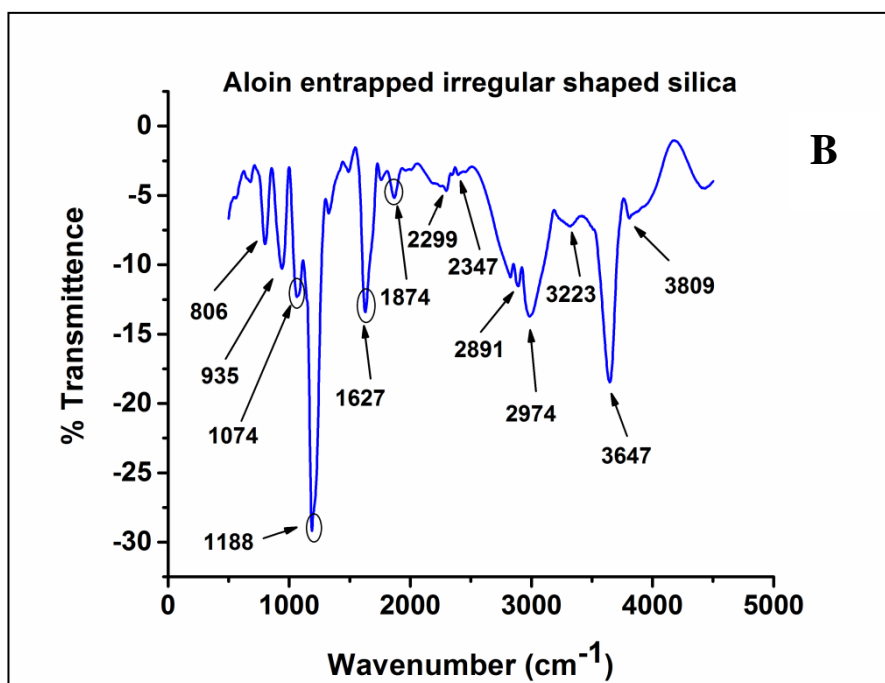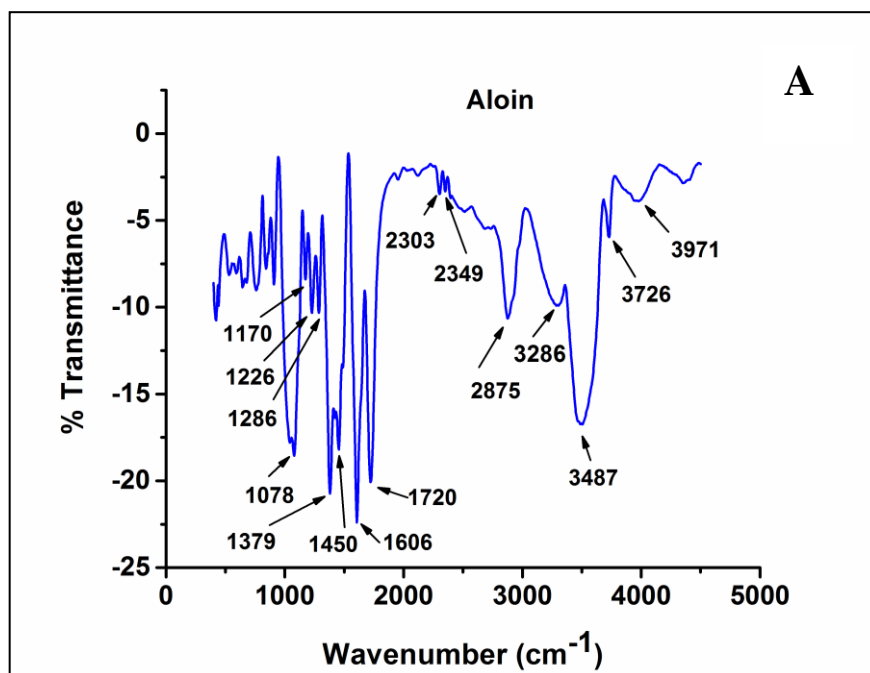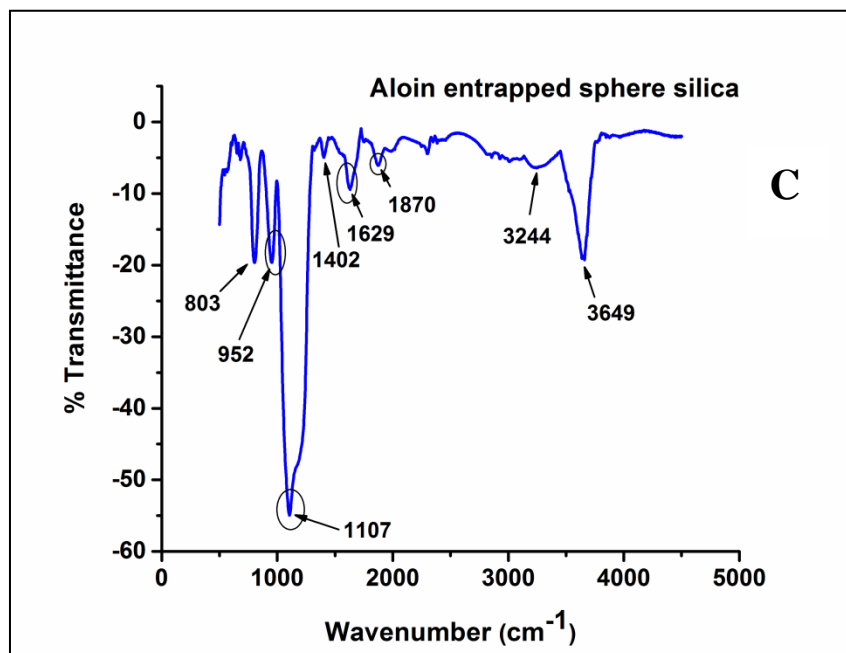
Fig 4.11: FTIR spectra of (A) Aloin and (B) Aloin entrapped irregular shaped silica sphere shaped silica(C)

1050-1250 cm^{-1} stretching is responsible for C-O-C bond which is present both in Fig 4.11A, 4.11B & 4.11C. Aromatic ring stretch frequency is 1600-1680 cm^{-1} for C=C-C.[10] 1606 cm^{-1} is present in pure aloin which is red-shifted to 1627 (4.11B) & 1633 (4.11C) to aloin entrapped silica particles. 1170 cm^{-1} stretching is for C-O bonds observed in 4.11A is red shifted to 1188 cm^{-1} in 4.11B and blue shifted to 1107 cm^{-1} in 4.11C. 1720 cm^{-1} is responsible for aliphatic ketones C=O which is red-shifted to 1753 cm^{-1} in 4.11B graph due to the entrapment of aloin. [12]

4.6.2 XRD analysis:

Samples of silica were subjected to XRD analysis in order to justify whether or not the crystalline phase was present in the drug as well as in the synthesized material.
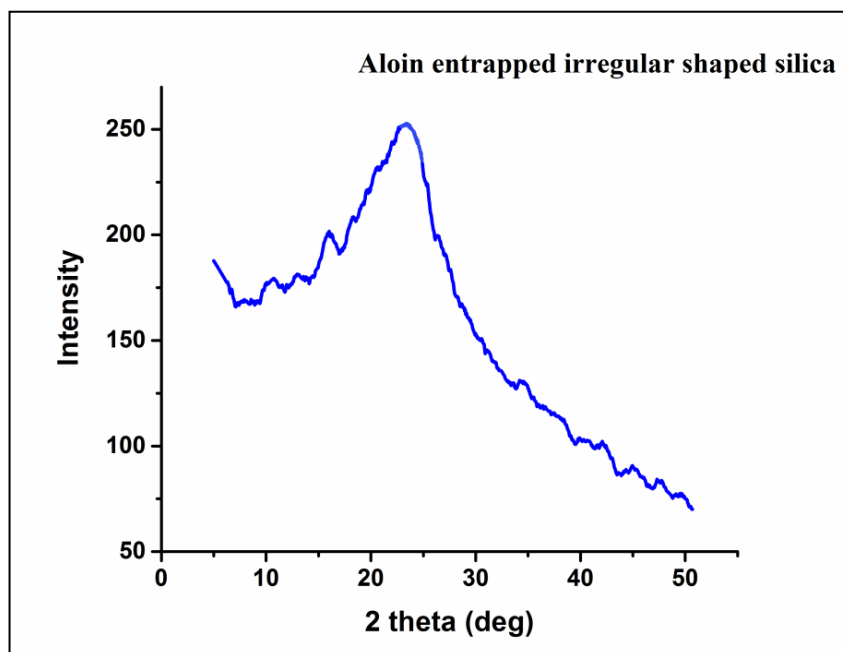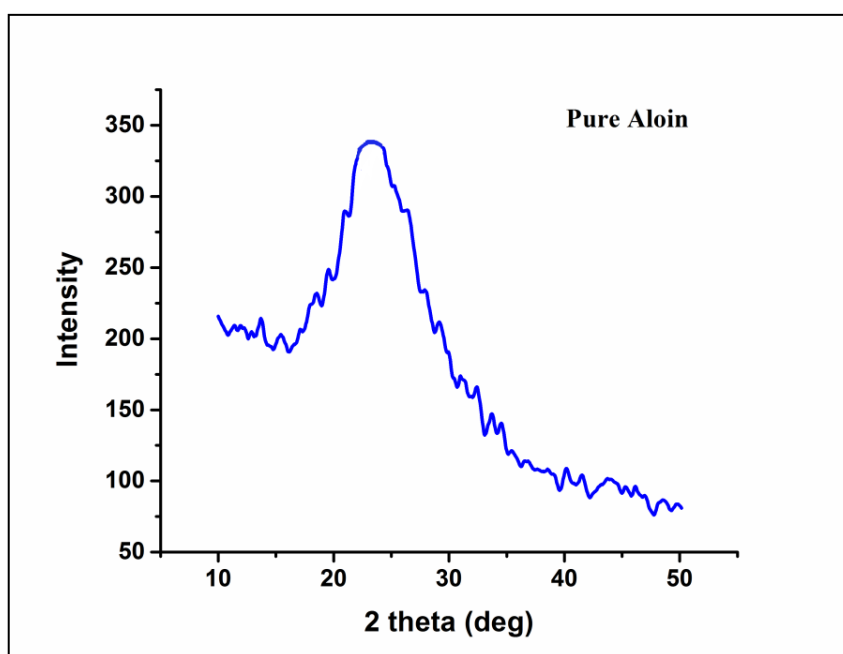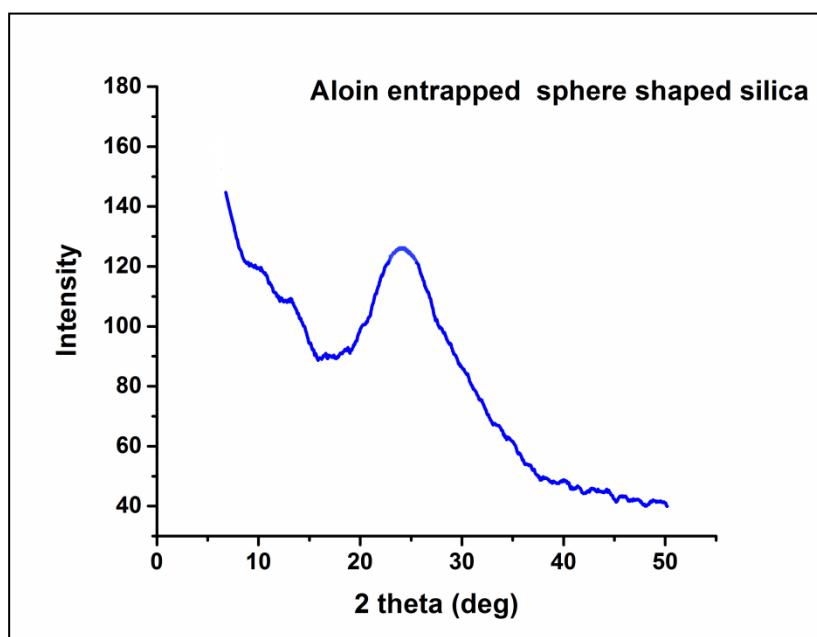
Fig 4.12: XRD analysis of pure (A) Aloin,(B)Aloin entrapped in irregular shapedsilica and (C) aloin entrapped sphere shaped silica

Fig 4.12 represents the XRD analysis of pure aloin and aloin entrapped irregular shaped, sphere shaped silica nanoparticles. All the XRD files show a hump between 15-30 deg which means the amorphous nature of both aloin and aloin entrapped irregular and sphere shaped silica particles. That also means aloin entrapped silica can be easily used as the drug delivery system for humans as amorphous silica is nontoxic and biodegradable.

4.7 Drug release studies of Aloin:

The prepared drug silica Nanoconjugate is immersed in two different release mediums namely SBF and SGF at 37°± 2° C in a BOD shaker at 110 rpm for 168 hours. During the time period a certain amount of medium is withdrawn at predetermined time intervals and immediately replaced with fresh medium. The concentration of aloin released in the medium is measured in UV-Vis spectrophotometer. For each type of drug-loaded silica, the whole experimental process is performed in triplicate.

Table 4.5: Cumulative release of Aloin in SBF & SGF from different irregular shaped silica particles

Sl no	Sample name	% Cumulative Release
1	AS2B (Aloin entrapped S2 silica, released in SBF)	37
2	AS4B (Aloin entrapped S4 silica, released in SBF)	45
3	AS6B(Aloin entrapped S6 silica, released in SBF)	52
4	AS2G (Aloin entrapped S2 silica, released in SGF)	38
5	AS4G (Aloin entrapped S4 silica, released in SGF)	54
6	AS6G (Aloin entrapped S6 silica, released in SGF)	68
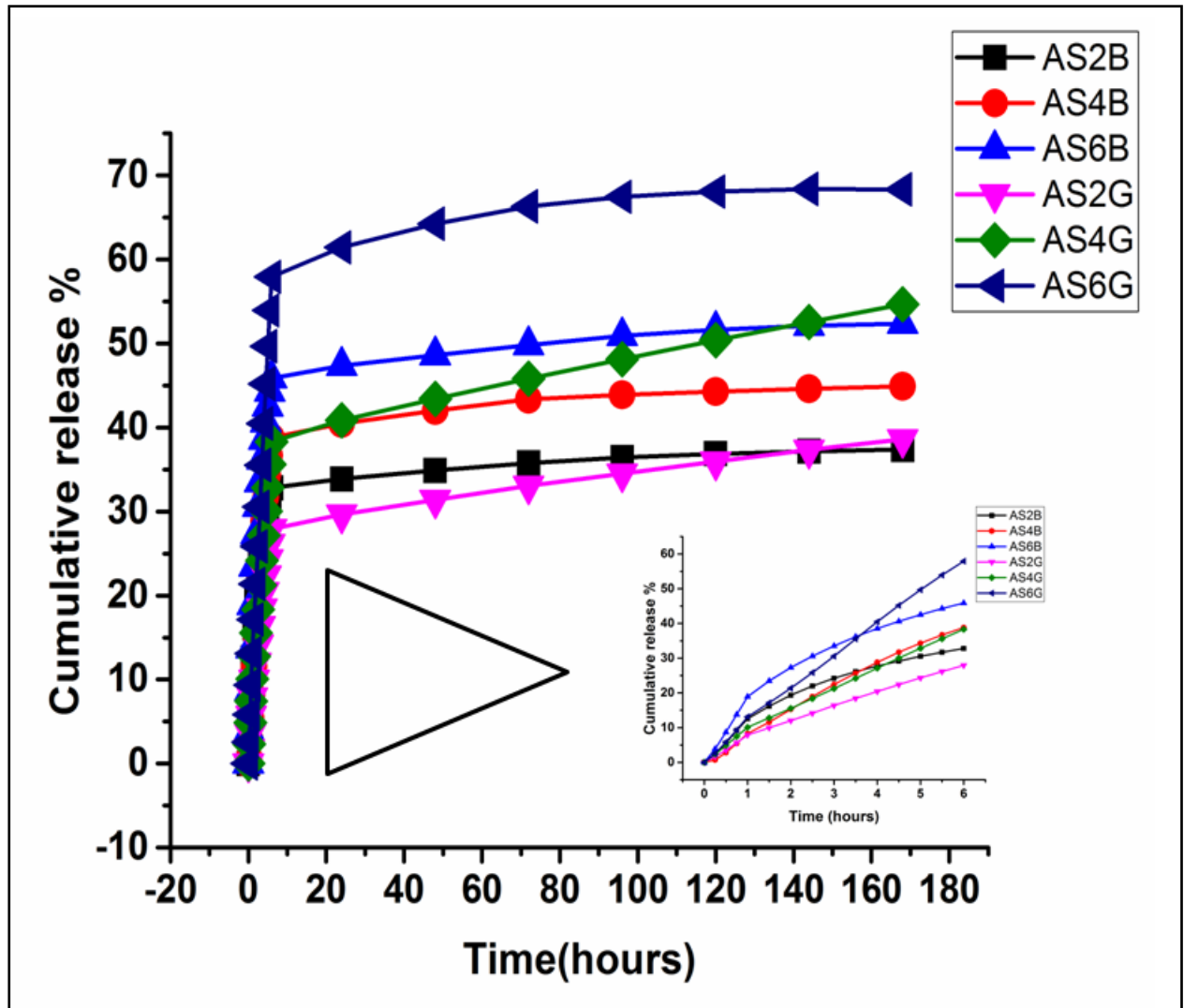
Fig 4.13: Dissolution profile of Aloin in SBF & SGF from irregular shape containing silica nanoparticles

4.8 Release kinetic study of aloin:

In the in vitro dissolution study three different samples (released from 3 different carriers) are examined and the optical values are considered making liquid liquid kinetics specially fitted on Zero order, First order, Higuchi model & Korsmeyerpeppas model. And the 'n' value from the korsmeyerpeppas model is used to find out the drug release mechanism. For the case of cylindrical tablets, $0.45 \leq n$ corresponds to a Fickian diffusion mechanism, $0.45 < n < 0.89$ to non-Fickian transport, $n = 0.89$ to Case II (relaxational) transport, and $n > 0.89$ to super case II transport. [13]

4.8.1 Drug release profile and kinetic behavior study of aloin from irregular shaped silica nanocarriers:

In monolithic (or matrix) dissolution systems release of any drug is always biphasic i.e a drug will be released from the matrix at two different rates or in two different periods of time. It provides an initial burst of drug release which is quickly followed by a constant rate of release comparatively slow over a definite time period. The released amount of aloin is measured through UV Vis spectroscopy at 298 nm wavelength. The rate and mechanism of drug release can be approximated by fitting the dissolution data in different liquid liquid kinetic models. Before that, a calibration curve is drawn with a respective concentration of the drug vs time. Different porosity-containing silica matrixes possess different drug release rates and percentages. Higher surface area containing matrix will release more percentage of drugs than lower surface area containing matrix over the selected time period.

4.8.1.1.A Release kinetic models of Aloin from S2 irregular SiO₂ in SBF for first 6 hours:

Fig 4.14: Kinetic models of Aloin released for first 6 hours from S2 silica in SBF medium

Table 4.6: Kinetic data of Aloin obtained from S2 irregular SiO₂ in SBF medium

Sample Name	Zero order (R^2 value)	First order (R^2 value)	Higuchi model (R^2 value)	Korsmeyer-peppas (R^2 value)	Korsmeyer-peppas n=release exponent
Aloin	BR	BR	BR	BR	BR
S2	0.985	**0.991**	0.979	0.986	1.65

Based on these kinetic models the best fitted model for burst release of aloin in SBF is First Order kinetic model. As the release exponent value is >0.89, the release mechanism is supercase II transport.

4.8.1.1.B Release kinetic models of Aloin from S2 irregular SiO₂ in SBF for 24-168 hours:

Fig 4.15: Kinetic models of Aloin released for 24-168 hours from S2 silica in SBF medium

Table 4.7: Kinetic data of Aloin obtained from S2 irregular SiO₂ in SBF medium

Sample Name	Zero order (R^2 value)	First order (R^2 value)	Higuchi model (R^2 value)	Korsmeyer-peppas (R^2 value)	Korsmeyer-peppas n=release exponent
Aloin	SR	SR	SR	SR	SR
S2	0.920	0.924	0.978	**0.993**	1.91

Based on these kinetic models the best fitted model for burst release of aloin in SBF is koresmeyerpeppas model. As the release exponent value is >0.89, the release mechanism is su8percase II transport.

4.8.1.1.C Release kinetic models of Aloin from S4 irregular SiO₂ in SBF for first 6 hours:

Fig 4.16: Kinetic models of Aloin released for first 6 hours from S4 silica in SBF medium.

Table 4.8: Kinetic data of Aloin obtained from S4 irregular SiO₂ in SBF medium.

Sample Name	Zero order (R^2 value)	First order (R^2 value)	Higuchi model (R^2 value)	Korsmeyer-peppas (R^2 value)	Korsmeyer-peppas n=release exponent
Aloin	BR	BR	BR	BR	BR
S4	0.990	**0.998**	0.961	0.961	1.69

Based on these kinetic models the best fitted model for burst release of aloin in SBF is First Order model. As the release exponent value is >0.89, the release mechanism is supercase II transport.

4.8.1.1.D Release kinetic models of Aloin from S4 irregular SiO₂ in SBF for 24-168 hours:

Fig 4.17: Kinetic models of Aloin released for 24-168 hours from S4 silicain SBF medium

Table 4.9:Kinetic data of Aloin obtained from S4 irregular SiO₂ in SBF medium

Sample Name	Zero order (R^2 value)	First order (R^2 value)	Higuchi model (R^2 value)	Korsmeyer-peppas (R^2 value)	Korsmeyer-peppas n=release exponent
Aloin	SR	SR	SR	SR	SR
S4	0.862	0.869	0.943	**0.986**	2.45

Based on these kinetic models the best fitted model for sustained release of aloin in SBF is koresmeyerpeppas model. As the release exponent value is >0.89, the release mechanism is supercase II transport.

4.8.1.1.E Release kinetic models of Aloin from S6 irregular SiO$_2$ in SBF for first 6 hours:

Fig 4.18: Kinetic models of Aloin released for first 6 hours from S6 silica in SBF medium

Table 4.10:Kinetic data of Aloin obtained from S6 irregular SiO$_2$ in SBF medium

Sample Name	Zero order (R^2 value)	First order (R^2 value)	Higuchi model (R^2 value)	Korsmeyer-peppas (R^2 value)	Korsmeyer-peppas n=release exponent
Aloin	BR	BR	BR	BR	BR
S6	0.913	0.958	**0.995**	0.951	1.96

Based on these kinetic models the best fitted model for burst release of aloin in SBF is First Order model. As the release exponent value is >0.89, the release mechanism is supercase II transport.

4.8.1.1.F Release kinetic models of Aloin from S6 irregular SiO₂ in SBF for 24-168 hours:

Fig 4.19: Kinetic models of Aloin released for 24-168 hours from S6 silica in SBF medium

Table 4.11:Kinetic data of Aloin obtained from S6 irregular SiO₂ in SBF medium

Sample Name	Zero order (R^2 value)	First order (R^2 value)	Higuchi model (R^2 value)	Korsmeyer-peppas (R^2 value)	Korsmeyer-peppas n=release exponent
Aloin	SR	SR	SR	SR	SR
S6	0.940	0.946	0.980	**0.984**	2.39

Based on these kinetic models the best fitted model for sustained release of aloin in SBF is koresmeyerpeppas model. As the release exponent value is >0.89, the release mechanism is supercase II transport.

4.8.1.2.A Release kinetic models of Aloin from S2 irregular SiO$_2$ in SGF for first 6 hours:

Fig 4.20: Kinetic models of Aloin released for first 6 hours from S2 silica in SGF medium

Table 4.12:Kinetic data of Aloin obtained from S2 irregular SiO$_2$ in SGF medium

Sample Name	Zero order (R^2 value)	First order (R^2 value)	Higuchi model (R^2 value)	Korsmeyer-peppas (R^2 value)	Korsmeyer-peppas n=release exponent
Aloin	BR	BR	BR	BR	BR
S2	0.988	**0.995**	0.980	0.987	1.91

Based on these kinetic models the best fitted model for burst release of aloin in SBF is First Order model. As the release exponent value is >0.89, the release mechanism is supercase II transport.

4.8.1.2.B Release kinetic models of Aloin from S2 irregular SiO₂ in SGF for 24-168 hours:

Fig 4.21: Kinetic models of Aloin released for 24-168 hours from S2 silica in SGF medium

Table 4.13:Kinetic data of Aloin obtained from S2 irregular SiO₂ in SGF medium

Sample Name	Zero order (R^2 value)	First order (R^2 value)	Higuchi model (R^2 value)	Korsmeyer-peppas (R^2 value)	Korsmeyer-peppas n=release exponent
Aloin	SR	SR	SR	SR	SR
S2	0.996	**0.998**	0.992	0.960	2.37

Based on these kinetic models the best fitted model for sustained release of aloin in SBF is first order model. As the release exponent value is >0.89, the release mechanism is supercase II transport.

4.8.1.2.C Release kinetic models of Aloin from S4 irregular SiO₂ in SGF for first 6 hours:

Fig 4.22: Kinetic models of Aloin released for first 6 hours from S4 silicain SGF medium

Table 4.14:Kinetic data of Aloin obtained from S4 irregular SiO₂ in SGF medium

Sample Name	Zero order (R^2 value)	First order (R^2 value)	Higuchi model (R^2 value)	Korsmeyer-peppas (R^2 value)	Korsmeyer-peppas n=release exponent
Aloin	BR	BR	BR	BR	BR
S4	0.994	**0.997**	0.976	0.992	1.85

Based on these kinetic models the best fitted model for burst release of aloin in SGF is First Order model. As the release exponent value is >0.89, the release mechanism is supercase II transport

4.8.1.2.D Release kinetic models of Aloin from S4 irregular SiO₂ in SGF for 24-168 hours:

Fig 4.23: Kinetic models of Aloin released for 24-168 hours from S4 silica in SGF medium

Table 4.15:Kinetic data of Aloin obtained from S4 irregular SiO₂ in SGF medium

Sample Name	Zero order (R^2 value)	First order (R^2 value)	Higuchi model (R^2 value)	Korsmeyer-peppas (R^2 value)	Korsmeyer-peppas n=release exponent
Aloin	SR	SR	SR	SR	SR
S4	0.998	**0.999**	0.962	0.950	2.31

Based on these kinetic models the best fitted model for sustained release of aloin in SGF is first order model. As the release exponent value is >0.89, the release mechanism is supercase II transport.

4.8.1.2.E Release kinetic models of Aloin from S6 irregular SiO$_2$ in SGF for first 6 hours:
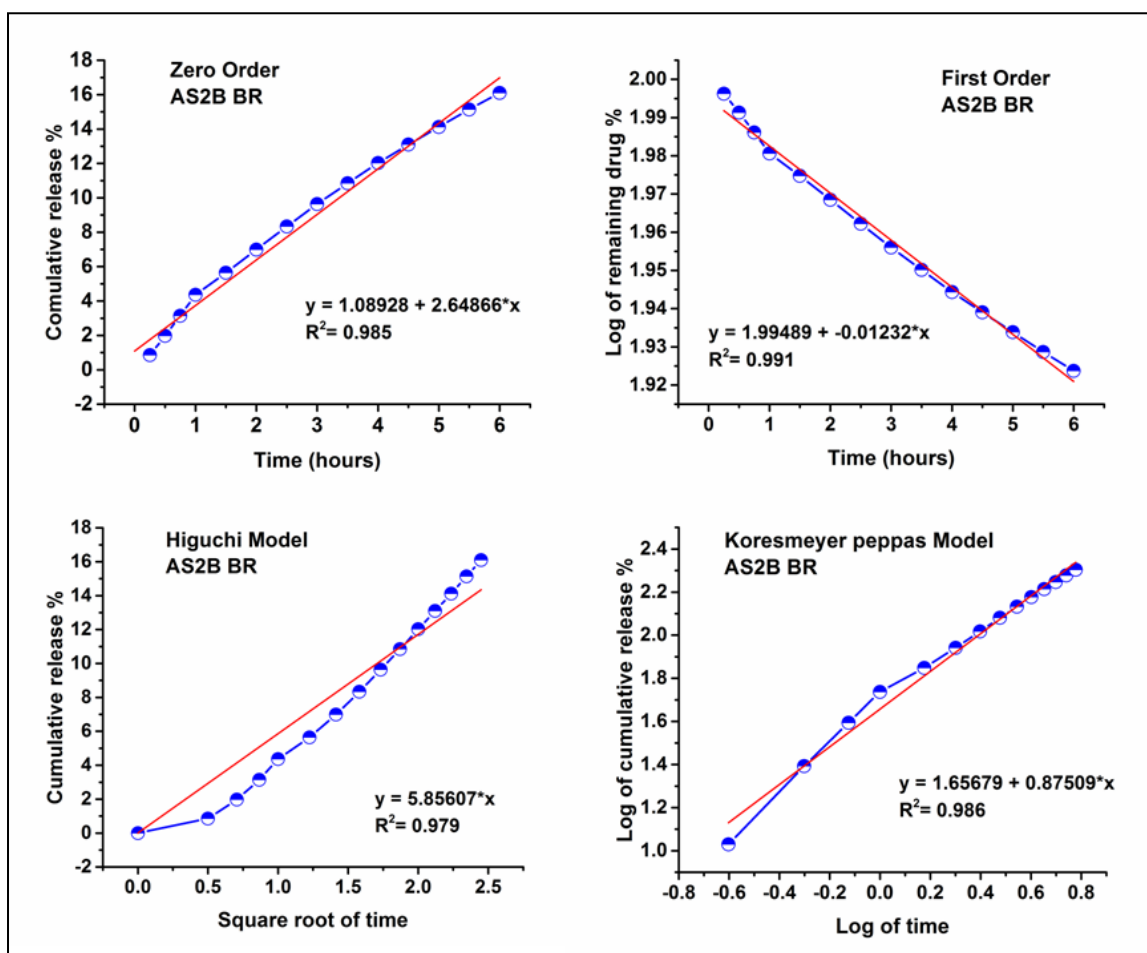

Fig 4.24: Kinetic models of Aloin released for first 6 hours from S6 silica in SGF medium

Table 4.16:Kinetic data of Aloin obtained from S6 irregular SiO$_2$ in SGF medium

Sample Name	Zero order (R^2 value)	First order (R^2 value)	Higuchi model (R^2 value)	Korsmeyer-peppas (R^2 value)	Korsmeyer-peppas n=release exponent
Aloin	BR	BR	BR	BR	BR
S6	**0.997**	0.991	0.963	0.993	1.84

Based on these kinetic models the best fitted model for burst release of aloin in SGF is Zero Order model. As the release exponent value is >0.89, the release mechanism is supercase II transport.

4.8.1.2.F Release kinetic models of Aloin from S6 irregular SiO₂ in SGF for 24-168 hours:
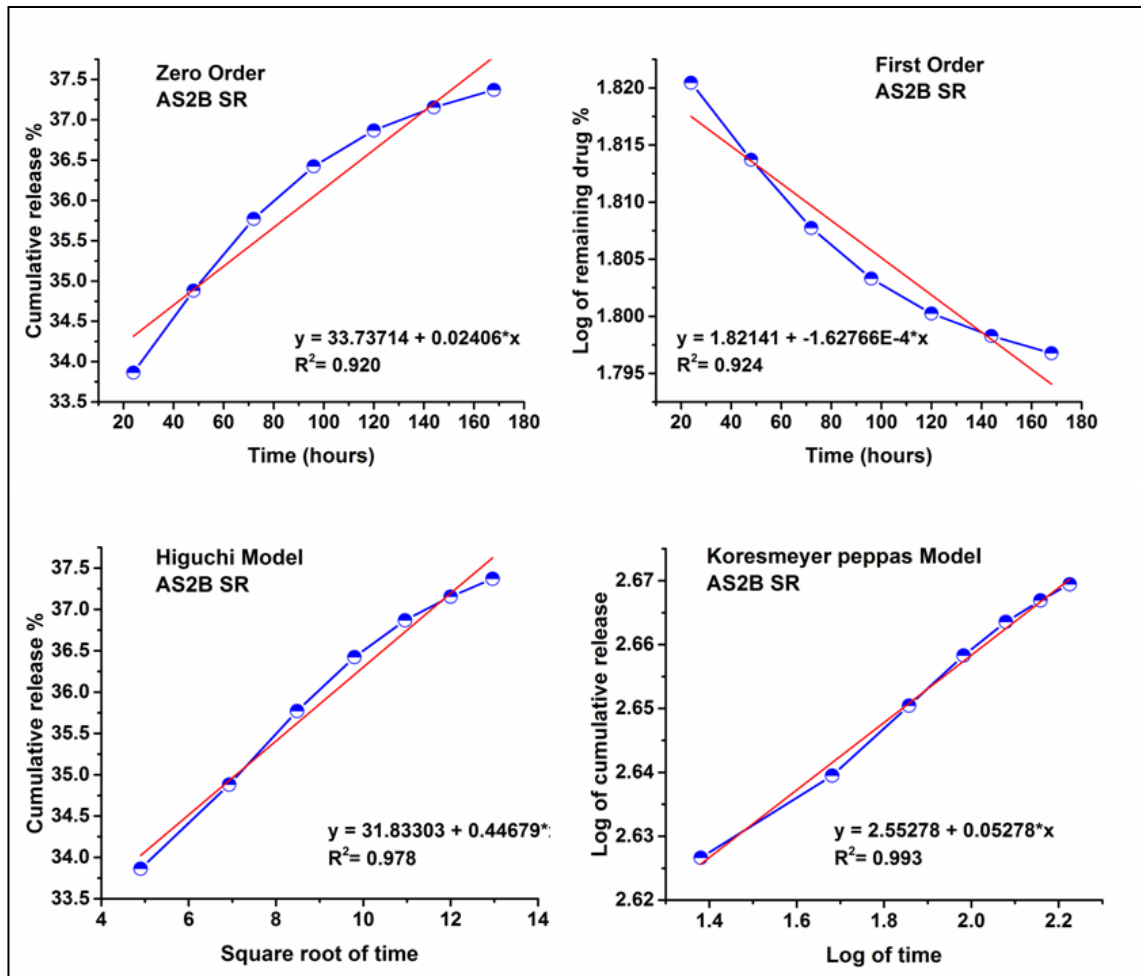

Fig 4.25: Kinetic models of Aloin released for 24-168 hours from S6 silica in SGF medium

Table 4.17:Kinetic data of Aloin obtained from S6 irregular SiO₂ in SGF medium

Sample Name	Zero order (R^2 value)	First order (R^2 value)	Higuchi model (R^2 value)	Korsmeyer-peppas (R^2 value)	Korsmeyer-peppas n=release exponent
Aloin	SR	SR	SR	SR	SR
S6	0.963	0.983	**0.997**	0.992	2.45

Based on these kinetic models the best fitted model for sustained release of aloin in SGF is Higuchi model .As the release exponent value is >0.89, the release mechanism is supercase II transport.

Depending on the regression coefficient values the best fitted models are obtained. All the regression coefficient values are given to their respective tables along with their kinetic models.

Table 4.18: Kinetic model of Aloin released from SiO$_2$ in SBF & SGF

Sl no	Sample name	Dissolution medium	Burst release	Sustained release
1	S2	SBF	First order model	Koresmeyer peppas model
		SGF	First order model	First order model
2	S4	SBF	First order model	Koresmeyer peppas model
		SGF	First order model	First order model
3	S6	SBF	Higuchi model	Koresmeyer peppas model
		SGF	Zero order model	Higuchi model

For all sets release exponent values are greater than 0.89 means the mechanism is super case II transport.

4.8.2 Drug release profile and kinetic behavior study of Aloevera from different porosity containing sphere shaped SiO$_2$ nano carriers:

Sphere shaped silica nanoparticles conjugated with drug aloin are also subjected to release in two different medium containing two different pH at a same set of procedures and kinetics models are plotted.

Table 4.19: Cumulative release of Aloin in SBF and SGF from different sphere shaped silica particles

Sl no	Sample name	% Cumulative Release
1	ASS2B (Aloin entrapped SS2 silica, released in SBF)	60
2	ASS4B (Aloin entrapped SS4 silica, released in SBF)	56
3	ASS6B(Aloin entrapped SS6 silica, released in SBF)	46
4	ASS2G (Aloin entrapped SS2 silica, released in SGF)	81
5	ASS4G (Aloin entrapped SS4 silica, released in SGF)	67
6	ASS6G (Aloin entrapped SS6 silica, released in SGF)	60
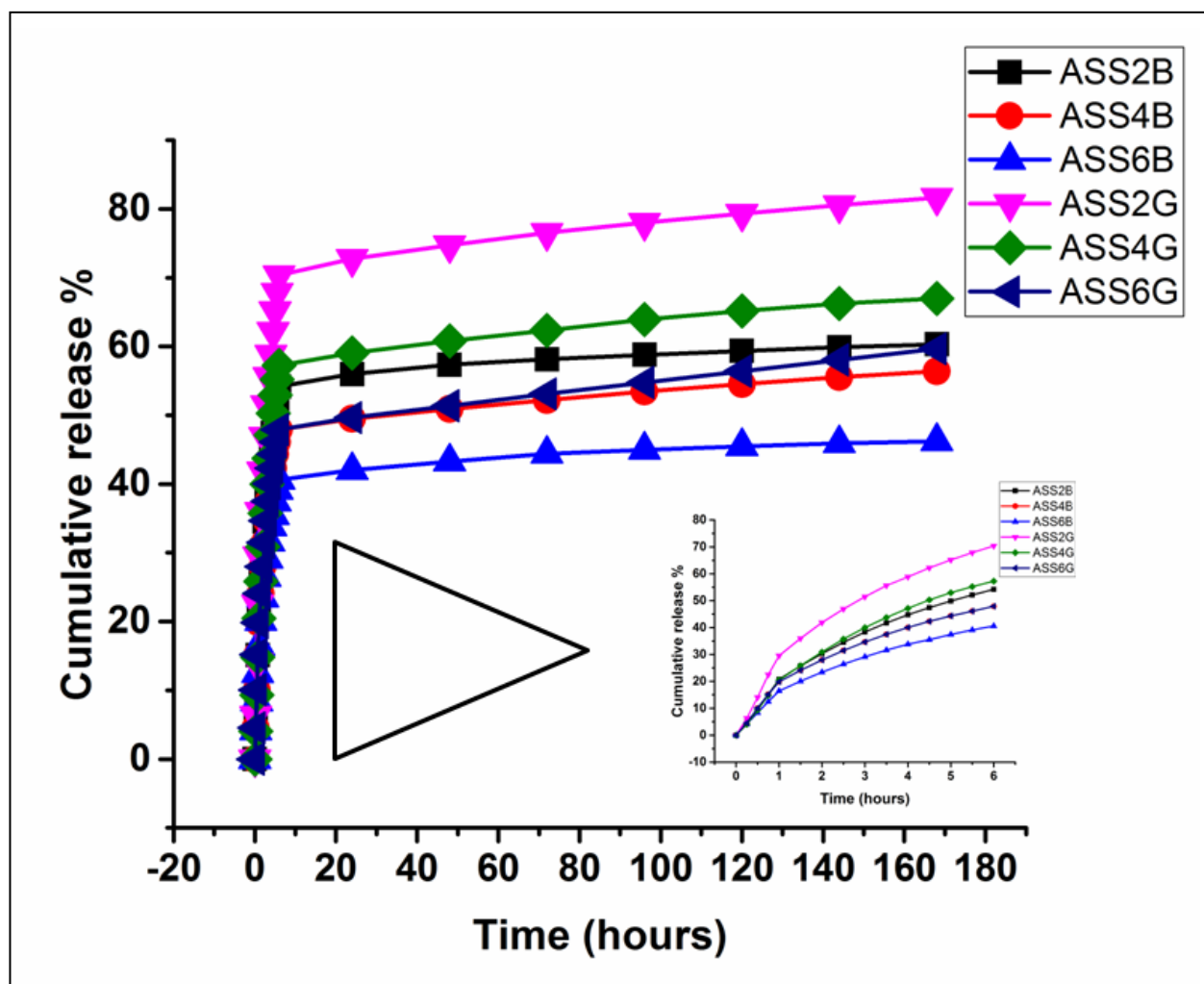
Fig 4.26: Dissolution profile of Aloin from sphere shape containing silica nanoparticles

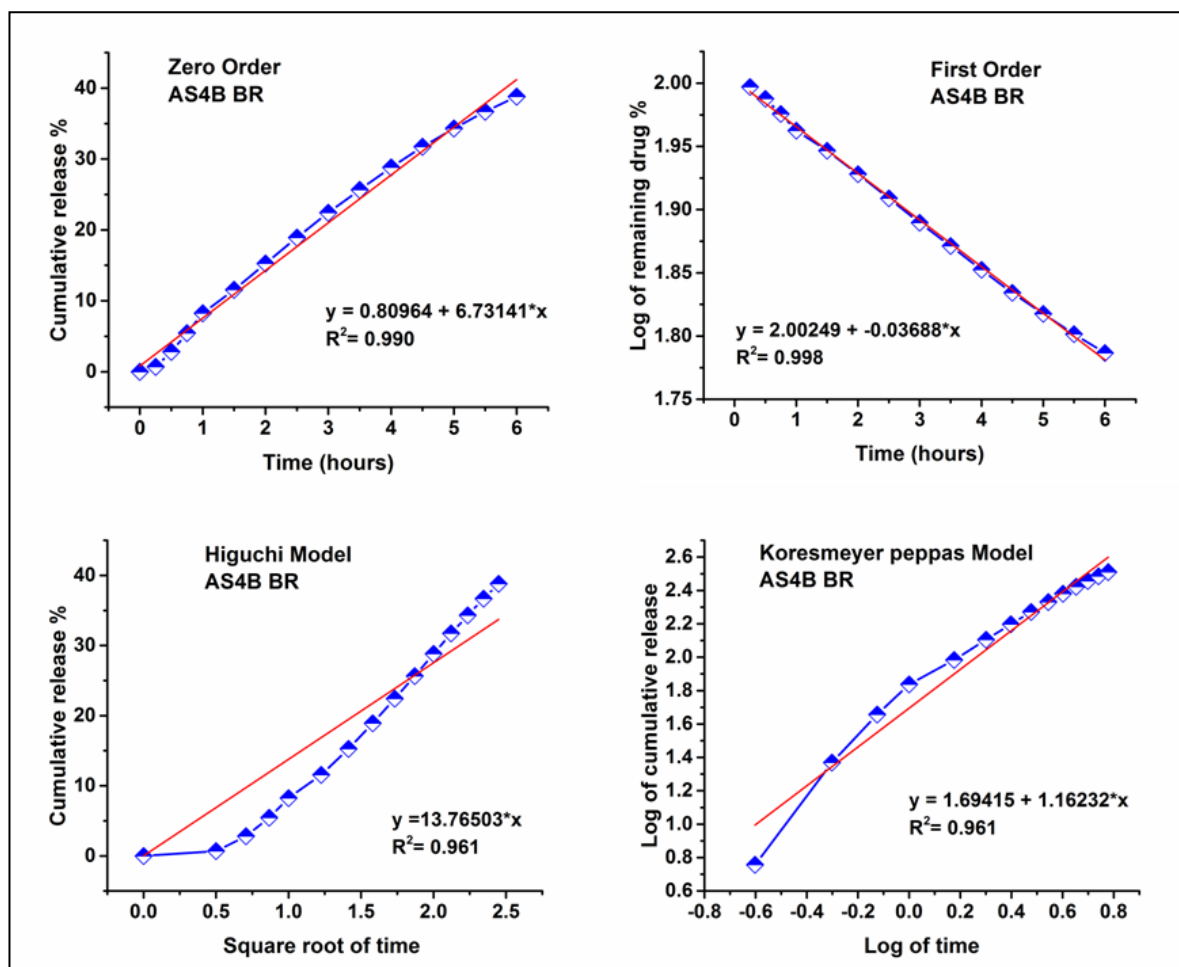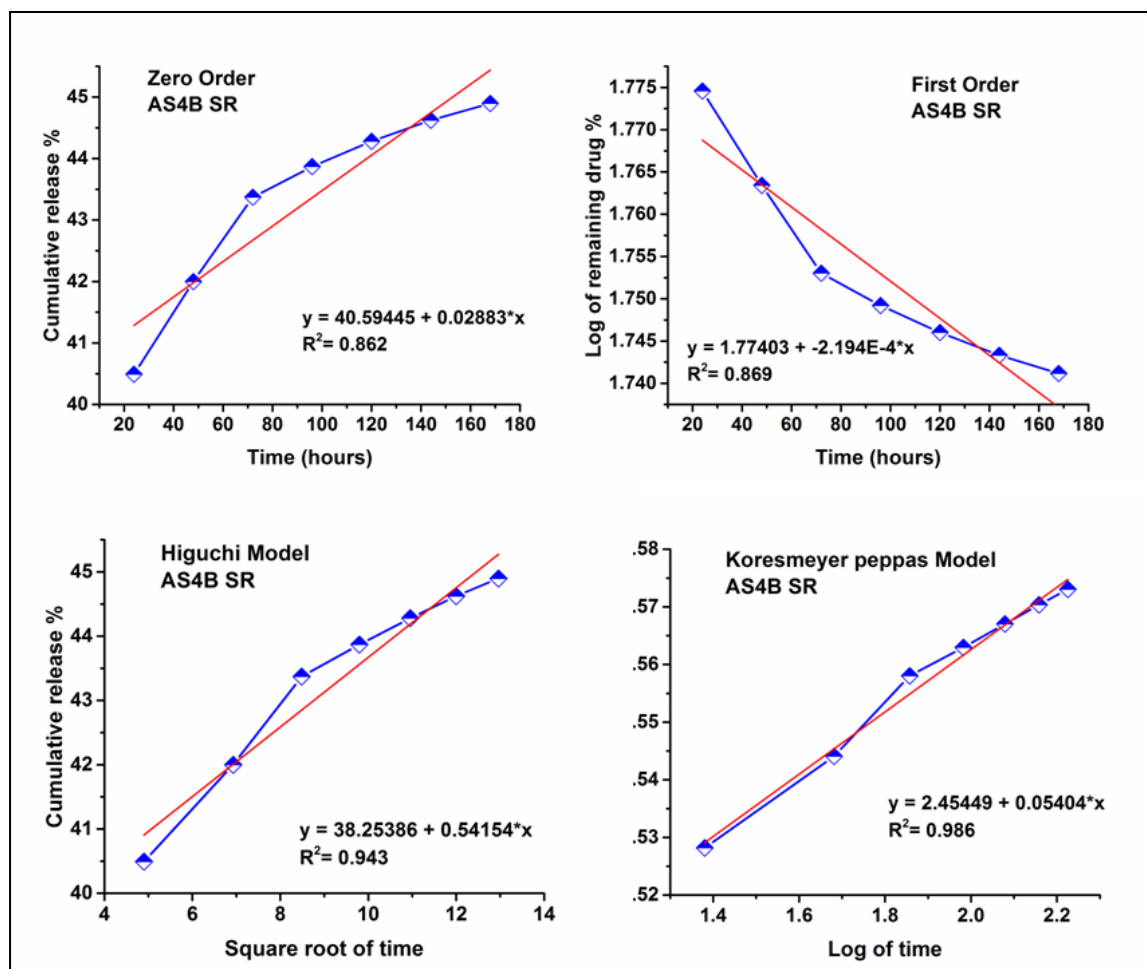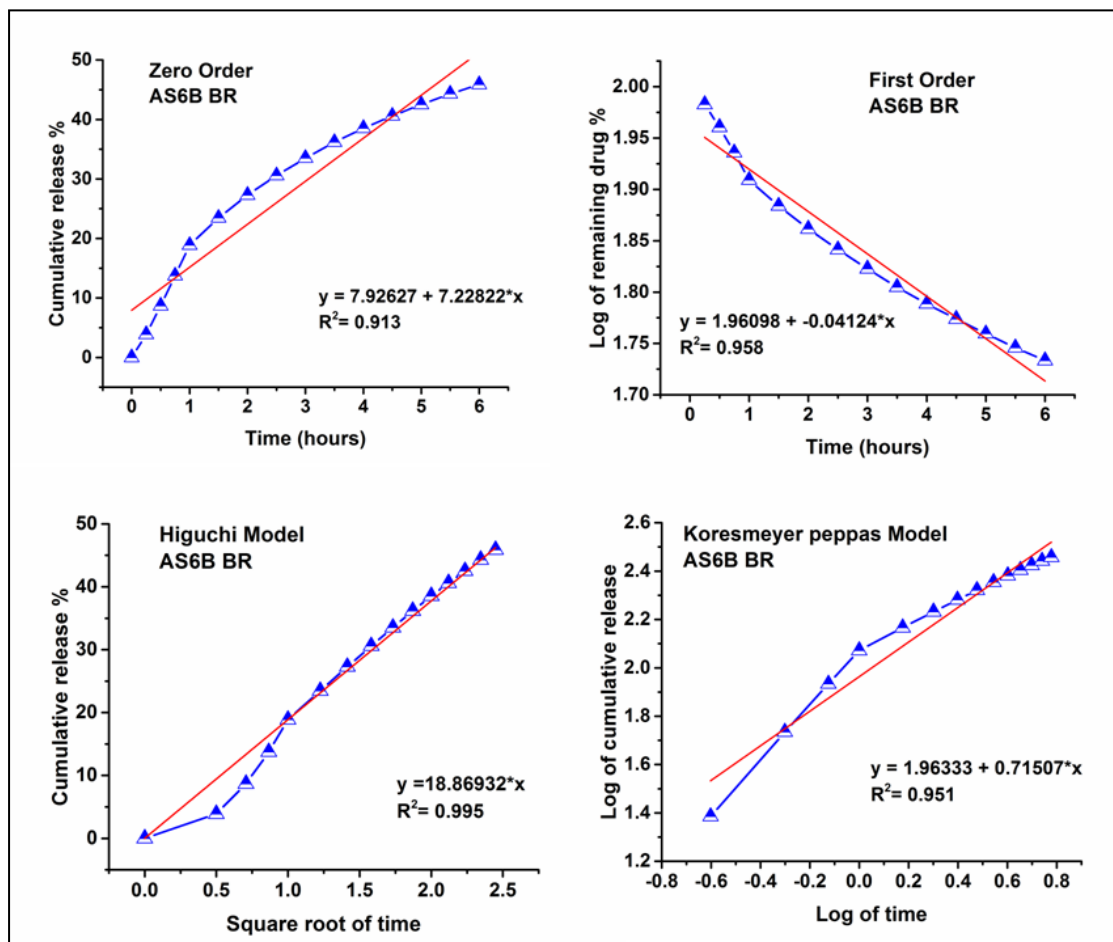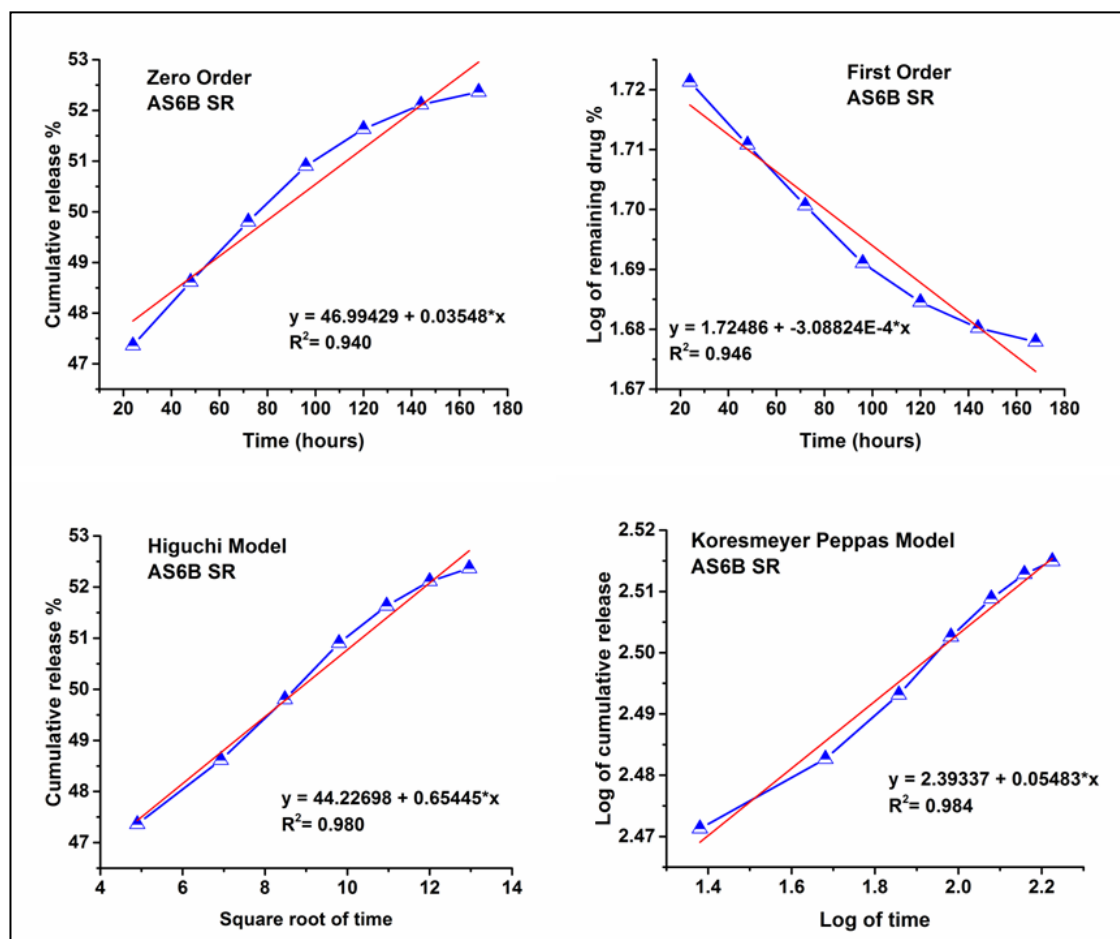**4.8.2.1.A Release kinetic models of Aloin from SS2 sphere SiO₂ in SBF for first 6 hours:**

Fig 4.27: Kinetic models of Aloin released for first 6 hours from SS2 silica in SBF medium

Table 4.20: Kinetic data of Aloin obtained from SS2 sphere SiO₂ in SBF medium

Sample Name	Zero order (R^2 value)	First order (R^2 value)	Higuchi model (R^2 value)	Korsmeyer-peppas (R^2 value)	Korsmeyer-peppas n=release exponent
Aloin	BR	BR	BR	BR	BR
SS2	0.934	0.979	**0.994**	0.970	2.02

Based on this regression coefficient value the best fitted model for burst release of aloin in SBF from SS2 is Higuchi model. As the release exponent value is >0.89, the release mechanism is supercase II transport.

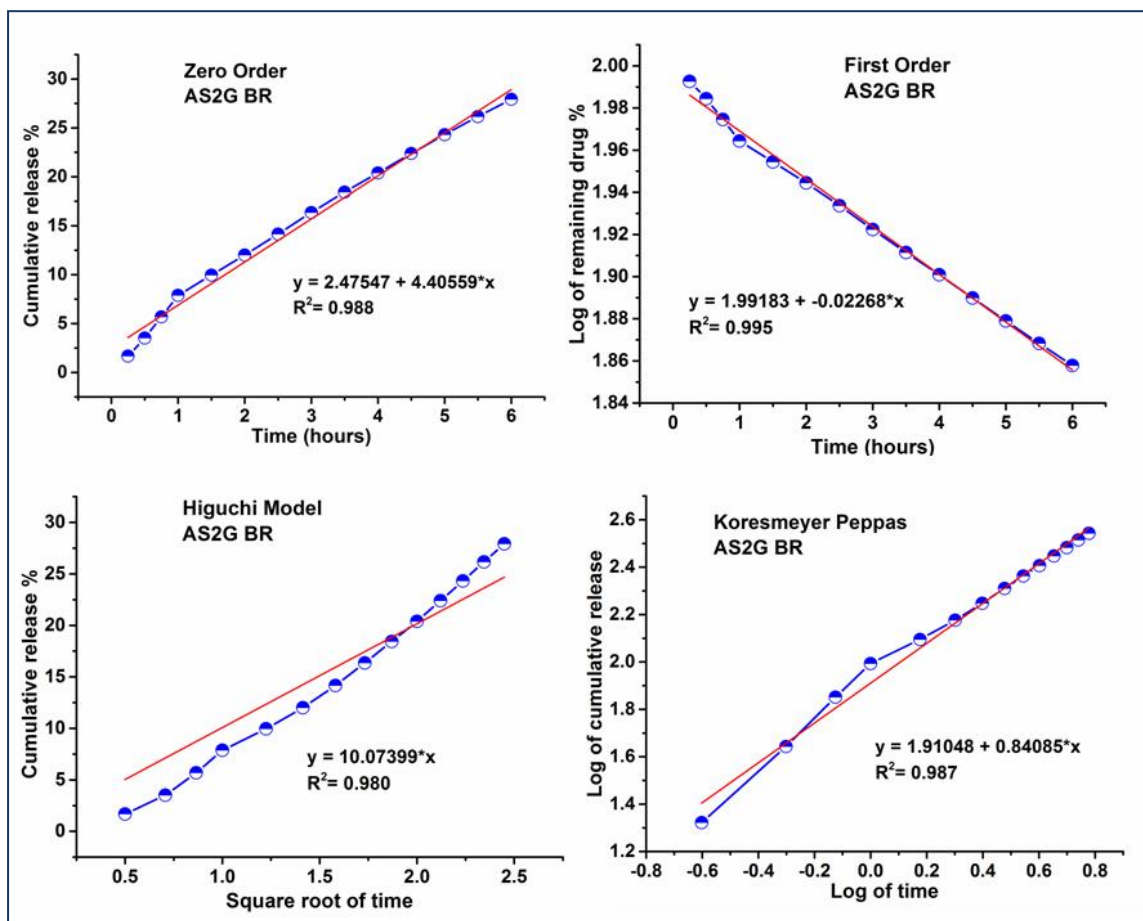**4.8.2.1.B Release kinetic models of Aloin from SS2 sphere SiO₂ in SBF for 24-168 hours:**

Fig 4.28: Kinetic models of Aloin released for 24-168 hours from SS2 silica in SBF medium

Table 4.21: Kinetic data of Aloin obtained from SS2 sphere SiO₂ in SBF medium

Sample name	Zero order (R^2 value)	First order (R^2 value)	Higuchi model (R^2 value)	Korsmeyer-peppas (R^2 value)	Korsmeyer-peppas n=release exponent
Aloin	SR	SR	SR	SR	SR
SS2	0.955	0.962	**0.994**	0.993	2.49

Based on this regression coefficient value the best fitted model for sustained release of aloinfrom SS2 in SBF is Higuchi model. As the release exponent value is >0.89, the release mechanism is supercase II transport.

4.8.2.1.C Release kinetic models of Aloin from SS4 sphere SiO$_2$ in SBF for first 6 hours:

Fig 4.29: Kinetic models of Aloin released for first 6 hours from SS4 silica in SBF medium

Table 4.22: Kinetic data of Aloin obtained from SS4 sphere SiO$_2$ in SBF medium

Sample name	Zero order (R^2 value)	First order (R^2 value)	Higuchi model (R^2 value)	Korsmeyer-peppas (R^2 value)	Korsmeyer-peppas n=release exponent
Aloin	BR	BR	BR	BR	BR
SS4	0.919	0.967	**0.996**	0.958	2.12

Based on this regression coefficient value the best fitted model for burst release of aloin from SS4 in SBF is Higuchi model. As the release exponent value is >0.89, the release mechanism is supercase II transport

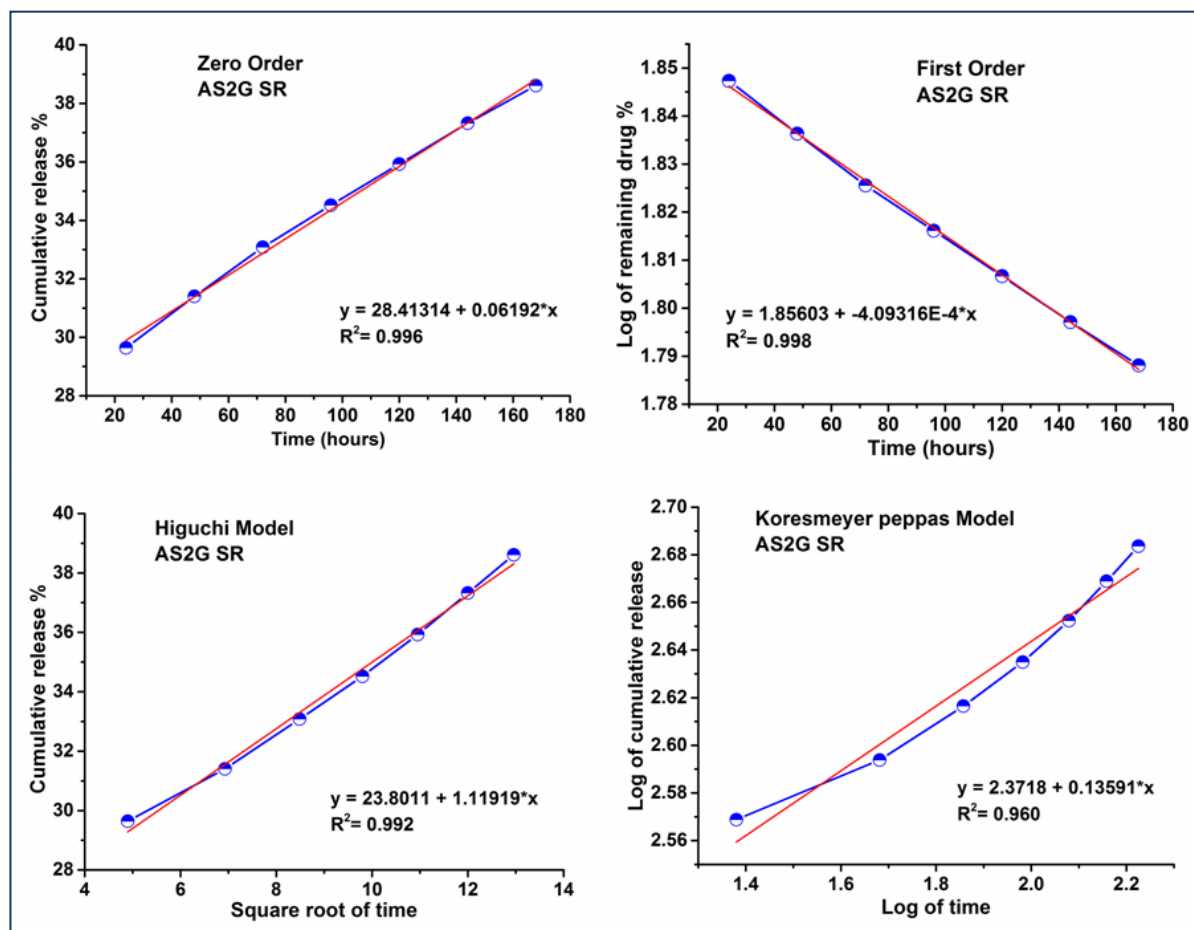**4.8.2.1.D Release kinetic models of Aloin from SS4 sphere SiO₂ in SBF for 24-168 hours:**
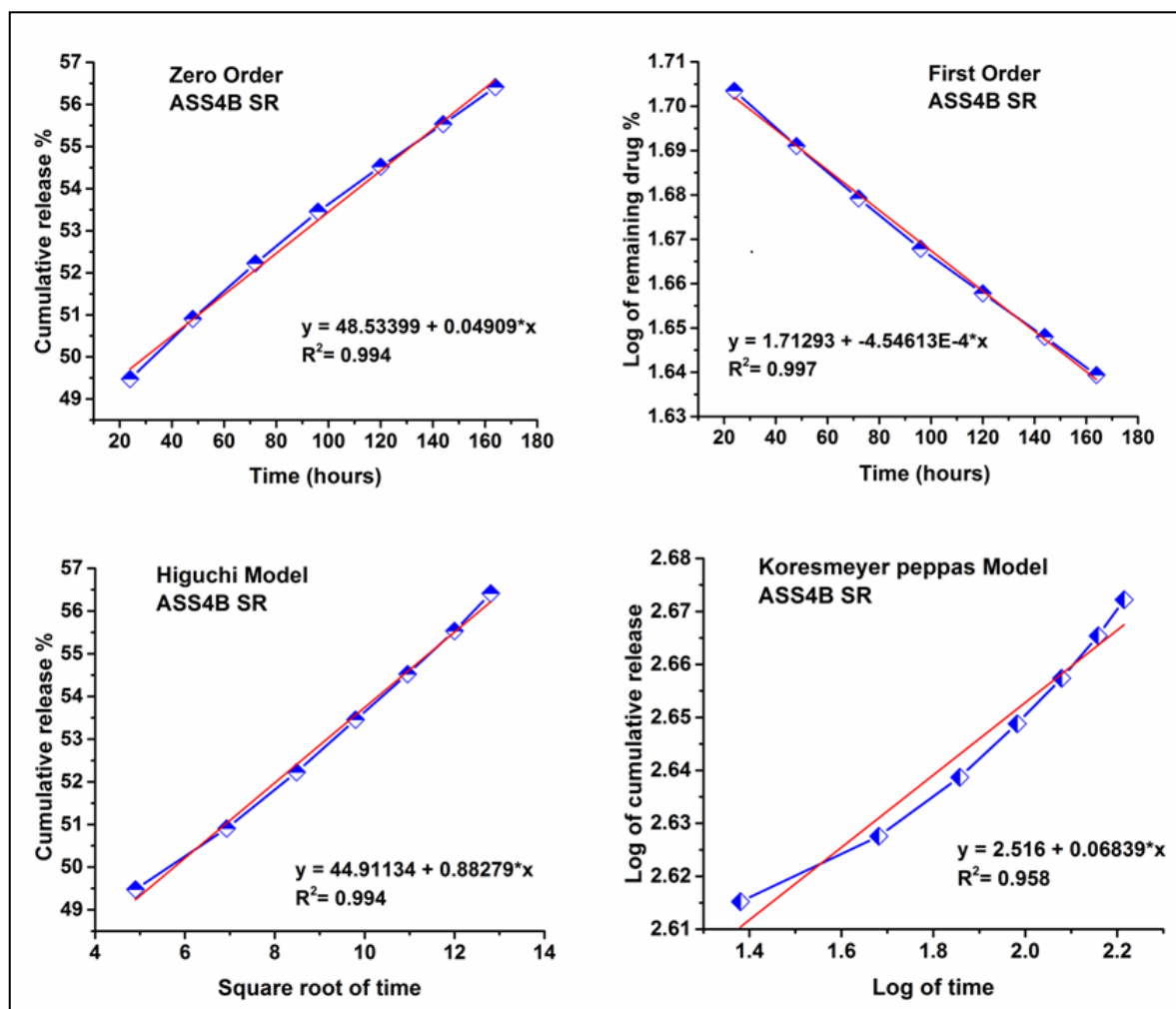
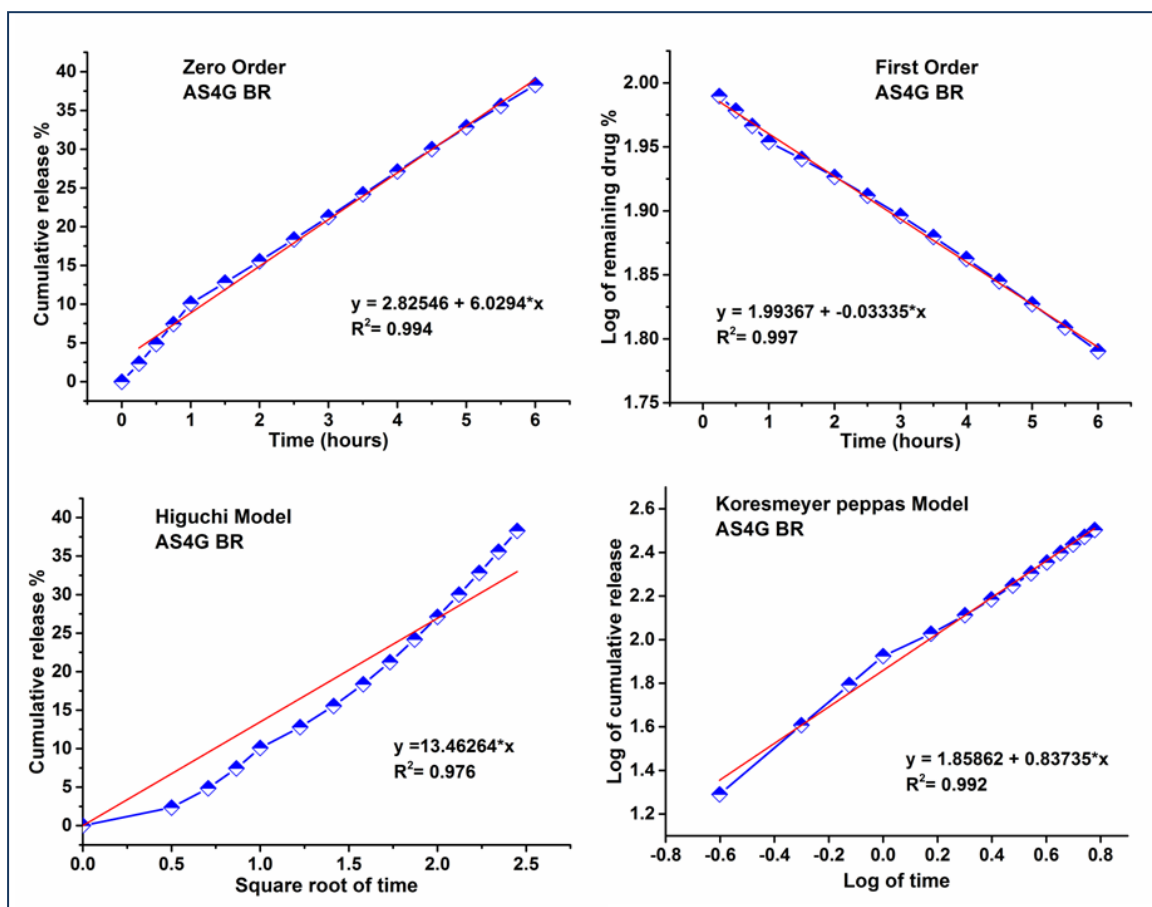**Fig 4.30: Kinetic models of Aloin released for 24-168 hours from SS4 silica in SBF medium**

Table 4.23: Kinetic data of Aloin obtained from SS4 sphere SiO₂ in SBF medium

Sample name	Zero order (R^2 value)	First order (R^2 value)	Higuchi model (R^2 value)	Korsmeyer-peppas (R^2 value)	Korsmeyer-peppas n=release exponent
Aloin	SR	SR	SR	SR	SR
SS4	0.994	**0.997**	0.994	0.958	2.51

Based on this regression coefficient value the best fitted model for sustained release of aloin from SS4 in SBF is First order model. As the release exponent value is >0.89, the release mechanism is supercase II transport.

4.8.2.1.E Release kinetic models of Aloin from SS6 sphere SiO₂ in SBF for first 6 hours:
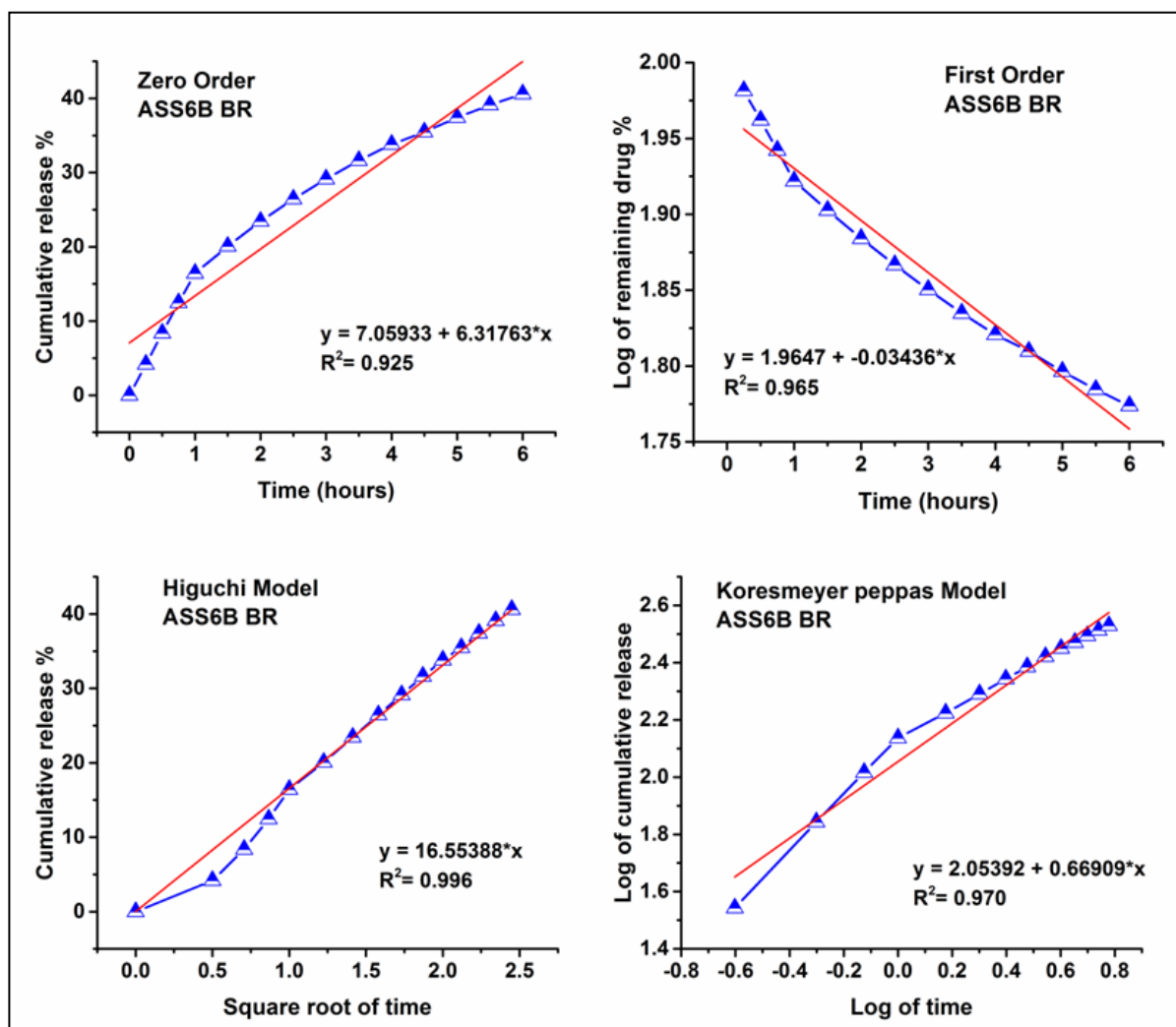
Fig 4.31: Kinetic models of Aloin released for first 6 hours from SS6 silica in SBF medium

Table 4.24: Kinetic data of Aloin obtained from SS6 sphere SiO₂ in SBF medium

Sample name	Zero order (R^2 value)	First order (R^2 value)	Higuchi model (R^2 value)	Korsmeyer-peppas (R^2 value)	Korsmeyer-peppas n=release exponent
Aloin	BR	BR	BR	BR	BR
SS6	0.925	0.965	**0.996**	0.970	2.05

Based on this regression coefficient value the best fitted model for burst release of aloin from SS6 in SBF is Higuchi model. As the release exponent value is >0.89, the release mechanism is supercase II transport.

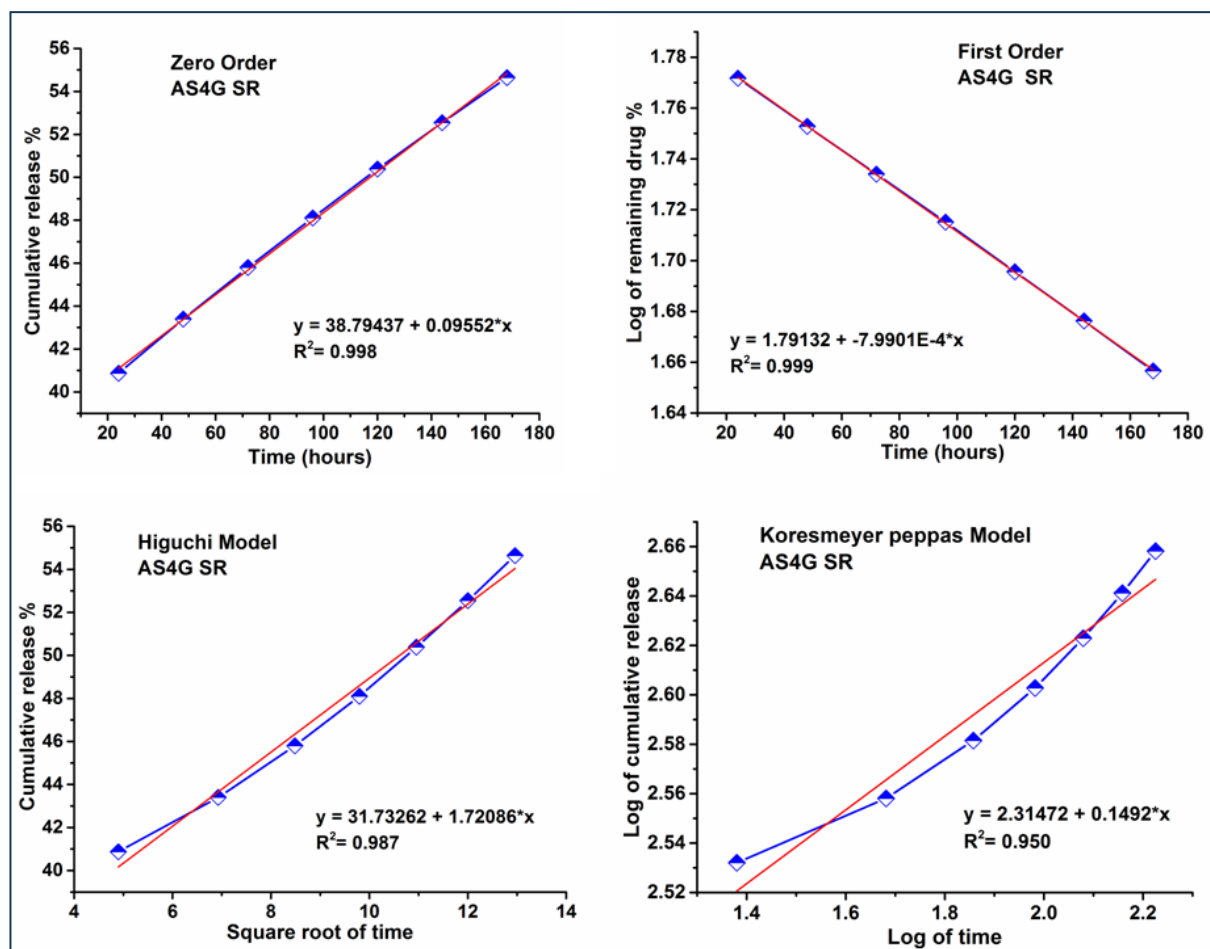**4.8.2.1.F Release kinetic models of Aloin from SS6 sphere SiO$_2$ in SBF for 24-168 hours:**
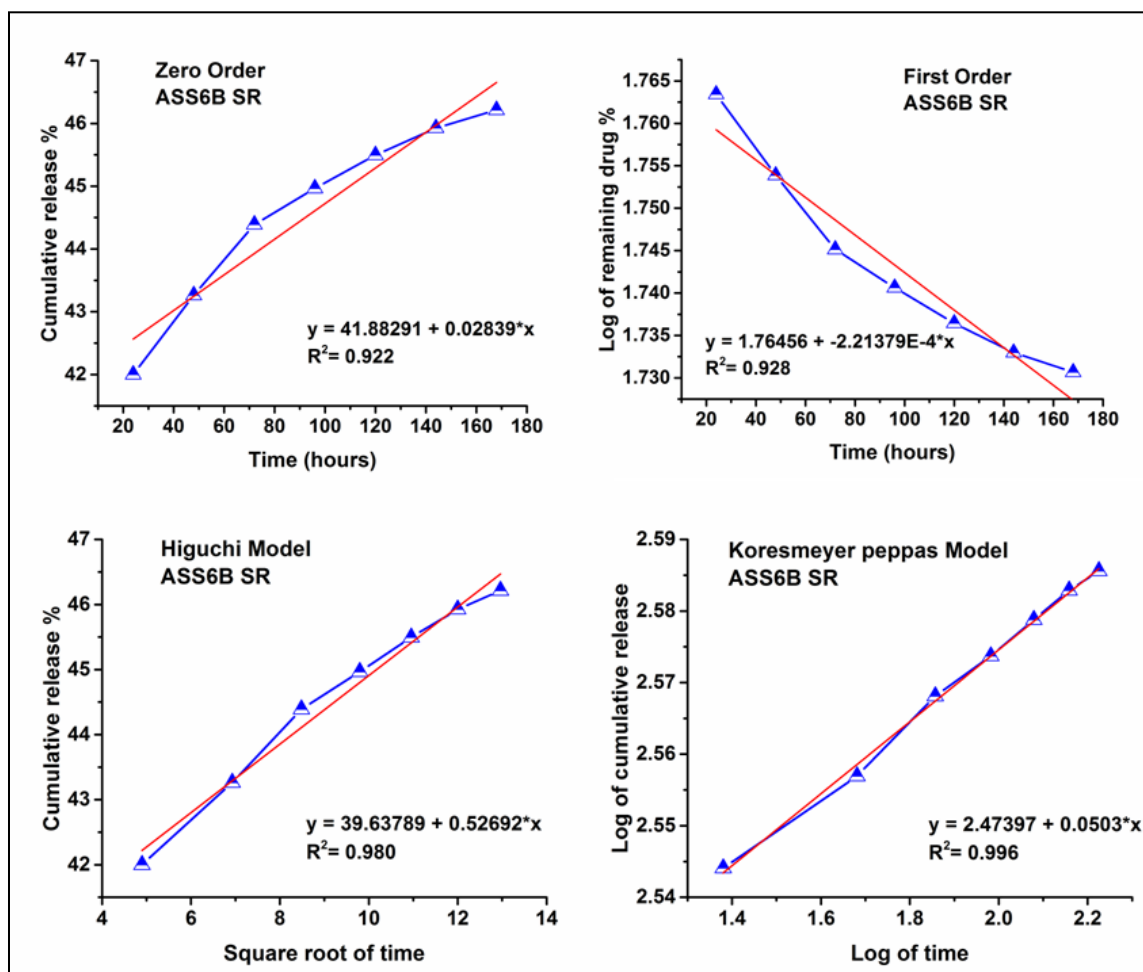
Fig 4.32: Kinetic models of Aloin released for 24-168 hours from SS6 silica in SBF medium

Table 4.25: Kinetic data of Aloin obtained from SS6 sphere SiO$_2$ in SBF medium

Sample name	Zero order (R^2 value)	First order (R^2 value)	Higuchi model (R^2 value)	Korsmeyer-peppas (R^2 value)	Korsmeyer-peppas n=release exponent
Aloin	SR	SR	SR	SR	SR
SS6	0.922	0.928	0.980	**0.996**	2.47

Based on this regression coefficient value the best fitted model for sustained release of aloin from SS6 in SBF is Koresmeyerpeppas model. As the release exponent value is >0.89, the release mechanism is supercase II transport.

4.8.2.2.A Release kinetic models of Aloin from SS2 sphere SiO₂ in SGF for first 6 hours:
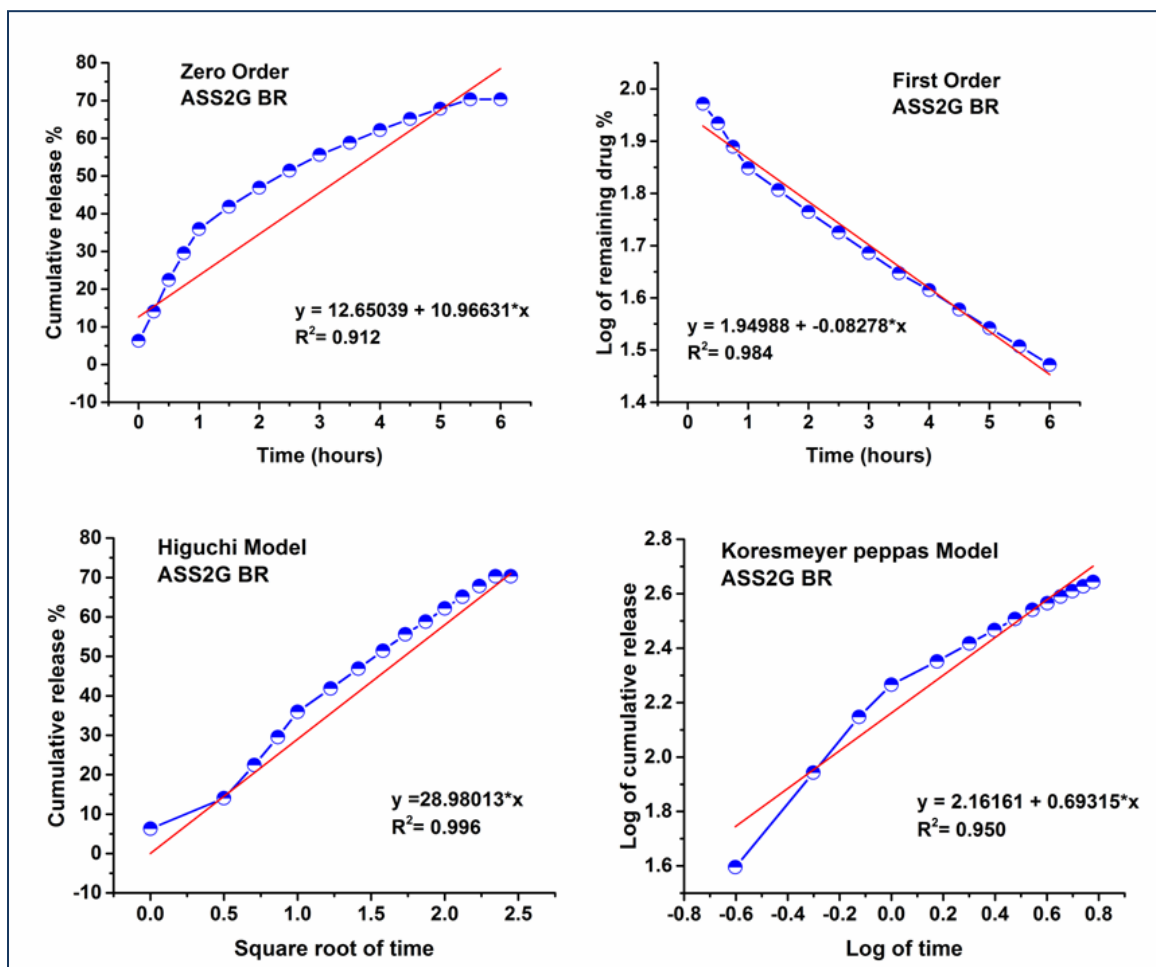
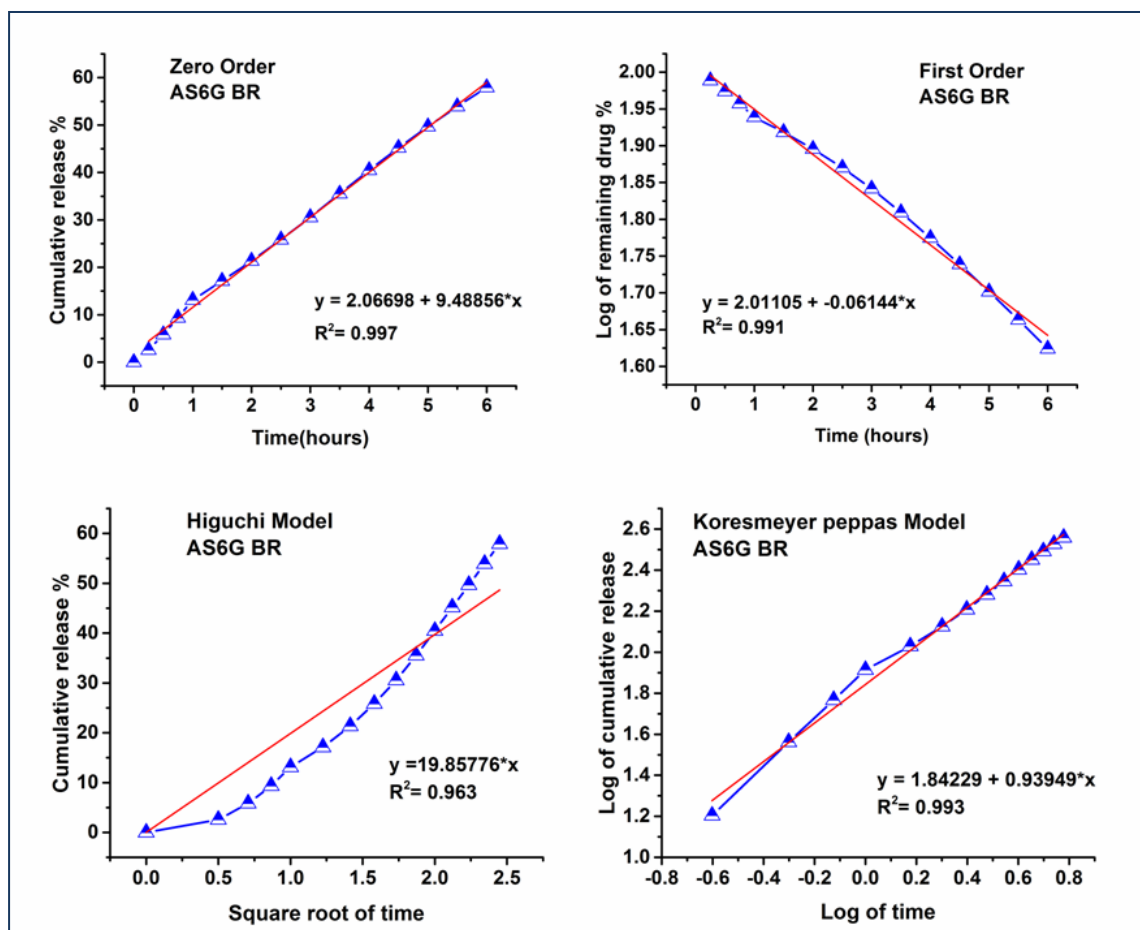**Fig 4.33: Kinetic models of Aloin released for first 6 hours from SS2 silica in SGF medium**

Table 4.26: Kinetic data of Aloin obtained from SS2 sphere SiO₂ in SGF medium

Sample name	Zero order (R^2 value)	First order (R^2 value)	Higuchi model (R^2 value)	Korsmeyer-peppas (R^2 value)	Korsmeyer-peppas n=release exponent
Aloin	BR	BR	BR	BR	BR
SS2	0.912	0.984	**0.996**	0.950	2.16

Based on this regression coefficient value the best fitted model for burst release of aloin from SS2 in SGF is Higuchi model. As the release exponent value is >0.89, the release mechanism is supercase II transport.

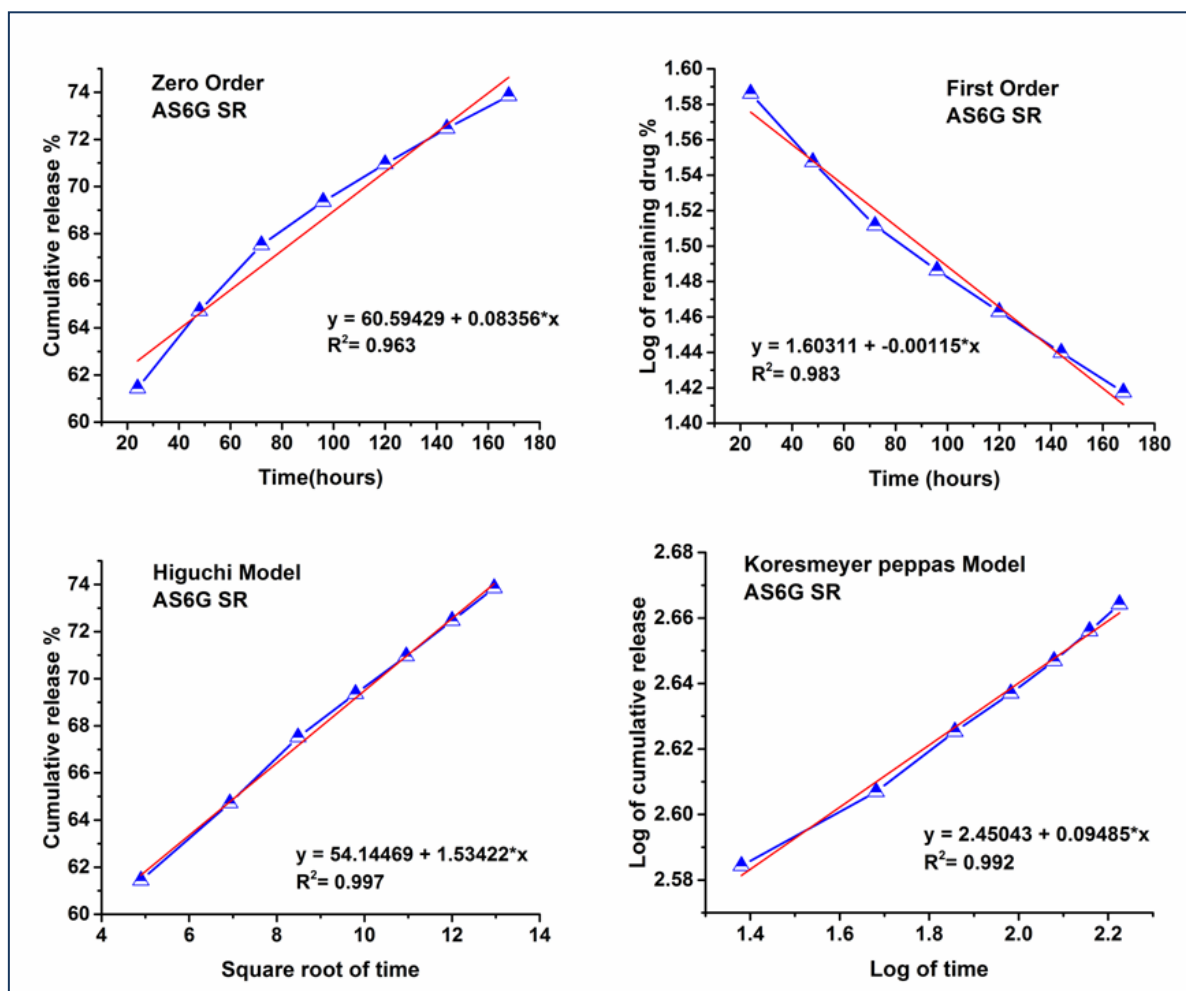**4.8.2.2.B Release kinetic models of Aloin from SS2 sphere SiO₂ in SGF for 24-168 hours:**
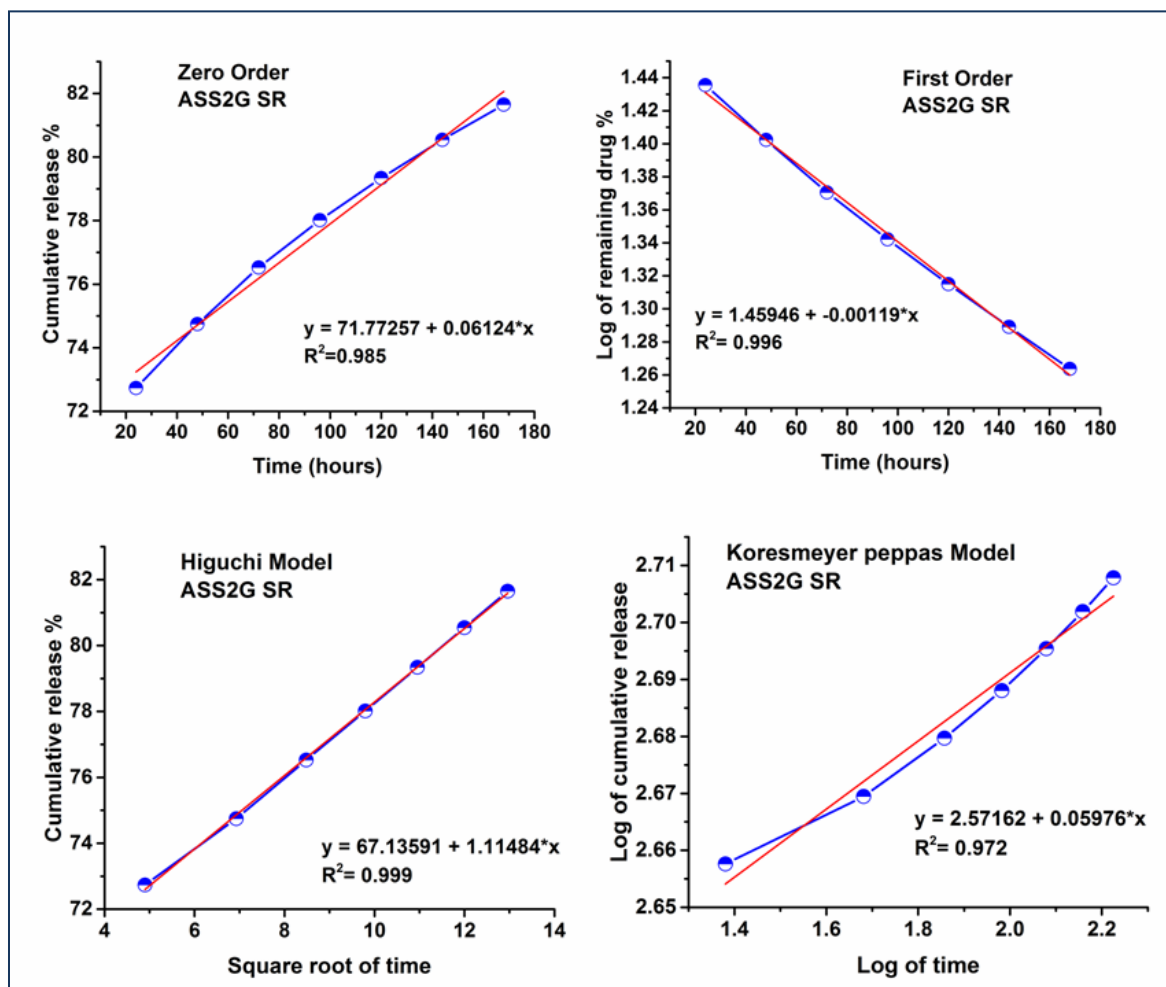
Fig 4.34: Kinetic models of Aloin released for 24-168 hours from SS2 silica in SGF medium

Table 4.27: Kinetic data of Aloin obtained from SS2 sphere SiO₂ in SGF medium

Sample name	Zero order (R^2 value)	First order (R^2 value)	Higuchi model (R^2 value)	Korsmeyer-peppas (R^2 value)	Korsmeyer-peppas n=release exponent
Aloin SS2	SR 0.985	SR 0.996	**SR** **0.999**	SR 0.972	SR 2.57

Based on this regression coefficient value the best fitted model for sustained release of aloin from SS2 in SGF is Higuchi model. As the release exponent value is >0.89, the release mechanism is supercase II transport.

4.8.2.2.C Release kinetic models of Aloin from SS4 sphere SiO₂ in SGF for first 6 hours:
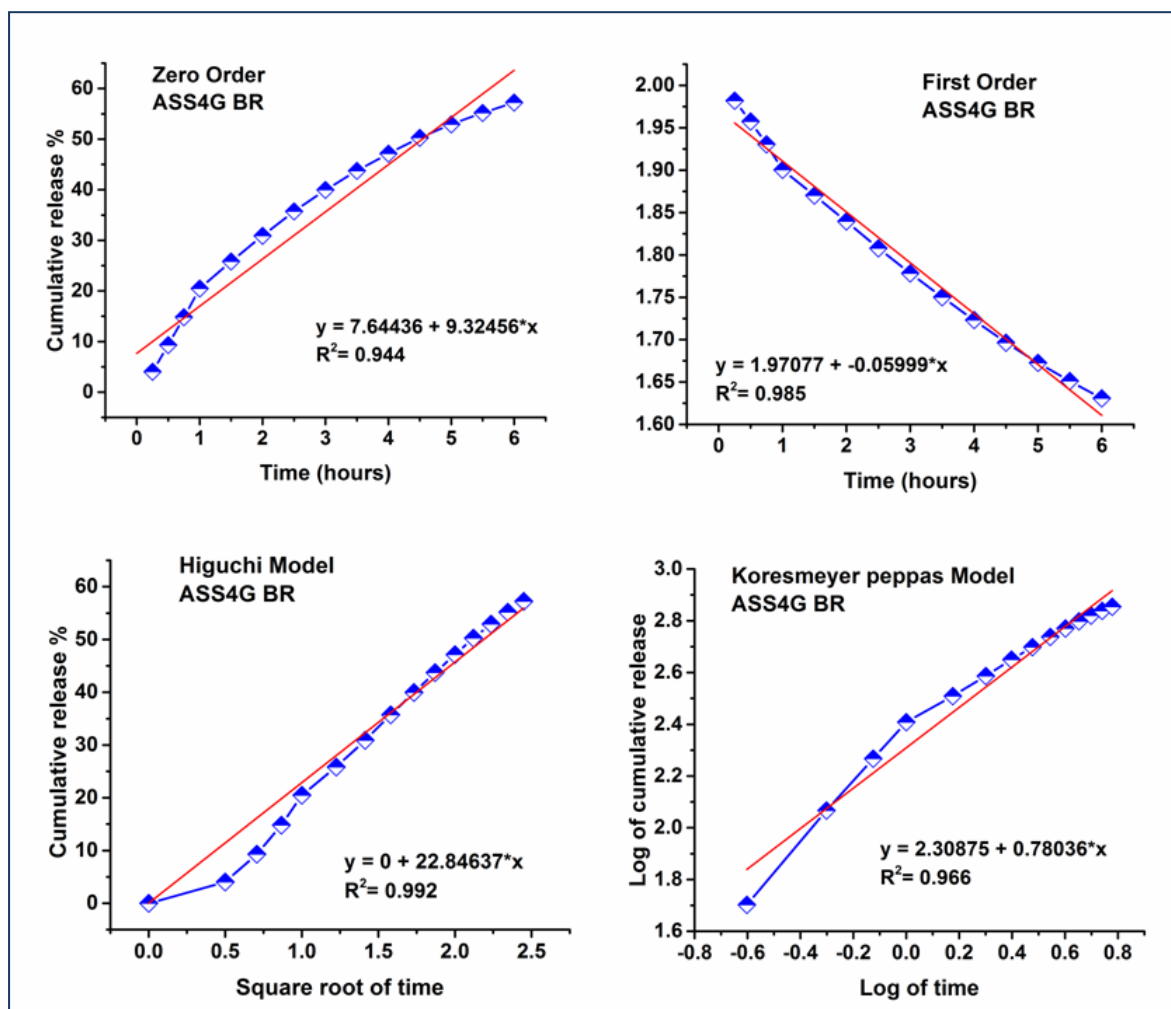
Fig 4.35: Kinetic models of Aloin released for first 6 hours from SS4 silica in SGF medium

Table 4.28: Kinetic data of Aloin obtained from SS4 sphere SiO₂ in SGF medium

Sample name	Zero order (R^2 value)	First order (R^2 value)	Higuchi model (R^2 value)	Korsmeyer-peppas (R^2 value)	Korsmeyer-peppas n=release exponent
Aloin	BR	BR	BR	BR	BR
SS4	0.944	0.985	**0.992**	0.966	2.30

Based on this regression coefficient value the best fitted model for burst release of aloin from SS4 in SGF is Higuchi model. As the release exponent value is >0.89, the release mechanism is supercase II transport.

4.8.2.2.D Release kinetic models of Aloin from SS4 sphere SiO₂ in SGF for 24-168 hours:
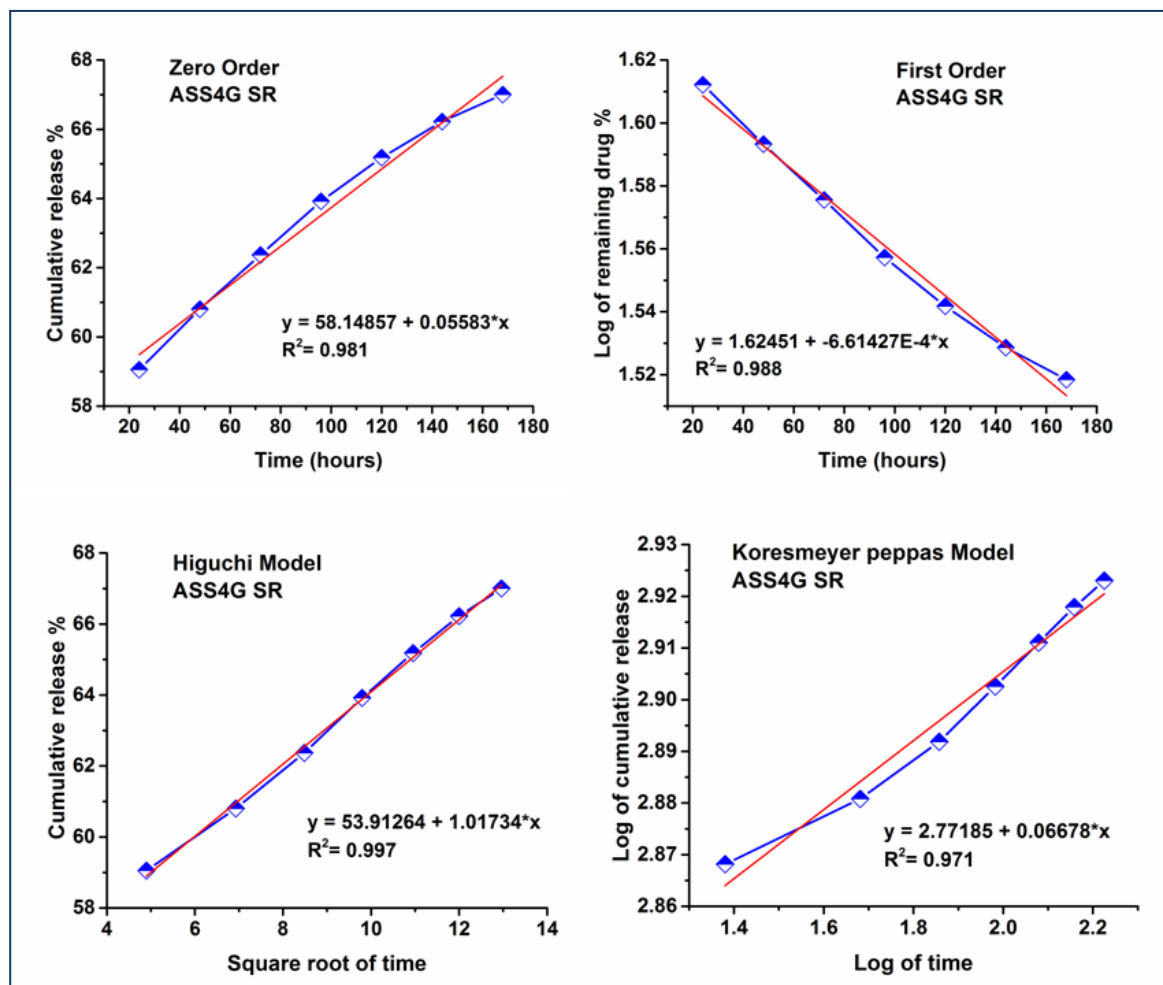
Fig 4.36: Kinetic models of Aloin released for 24-168 hours from SS4 silica in SGF medium

Table 4.29: Kinetic data of Aloin obtained from SS4 sphere SiO₂ in SGF medium

Sample name	Zero order (R^2 value)	First order (R^2 value)	Higuchi model (R^2 value)	Korsmeyer-peppas (R^2 value)	Korsmeyer-peppas n=release exponent
Aloin	SR	SR	SR	SR	SR
SS4	0.981	0.988	**0.997**	0.971	2.77

Based on this regression coefficient value the best fitted model for sustained release of aloin from SS4 in SGF is Higuchi model. As the release exponent value is >0.89, the release mechanism is supercase II transport.

4.8.2.2.E Release kinetic models of Aloin from SS6 sphere SiO₂ in SGF for first 6 hours:
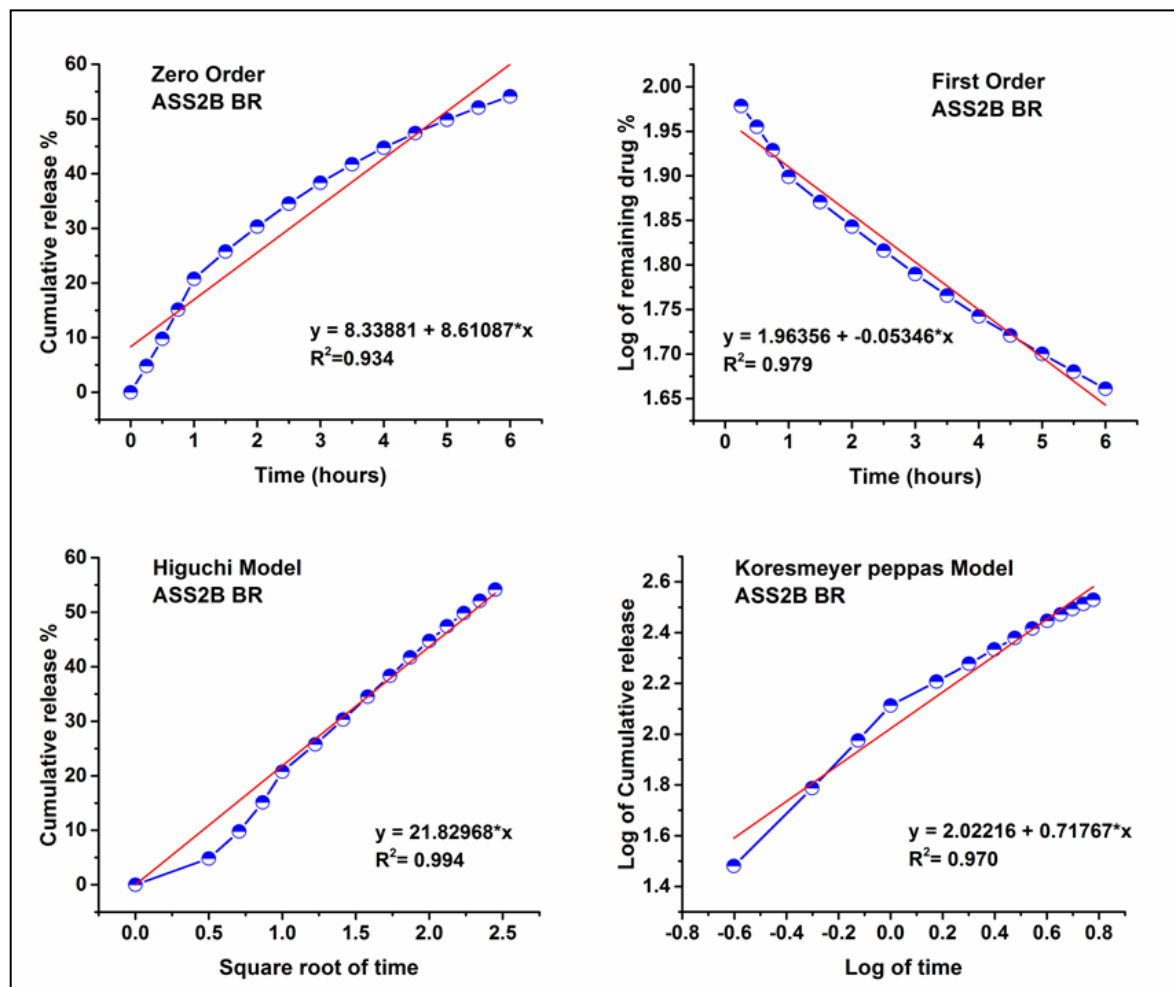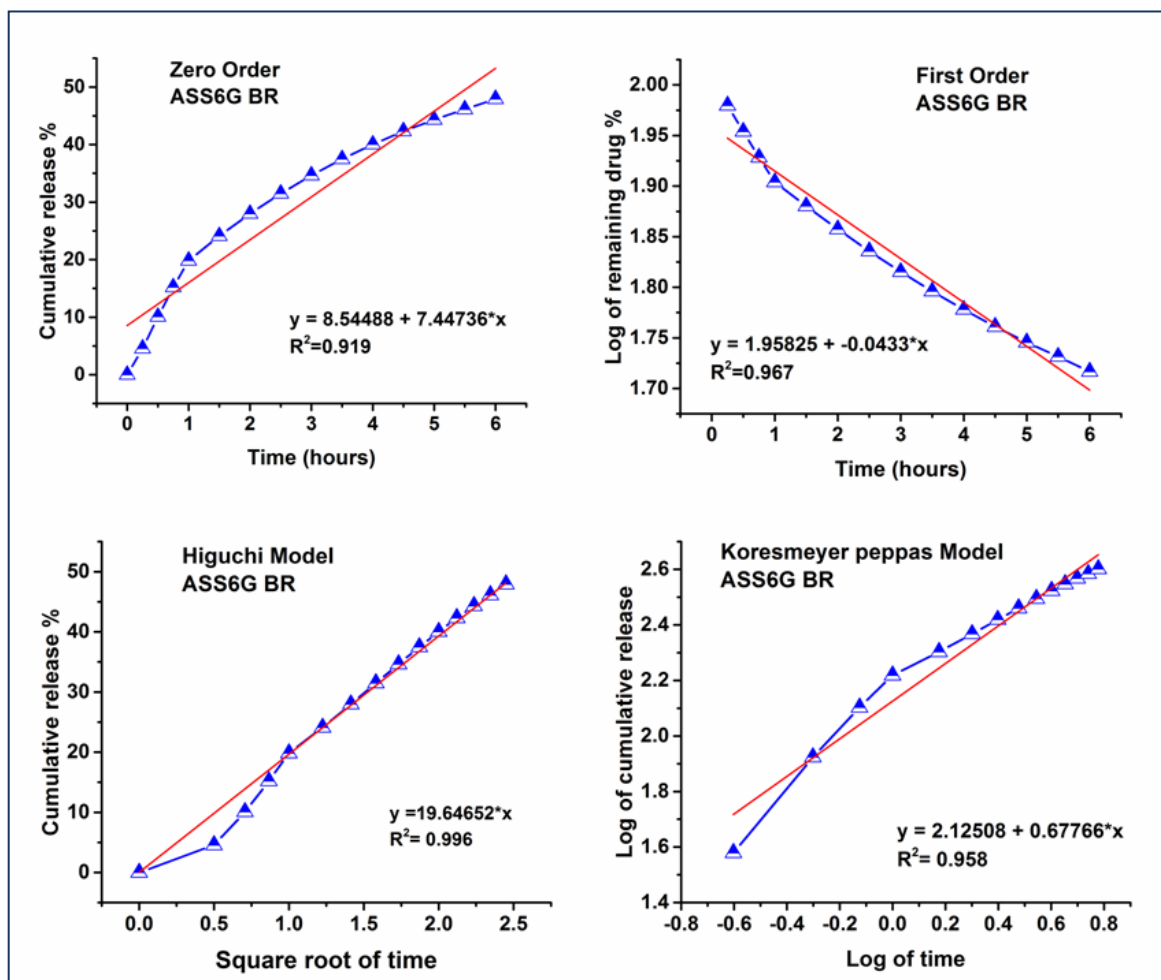

Fig 4.37: Kinetic models of Aloin released for first 6 hours from SS6 silica in SGF medium

Table 4.30: Kinetic data of Aloin obtained from SS6 sphere SiO₂ in SGF medium

Sample name	Zero order (R^2 value)	First order (R^2 value)	Higuchi model (R^2 value)	Korsmeyer-peppas (R^2 value)	Korsmeyer-peppas n=release exponent
Aloin	BR	BR	BR	BR	BR
SS6	0.919	0.967	**0.996**	0.958	2.12

Based on this regression coefficient value the best fitted model for burst release of aloin from SS4 in SGF is Higuchi model. As the release exponent value is >0.89, the release mechanism is supercase II transport.

4.8.2.2.F Release kinetic models of Aloin from SS6 sphere SiO₂ in SGF for 24-168 hours:
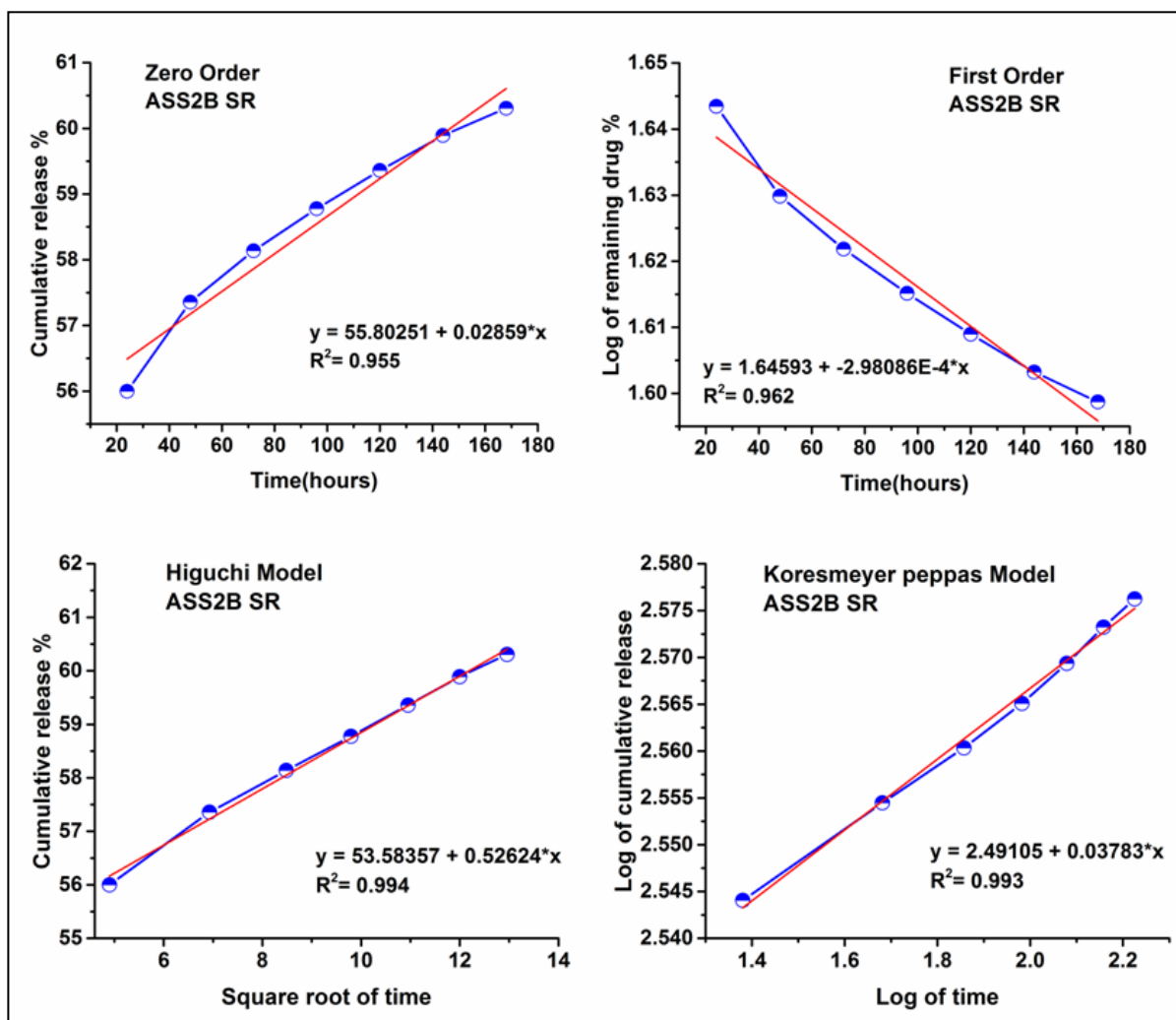

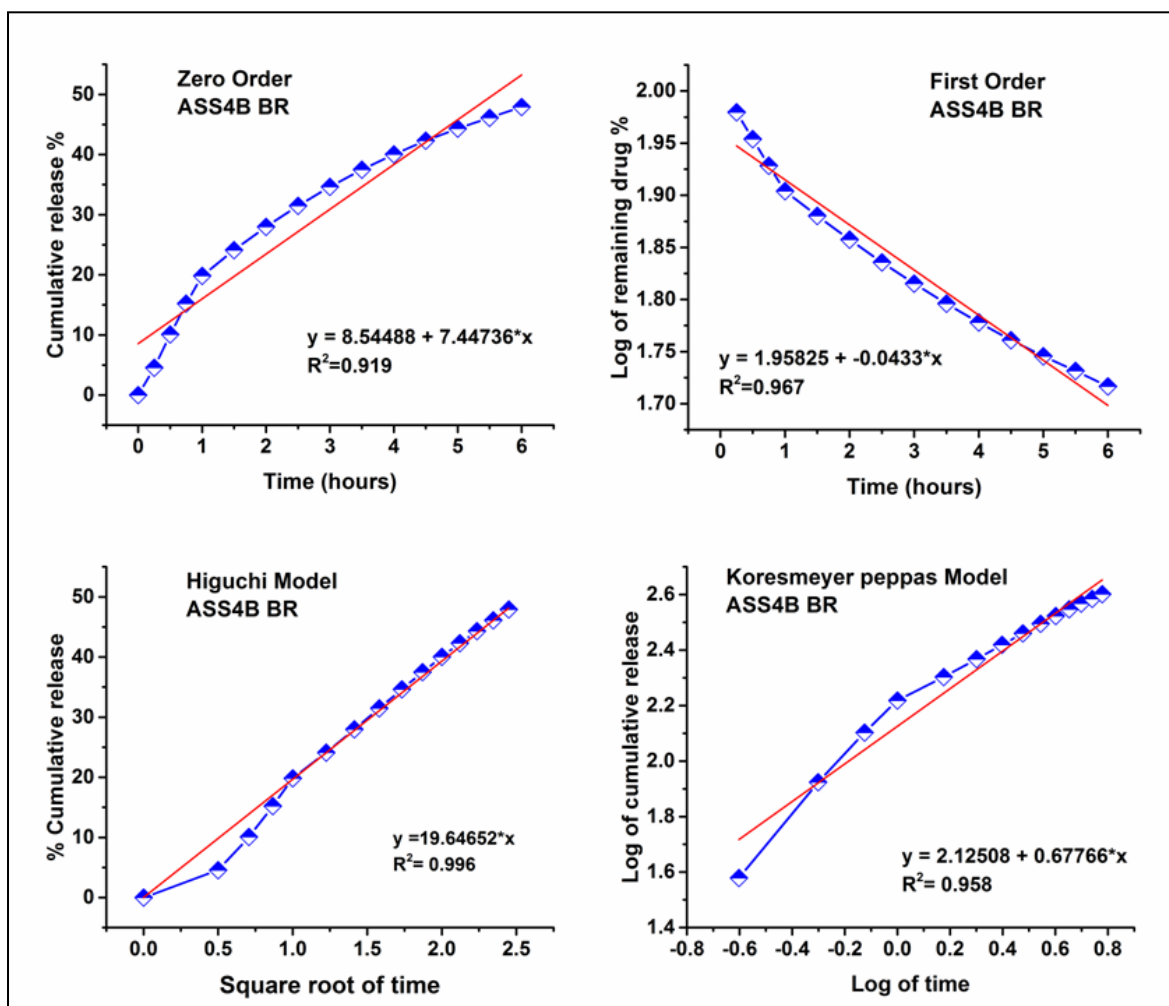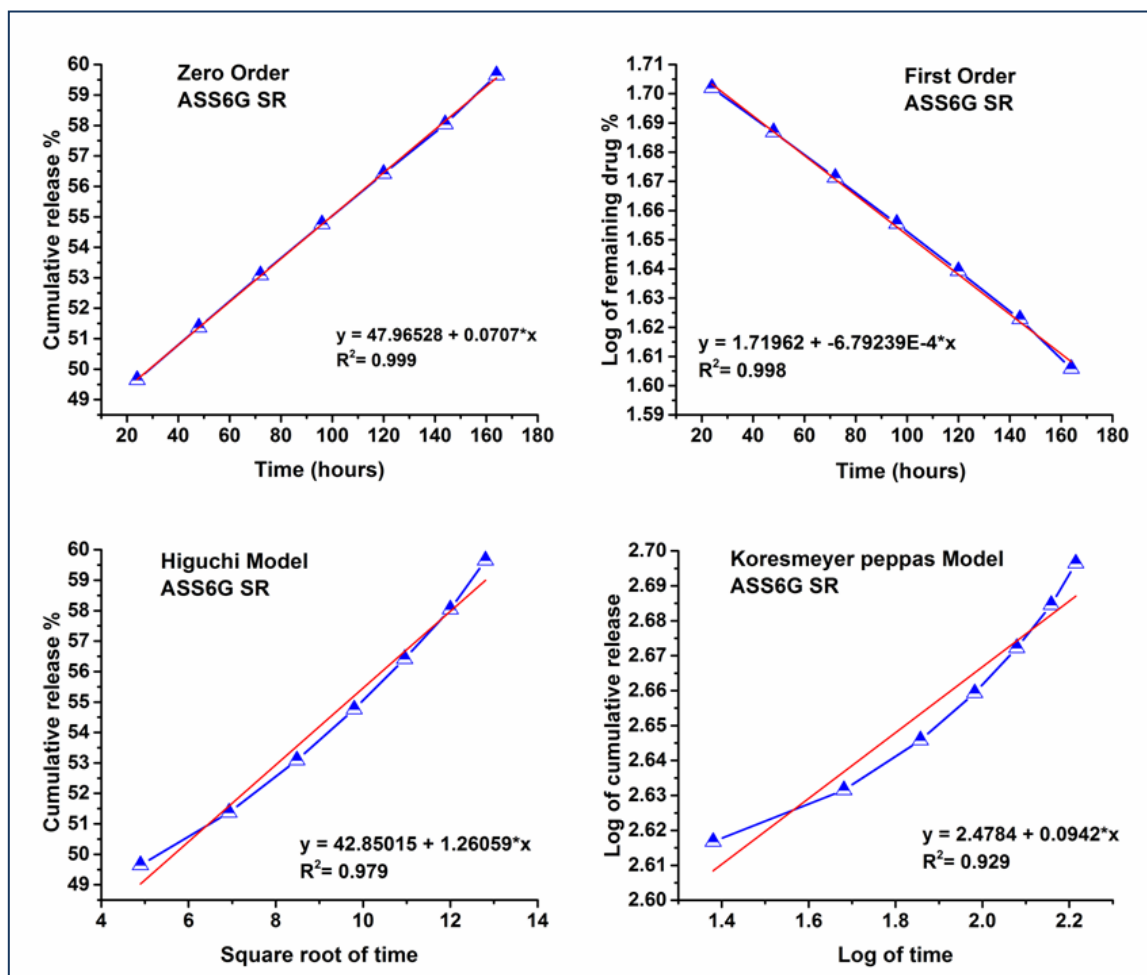**Fig 4.38: Kinetic models of Aloin released for 24-168 hours from SS6 silica in SGF medium**

Table 4.31: Kinetic data of Aloin obtained from SS6 sphere SiO₂ in SGF medium

Sample name	Zero order (R^2 value)	First order (R^2 value)	Higuchi model (R^2 value)	Korsmeyer-peppas (R^2 value)	Korsmeyer-peppas n=release exponent
Aloin	SR	SR	SR	SR	SR
SS6	**0.999**	0.998	0.979	0.929	2.47

Based on this regression coefficient value the best-fitted model for the sustained release of aloin from SS6 in SGF is the Zero-order model. As the release exponent value is >0.89, the release mechanism is supercase II transport.

From all the release data, the highest percentages of the release of drugs from the respective carriers are to be considered for the next application part. Morphology as well as the porosity of SiO_2 nanoparticle is the main key factor for the adsorption of the drug followed by a release in the medium. Here, one more important thing is the nature of the drug mainly the solubility of the drug. To mimic the in vivo condition, two different pH medium is used for drug release 1.2 and 7.4 for oral and intravenous delivery respectively. Here aloin is more soluble in acidic pH because of its physical nature. So, the highest percentage of release is seen in the SGF medium compared to the SBF medium. In the case of both structures, the same nature is observed. Besides this porosity of the nanoparticles along with the surface area insist on the release percentage for specific time duration. To examine all the applications, one released sample from the two highest percentages along with the raw drug are used.

Based on the regression coefficient values of all the kinetic models best fitted models are obtained. All the regression coefficient values are given to the respective tables along with the graphs. Kinetic models of released aloin in SBF & SGF are summarized and given in table 4.32.

Table 4.32: Kinetic model of Aloin released from SiO_2 in SBF & SGF

Sl no	Sample name	Dissolution medium	Burst release	Sustained release
1	SS2	SBF	Higuchi model	Higuchi model
		SGF	Higuchi model	Higuchi model
2	SS4	SBF	Higuchi model	First order model
		SGF	Higuchi model	Higuchi model
3	SS6	SBF	Higuchi model	Koresmeyer peppas model
		SGF	Higuchi model	Zero order model

Morphology of the silica nanoparticles mainly the surface area of the nanoparticles and the nature of both the drugs and dissolution medium are responsible for the percentage dissolution of aloin in SBF & SGF. Since, porosity of S6 SiO_2 samples are more on the surface compared to S2, more drug is not released from S6 in short time as drugs are adsorbed within pores of the sample. Since aloin is basic in character, dissolution of aloin in SGF (pH-1.2) is more compared

to SBF (pH-7.4). Again release of aloin is more from sphere shaped SiO_2 than irregular shaped SiO_2 because availability of higher surface area.

4.9 Antimicrobial activity assay:

4.9.1 Bacteria strain preparation: *Salmonella typhi* was procured from the American Type culture collection (ATCC). The bacterial strain was cultured in nutrient broth (NB) for 24 hours at 37°C in a BOD incubator at 150 rpm with agitation.

4.9.2 MIC study: According to the CLSI guidelines, the broth microdilution method is used to find out the MIC (minimum inhibitory concentration) and MBC (minimum bactericidal concentration) values. The MIC assay is performed in a flat-bottomed microtiter 96-well plate with a standard broth dilution method. Here the chemical compound means the drug is serially twofold diluted from the stock concentration starting with the 1st column to 12th column. Column 1st belongs to the highest concentration and 12th is the lowest concentration of the drug. 10 µL of 0.5 McFarland standard concentrated bacterial inoculum suspensions as culture is added to each well. Then the 96 well-plate is incubated for 24 hours at 37°C. All the experiment is performed in triplicate. MIC is defined as the lowest concentration of antibacterial agent which can inhibit the growth of microbial suspension. MBC value is the concentration of antimicrobial agent that completely kills the bacteria on the agar plate. MBC assay is performed on an agar plate. Here actually the suspension from each well of the microtiter plate is plated on an agar plate. The agar plates are incubated at 37°C overnight. The lowest concentration which results in no visible growth on the agar plate regarded as MBC value.

Table 4.33: MIC values of Aloin over *S. typhi* bacteria

Sl no	Microoganism used	Aloin concentration
1	*Salmonella typhi*	2.5 mg/ml

4.9.3 Zone of Inhibition Study: The antimicrobial activity of aloin against the previously selected gram-negative water-borne pathogen *S. typhi* is carried out using the disk diffusion process by the Kirby-Bauer method. At first 24 hours fresh culture of *S. typhi* bacterial strain is

prepared. From that fresh culture, 0.5 McFarland standard concentrated bacterial culture is considered as culture medium and spread out on the nutrient agar plate using an autoclaved sterile spreader. The disks are already dipped into drug solutions and soaked for 30 minutes. Then these disks are put on the four quadrants on the plate respectively mentioned as different concentrations. Four different concentrations are prepared from the stock concentration of drug aloin. These four concentrations are prepared based on the MIC values of aloin over *S. typhi* bacteria. ½ MIC, MIC, 2MIC, and 4 MIC concentrations are considered as a sample for aloin drug to see the differences in the effect of the above concentrations. A bar graph (Fig 4.39) is prepared for the drug aloin using the data obtained after 24 hours of incubation in a BOD incubator at 37° C after this assay.
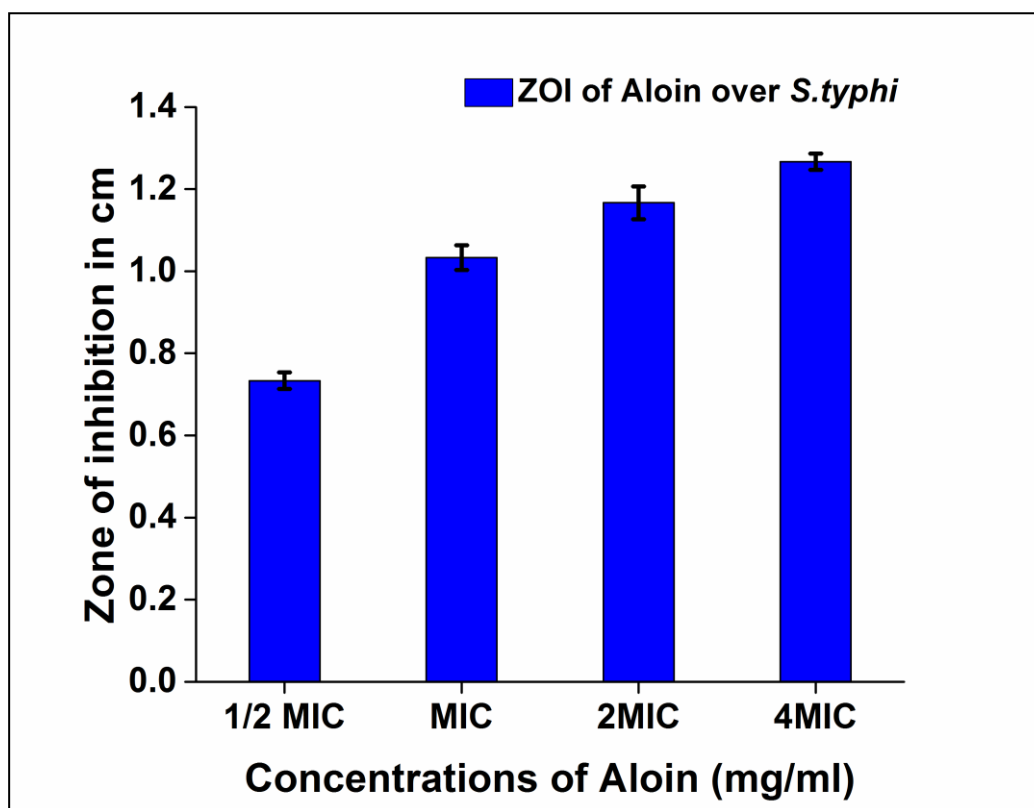
Fig 4.39: Zone of inhibition study results of Aloin over *S. typhi*
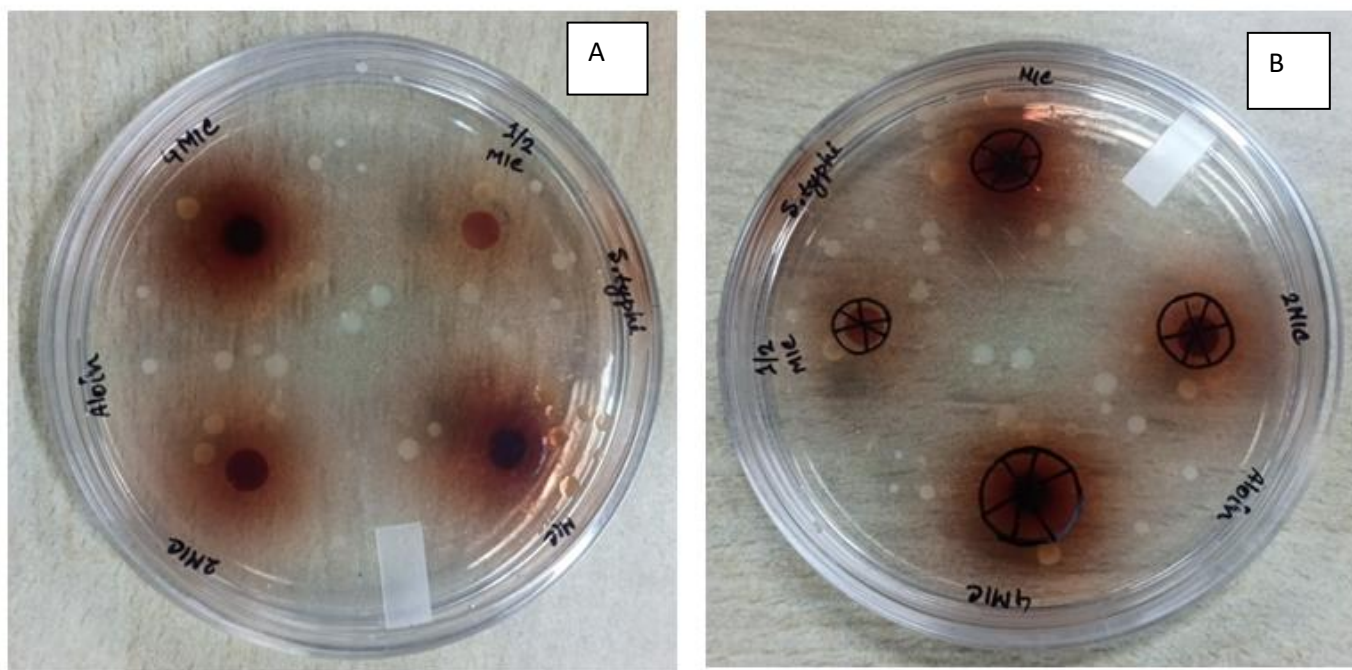
Fig 4.40: Nutrient agar plate of zone of inhibition study of aloin over *S. typhi*. Figure A & B both represent the same picture. How the zone of inhibition is measured shown in figure B

This assay concludes a distinct difference in the concentration effect of any drug over the bacterial growth or inhibition of growth. Theoretically, as concentration increases from lower to higher zone of inhibition is increased. In the case of aloin, the highest concentration and lowest concentration reflect their colour as the drug is colourful. The result of this assay is determined over an eye inspection. Always the measurement is taken three times as depicted in the picture and the mean data is reflected in the above bar graph. The MIC value is enough capable of inhibiting the growth of bacteria. If we want that much affectivity, the calculated amount over MIC concentration should be entrapped within the carriers. This amount will depend upon the drug loading efficiency of the drug within the nanocarriers.

4.9.4 Growth Curve Analysis: 24 hours fresh culture of *S. typhi* is taken to perform this assay. The culture is incubated in 25 ml nutrient broth medium containing different concentrations (½ MIC, MIC, 2MIC, and 4 MIC) of prepared drugs at 37˚C for 6 hours with 150 rpm shaking. After incubation, the optical density is measured at 600 nm through UV Vis spectrophotometer.
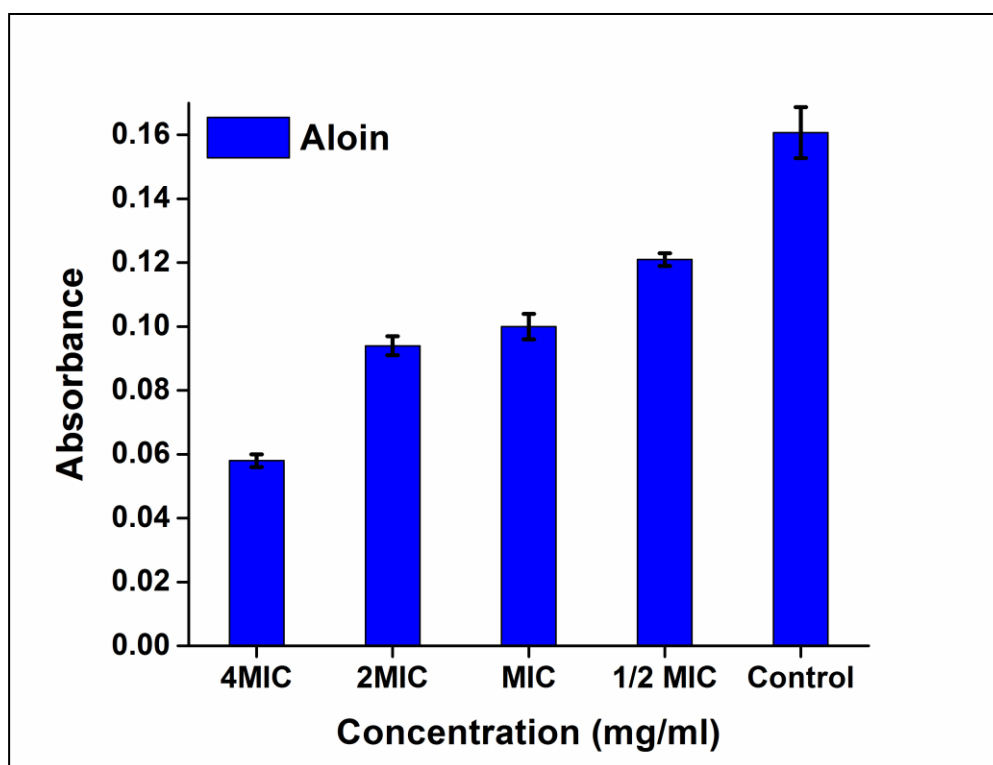
Fig 4.41: Growth curve of *S.typhi* after treatment with Aloin

Even if comparing to the control 4MIC concentration and MIC concentration percentage of inhibition is much higher in 4MIC concentration with respect to control growth. If judged against all the concentrations the MIC value is the strongest one which can destroy the highest percentage of the bacterial population represented in a bar diagram of Fig 4.41.

4.9.5 CFU Count Study: Continuation with the growth curve analysis assay, 10 μL of aliquots from each container having different concentrations (½ MIC, MIC, 2MIC and 4 MIC) of drug with *S. typhi* microorganism is taken and spread on agar media with a spreader. Before spreading the spreader is either sterilized with ethanol or autoclaved. These agar plates are incubated at 37 ˚C for 24 hours. Next day the plates are taken and colonies are counted. The whole procedure is done in triplicate and the mean value is considered final.

Table 4.34: Number of colonies of *S. typhi* microorganism over the drug Aloin at the respective concentration

Drug	ASS2G	4MIC	2MIC	MIC	½ MIC	Control
Aloin CFU	56	5	29	39	112	226

As depicted in the growth curve (Fig 4.41), MIC gives a significant low count compared to control in both drugs though a number of colonies vary with the drugs.

4.9.6 Microscopic analysis: After completing all the above assays microscopic analysis is done to observe the actual morphological changes affected by the drugs on *S. typhi* bacteria. The procedure of preparing bacterial strain to get some beautiful SEM pictures. Here, the treated bacterial sample with aloin along with the control bacterial sample is prepared for microscopic view maintaining the proper procedure given in the flowchart. In one step a serial dilution of ethanol is used from 70%, 80%, 90%, and 100% at 25˚C (1*10 min). Before use pH is measured of PBS at 7.3. All the procedure is done at room temperature.
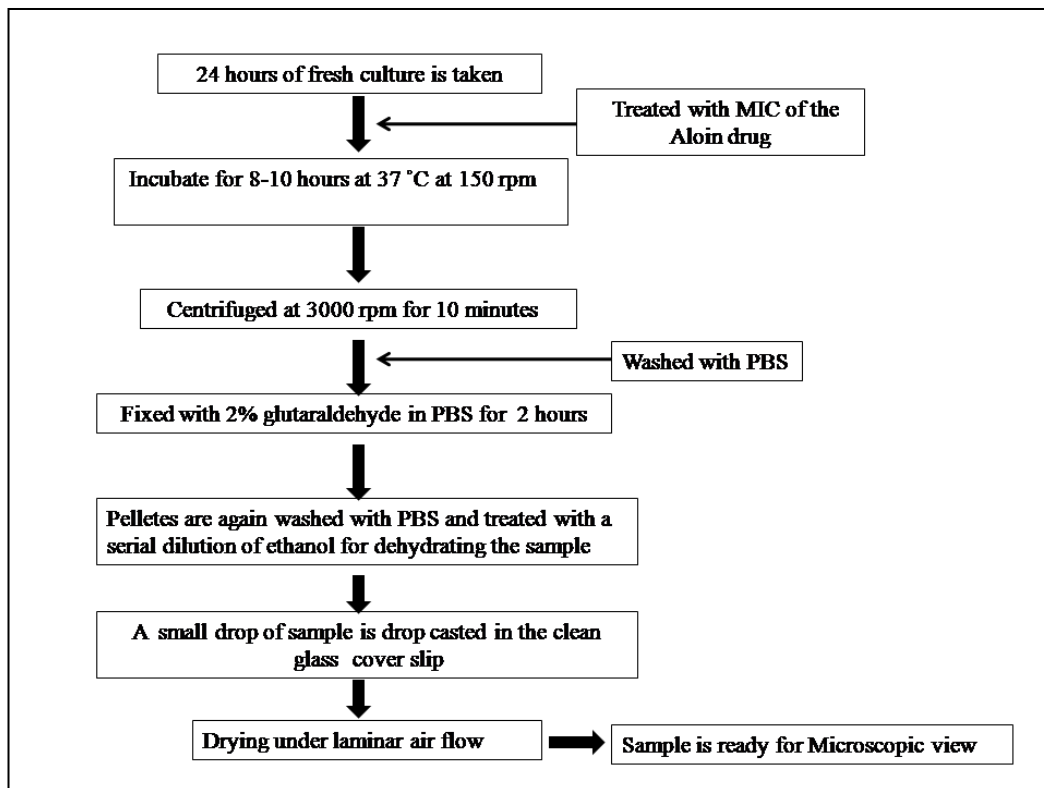
Fig 4.42: Flowchart of preparation of bacterial sample for microscopic analysis
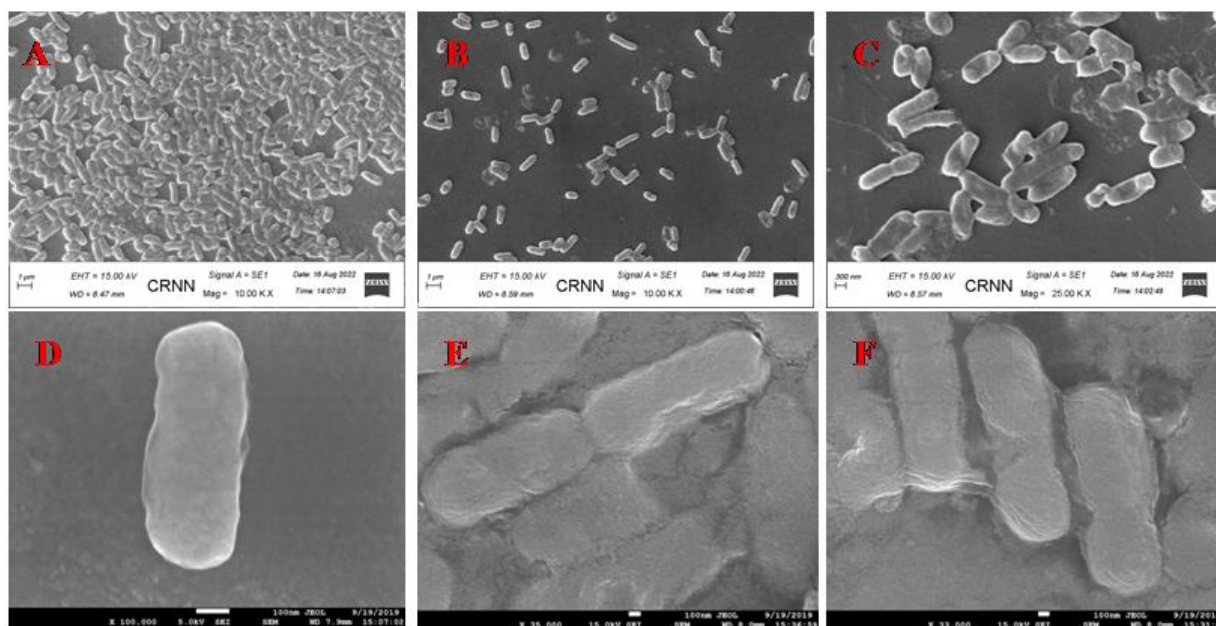
Fig 4.43: Microscopic view of control *S. typhi* bacteria (A-F)
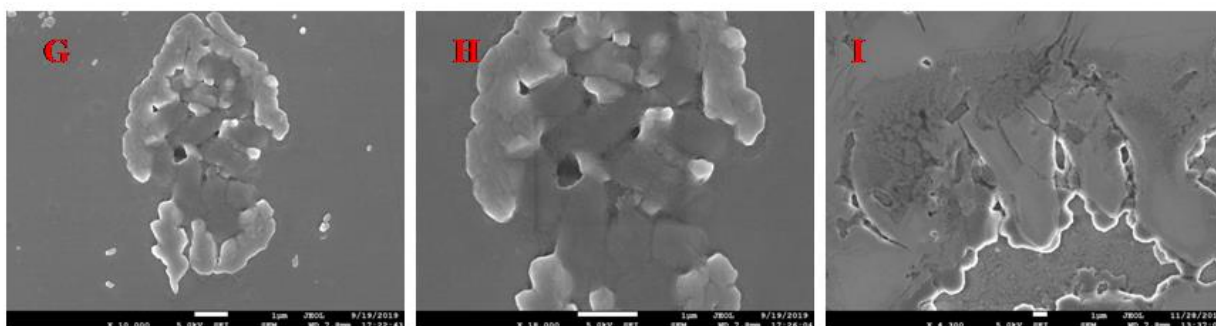
Fig 4.44: Microscopic view of *S. typhi* after treatment with Aloin (G-I)

Result: Microscopic analysis revealed the structure of bacteria treated with sustained released drugs from drug-entrapped nanocarriers. Numerous mechanisms are reported regarding the mode of action of aloin over the microorganism. Here the cell wall of all the bacteria was deformed; they became smaller in size, mostly fused together, and appeared almost like the cell wall deficient L forms after treatments. Aloin or aloe-emodin (metabolites of aloin) can interacts with cell wall protein resulting in increases permeability of outer fluids causing bacterial death as well as it cause interference in membrane and respiration transport.

4.10 Anticancer assay:

In this study, aloin is used over the HCC cell line HepG2. To see the effectiveness of aloin against this cancer cell line followings assays are done with established procedures.

4.10.1 MTT assay:

MTT (3-(4,5-dimethylthiazol-2-yl)-2–5-diphenyltetrazolium bromide) assay is one of the most commonly used colorimetric assays to assess cytotoxicity or cell viability. This assay determines principally cell viability through the determination of the mitochondrial function of cells by measuring the activity of mitochondrial enzymes such as succinate dehydrogenase. In this assay, MTT is reduced to purple formazan by NADH (nicotinamide adenine dinucleotide (NAD) + hydrogen (H).The NADH produced by the body is involved in making energy in the body. This product can be quantified by light absorbance at a specific wavelength. [14]

Additional control experiments should be conducted to reduce false-positive or false-negative results caused by background interference due to the inclusion of particles. This interference could lead to an overestimation of cell viability. This can often be controlled by subtraction of the background absorbance of the cells in the presence of the particles, but without the assay reagents. [15]

Procedure:

HepG2 cells are grown in DMEM (Dulbecco's minimal Essential Medium) supplemented with 10% heat-inactivated FBS (fetal bovine serum) and antibiotics such as penicillin, streptomycin, and amphotericin B. The cells are cultured in 12 well plates in an atmospheric condition of 5% CO_2 and 95% air at 37 C for 48-72 hours. After proper incubation, cell growth is monitored by microscopic examination. If suitable growth is observed then these cells are allowed for the experiment. This experiment is the assessment assay for cell viability. The whole assay is done in 96 well plates in quintuplicate and the mean value is considered.

At first, drugs are diluted in 100-10ug/ml concentrations to see the IC_{50} value. Cells are seeded with DMEM media and treated with a defined dose of drugs 10μl each followed by 1-hour incubation. After incubation 10 μl MTT reagents are added for at least 4 hours. After 4 hours 100 μl solubilizing agent is added to solubilize the MTT crystal and kept for 24 hours. The next

day,the absorption density is measured at 570 nm. As a control, only DMEM media, only cells within the media, and media with drugs of each dilution is given.
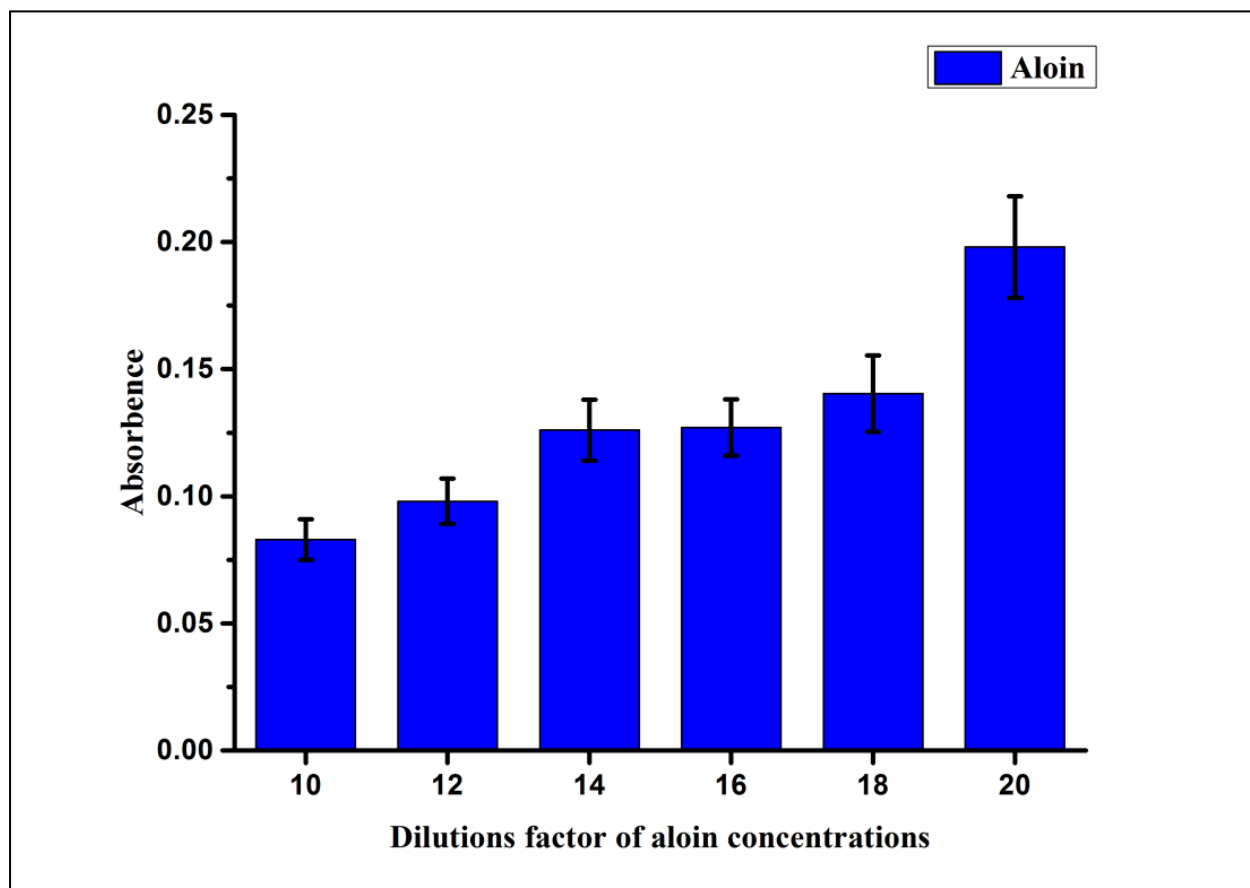
Fig 4.45: Graphical representation of absorbance with concentrations of Aloin. Aloin is diluted 10 to 20 times from the stock concentration. Absorbance is directly proportional to the living cells present in the respective wells

Result: As the concentrations decrease of drug aloin automatically number of living cells is increasing in the respective wells. This data is recorded from spectrophotometric analysis. The IC_{50} value is the 12th dilution of aloin. But for the chemical and sample colours, this data may misinterpret sometimes. To confirm this experimental data methylene blue assay is also done.

4.10.2 Methylene Blue assay:

Live cell examination or cell counting is an important technique in the molecular biology section. Here this technique is the key determination technique for cell cytotoxicity measurement, cell growth, cell proliferation, cell doubling time determinations etc. There are many traditional cell counting methods already applied over time but some limitations influence the resulting methods. Such as the trypan blue method miscalculates the cell number whereas the lowry protein method results differently over the cell cycle in culture medium.

In the trypan blue staining method some of the cells in culture media degrade in the trpsinization step due to the breakage of chromatin by the trypsin enzyme. As a result cell number decreases which underestimates the overall cell count. This affects the accuracy of hemocytometer cell count.

In the lowry protein method, the results are directly proportional to the protein content of cells. But this protein content fluctuates over every stage of the cell cycle because protein production of a cell increases in the G2 phase as well as decreases at G0 phase. Therefore the cell number is fixed but the protein content is varying over time. So, in this situation, cell number cannot be directly proportional to the protein present. [16]

An urgent need exists for a method of cell counting that is both accurate and versatile and can perfectly distinguish between living and dead cells on the culture plate.

In 1984 a modified methylene blue assay is introduced by Finley et al to measure the cytotoxicity of drugs, phytochemicals, and any natural compounds on the treated cell lines. Compared with trypan blue assay cell protein accumulation in the G2 phase does not affect methylene blue assay and direct cell counting or live dead cell differentiation. This assay interprets the interactions between the adherent cell lines with applied drugs especially how the drug reacts with internal compounds like hormones, inhibitors, nutrients etc. [17]

Procedure:

HepG2 cells are grown in DMEM (Dulbecco's minimal Essential Medium) supplemented with 10% heat-inactivated FBS (fetal bovine serum) and antibiotics such as penicillin, streptomycin,

and amphotericin B. The cells are cultured in 12 well plates in an atmospheric condition of 5% CO_2 and 95% air at 37 C for 48-72 hours.

After incubation, the cells are detached and seeded into 06 well plates and cultivated in an incubator at 37°C with 5% CO2 for 48 hours to pursue the methylene blue staining assay. Here the concentrations of drugs are considered at IC_{50} values. This assay is analyzed with inverted microscopic observations.
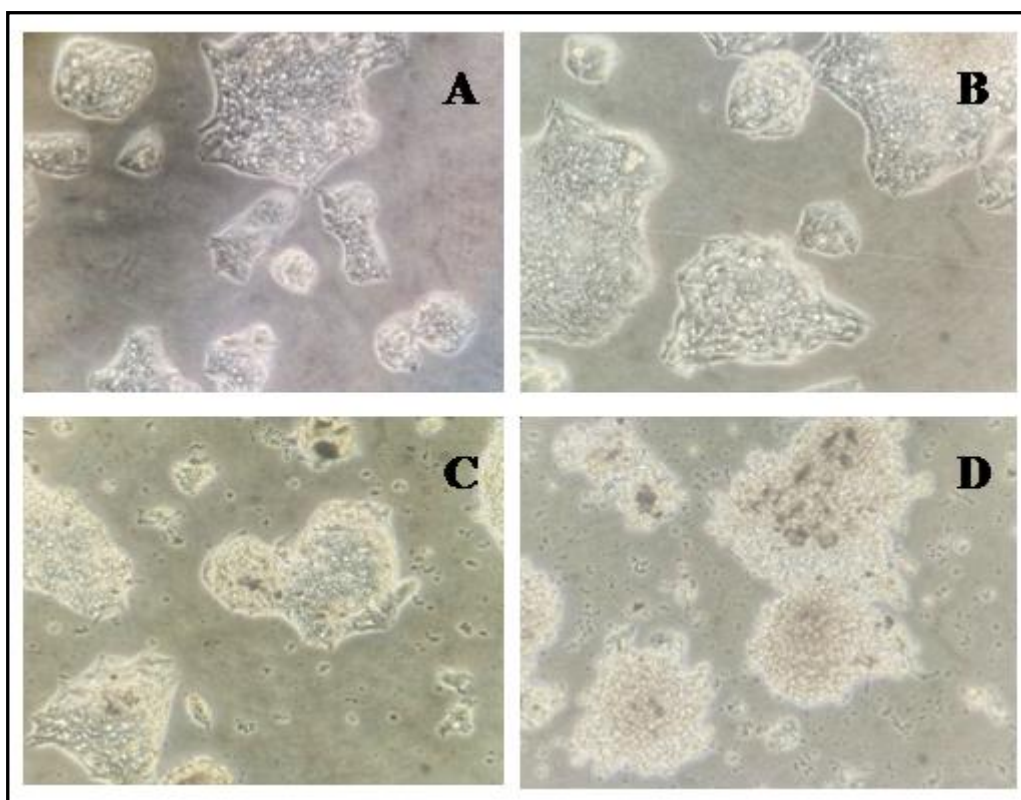
Fig 4.46: Microscopic analysis of HepG2 cell lines in set of methylene blue assay. For control sample freshly cultured and 24 hr incubated bare HepG2 cells are considered. HepG2 cells of 0 hr and 24 hr incubation (A) and (B) respectively for control sample. 1 hr and 24 hr incubation of HepG2 cells with Aloin treatment (C) and (D) respectively
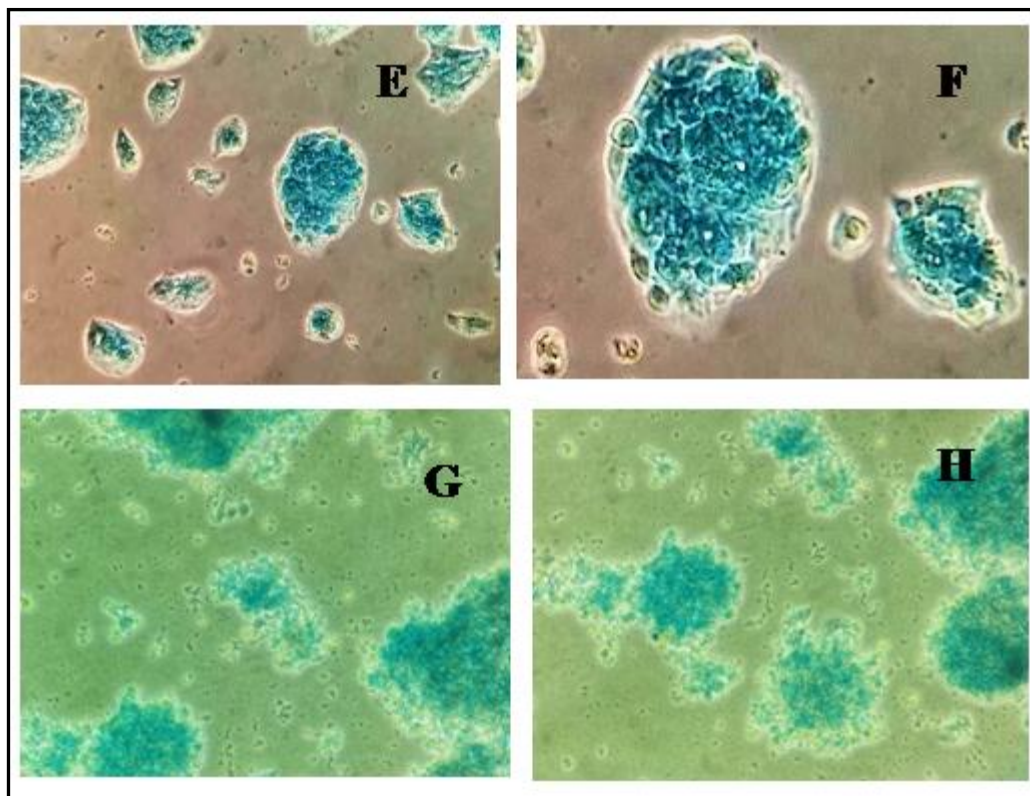
Fig 4.47: Figure E & F represent the control cells with methylene blue staining and G&H represent Aloin treated HepG2 cells of methylene blue staining

At first, the seeded cells are rinsed with PBS gently to remove excess media from the wells. Then predetermined volumes of drugs are given to the wells followed by incubation of 10 hours at 37°C. After that appropriate volume of methylene blue solution is added to each well of 6 well culture plate which includes a homogenous mixture of HBSS + 1.25% glutaraldehyde + 0.6% methyleneblue. Microscopic observations of samples are done at 0 hr incubation, 1 hr incubation, and 24 hours of incubation. After 24 hours of incubation the culture plate is washed with PBS and microscopic analysis is done.

All the microscopic observations are depicted in Fig 4.46 & 4.47. The selected drug aloin treated HepG2 cell lines are subjected to methylene blue assay to interpret the effectivity of drugs over the cell line. To compare the effectiveness control cell line was also presented. After treatment with aloin, to study the effectiveness of the drugs the well plates are stained with methylene blue. Methylene blue stains both nuclei and cytoplasm of both living and dead cells. If methylene blue

is applied to live cells, enzymes present within live cells reduce the dye and become colourless which dead cells cannot. So, dead cells remain blue in colour and live cells become white after PBS wash. It is prominent that aloin treatment affects almost 80-90% of cells that are dead represented in figure 4.47.

Results:

All the microscopic observations are depicted in Fig 4.46 & 4.47. The drug-aloin-treated HepG2 cell lines are subjected to methylene blue assay to interpret the effectiveness of the drug over the cancer cell line. To compare the effectiveness control cell line (Fig 4.46.A, 4.46.B) also presented. After treatment with aloin, to study the effectiveness of the drugs the well plates are stained with methylene blue. Methylene blue stains both nuclei and cytoplasm of both living and dead cells. If methylene blue is applied to live cells, enzymes present within live cells reduce the dye and become colourless which dead cells cannot. So, dead cells remain blue in colour and live cells become white after PBS wash. In the case of aloin treatment, this is prominent that 80-90% of cells are dead represented in figure 4.47.

4.11 Antiviral assay:

For the antiviral assay, Delta SARS-CoV-2 spike RBD protein is selected as a viral agent. The total experiment is done in *Gallus gallus* domesticus chicken eggs. To do the experiment chicken eggs from the Government State Poultry Farm in Kolkata, India, which are embryonated at 13 days old and free of pathogens, are purchased. To clean the eggs' surface distilled water and rectified spirit are used. Then the cleaned eggs are candled and incubate each at 38°C and 60–80% humidity. On the fourteenth day, the eggs were divided into seven distinct groups. All groups, with the exception of the normal control, injected 100 μL of each sample material a tiny whole done by a sterilized syringe which actually goes to the amniotic sac. Following inoculation, the eggs were candled, rotated three times throughout the day, and incubated as previously stated. 5–10 mL of allantoic fluids were collected in sterile vials and stored at 80 °C for further analysis after 48 hours (on the 16th day) of incubation. Before that, all the eggs are exposed at 2–8 °C for 2 hours. Besides this, each embryo's physical conditions were observed.

Table 4.35: All the sample name with their code for antiviral experimental analysis

Sl no	Sample name	Sample code
1	Aloin raw	AR
2	Aloin released in SBF	ARS
3	Ag challenged by Aloin raw	DAR
4	Ag challenged by Aloin released in SBF	DARS
5	SBF Control	SC
6	Ag challenged by SBF control	DSC
7	Antigen	AG

To conduct comparative gene expression studies real-time PCR with dNTPs, Taq polymerase, MgCl2, buffer, and SYBR Green-tagged primers are used. The changes in expression are compared to the housekeeping gene ß-actin and calculated as a fold increase or decrease from the value of the normal control.

Table 4.36: Increase in cytokines (fold increase in comparison with normal control) in different experimental sets after 48 hours

SET	IFNα	IFNß	IL-6	IL-8	IL-1B	IL-10
AR	8026.95	54.16	4.39	0.158	41.21	734.18
ARP	811.68	179.66	211.57	194.68	60.8	385.34
DAR	30.06	23.98	122.36	51.44	70.27	1016.92
DARP	39.64	11.29	193.34	89.57	84.23	680.28
SC	0.27	7.05	0	0	0.29	0.88
DSC	4	2.89	15.08	20.75	12.51	13.64
AG	1692.57	149.09	7.285	3.02	2.02	2.94
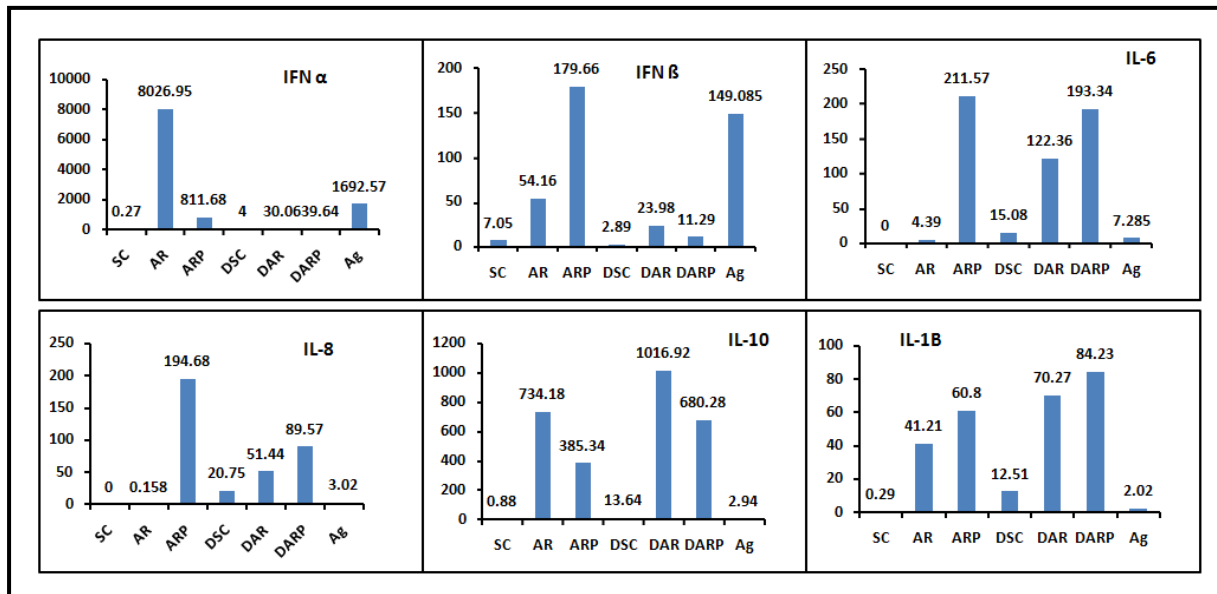
Fig 4.48: Relative fold change in expression of selected gene in respect of housekeeping gene ß-actin
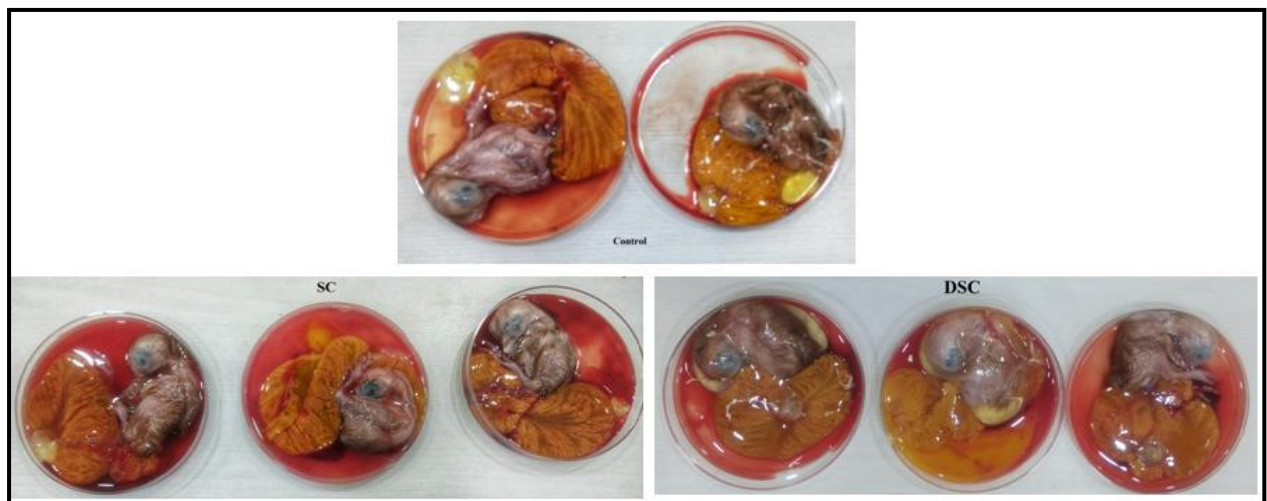
Fig 4.49: Egg embryo picture after 48 hours of incubation of control samples
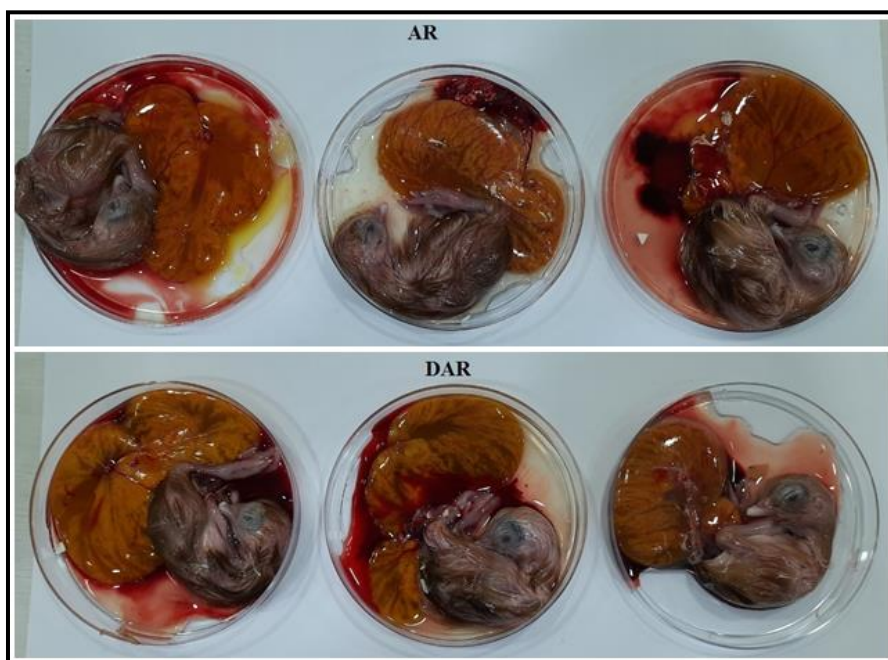
Fig 4.50: Picture of egg embryo after treated with Aloin raw (AR) and Ag challenged by Aloin raw (DAR)
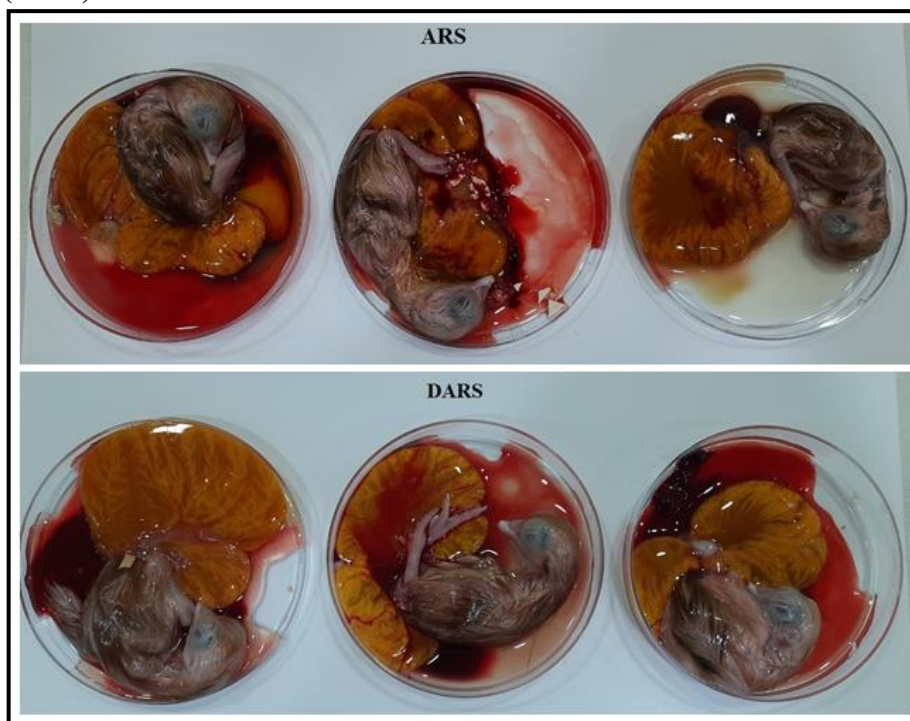
Fig 4.51: Picture of egg embryo after treated with Aloin released (ARS) and Ag challenged by Aloin released (DARS) from nanoparticles

Results:

IFNα: Raw aloin markedly increased IFNα gene expression, and direct antigen and aloin released in SBF significantly increased IFNα gene expression. In all other experimental sets, IFNα gene expression is mildly increased.

IFNβ: Raw aloin, direct antigen, and aloin released in SBF increased IFNβ gene expression, and in preventive sets with aloin this gene expression is mildly increased.

IL-6: Although raw aloin could decrease IL-6 gene expression increased by direct antigen, in preventive experiments with this, the gene expression is increased.

IL-8: Similar findings like IL-6 gene expressions were also observed, with IL-8 gene expression.

IL-1β: In all experimental sets with aloin, IL-1β gene expression was increased.

IL-10: It is important to note that direct antigen could not increase IL-10 gene expression significantly. However, with raw aloin and in the preventive sets with aloin, this gene expression was increased much more than all the pro-inflammatory gene expressions.

Aloin in the preventive experimental sets in the chicken egg model could counteract, and prevent damaging action of pro-inflammatory cytokines IL-6, IL-8 and IL-1β by increasing gene expression of anti-inflammatory cytokine IL-10. It indicates that aloin could prevent the damage of different organs in a cytokine storms, which is the main pathogenic factor in morbidity and mortality in SARS-CoV-2 infections, mediated mainly by the S-protein of the virus. IFNα and IFNβ are also mildly increased indicating a beneficial role in this condition.

4.12 Conclusion:

Amorphous SiO_2 nanocarriers of irregular shape & sphere shape are synthesized by sol gel method using acid and base catalyst. XRD study confirms the amorphous nature of SiO_2 nanopaticles. BET study reveals the surface area and it is observed that spherical SiO_2 nanoparticles have more surface area compared to irregular shaped SiO_2 nanopaticles of same ratio of precursors TEOS, ethyl alcohol and water. SEM microphotographs help to see the images of irregular shaped and sphere shaped SiO_2 nanopaticles. The size of SiO_2 sphere nanopaticles is found to be in the range of 25-140 nm.

Aloin is extracted in ethanol medium and entrapped in both type of SiO_2 nanocarriers. The entrapment of aloin in SiO_2 nanopaticles is confirmed by FTIR analysis. Presence of C=C-C within 1600-1680 cm^{-1}, C-O-C within 1050-1250 cm^{-1} stretching in FTIR plot of aloin entrapped SiO_2 nanopaticles confirms the presence of aloin phytochemicals within SiO_2 nanopaticles.

Aloin is released from SiO_2 nanocarriers into SBF & SGF and the cumulative dissolution percentage is calculated using UV-Vis spectrophotometer. It is observed that 68% aloin is released in SGF and 52% aloin is released in SBF for irregular shaped SiO_2. Whereas, dissolution percentage of aloin is increased in both media in case of sphere shaped SiO_2 nanoparticles. In this case 81% and 60% aloin is released in SGF and SBF media respectively. Nano carriers with high surface area and higher percentage of released drug are considered to be better for application in drug delivery. So, the process parameters for the synthesis of silica nano carrier as a porous substrate for use in drug delivery is optimized at 1: 2: 1 of TEOS: ethyl alcohol: water with CTAB surfactant in basic medium.

Release kinetics study (both burst and sustained release) of aloin in SBF & SGF for irregular shaped and sphere shaped SiO_2 is carried out. In each case using regression coefficient model the best fitted kinetic model is identified.

Release kinetic study of aloin in SBF from three different irregular shaped silica nano carriers reveals that burst release of aloin from samples S2 & S4 fit to first order model and S6 best fit to Higuchi model. Sustained release of aloin from sample S2, S4 & S6 of the same set of silica samples in SBF follows koresmeyer peppas model. Burst & sustain release aloin in SGF from S2

& S4 follow first order kinetic model, whereas, release from S6 set is found to match zero order and higuchi model for burst and sustained release respectively. In every model 'n' value is greater than 0.89 that means all release mechanisms are super case II transport.

In the kinetic study of release of aloin from three different sphere samples of silica nano carriers in SBF, burst release from SS2, SS4 & SS6 fit to Higuchi model whereas, sustained release from SS2, SS4 & SS6 follows higuchi model, first order model and koresmeyer peppas model respectively. For release of aloin in SGF, burst release from all three types of silica samples match to higuchi model. Sustained release from SS2 and SS4 fit to higuchi model and release from SS6 samples follows zero order model. In every model 'n' value is greater than 0.89 indicating all release mechanisms are super case II transport.

In the application part, released aloin from irregular and sphere shaped are compared and highest percentage of released aloin is considered for the applications as already mentioned. The highest aloin release is found to the very effective as an antimicrobial agent for *Salmonella typhi* bacteria. The MIC value calculated is 2.5 mg/ml. The zone of inhibition is 1.66 mm for MIC concentration. The CFU count is 56 for *S. typhi* with released aloin which is close to the CFU count when treated at MIC value of aloin. Microscopic view shows the deformation of bacterial sample comparing to the control sample after treatment with released aloin.

In anticancer study, at first IC_{50} value of pure drugs is determined. For this aloin drugis diluted from 10 to 20 times from a stock concentration of 1mg/ml. From spectrophotometric analysis IC_{50} value is obtained as 12th dilution for aloin which is considered for methylene blue assay. In the methylene blue assay dead cells are present as debries. After treatment with IC_{50} concentration of aloin, it is found to be highly effective for HCC cancer cell line.

In the antiviral assay it is observed that aloin can prevent damaging action of pro-inflammatory cytokines IL-6, IL-8 and IL-1β by increasing gene expression of anti-inflammatory cytokine IL-10. It indicates that aloin could prevent the damage of different organs in a cytokine storms, which is the main pathogenic factor in morbidity and mortality in SARS-CoV-2 infections, IFNα and IFNβ are also mildly increased by aloin action indicating a beneficial role in this condition.

References:

1.M. Manzano and M. Vallet-Regí, Mesoporous Silica Nanoparticles for Drug Delivery, *Adv. Funct. Mater.* 2020, *30*, 1902634

2. M. Ramos, L. Toledo ,G. Calixto , B. Bonifácio , M. Araújo , L. Santos ,M. Almeida, M. Chorilli and T. Bauab, Syngonanthus nitens Bong. (Rhul.)-Loaded Nanostructured System for VulvovaginalCandidiasis Treatment, Int. J. Mol. Sci. 2016, 17, 1368; doi:10.3390/ijms17081368

3. F. Arriagada , G. Günther , J. Nos , S. Nonell , C. Olea-Azar and J. Morales, Antioxidant Nanomaterial Based on Core–Shell Silica Nanospheres with Surface-Bound Caffeic Acid: A Promising Vehicle for Oxidation-Sensitive Drugs, Nanomaterials 2019, 9, 214; doi:10.3390/nano9020214

4. P. K. Bharti; U.K. Niyogi, Plankton diversity and aquatic ecology of a freshwater lake (L3) at Bharti Island, Larsemann Hills, east Antarctica.Global J. Environ. Sci. Manage., 1(2): 137-144, Spring 2015

5. H. Hanif, S. Nazir, K. Mazhar, M. Waseem, S. Bano, U. Rashid, Targeted delivery of mesoporous silica nanoparticles loadedmonastrol into cancer cells: an in vitro study, Appl Nanosci (2017) 7:549–555, https://doi.org/10.1007/s13204-017-0593-8

6. G. C. Carvalho, R. M. Sabio, M. Chorilli,An overview of properties and analytical methods for lycopene in organic nanocarriers, Critical reviews in analytical chemistry, 51(7); 1-13.

7. M. L. Kaushik,&S. S Jalalpure, Asian Journal of Pharmaceutical and Clinical Research. *Asian Journal ofPharmaceutical and Clinical Research*, 2011; *4*(3), 9–11.

8. P. Pukkela , S. Borra . Machine Learning Based Plant Leaf Disease Detection and Severity Assessment Techniques: Stateof- the-Art. Lecture Notes in Computational Vision and Biomechanics: Springer International Publishing; 2017. 199-226.

9. R. K. Nariyal, P. Kothari,& B. Bisht, FTIR Measurements of SiO2 Glass Prepared by Sol-Gel Technique. *ChemicalScience Transactions*, 2014; *3*(3), pp. 1064–1066.

10. P. Innocenzi, infrared spectroscopy of sol gel derived silica based films: a spectra-microstructure overview. Journal of non-crystalline solids 316,2003, 309-319.

11. D. Dutta , B. Paul , B. Mukherjee , L. Mondal , S. Sen , C. Chowdhur & M. Chatterjee Debnath, Nanoencapsulated betulinic acid analogue distinctively improves colorectal carcinoma in vitro and in vivo,Scientific Reports 2019, *9:11506.*

12. J. Coates, interpretation of infrared spectra, apractical approach. Encyclopedia of analytical chemistry R A Meyers 9Ed0 copyright Q john wiley & Sons Ltd.

13. S. Dash, P. Narasimha Murthy, L. Nath, P. Chowdhury, Kinetic modeling on drug release from controlled drug delivery systems, Acta Poloniae Pharmaceutica n Drug Research, 2010, 67. 3; 217-223.

14. T. Mosmann. Rapid colorimetric assay for cellular growth and survival: Application to proliferation an cytotoxicity assays. Journal of Immunological Methods. 1983;65(1-2):55-63

15. O.S. Aslantürk, T. Aşkın Çelik , B. Karabey , F. Karabey , Active phytochemical detecting,antioxidant, cytotoxic, apoptotic activities of ethyl acetate and methanol extracts ofGalium aparine L. British Journal of Pharmaceutical Research. 2017;15(6):1-16

16. O. H. Lowry, N. J. Rosenbrough, A. L. Farr,&R. J. Randall, Protein measurement with the Folin phenol reagent. Journal of Biological Chemistry, 1951, 193, 265–275.

17. G. J. Finlay, B. C. Baguley, &W. R. Wilson, A semiautomated microculture method for investigating growth effects of cytotoxic compounds on exponentially growing carcinoma cells. Analytical Biochemistry, 1984;139, 272–277.

CHAPTER 5

Release kinetic study of garlic (Allium sativum) from SiO$_2$ nano carrier and its application

5.1 Introduction: Phytochemicals present in herbs is an important aspect now a day due to their lethal property on microorganisms as well as fewer side effects compared to chemically synthesized drug. There is a better future for herbal medicine if it blends with nanotechnology. Nanomaterials have the capability to invade all the biological membranes present in our body. If phytochemicals are being entrapped within any nanomatrix then it will be very trouble-free for the particular herbal values to reach any part of the body in undamaged condition. [1] Mesoporous silica nanomaterial (MSNs) has attracted much interest as a carrier of holding drugs. The physical properties of silica nanomaterial (like shape, size, porosity, mesostructureetc), and chemical natures (like surface chemistry, surface functionalization, electric charge etc) can be molded as per experimental needs is why silica-based materials are very welcoming in the biological world. Inorganic porous silica materials are durable drug carriers compared to organic polymers because they can protect the loaded drug from any chemical or biological degradation efficiently. Silica materials also have the resistant power to *in vivo* microenvironment's interruption like changes in ion concentration, pH, and sometimes temperature, pressure etc as it has extremely high thermal stability and chemical inertness than other polymers. Mesoporous silica nanoparticles have a large surface area, multifunctional properties like integrating drug carriers, success in diagnostic and curative purposes, act as biocatalysts/ biosensing agents, and thus become more and more useful in the biological field. [2] The literature says in contrast with allopathic drugs, plant-based natural yields are paying special attention in chemo-prevention because they have less or no side effects. It has been noticed that naturally occurring phytochemicals like Diallyl disulfide (DADS) have many health-beneficial effects. DADS is one of the main constituents of garlic (*Allium sativum*) as well as in onions(*Allium cepa*) and it is also the major constituent of secondary metabolites. [3] There are almost 700 species that widely exist inthe world of genus Allium. [4] The species are dissimilar in taste and morphology but they areappreciated because of their easy growth, flavor, long storage time, and obviously their nearly similar phytochemical and biochemical property. The main constituent of these *Allium* species is organosulfur compounds which are the causative agents for organoleptic parameters. [5] These volatile constituents are the main parts of essential oils that have antioxidant and antimicrobial properties. [6-11] Alliin is the primary form of organosulfur compound which is transferred into allicin through the enzyme allinase after cutting garlic. Allicin is also an unstable compound and it immediately breaks down into its oil-soluble derivatives (essential oil) which

include diallyl sulfide (DAS), diallyl disulfide (DADS), diallyl trisulfide (DATS), vinyl dithiin and ajoene under their respective favorable conditions. [12] Banerjee et. al. & Kim et. al. have reported through GC-MS analysis that more than 94.63%of a constituent of garlic essential oil is organosulfur compounds. These organosulfur compounds include diallyl disulfide (37.90%), diallyl trisulfide (28.06%), allyl methyl trisulfide (7.26%), Diallyl sulfide (6.59%), Diallyl tetrasulfide (4.14%) and allylmethyl disulfide (3.69%). [13] These Diallyl sulfides show antimicrobial activity as well as antioxidant properties because of a greater number of sulfur atom spresent in them. So, the richness of sulfur atoms in garlic essential oil makes it more effective to exert above mentioned properties. [6,14,15,16] Among all the essential oils, diallyl disulfide (DADS) and diallyl trisulfide (DATS) is comparatively stable compounds. From the previous studies, it has been observed that drug metabolism and pharmacokinetics of organosulfur compounds from garlic have been generally restricted in rodents. Literature gives us information on metabolism and pharmacokinetics data mainly about DADS among all the organosulfur components of garlic. [12] Moreover, sulfide atoms do react with -SH groups of cellular proteins and generate mixed disulfides resulting in damage to microbial cells are reported by Mynaer et al 2014. [13] Different carriers for example liposomes, nanoparticles, and micro emulsion have been developed for the implementation of sustained release of the drug which enhances the bioavailability, systemic circulation, and constancy rate of the drug. Depending on the stable and active organosulfur components, a stable drug delivery system is prepared for the development of potential pharmaceuticals. The released molecules are evaluated as biopharmaceuticals. [12]

In this chapter, proper entrapment of DADS, the active component of *Allium sativum* in the different porosity containing silica nanoparticles and the study of release kinetics from the carrier as well as evaluation through kinetic modeling along with antimicrobial, anticancer, and antiviral properties is done.

5.2 Methodology

5.2.1 Synthesis of irregular shaped silica nanoparticles:

SiO_2 nanoparticles are synthesized by conventional sol-gel route with TEOS as the precursor for SiO_2. The process is discussed in detail in chapter 4. During the synthesis of silica nanoparticles hydrolysis of the silica precursor and subsequent condensation are the fundamental chemical reactions which are taking place at room temperature. The simultaneous happening hydrolysis and condensation reactions are multistep processes. In hydrolysis reaction alkoxide groups are replaced by hydroxyl groups which are acid catalysed. Condensation reactions result in the formation of a three-dimensional polymeric network through siloxane bridges.

The details procedure is mentioned in chapter 4 (section 4.2.1).

5.2.2 Synthesis of sphere-shaped silica nanoparticles:

Sphere-shaped silica particles are also obtained by sol-gel process with the addition of a base catalyst (NH_4OH) and a surfactant CTAB is also added to make uniform sphere molecules of silica particles. Here a white colour precipitation will result after the addition of catalyst. Then the dried white material is calcined and ready for characterization.

The details procedure is mentioned in chapter 4 (section 4.2.2).

5.3 Characterization of synthesized silica nanoparticles:

Synthesized silica nanomaterial is characterized by FTIR, XRD, SEM, and BET instruments. Details of this are already mentioned in chapter 3 (section: 3.3).

5.4 Results and discussions:

5.4.1 XRD Analysis:

Fig 4.5 & 4.6 of the previous chapter represent the XRD plot of synthesized SiO_2 nanoparticles. . Irregular and sphere shaped silica nanoparticles present of the hump at 3-15 degrees confirms the formation of SiO_2. Based on this technique the nature of the synthesized material can be

determined. Depending upon the physical property of any material like in which plane it is lying, the incident beam of X-ray behaves or is scattered accordingly. An amorphous silica nanoparticle gives a hump between 15-30 deg which authenticates the nontoxicity and biodegradability of the nanoparticles mentioned in chapter 4 (section 4.4.2).

5.4.2 FTIR Analysis:

The absorption band shown in the FTIR spectrum assures the formation of chemical bonding between the chemical used in the making of silica nanoparticles. The significant bond vibrations are present in the FTIR graph of synthesized silica nanoparticles already mentioned in chapter 4 (section 4.4.1) which give confirmation of the proper synthesis of the particles which can be used for further experiments.

FTIR spectrum (Fig 4.3 & 4.4) as shown in chapter 4 represents the bands present in SiO_2 nanoparticles are validating the XRD confirmation of SiO_2 nanoparticle formation.

5.4.3 BET Analysis:

This analysis gives an idea about the porosity, surface area, and pore volume of any porous material. Section 4.4.3 of chapter 4 describes the details of this analysis of different porosity and shape containing silica nanoparticles.

5.4.4 Microscopic Analysis:

All the synthesized silica nanoparticles have different sizes and shapes which are ultimately proven by the microscopic analysis. Where overall morphology, as well as distribution of particles, are also seen. The homogeneity of the particles is also verified by this. If there any different morphological particles are present or not. Different sets of microscopic view with the lowest and highest magnification are presented in chapter 4 (section 4.4.4)

5.5 Drug loading determination:

To determine the drug loading percentage, continuous stirring is used to disperse the DADS in a solution of 2% ethanol. Two milligrams of silica are added, and the mixture is stirred for at least 24 hours at 37 degrees Celsius and 250 rpm. The drug's concentration is determined using a UV-Vis spectrophotometer at 211 nm.

The loading percentage of a drug within any matrix or vehicle is determined through this equation (1)

$$\text{Drug loading \% (Actual)} = \frac{Amount\,of\,drug\,in\,nanoparticles}{Amount\,of\,nanoparticles} \times 100 \qquad (1)$$

Drug loading within the delivering carrier is an important parameter to evaluate the therapeutic efficacy of the particular drug delivery because it determines the administered formulation.

Encapsulation efficiency is determined through equation (2)

$$\text{Encapsulation efficiency (\%)} = \frac{Drug\,loading\,\%\,(Actual)}{Drug\,loading\,\%\,(Theoritical)} \times 100 \qquad (2)[17]$$

In each case, 5 mg drug DADS is encapsulated and during the drug loading procedure 2 mg nanoparticles of SiO_2 are taken**.**

Table 5.1: Sample name with drug loading and encapsulation efficiency

Sl no	Sample name	Drug loading (%)	Encapsulation efficiency (%)
1	DS2 (DADS entrapped irregular shaped S2 SiO_2)	0.3	71.44
2	DS4 (DADS entrapped irregular shaped S4 SiO_2)	0.33	87.22
3	DS6 (DADS entrapped irregular shaped S6 SiO_2)	0.4	91.62
4	DSS2 (DADS entrapped sphere shaped SS2 SiO_2)	0.71	95.75
5	DSS4 (DADS entrapped sphere shaped SS4 SiO_2)	0.54	94.05
6	DSS6 (DADS entrapped sphere shaped SS6 SiO_2)	0.52	93.92

From table 5.1 it is observed that with increase in drug loading %, encapsulation efficiency also increases.

5.6 Characterization of DADS entrapped silica particles:

5.6.1 FTIR analysis:
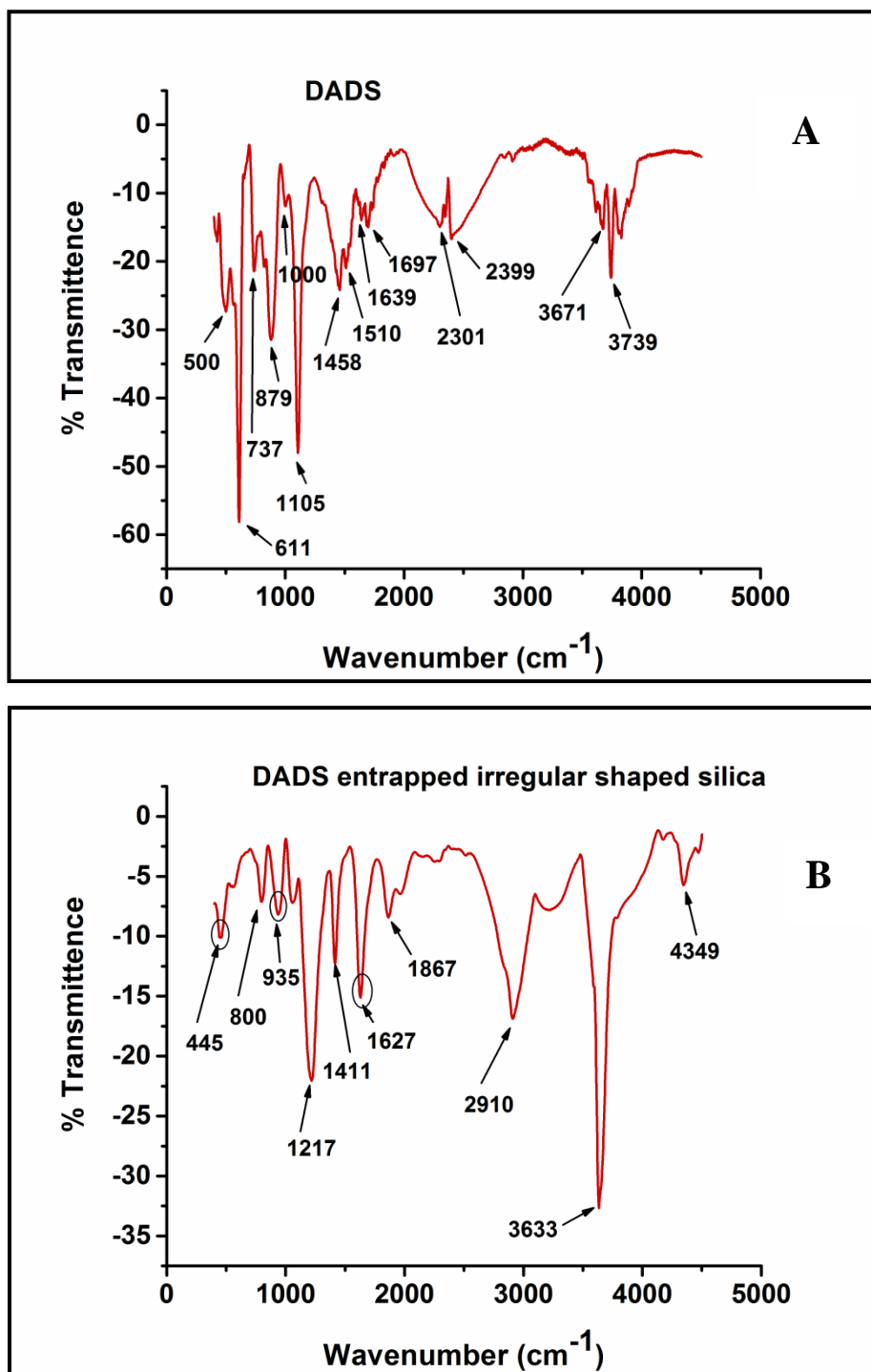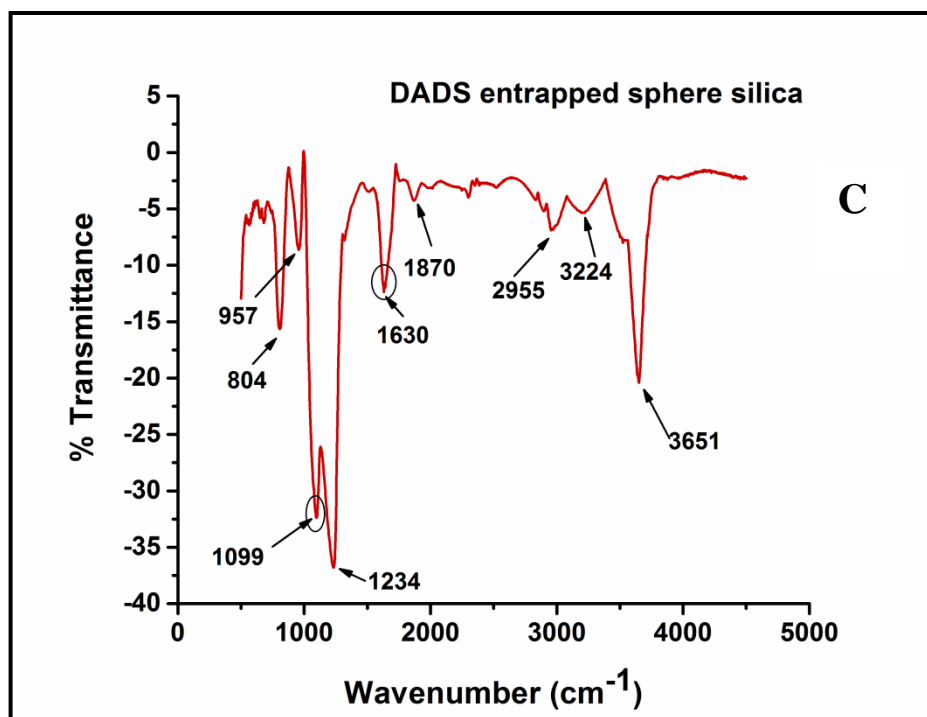
Fig 5.1: FTIR graph of pure DADS (A) and DADS entrapped irregular shaped silica (B) and DADS entrapped sphere silica (C) particles

Comparing with two graphs 5.1B & 5.1C with 5.1A, there are much new absorption found in the spectrum of dialyl disulfide entrapped irregular shaped silica and sphere shaped silica which is the result of DADS entrapment. 900-1100 cm^{-1} is for the C-S bond. 400-700 cm^{-1}is assigned to S-S stretching and 1600-1680 cm^{-1}comprise for C-C=C symmetric vibrations. In graph A 426 cm^{-1}is found for the bond vibration of S-S stretching which comes from diallyl disulfide compound which is red-shifted to 445 cm^{-1}in graph 5.1B [18]. 1000 cm^{-1} in graph A is responsible for the C-S bond which is reduced to 935 cm^{-1} in graph 5.1B and increased to 1099 cm^{-1} in graph 5.1C due to the entrapment of drug within it [19]. 1639 cm^{-1} vibration is reduced to 1627 cm^{-1} to graph 5.1B and 1630 cm^{-1} to graph 5.1C due to a blue shift [20]. All these vibrations confirmed the proper entrapment of diallyl disulfide within the irregular shaped and sphere shaped silica nanoparticles.

5.6.2 XRD analysis:
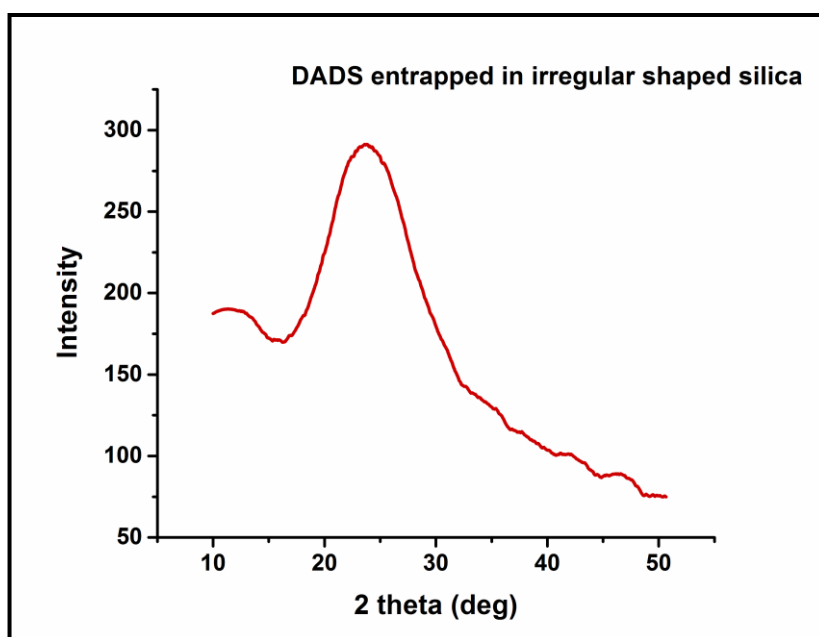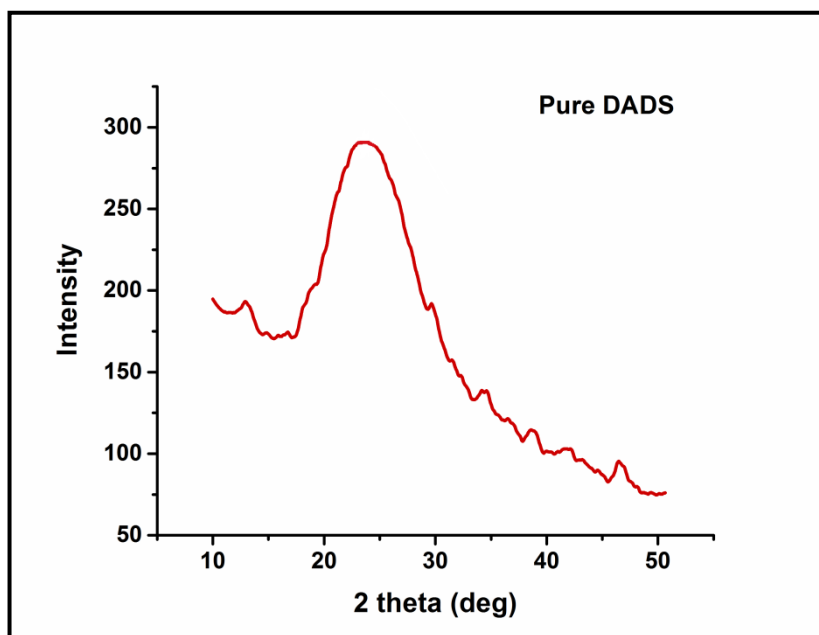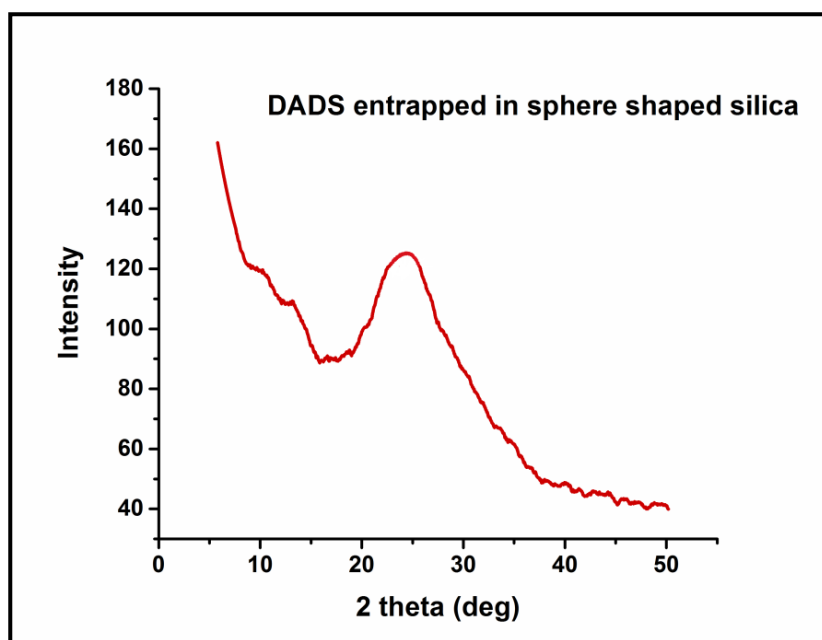
Fig 5.2: XRD analysis of DADS (A) and DADS entrapped irregular shaped (B) and DADS entrapped sphere (C) silica

There are such no differences between the two XRD graphs of pure DADS and pure DADS entrapped silica particles. This indicates that the property of bare silica along with drug-entrapped irregular and sphere silica shows similar amorphous nature. So, like bare silica these DADS entrapped silica carriers are nontoxic to the body and biocompatible.

5.7 Drug release studies:

The prepared drug silica nano conjugate i.e; DADS entrapped silica nanoparticle is immersed in two distinct release mediums, SBF and SGF, at 37 degrees Celsius in a BOD shaker at 110 rpm for 168 hours. During this time, a certain amount of medium is taken out at predetermined intervals, and immediately replaced with a new medium, and the collected sample is analyzed using a spectrophotometer. The absorbance values of the released DADS are used to calculate their concentrations over time using a standard curve. The entire experimental procedure is carried out in triplicate for each kind of drug-loaded silica.

Table 5.2: Cumulative release of DADS in SBF and SGF from different irregular shaped silica particles

Sl no	Sample name	% Cumulative Release
1	DS2B (DADS entrapped S2 silica, released in SBF)	36
2	DS4B (DADS entrapped S4 silica, released in SBF)	37
3	DS6B(DADS entrapped S6 silica, released in SBF)	39
4	DS2G (DADS entrapped S2 silica, released in SGF)	45
5	DS4G (DADS entrapped S4 silica, released in SGF)	53
6	DS6G (DADSentrapped S6 silica, released in SGF)	57
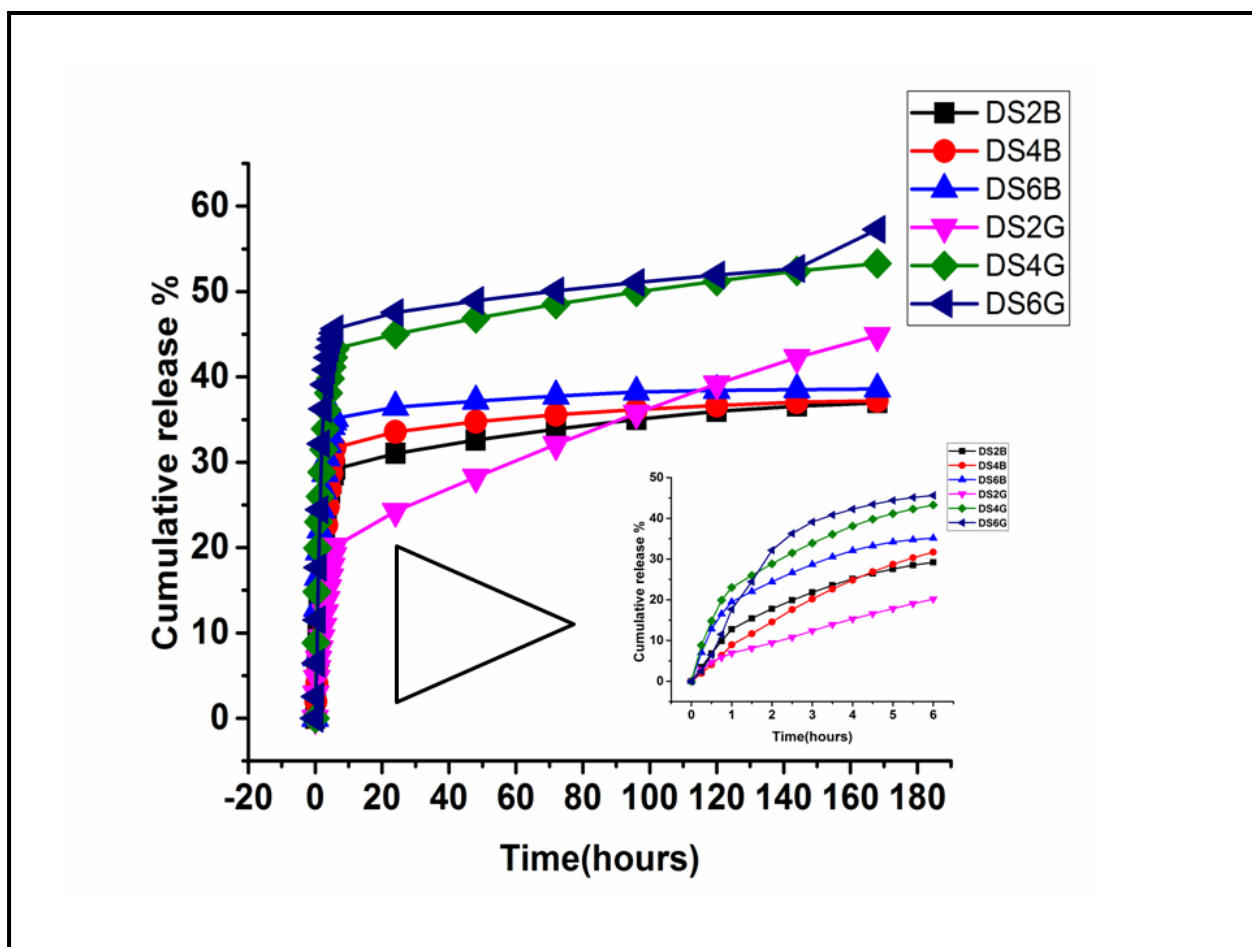
Fig 5.3: Dissolution profile of DADS in both SBF and SGF medium from irregular shape containing silica nanoparticles for both sustained and burst release

From the dissolution profile of DADS in both pH medium from irregular and sphere shaped silica it is observed that most cumulative release percentage is seen in SGF medium means at pH 1.2 for both structures. In irregular shaped silica highest percentage of release is seen from S6 samples. In sphere shaped silica highest percentage of release is seen from SS2 structure.

5.8 Release kinetic study:

5.8.1 Drug release profile and kinetic behavior study of DADS samples from different porosity containing irregular silica nanocarriers:

The in vitro drug release study is done in both SBF and SGF at room temperature in a BOD shaker for 168 hours. This release is biphasic in nature means shows rapid and slow release over the total time period of release. The release of DADS that is adsorbed on the surface of silica matrices is the cause of the burst release in the first phase. Additionally, a higher DADS concentration gradient between the silica matrices and the dissolution medium, in the beginning, was responsible for the drug's higher initial dissolution in the first phase. The drug is released from the three-dimensional polymeric network regions, where an internal tension exists, resulting in the sustained release. This sustained release part is primarily a slow process in the second phase of the entire release process. At physiological pH (pH = 7.4), silica has an equilibrium solubility of approximately 120 ppm, which enables the drug to quickly reach its saturation level. Because of this, the drug's rate of release slowed down, resulting in an incomplete release.

5.8.1.1.A Release kinetic models of DADS released from irregular shaped silica in SBF:

Fig 5.4: Kinetic models of DADS release for first 6 hours from S2 silica in SBF

Table 5.3: Kinetic data of DADS releasedfrom S2 irregular SiO₂ in SBF medium

Sample name	Zero order (R^2 value)	First order (R^2 value)	Higuchi model (R^2 value)	Korsmeyer-peppas (R^2 value)	Korsmeyer-peppas n=release exponent
DADS	BR	BR	BR	BR	BR
S2	0.906	0.942	**0.997**	0.966	0.99

Based on these kinetic models the best fitted model for burst release of DADS in SBF is Higuchi model. As the release exponent value is >0.89, the release mechanism is supercase IItransport

5.8.1.1.B Release kinetic models of DADS from S2 irregular SiO₂ in SBF for 24-168 hours:

Fig 5.5: Kinetic models of DADS released for 24-168 hours from S2 silica in SBF

Table 5.4: Kinetic data of DADS obtained from S2 irregular SiO₂ in SBF medium

Sample name	Zero order (R^2 value)	First order (R^2 value)	Higuchi model (R^2 value)	Korsmeyer-peppas (R^2 value)	Korsmeyer-peppas n=release exponent
DADS S2	SR 0.953	SR 0.958	SR **0.992**	SR 0.989	SR 1.33

Based on these kinetic models the best fitted model for sustained release of DADS in SBF is Higuchi model. As the release exponent value is >0.89, the release mechanism is supercase II transport.

5.8.1.1.C Release kinetic models of DADS from S4 irregular SiO₂ in SBF for first 6 hours:

Fig5.6: Kinetic models of DADS release for first 6 hoursfrom S4 silica in SBF

Table 5.5: Kinetic data of DADS obtained from S4 irregular SiO₂ in SBF medium

Sample name	Zero order (R^2 value)	First order (R^2 value)	Higuchi model (R^2 value)	Korsmeyer-peppas (R^2 value)	Korsmeyer-peppas n=release exponent
DADS	BR	BR	BR	BR	BR
S4	0.977	**0.989**	0.982	0.988	0.85

Based on these kinetic models the best fitted model for burs release of DADS in SBF is First order model. As the release exponent value is <0.89, the release mechanism is non Fickian transport.

5.8.1.1.D Release kinetic models of DADS from S4 irregular SiO$_2$ in SBF for 24-168 hours:

Fig 5.7: Kinetic models of DADS release for 24-168 hours from S4 silica in SBF

Table 5.6: Kinetic data of DADS obtained from S4 irregular SiO$_2$ in SBF medium

Sample name	Zero order (R^2 value)	First order (R^2 value)	Higuchi model (R^2 value)	Korsmeyer-peppas (R^2 value)	Korsmeyer-peppas n=release exponent
DADS S4	SR 0.932	SR 0.935	SR 0.984	SR **0.997**	SR 1.42

Based on these kinetic models the best fitted model for burst release of DADS in SBF is Koresmeyer peppas model. As the release exponent value is >0.89, the release mechanism is supercase II transport.

5.8.1.1.E Release kinetic models of DADS from S6 irregular SiO₂ in SBF for first 6 hours:

Fig 5.8: Kinetic models of DADS release for first 6 hours from S6 silica in SBF

Table 5.7: Kinetic data of DADS obtained from S6 irregular SiO₂ in SBF medium

Sample name	Zero order (R^2 value)	First order (R^2 value)	Higuchi model (R^2 value)	Korsmeyer-peppas (R^2 value)	Korsmeyer-peppas n=release exponent
DADS	BR	BR	BR	BR	BR
S6	0.829	0.908	**0.993**	0.955	1.20

Based on these kinetic models the best fitted model for burst release of DADS in SBF is Higuchi model. As the release exponent value is >0.89, the release mechanism is supercase II transport.

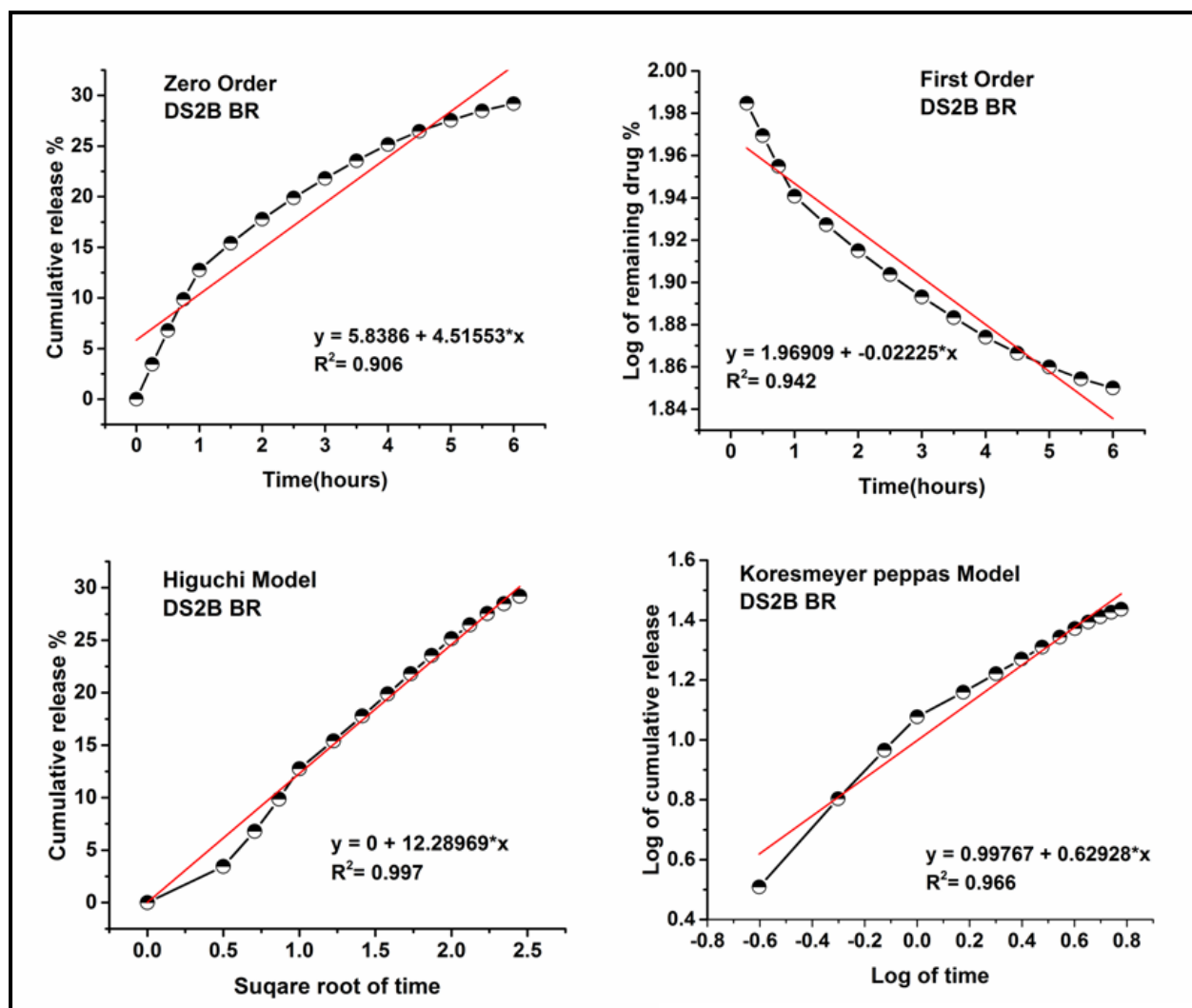**5.8.1.1.F Release kinetic models of DADS from S6 irregular SiO$_2$ in SBF for 24-168 hours:**

Fig 5.9: Kinetic models of DADS release for 24-168 hours from S6 silica in SBF

Table 5.8: Kinetic data of DADS obtained from S6 irregular SiO$_2$ in SBF medium

Sample name	Zero order (R^2 value)	First order (R^2 value)	Higuchi model (R^2 value)	Korsmeyer-peppas (R^2 value)	Korsmeyer-peppas n=release exponent
DADS	SR	SR	SR	SR	SR
S6	0.851	0.935	0.853	**0.979**	1.42

Based on these kinetic models the best fitted model for sustained release of DADS in SBF is Koresmeyer peppas model. As the release exponent value is >0.89, the release mechanism is supercase II transport.

5.8.1.2.A Release kinetic models of DADS from S2 irregular SiO₂ in SGF for first 6 hours:

Fig 5.10: Kinetic models of DADS for first 6 hours of release from S2 irregular shaped in SGF

Table 5.9: Kinetic data of DADS obtained from S2 irregular SiO₂ in SGF medium

Sample name	Zero order (R^2 value)	First order (R^2 value)	Higuchi model (R^2 value)	Korsmeyer-peppas (R^2 value)	Korsmeyer-peppas n=release exponent
DADS	BR	BR	BR	BR	BR
S2	0.974	**0.995**	0.994	0.994	0.79

Based on these kinetic models the best fitted model for burst release of DADS in SGF is First Order model. As the release exponent value is <0.89, the release mechanism is non fickian transport.

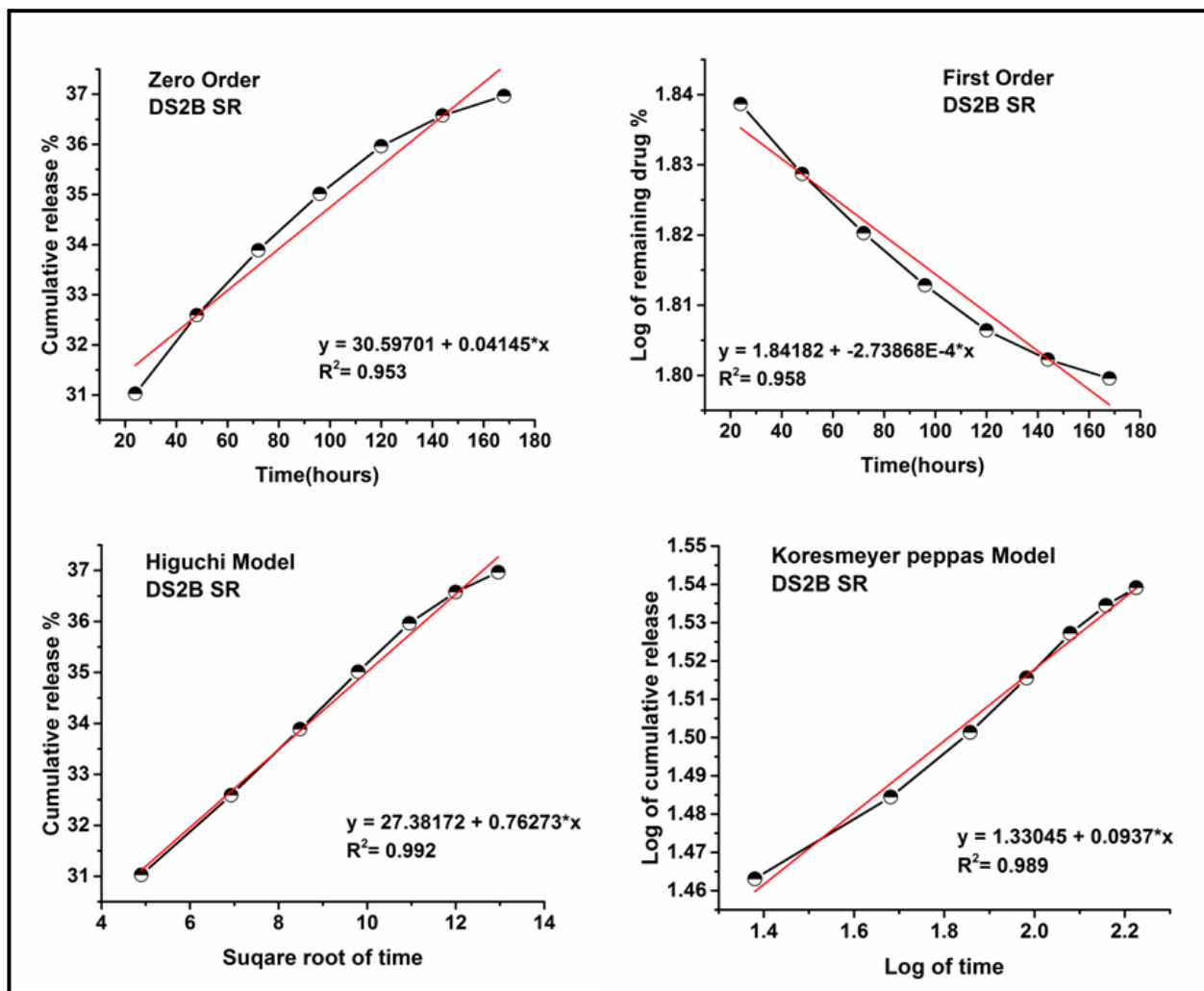**5.8.1.2.B Release kinetic models of DADS from S2 irregular SiO$_2$ in SGF for 24-168 hours:**
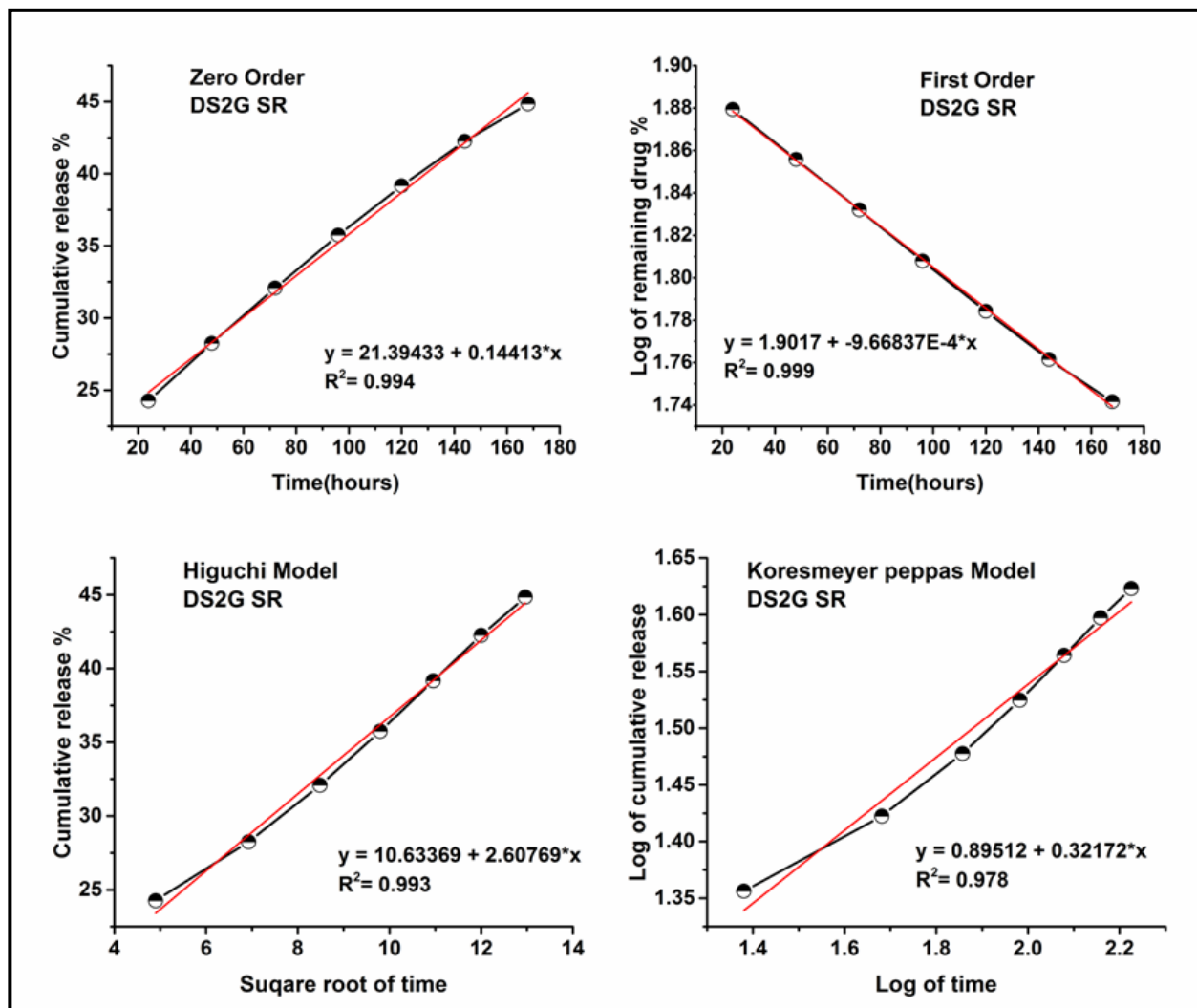
Fig 5.11: Kinetic models of DADS for 24- 168 hours of release from S2 irregular shaped in SGF

Table 5.10: Kinetic data of DADS obtained from S2 irregular SiO$_2$ in SGF medium

Sample name	Zero order (R^2 value)	First order (R^2 value)	Higuchi model (R^2 value)	Korsmeyer-peppas (R^2 value)	Korsmeyer-peppas n=release exponent
DADS S2	SR 0.994	SR **0.999**	SR 0.993	SR 0.978	SR 0.895

Based on these kinetic models the best fitted model for sustained release of DADS in SGF is first order model. As the release exponent value is >0.89, the release mechanism is supercase II transport.

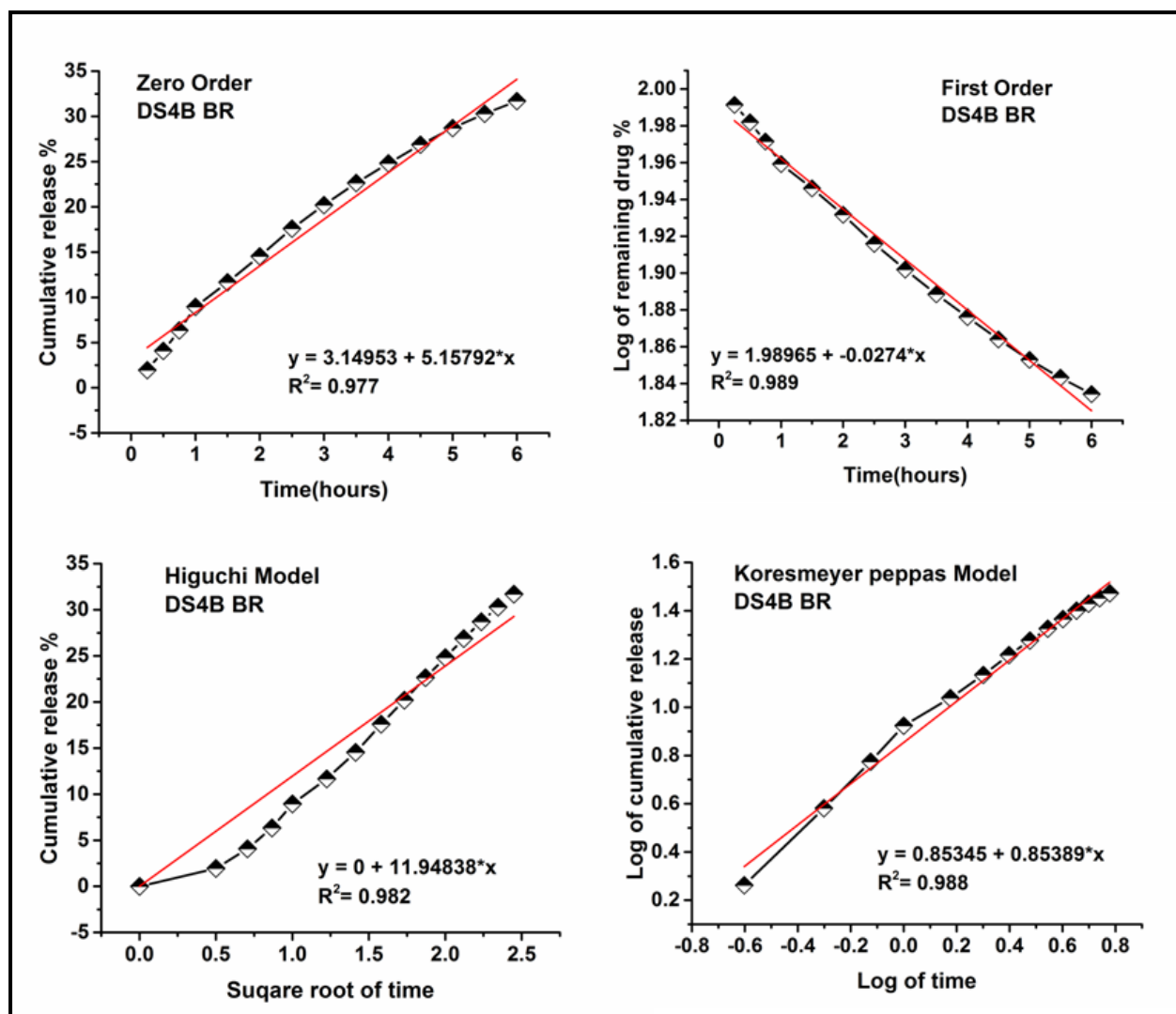**5.8.1.2.C Release kinetic models of DADS from S4 irregular SiO$_2$ in SGF for first 6 hours**
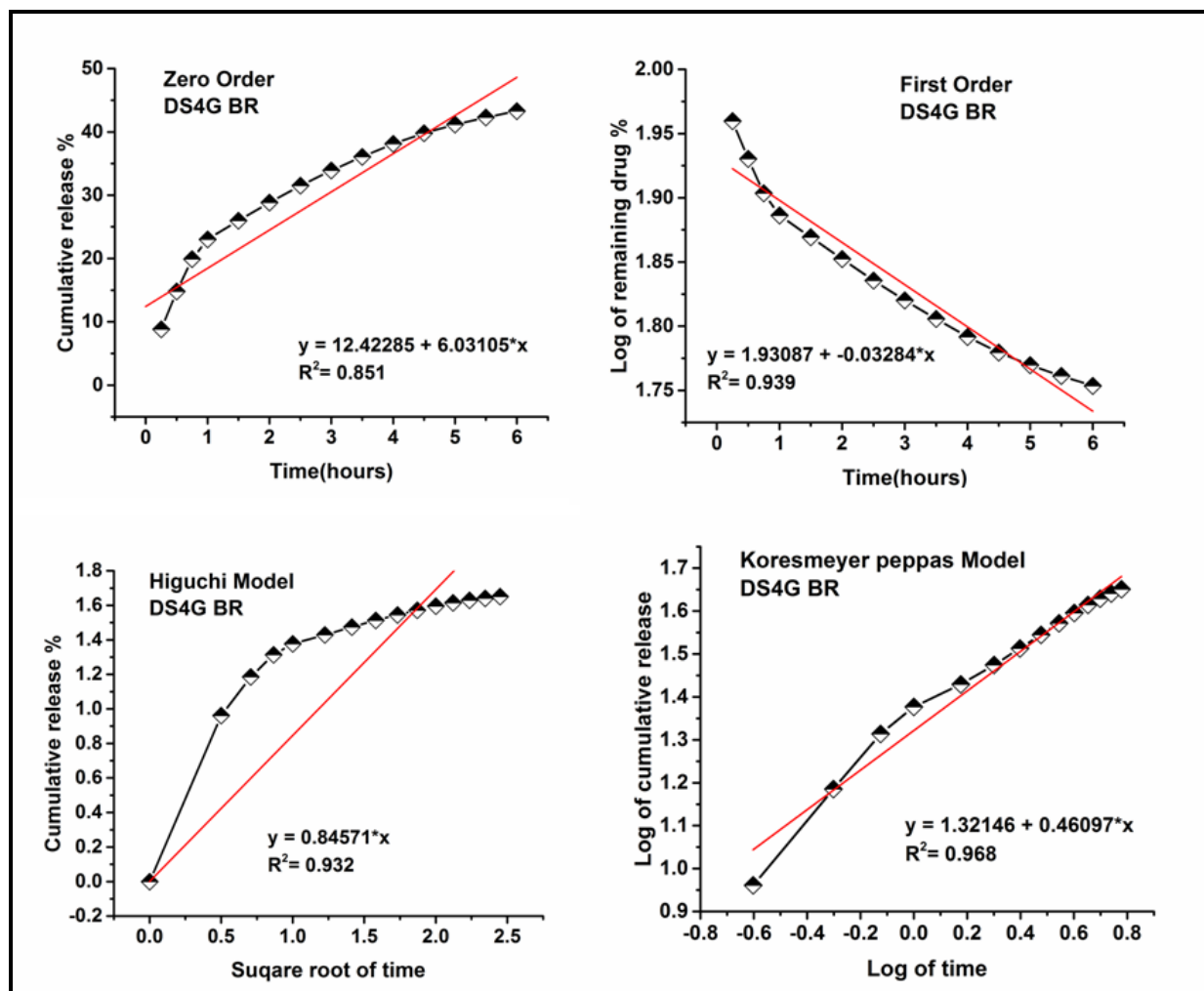
Fig 5.12: Kinetic models of DADS for first 6 hours of release from S4 irregular shaped in SGF

Table 5.11: Kinetic data of DADS obtained from S4 irregular SiO$_2$ in SGF medium

Sample name	Zero order (R^2 value)	First order (R^2 value)	Higuchi model (R^2 value)	Korsmeyer-peppas (R^2 value)	Korsmeyer-peppas n=release exponent
DADS	BR	BR	BR	BR	BR
S4	0.851	0.939	0.932	**0.968**	1.32

Based on these kinetic models the best fitted model for burst release of DADS in SGF is Koresmeyer peppas model. As the release exponent value is >0.89, the release mechanism is supercase II transport.

5.8.1.2.D Release kinetic models of DADS from S4 irregular SiO₂ in SGF for 24-168 hours:
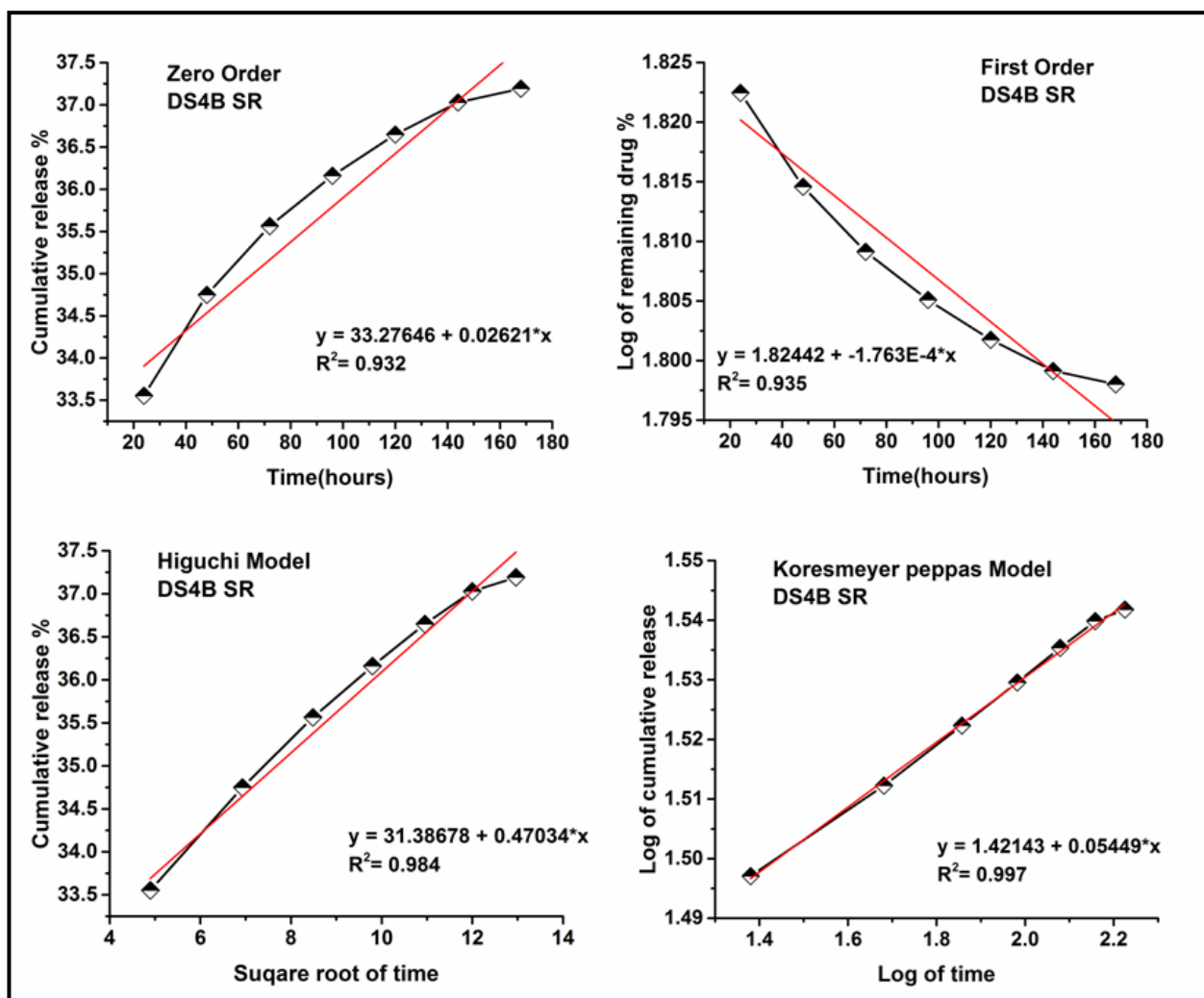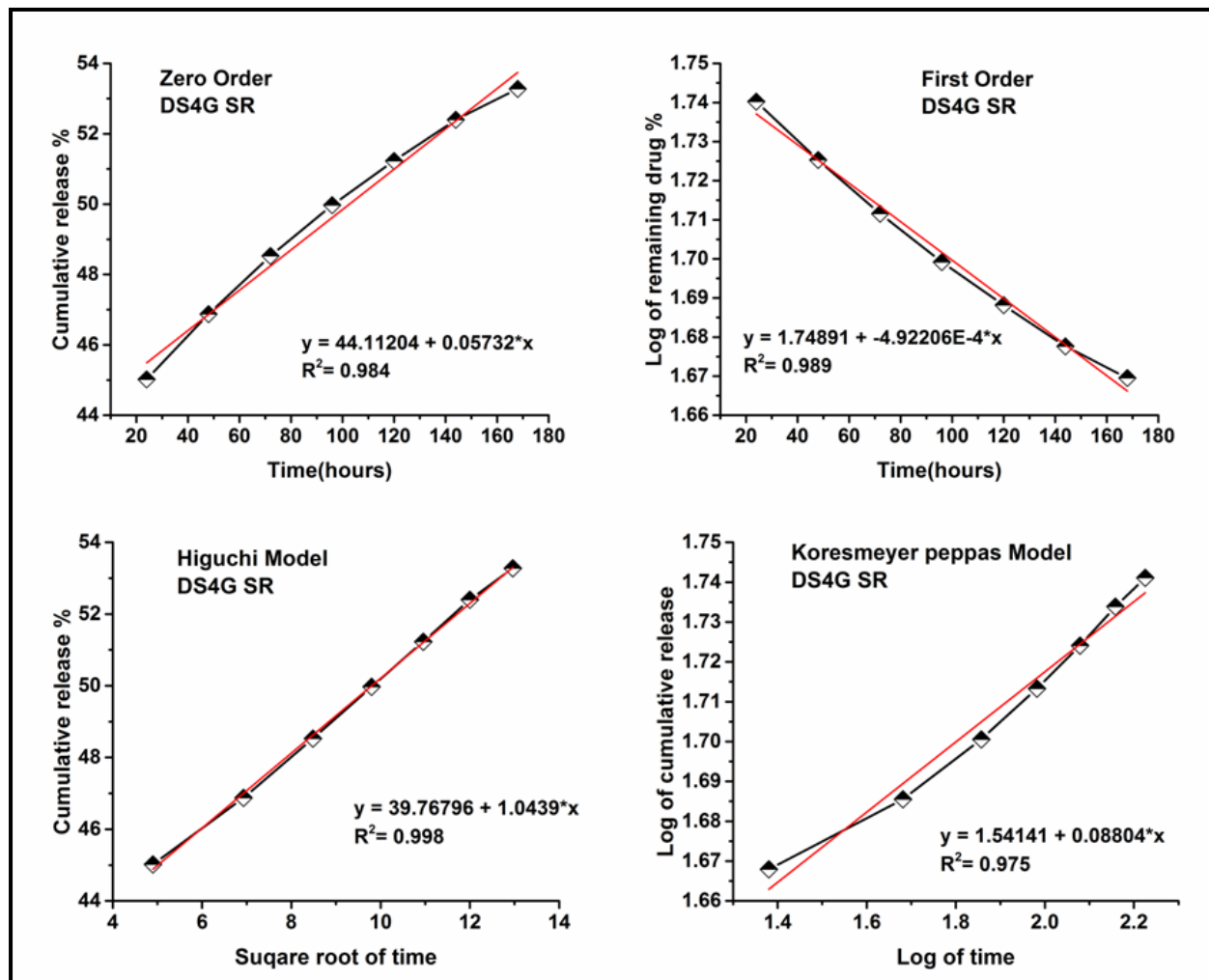

Fig 5.13: Kinetic models of DADS for 24-168 hours of release from S4 irregular shaped in SGF

Table 5.12: Kinetic data of DADS obtained from S4 irregular SiO₂ in SGF medium

Sample name	Zero order (R^2 value)	First order (R^2 value)	Higuchi model (R^2 value)	Korsmeyer-peppas (R^2 value)	Korsmeyer-peppas n=release exponent
DADS	SR	SR	SR	SR	SR
S4	0.984	0.989	**0.998**	0.975	1.54

Based on these kinetic models the best fitted model for sustained release of DADS in SGF is Higuchi model. As the release exponent value is >0.89, the release mechanism is supercase II transport.

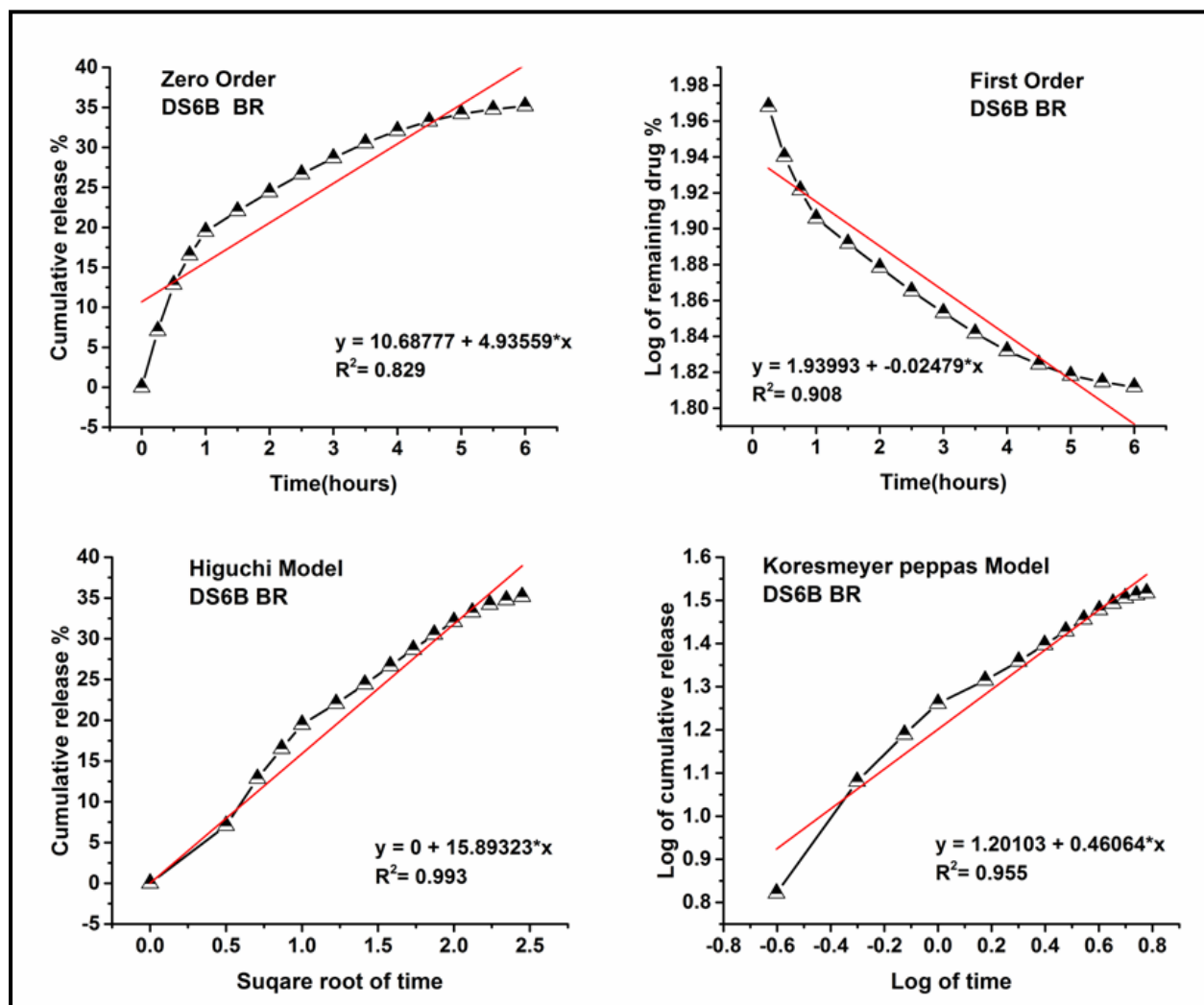**5.8.1.2.E Release kinetic models of DADS from S6 irregular SiO₂ in SGF for first 6 hours:**
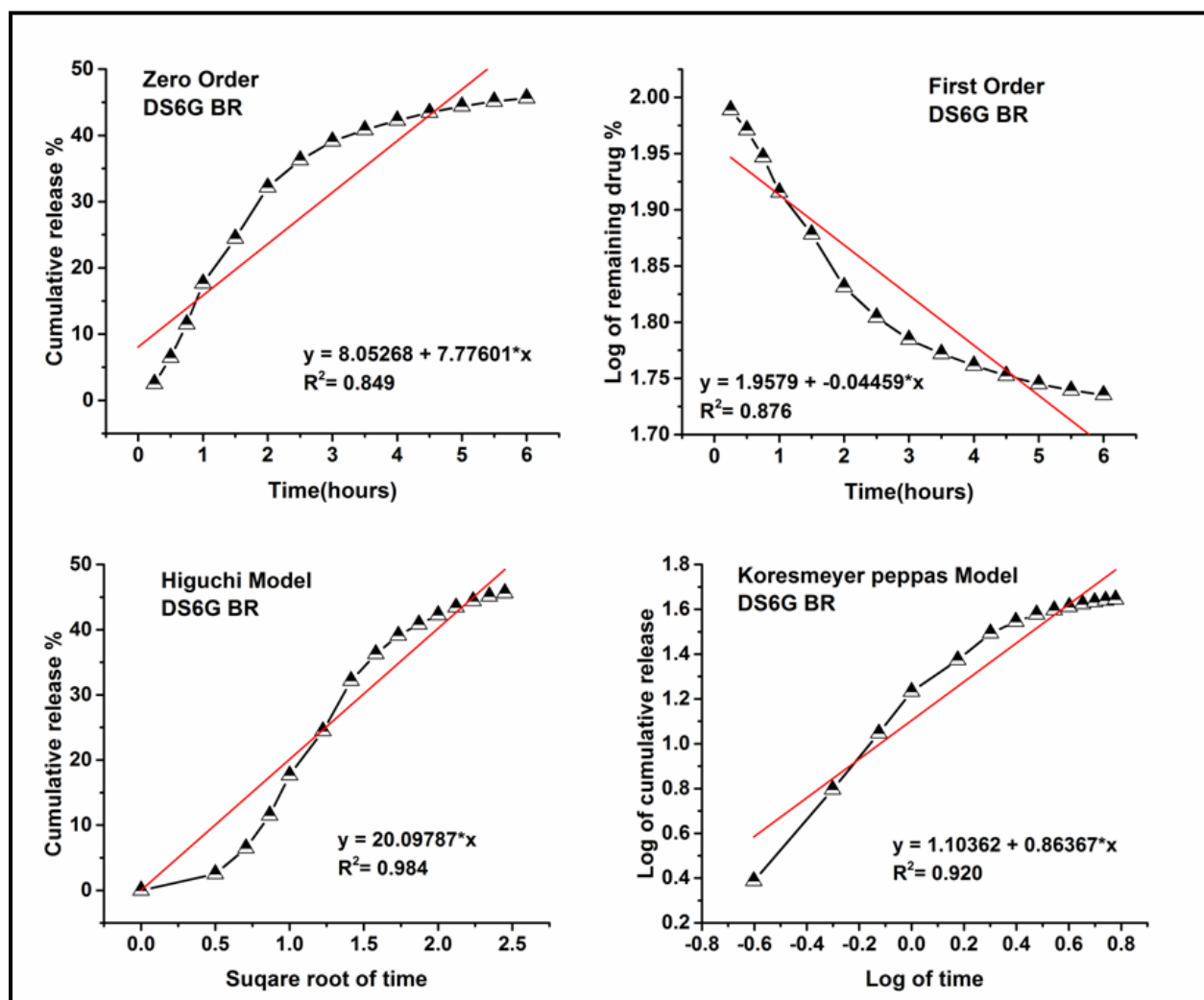
Fig 5.14: Kinetic models of DADS for first 6 hours of release from S6 irregular shaped in SGF

Table 5.13: Kinetic data of DADS obtained from S6 irregular SiO₂ in SGF medium

Sample name	Zero order (R^2 value)	First order (R^2 value)	Higuchi model (R^2 value)	Korsmeyer-peppas (R^2 value)	Korsmeyer-peppas n=release exponent
DADS	BR	BR	BR	BR	BR
S6	0.849	0.876	**0.984**	0.920	1.10

Based on these kinetic models the best fitted model for burst release of DADS in SGF is Higuchi model. As the release exponent value is >0.89, the release mechanism is supercase II transport.

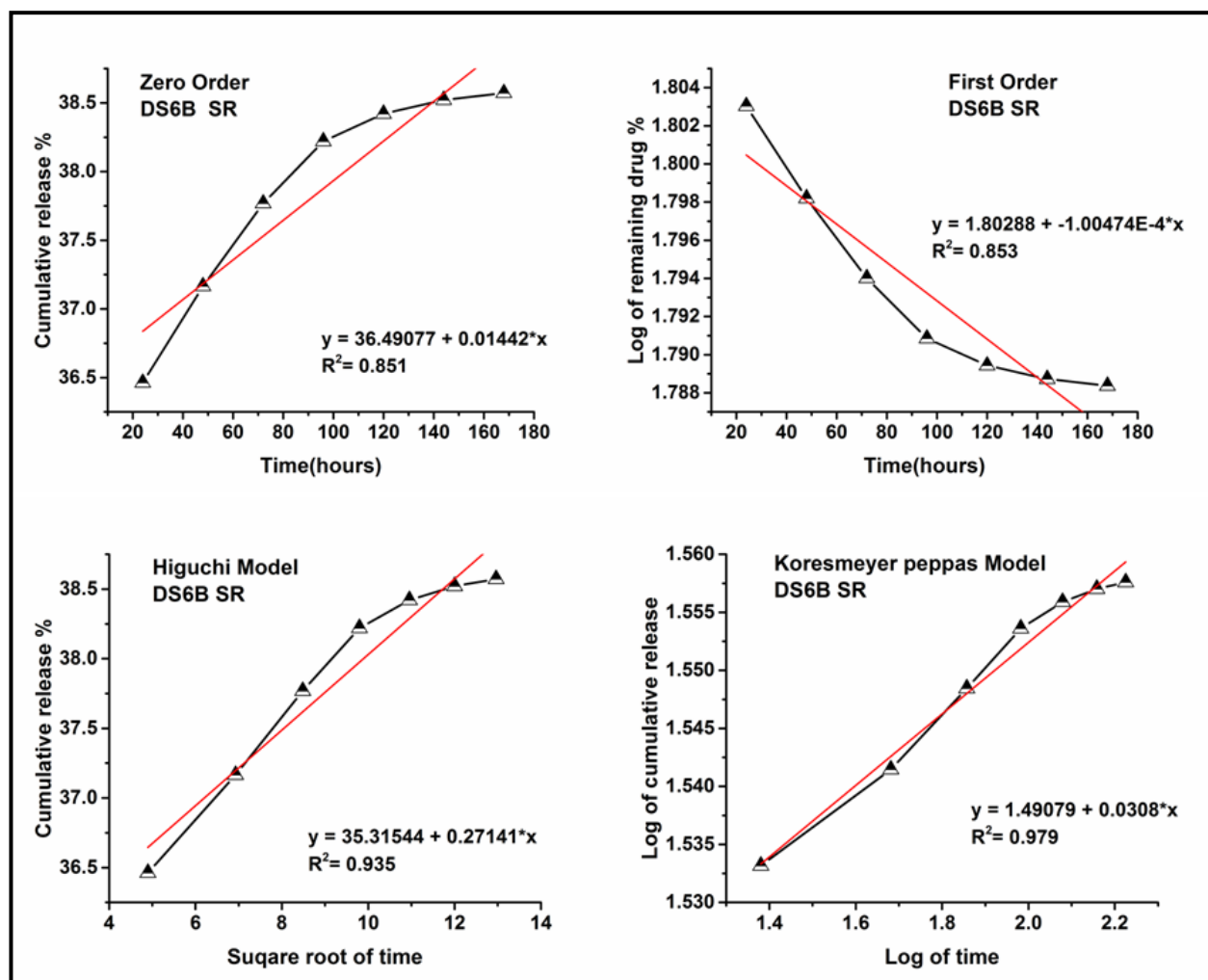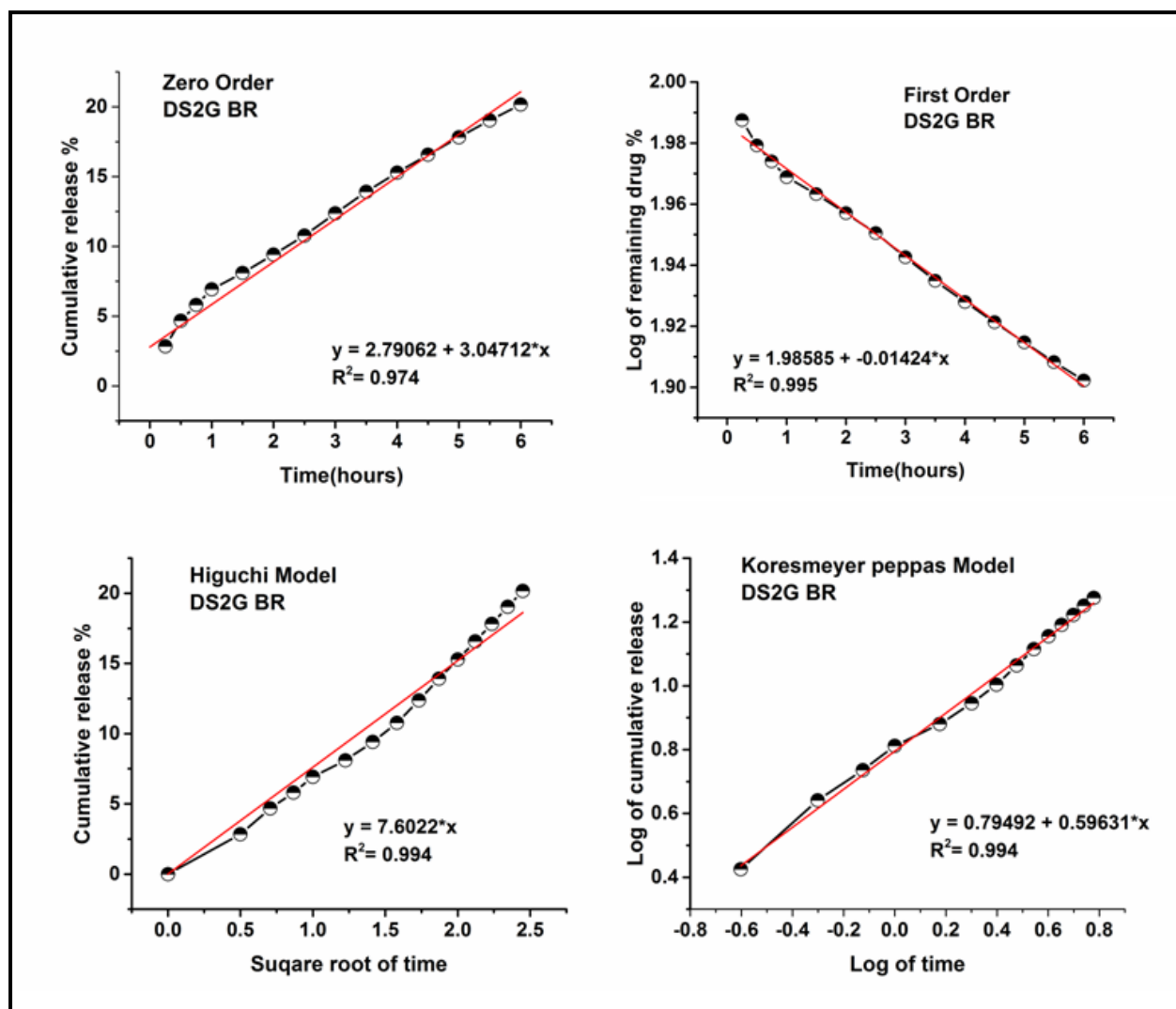**5.8.1.2.F Release kinetic models of DADS from S6 irregular SiO₂ in SGF for 24-168 hours.**

Fig 5.15: Kinetic models of DADS for 24-168 hours of release from S6 irregular shaped in SGF

Table 5.14: Kinetic data of DADS obtained from S6 irregular SiO₂ in SGF medium

Sample name	Zero order (R^2 value)	First order (R^2 value)	Higuchi model (R^2 value)	Korsmeyer-peppas (R^2 value)	Korsmeyer-peppas n=release exponent
DADS	SR	SR	SR	SR	SR
S6	**0.876**	0.852	0.814	0.754	1.54

Based on these kinetic models the best fitted model for sustained release of DADS in SGF is Zero order model .As the release exponent value is >0.89, the release mechanism is supercase II transport.

Based on the R^2 value, the best-fitted model of the released drug (DADS) in SBF & SGF medium from irregular shaped silica is determined. All sets of regression coefficient values (R^2) are given in the previous tables respectively. Table 5.15 summarizes the kinetic study result of DADS release from three different irregular silica nano carriers in SBF and SGF media.

Table 5.15: Kinetic models of DADS released from SiO$_2$ in SBF & SGF

Sl no	Sample name	Dissolution medium	Burst release	Sustained release
1	S2	SBF	Higuchi model	Higuchi model
		SGF	First order model	First order model
2	S4	SBF	First order model	Koresmeyer peppas model
		SGF	Koresmeyer peppas model	Higuchi model
3	S6	SBF	Higuchi model	Koresmeyer peppas model
		SGF	Higuchi model	Zero order model

In all cases release exponent values are greater than 0.89 except the burst release from S4 sample in SBF medium and burst release from S2 sample in SGF medium.

Release exponent value is greater than 0.89 means the release mechanism is supercase II transport and less than 0.89 means non-fickian diffusion.

5.8.2 Drug release profile and kinetic behavior study of DADS samples from different porosity-containing sphere silica nanocarriers:

Liquid liquid kinetic models are done and described here all from the collected data of UV Vis spectrophotometric analysis of released DADS from sphere-shaped silica particles. All kinetic models are applied for both released medium SBF and SGF. Three different porosity-containing sphere silica DADS conjugate samples are allowed for drug release in two different pH mediums.

Table 5.16: Cumulative release of DADS in SBF from different sphere shaped silica nanoparticles.

Sl no	Sample name	% Cumulative Release
1	DSS2B (DADS entrapped SS2 silica, released in SBF)	70
2	DSS4B (DADS entrapped SS4 silica, released in SBF)	66
3	DSS6B(DADS entrapped SS6 silica, released in SBF)	64
4	DSS2G (DADS entrapped SS2 silica, released in SGF)	81
5	DSS4G (DADS entrapped SS4 silica, released in SGF)	70
6	DSS6G (DADS entrapped SS6 silica, released in SGF)	66
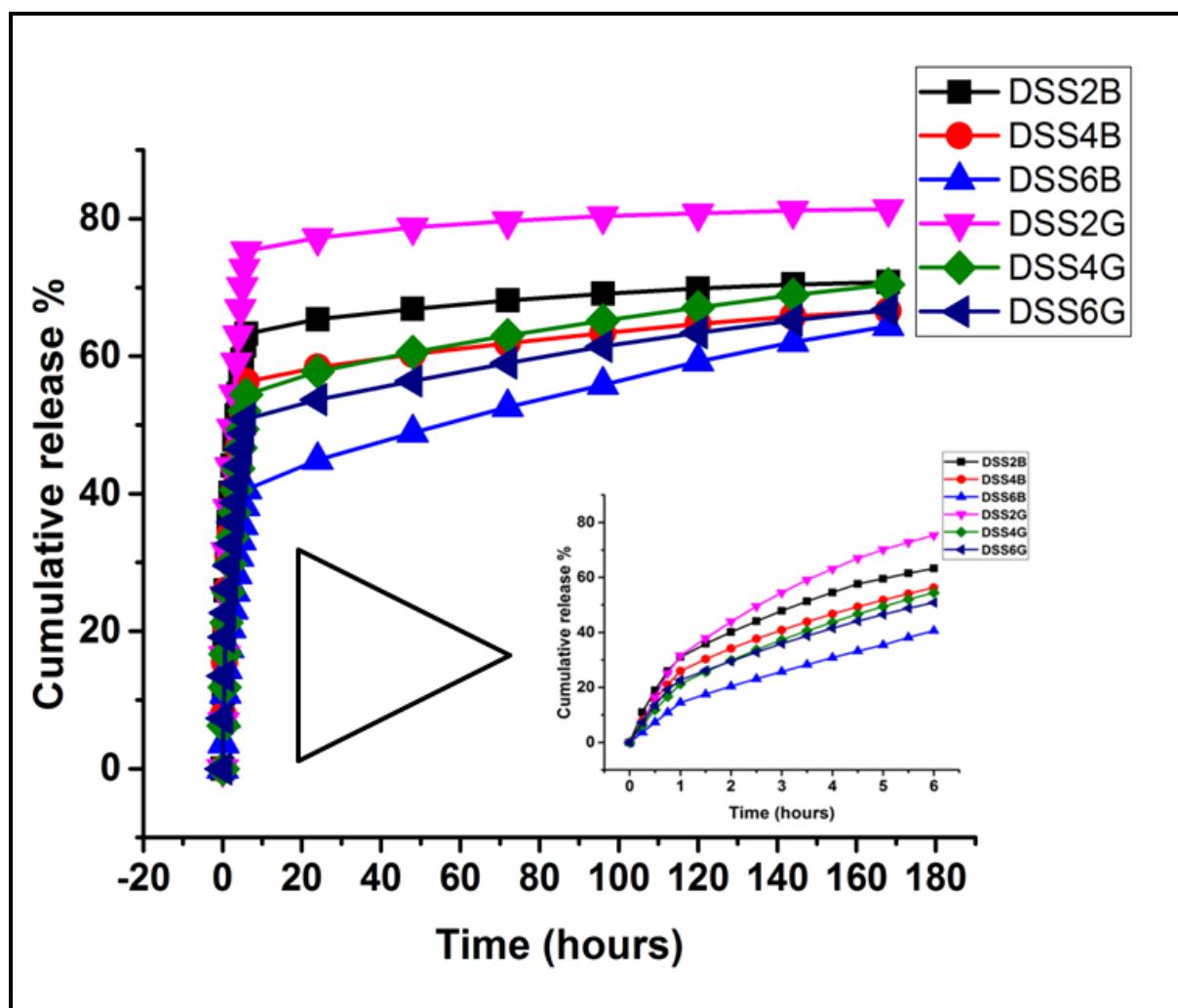
Fig 5.16: Dissolution profile of DADS in both SBF and SGF medium from sphere shape containing silica nanoparticles for both sustained and burst release

5.8.2.1.A Release kinetic models of DADS from SS2 sphere SiO₂ in SBF for 6 hours

Zero Order DSS2B BR

$y = 15.7799 + 9.14308*x$
$R^2 = 0.883$

First Order DSS2B BR

$y = 1.91954 + -0.06317*x$
$R^2 = 0.973$

Higuchi Model DSS2B BR

$y = 1.52758 + 26.2837*x$
$R^2 = 0.989$

Koresmeyer peppas Model DSS2B BR

$y = 1.4136 + 0.51334*x$
$R^2 = 0.973$
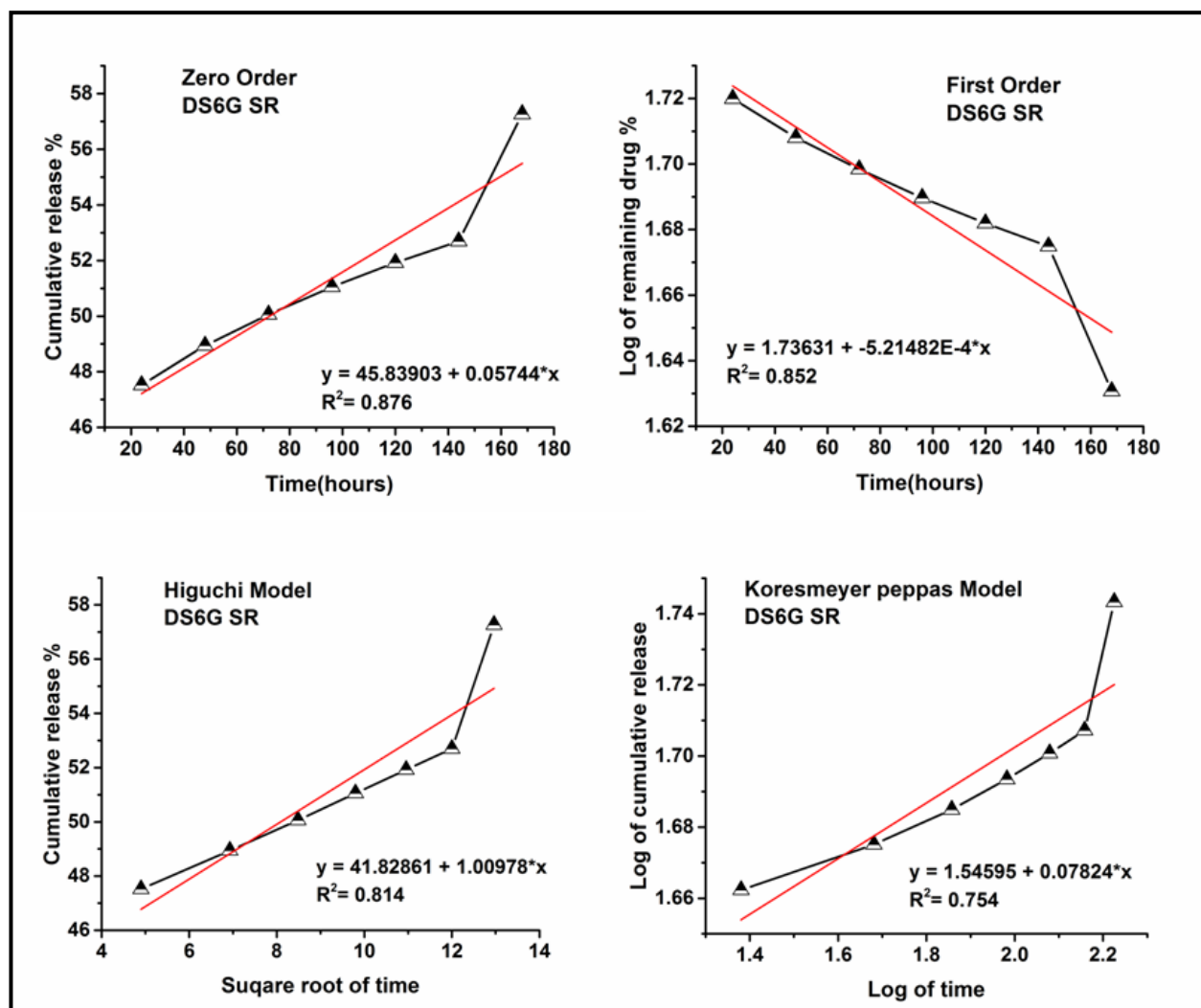
Fig 5.17: Kinetic models of DADS for first 6 hours of release from SS2 in SBF

Table 5.17: Kinetic data of DADS obtained from SS2 sphere SiO₂ in SBF medium

Sample name	Zero order (R^2 value)	First order (R^2 value)	Higuchi model (R^2 value)	Korsmeyer-peppas (R^2 value)	Korsmeyer-peppas n=release exponent
DADS	BR	BR	BR	BR	BR
SS2	0.883	0.973	**0.989**	0.973	1.41

Based on this regression coefficient value the best fitted model for burst release of DADS in SBF from SS2 is Higuchi model. As the release exponent value is >0.89, the release mechanism is supercase II transport.

5.8.2.1.B Release kinetic models of DADS from SS2 sphere SiO₂ in SBF for 24-168 hours:

Fig 5.18: Kinetic models of DADS for 24-168 hours of release from SS2 in SBF

Table 5.18: Kinetic data of DADS obtained from SS2 sphere SiO₂ in SBF medium

Sample name	Zero order (R^2 value)	First order (R^2 value)	Higuchi model (R^2 value)	Korsmeyer-peppas (R^2 value)	Korsmeyer-peppas n=release exponent
DADS SS2	SR	SR	SR	SR	SR
	0.944	0.955	0.990	**0.992**	1.73

Based on this regression coefficient value the best fitted model for sustained release of DADS from SS2 in SBF is Koresmeyer peppas model. As the release exponent value is >0.89, the release mechanism is supercase II transport.

5.8.2.1.C Release kinetic models of DADS from SS4 sphere SiO₂ in SBF for first 6 hours:

Fig 5.19: Kinetic models of DADS for first 6 hours of release from SS4 in SBF

Table 5.19: Kinetic data of DADS obtained from SS4 sphere SiO₂ in SBF medium

Sample name	Zero order (R^2 value)	First order (R^2 value)	Higuchi model (R^2 value)	Korsmeyer-peppas (R^2 value)	Korsmeyer-peppas n=release exponent
DADS	BR	BR	BR	BR	BR
SS4	0.901	0.973	**0.998**	0.965	1.32

Based on this regression coefficient value the best fitted model for burst release of DADS from SS4 in SBF is Higuchi model. As the release exponent value is >0.89, the release mechanism is supercase II transport.

5.8.2.1.D Release kinetic models of DADS from SS4 sphere SiO₂ in SBF for 24-168 hours:

Fig 5.20: Kinetic models of DADS for 24-168 hours of release from SS4 in SBF

Table 5.20: Kinetic data of DADS obtained from SS4 sphere SiO₂ in SBF medium

Sample name	Zero order (R² value)	First order (R² value)	Higuchi model (R² value)	Korsmeyer-peppas (R² value)	Korsmeyer-peppas n=release exponent
DADS SS4	SR 0.979	SR 0.987	SR **0.998**	SR 0.967	SR 1.64

Based on this regression coefficient value the best fitted model for sustained release of DADS from SS4 in SBF is Higuchi model. As the release exponent value is >0.89, the release mechanism is supercase II transport.

5.8.2.1.E Release kinetic models of DADS from SS6 sphere SiO₂ in SBF for first 6 hours:

Fig 5.21: Kinetic models of DADS for first 6 hours of release from SS6 in SBF

Table 5.21: Kinetic data of DADS obtained from SS6 sphere SiO₂ in SBF medium

Sample name	Zero order (R^2 value)	First order (R^2 value)	Higuchi model (R^2 value)	Korsmeyer-peppas (R^2 value)	Korsmeyer-peppas n=release exponent
DADS	BR	BR	BR	BR	BR
SS6	0.961	0.988	**0.993**	0.981	1.09

Based on this regression coefficient value the best fitted model for sustained release of DADS from SS6 in SBF is Higuchi model. As the release exponent value is >0.89, the release mechanism is supercase II transport.

5.8.2.1.F Release kinetic models of DADS from SS6 sphere SiO₂ in SBF for 24-168 hours:
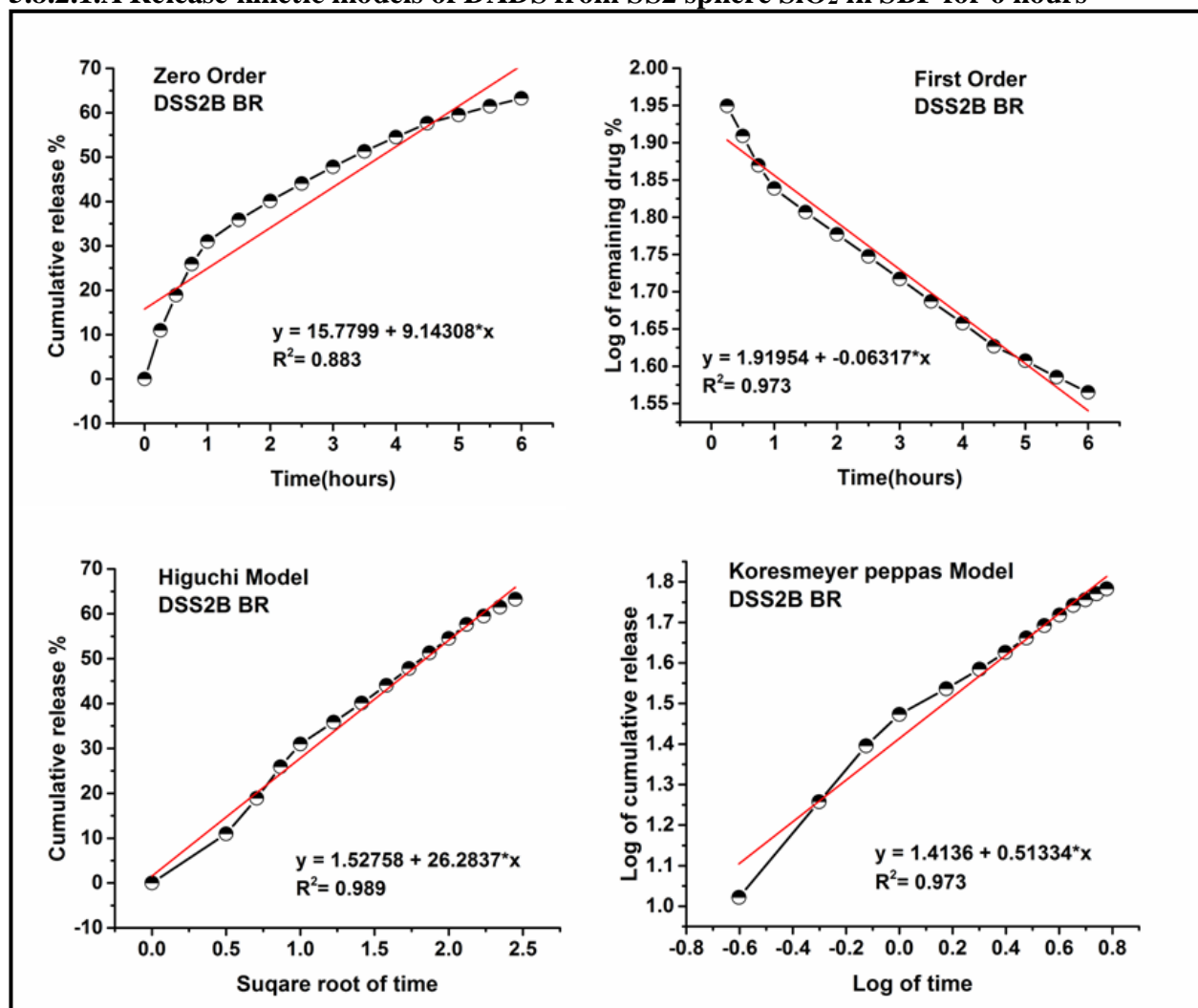

Fig 5.22: Kinetic models of DADS for 24-168 hours of release from SS6 in SBF

Table 5.22: Kinetic data of DADS obtained from SS6 sphere SiO₂ in SBF medium

Sample name	Zero order (R^2 value)	First order (R^2 value)	Higuchi model (R^2 value)	Korsmeyer-peppas (R^2 value)	Korsmeyer-peppas n=release exponent
DADS	SR	SR	SR	SR	SR
SS6	0.992	**0.999**	0.995	0.972	1.39

Based on this regression coefficient value the best fitted model for sustained release of DADS from SS6 in SBF is First order model. As the release exponent value is >0.89, the release mechanism is supercase II transport.

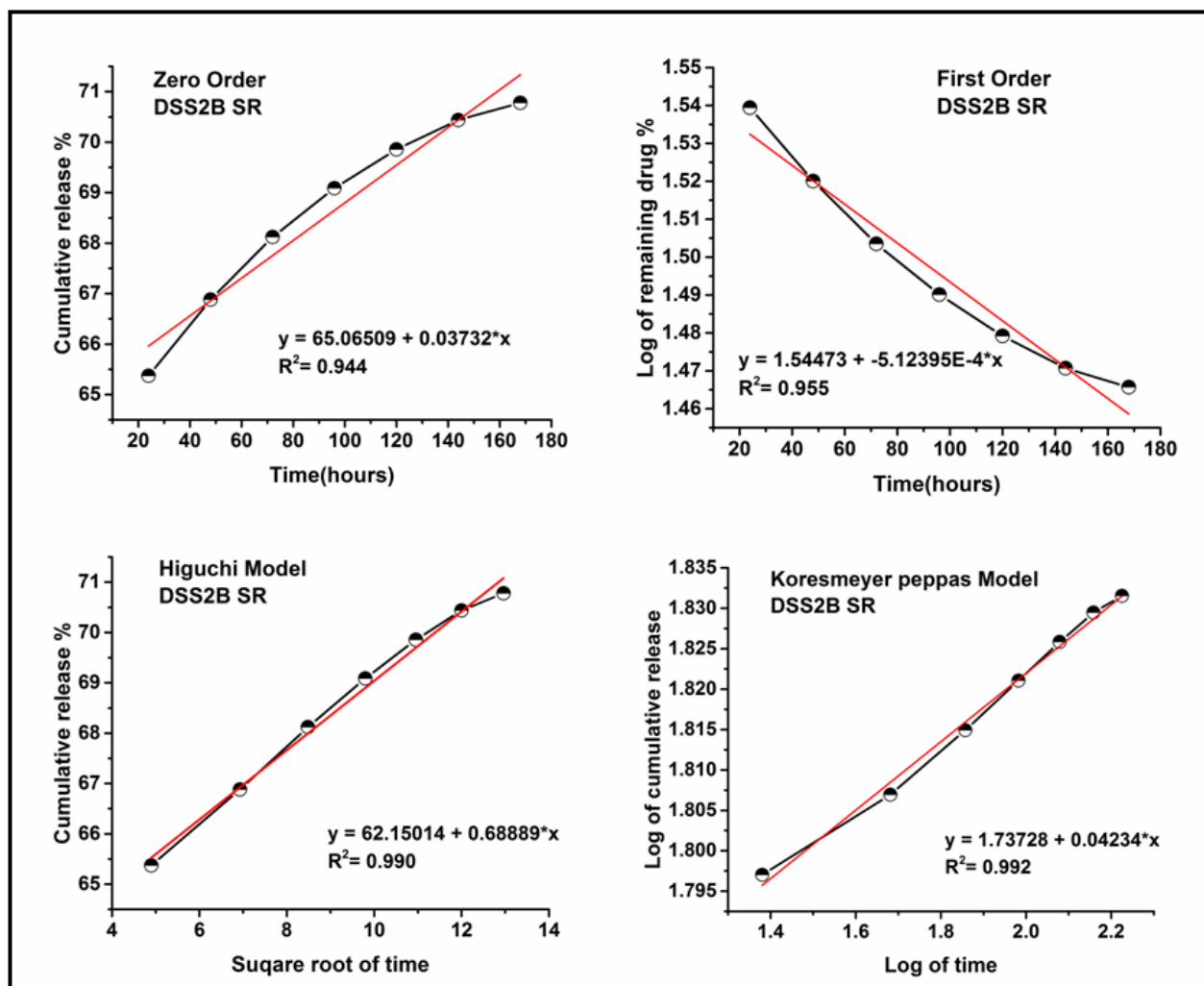**5.8.2.2.A Release kinetic models of DADS from SS2 sphere SiO₂ in SGF for first 6 hours:**
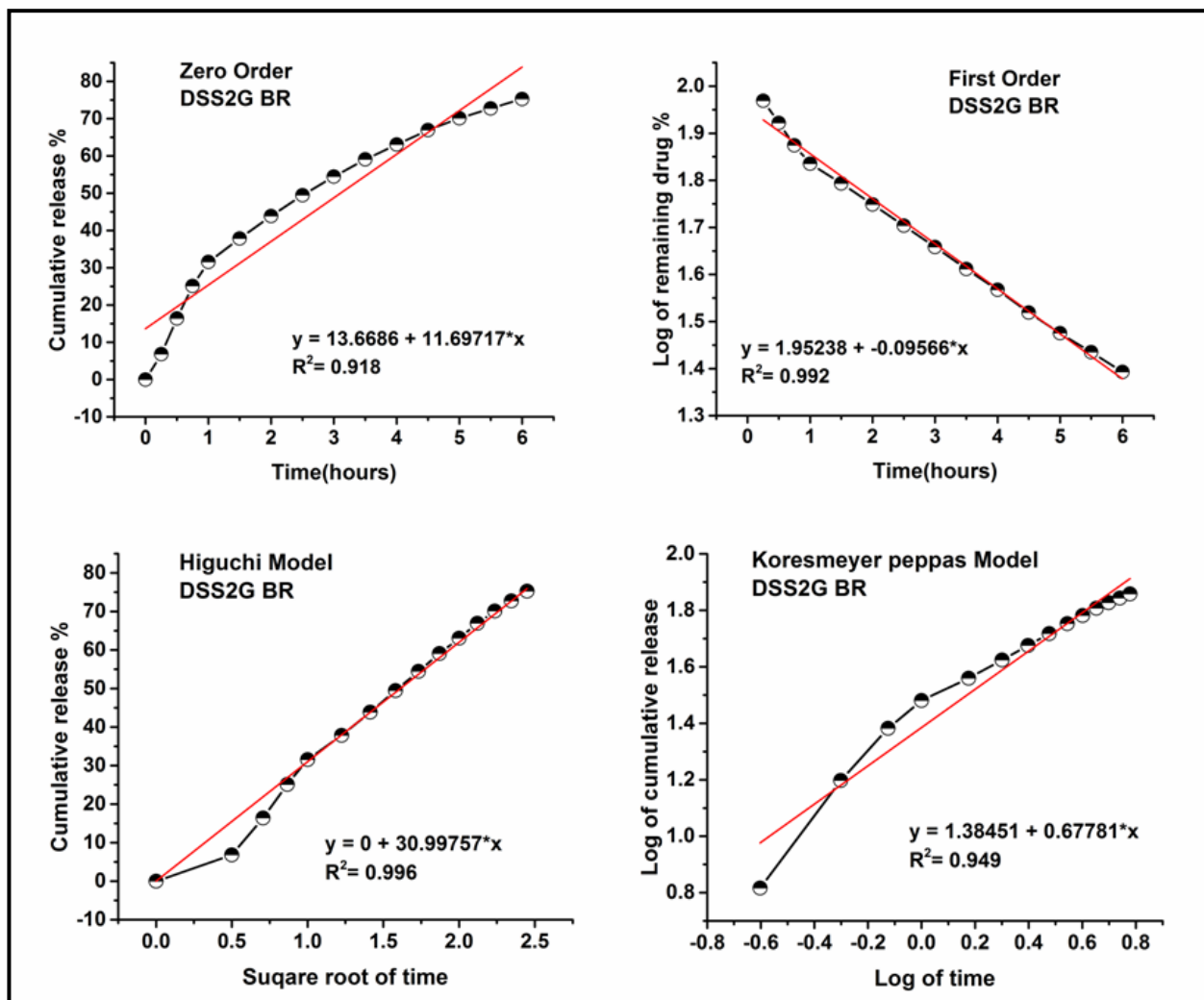
Fig 5.23: Kinetic models of DADS for first 6 hours of release from SS2 in SGF

Table 5.23: Kinetic data of DADS obtained from SS2 sphere SiO₂ in SGF medium

Sample name	Zero order (R^2 value)	First order (R^2 value)	Higuchi model (R^2 value)	Korsmeyer-peppas (R^2 value)	Korsmeyer-peppas n=release exponent
DADS	BR	BR	BR	BR	BR
SS2	0.918	0.992	**0.996**	0.949	1.38

Based on this regression coefficient value the best fitted model for burst release of DADS from SS2 in SGF is Higuchi model. As the release exponent value is >0.89, the release mechanism is supercase II transport.

5.8.2.2.B Release kinetic models of DADS from SS2 sphere SiO₂ in SGF for 24-168 hours:
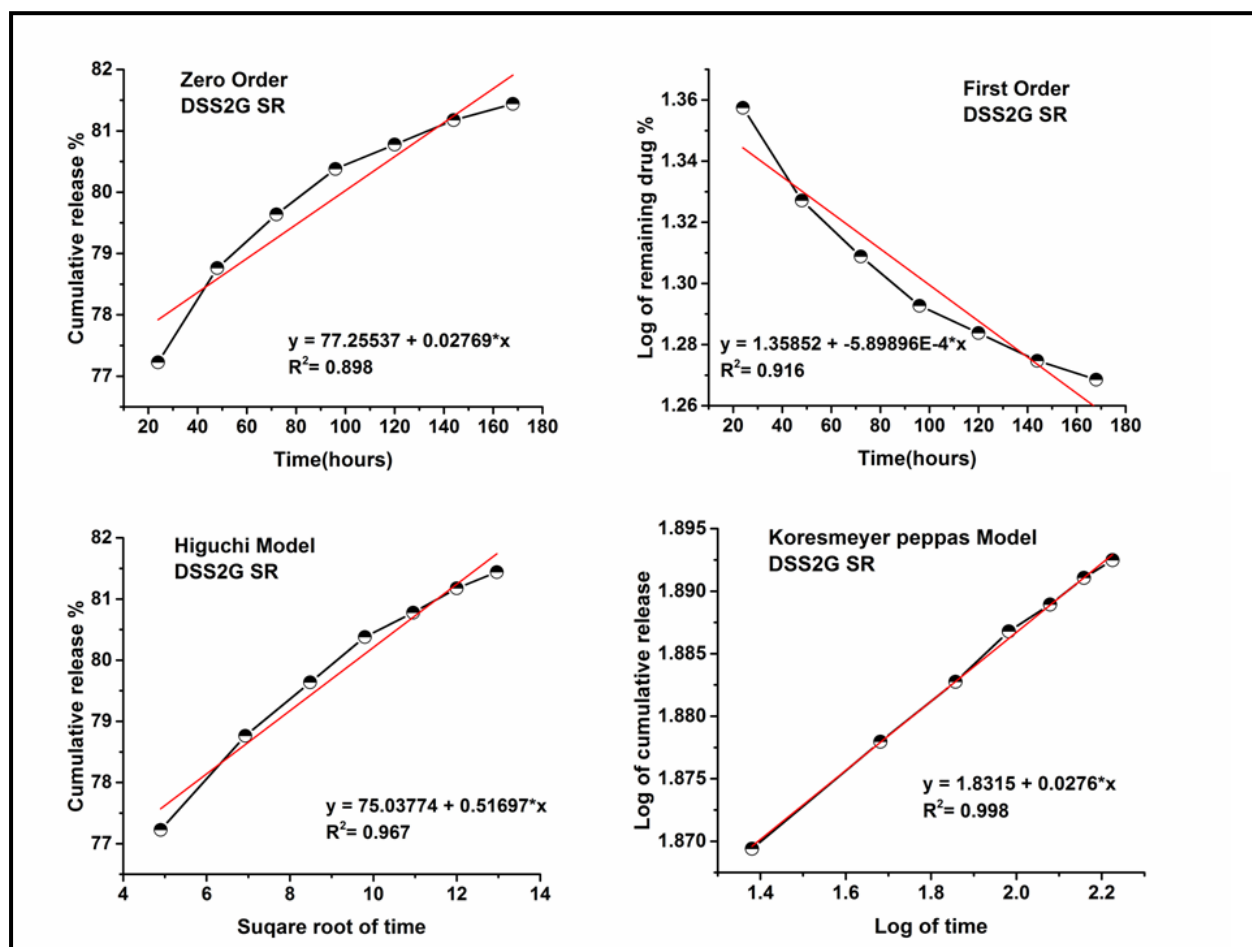
Fig 5.24: Kinetic models of DADS for 24-168 hours of release from SS2 in SGF

Table 5.24: Kinetic data of DADS obtained from SS2 sphere SiO₂ in SGF medium

Sample name	Zero order (R^2 value)	First order (R^2 value)	Higuchi model (R^2 value)	Korsmeyer-peppas (R^2 value)	Korsmeyer-peppas n=release exponent
DADS	SR	SR	SR	SR	SR
SS2	0.898	0.916	0.967	**0.998**	1.83

Based on this regression coefficient value the best fitted model for sustained release of DADS from SS2 in SGF is Koresmeyer peppas model. As the release exponent value is >0.89, the release mechanism is supercase II transport.

5.8.2.2.C Release kinetic models of DADS from SS4 sphere SiO_2 in SGF for first 6 hours:
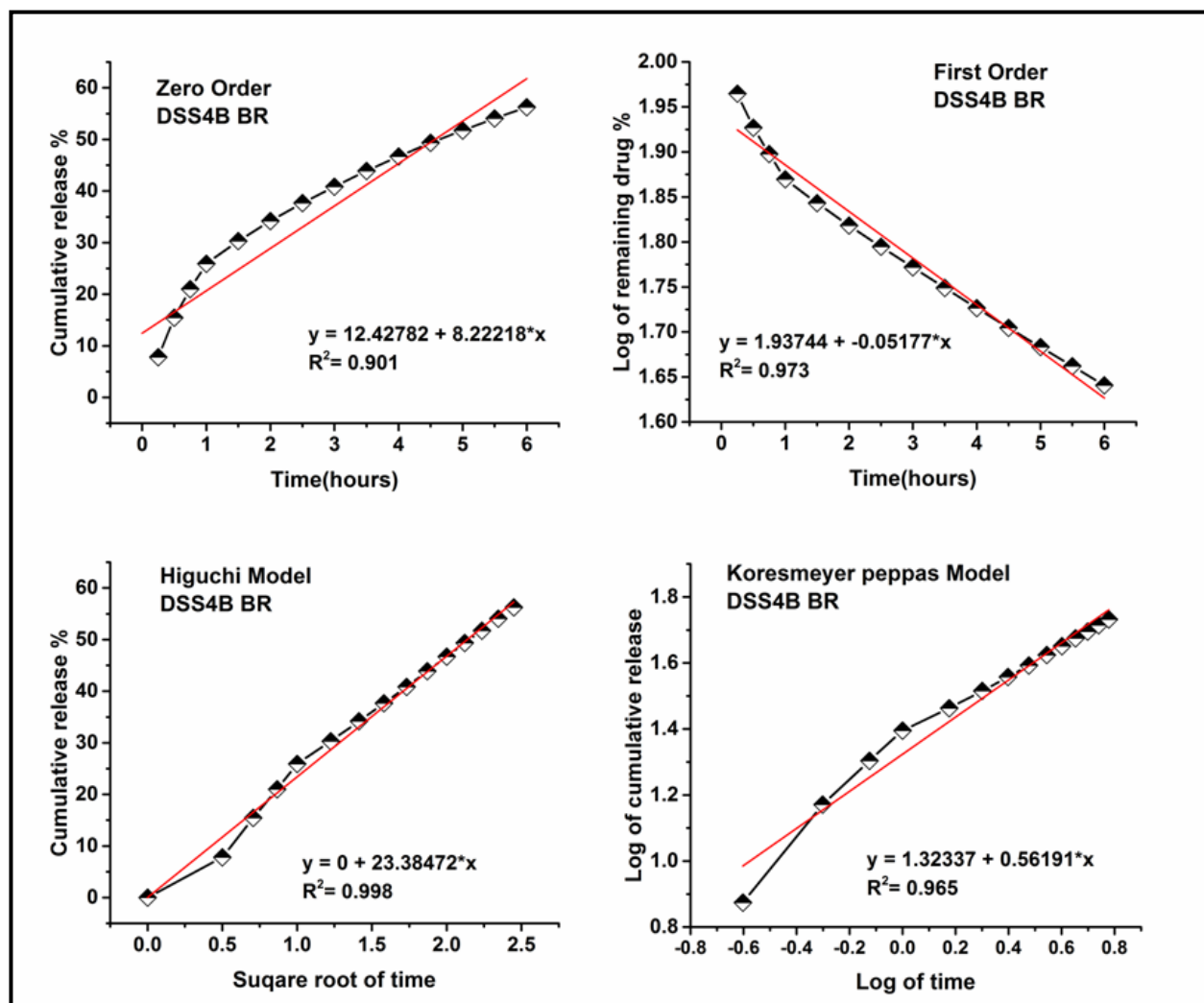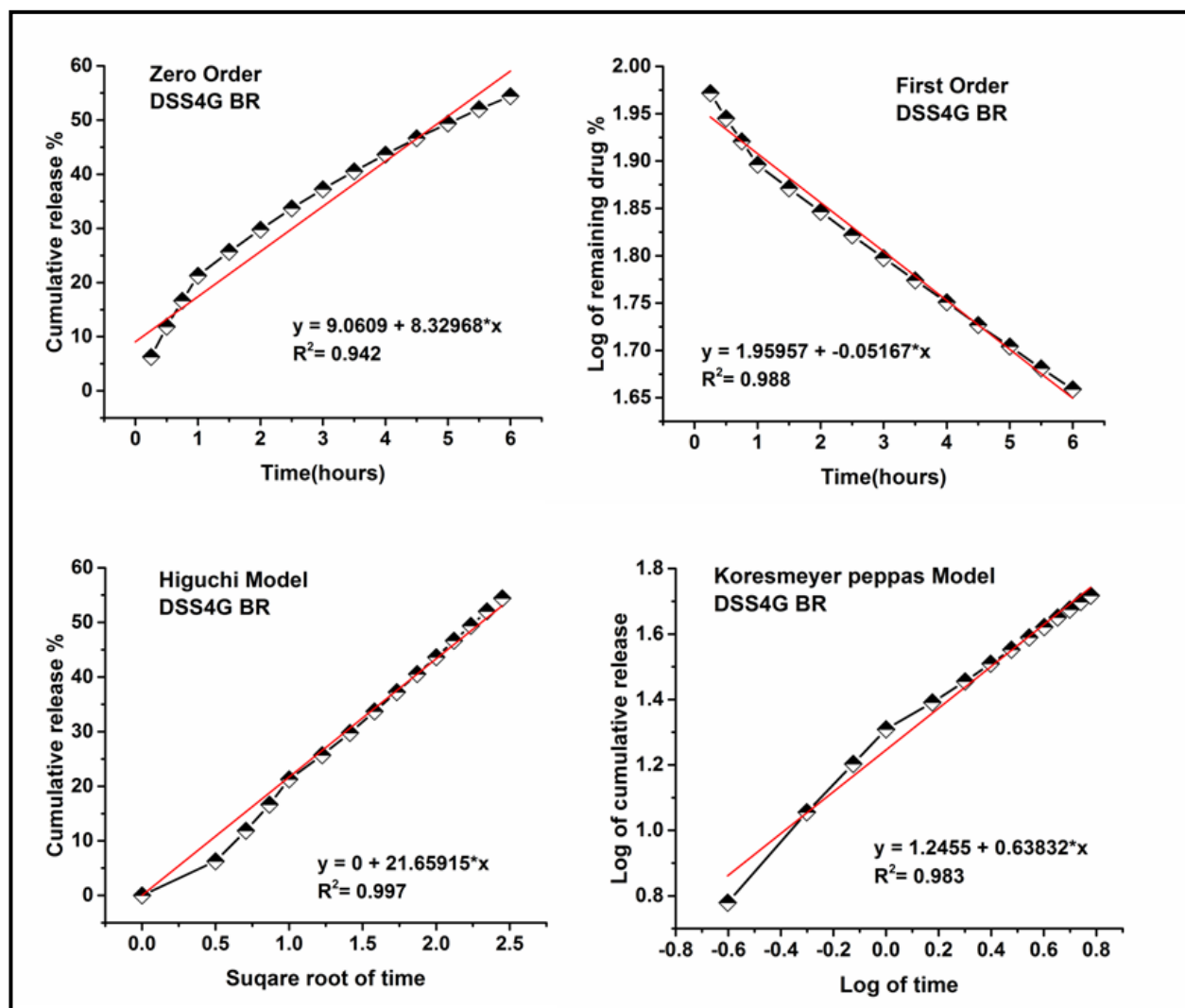

Fig 5.25: Kinetic models of DADS for first 6 hours of release from SS4 in SGF

Table 5.25: Kinetic data of DADS obtained from SS4 sphere SiO_2 in SGF medium

Sample name	Zero order (R^2 value)	First order (R^2 value)	Higuchi model (R^2 value)	Korsmeyer-peppas (R^2 value)	Korsmeyer-peppas n=release exponent
DADS	BR	BR	BR	BR	BR
SS4	0.942	0.988	**0.997**	0.983	2.30

Based on this regression coefficient value the best fitted model for burst release of DADS from SS4 in SGF is Higuchi model. As the release exponent value is >0.89, the release mechanism is supercase II transport.
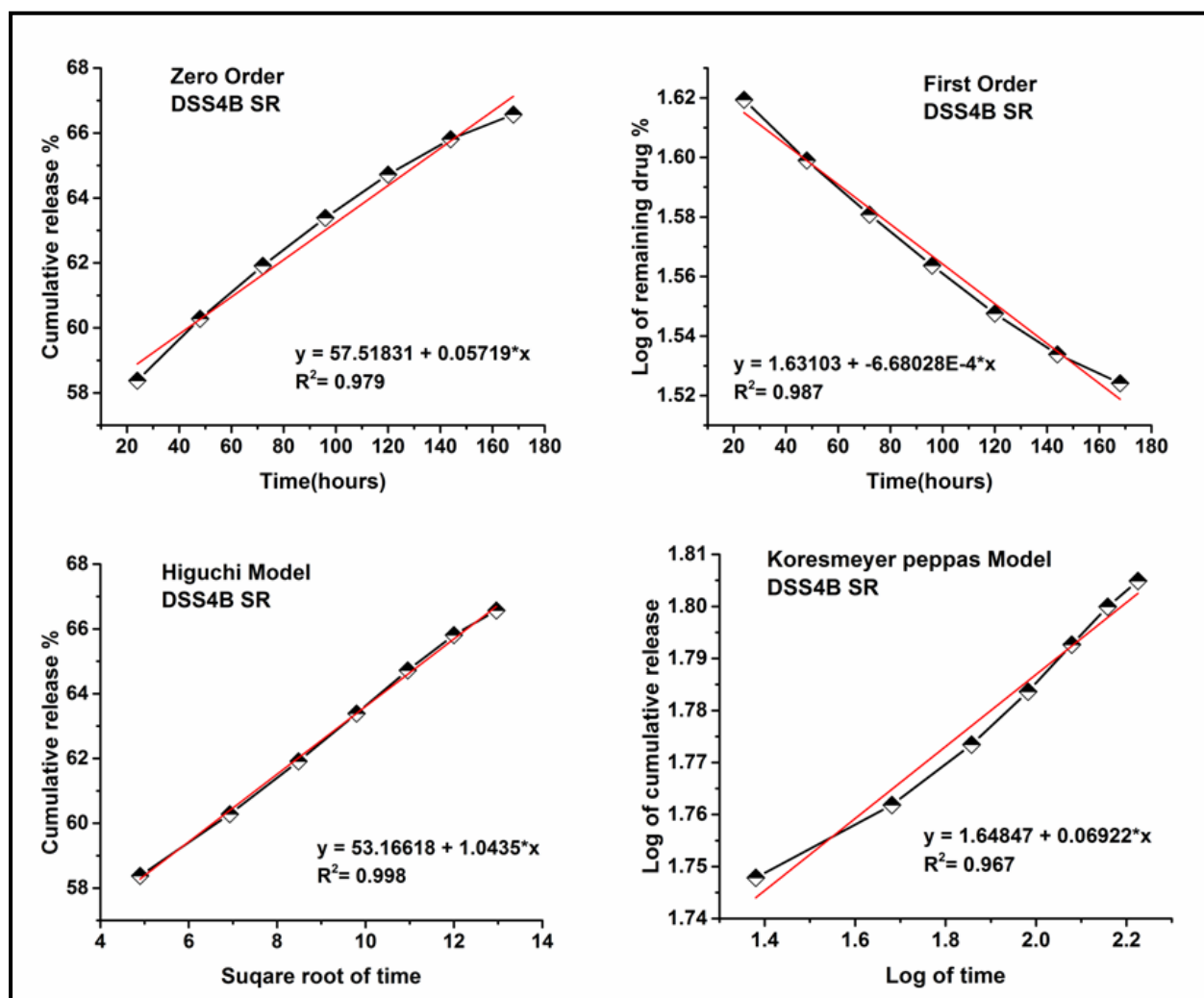
5.8.2.2.D Release kinetic models of DADS from SS4 sphere SiO₂ in SGF for 24-168 hours:
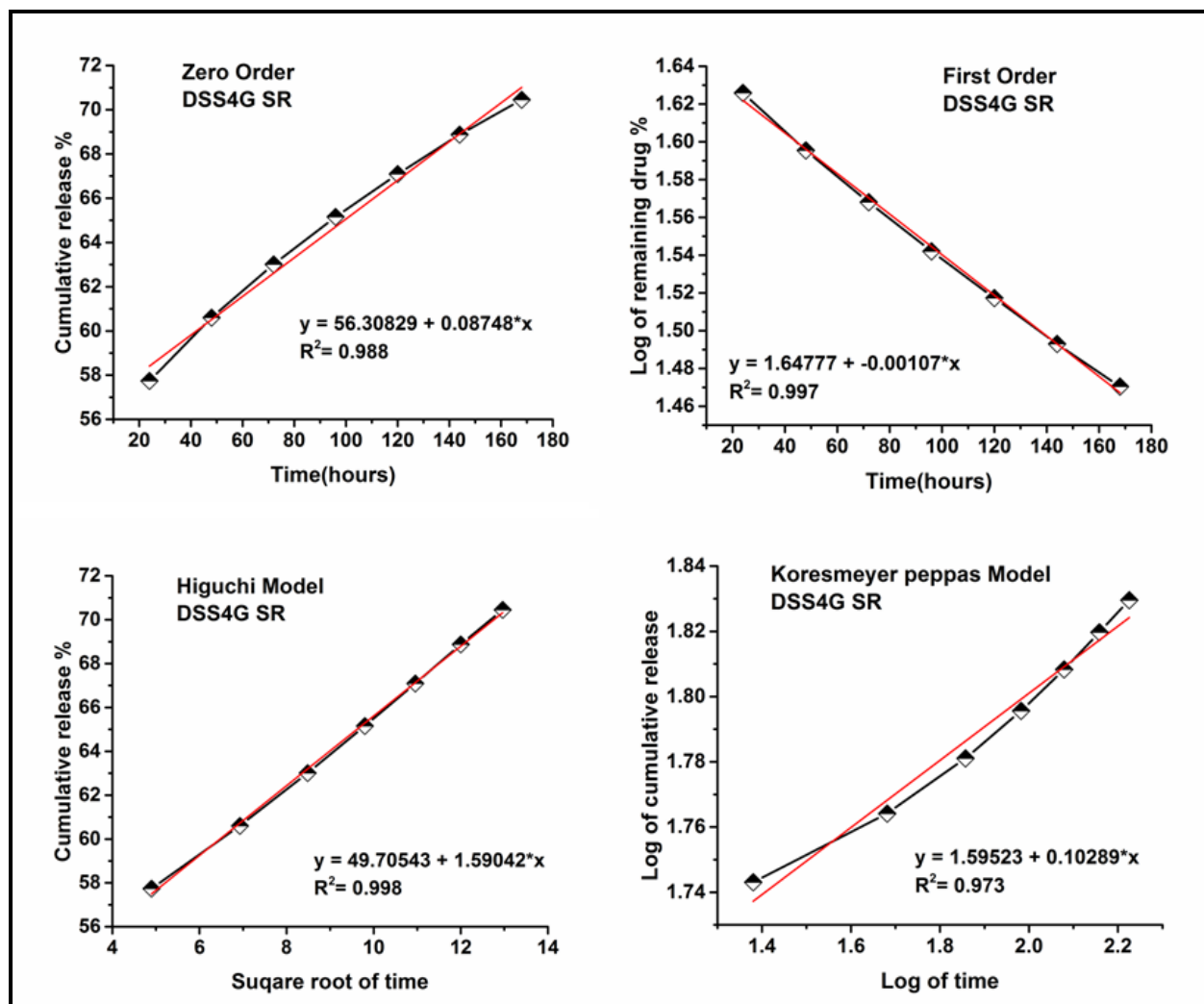
Fig 5.26: Kinetic models of DADS for 24-168 hours of release from SS4 in SGF

Table 5.26: Kinetic data of DADS obtained from SS4 sphere SiO₂ in SGF medium

Sample name	Zero order (R^2 value)	First order (R^2 value)	Higuchi model (R^2 value)	Korsmeyer-peppas (R^2 value)	Korsmeyer-peppas n=release exponent
DADS	SR	SR	SR	SR	SR
SS4	0.988	0.997	**0.998**	0.973	1.59

Based on this regression coefficient value the best fitted model for burst release of DADS from SS4 in SGF is Higuchi model. As the release exponent value is >0.89, the release mechanism is supercase II transport.

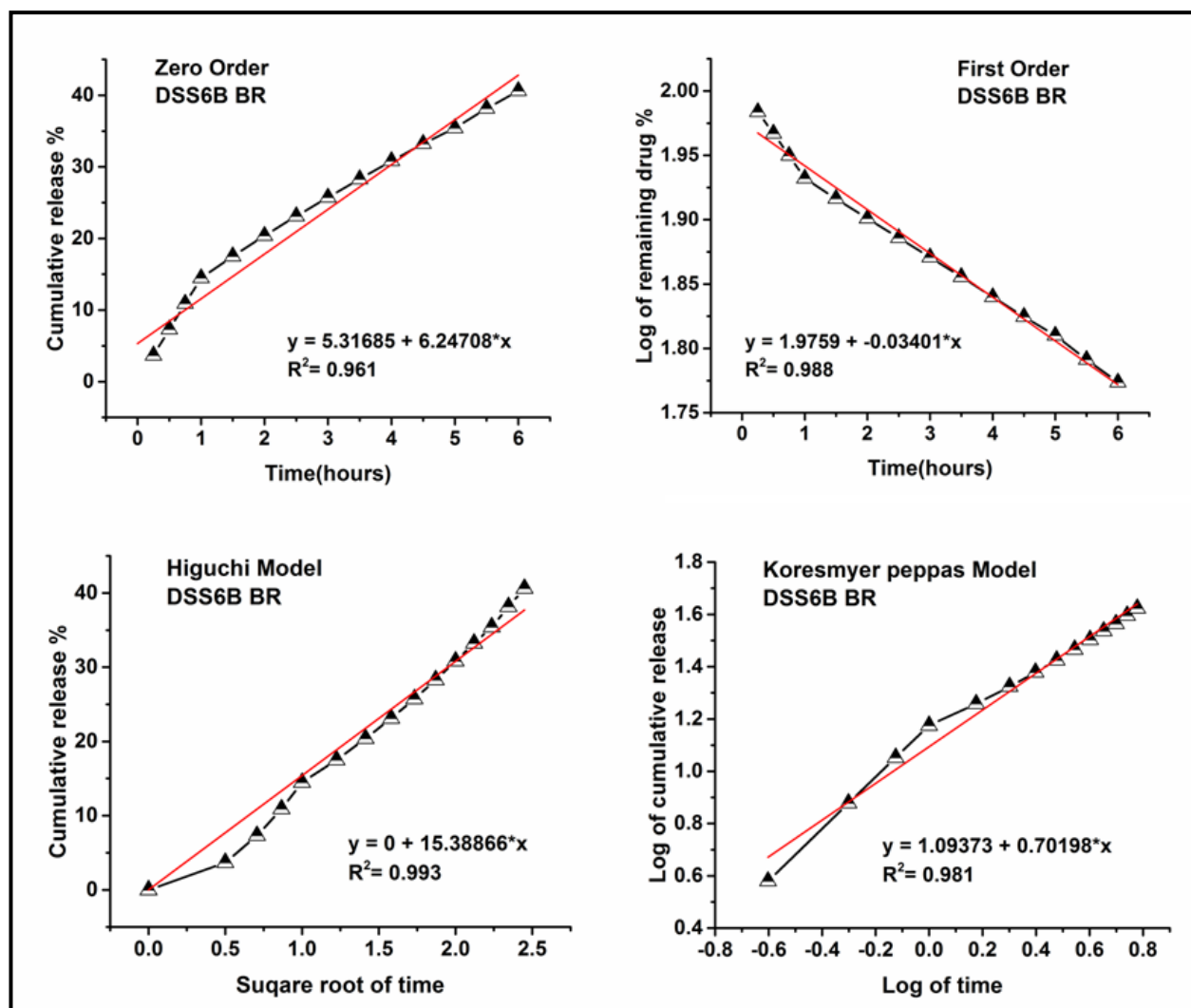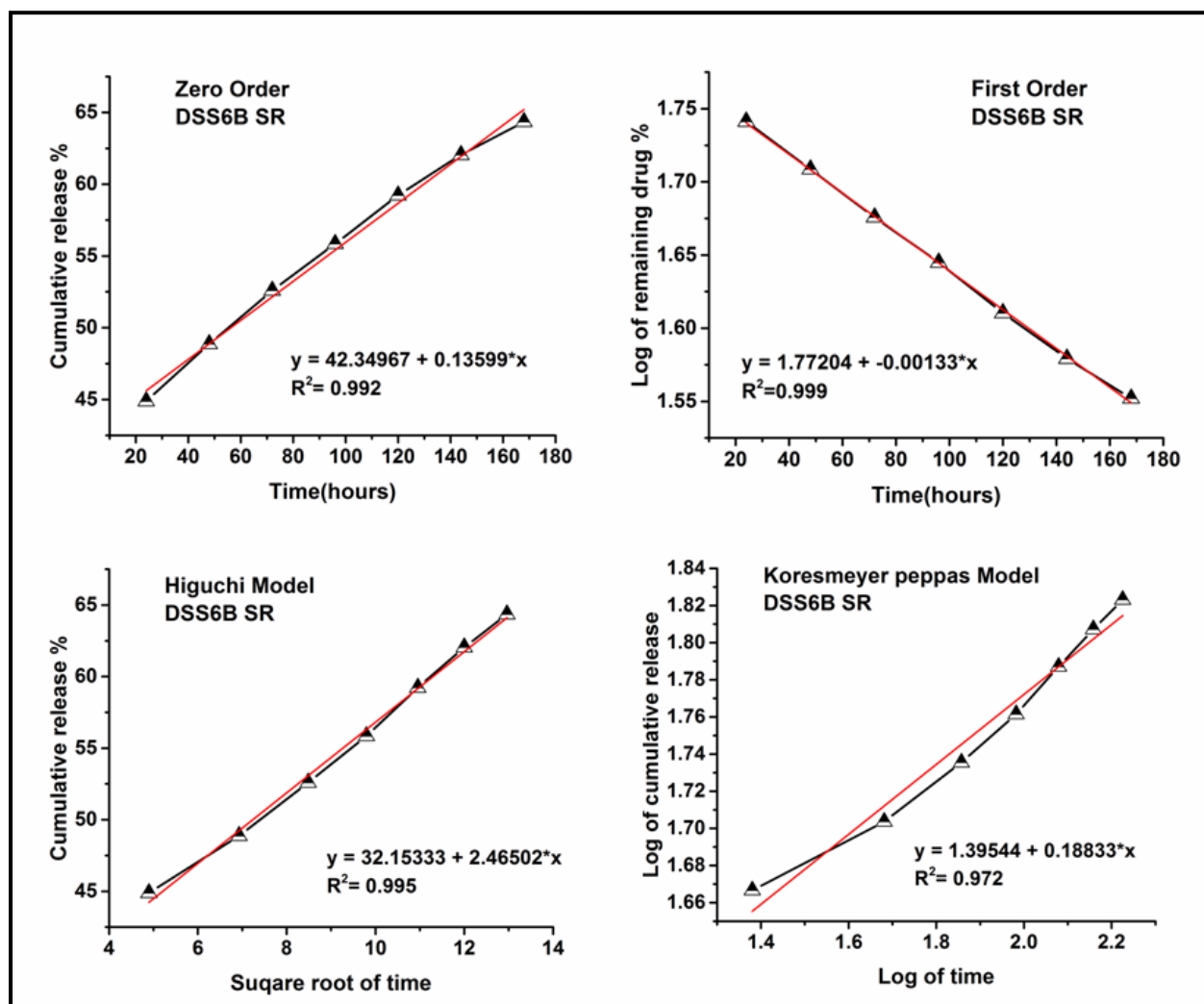**5.8.2.2.E Release kinetic models of DADS from SS6 sphere SiO₂ in SGF for first 6 hours:**
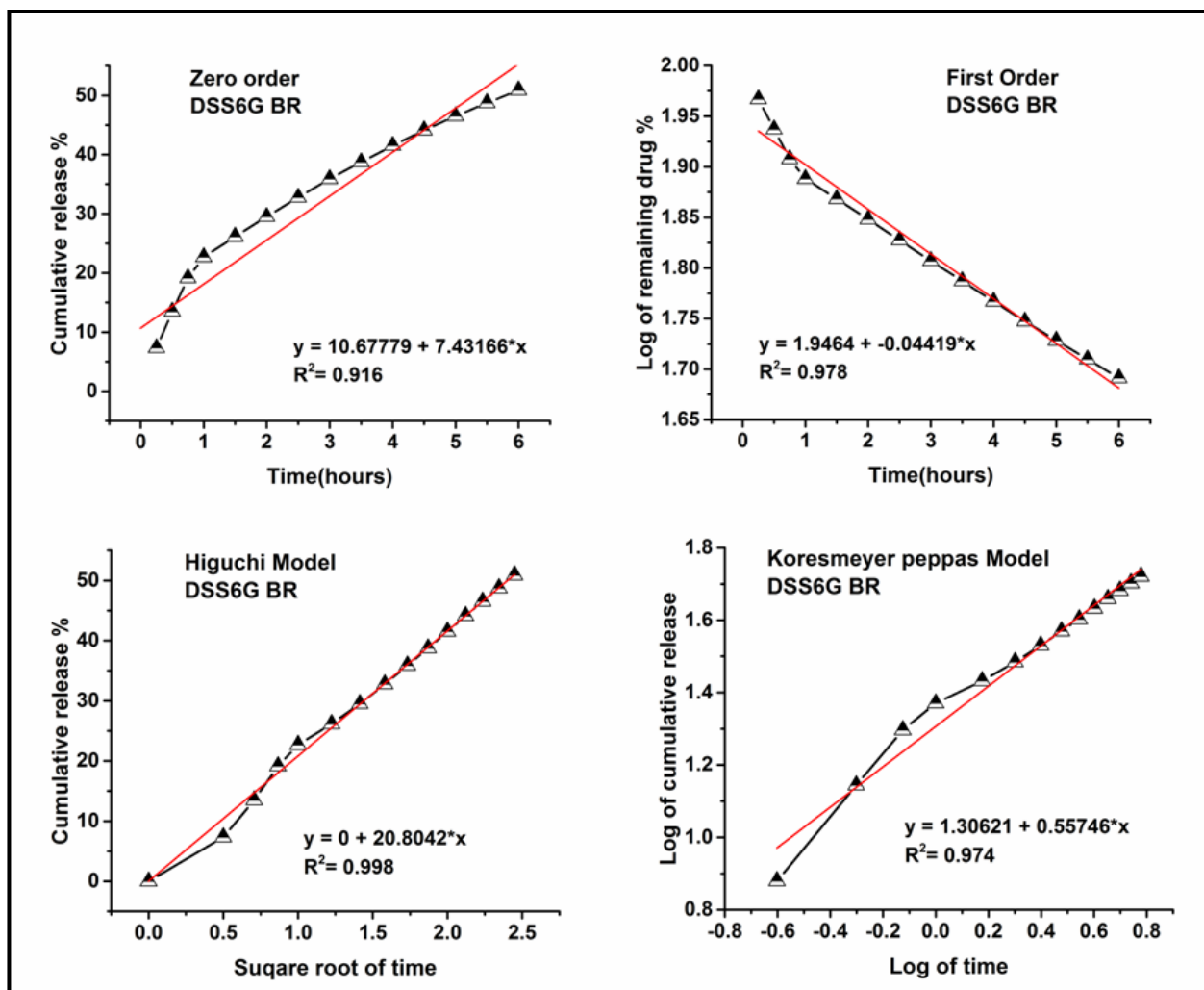
Fig 5.27: Kinetic models of DADS for first 6 hours of release from SS6 in SGF

Table 5.27: Kinetic data of DADS obtained from SS6 sphere SiO₂ in SGF medium

Sample name	Zero order (R^2 value)	First order (R^2 value)	Higuchi model (R^2 value)	Korsmeyer-peppas (R^2 value)	Korsmeyer-peppas n=release exponent
DADS	BR	BR	BR	BR	BR
SS6	0.916	0.978	**0.998**	0.974	1.30

Based on this regression coefficient value the best fitted model for burst release of DADS from SS6 in SGF is Higuchi model. As the release exponent value is >0.89, the release mechanism is supercase II transport.

5.8.2.2.F Release kinetic models of Aloin from SS6 sphere SiO₂ in SGF for 24-168 hours:
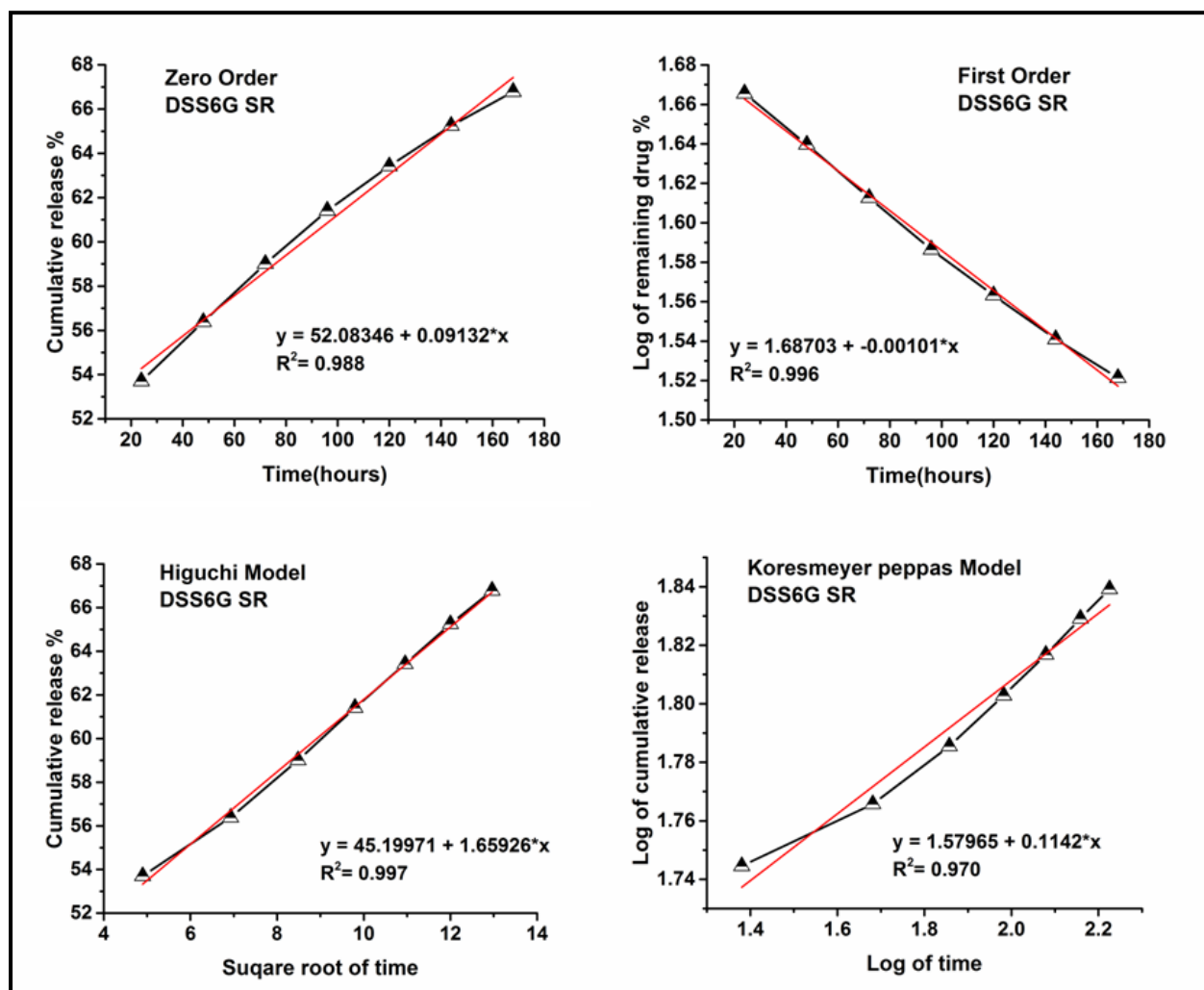
Fig 5.28: Kinetic models of DADS for 24-168 hours of release from SS6 in SGF

Table 5.28: Kinetic data of DADS obtained from SS6 sphere SiO₂ in SGF medium

Sample name	Zero order (R^2 value)	First order (R^2 value)	Higuchi model (R^2 value)	Korsmeyer-peppas (R^2 value)	Korsmeyer-peppas n=release exponent
DADS	SR	SR	SR	SR	SR
SS6	0.988	0.996	**0.997**	0.970	1.57

Based on this regression coefficient value the best-fitted model for the sustained release of DADS from SS6 in SGF is the Higuchi model. As the release exponent value is >0.89, the release mechanism is supercase II transport.

Based on the R^2 value, the best-fitted model of the released drug (DADS) in SBF medium from sphere shaped silica is determined. All sets of R^2 values are given in the respective tables. Table 5.29 summarizes the kinetic study result of DADS release from three different irregular silica nano carriers in SBF and SGF media.

Table 5.29: Kinetic model of DADS released from SiO₂ in SBF & SGF

Sl no	Sample name	Dissolution medium	Burst release	Sustained release
1	SS2	SBF	Higuchi model	Koresmeyer peppas model
		SGF	Higuchi model	Koresmeyer peppas model
2	SS4	SBF	Higuchi model	Higuchi model
		SGF	Higuchi model	Higuchi model
3	SS6	SBF	Higuchi model	First order model
		SGF	Higuchi model	Higuchi model

For all burst and sustained released samples n> 0.89 so, the all mechanisms are super case II transport.

5.9 Antimicrobial activity assay:

5.9.1Bacteria strain preparation: *Salmonella typhi* bacterial starin is prepared in nutrient broth medium at 37˚C in BOD shaker with proper agitation.

5.9.2 MIC study:

To determine the MIC (minimum inhibitory concentration) and MBC (minimum bactericidal concentration), the CLSI guidelines recommend using the broth microdilution method. Using the standard broth dilution method, the MIC assay is carried out in a 96-well plate with a flat bottom. This assay is done at room temperature. MIC is that much of the concentration of any drug which can inhibit the growth of any tested microorganism. Details procedure is mentioned in chapter 4 (section 4.9.2)

Table 5.30: MIC values of DADS over *S. typhi* bacteria

Sl no	Microogranism used	DADS concentration
1	*Salmonella typhi*	0.941 mg/ml

5.9.3 Zone of Inhibition Study:

In the Zone of Inhibition study, a petri dish containing a nutrient agar is spread with the *S. typhi* bacteria culture. The agar plate is incubated at 37˚C temperature appropriate for the test microorganism for 18 to 24 hours. If this antimicrobial agent leaches from the disk into the agar and inhibits growth. A clear zone (the zone of inhibition) appears around the test product here the drug DADS. Due to the presence of a drug that hinders their growth, bacteria cannot grow in this area of the media. The details procedure is mentioned in chapter 4 (section 4.9.3).
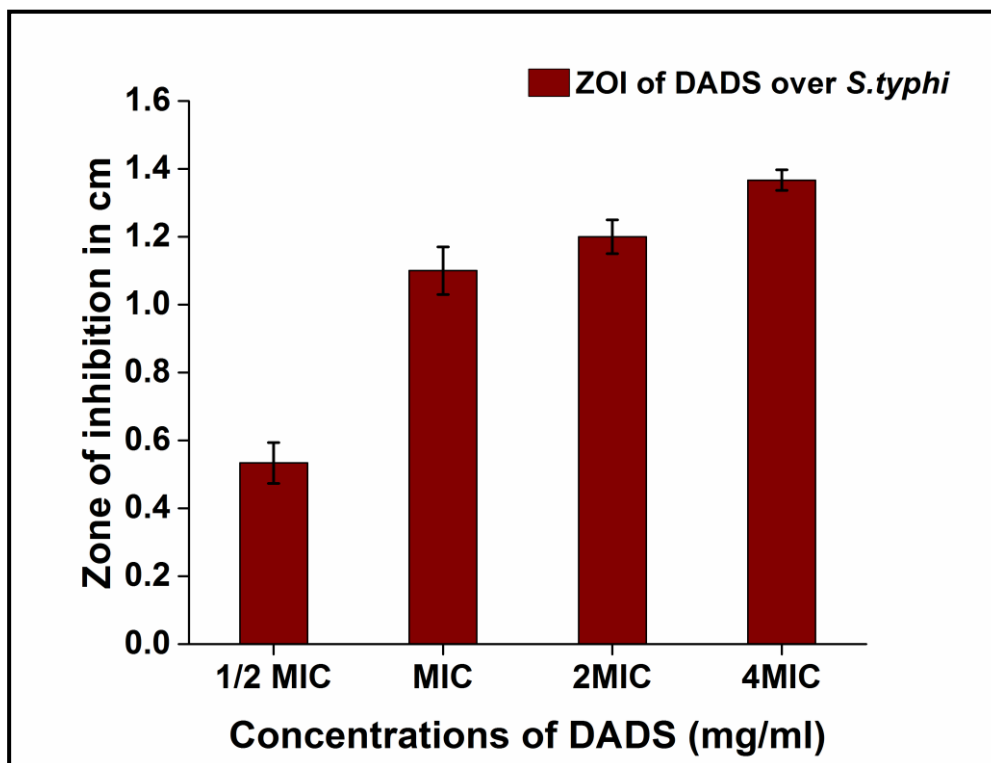
Fig 5.29: ZOI study results of DADS over *S. typhi*
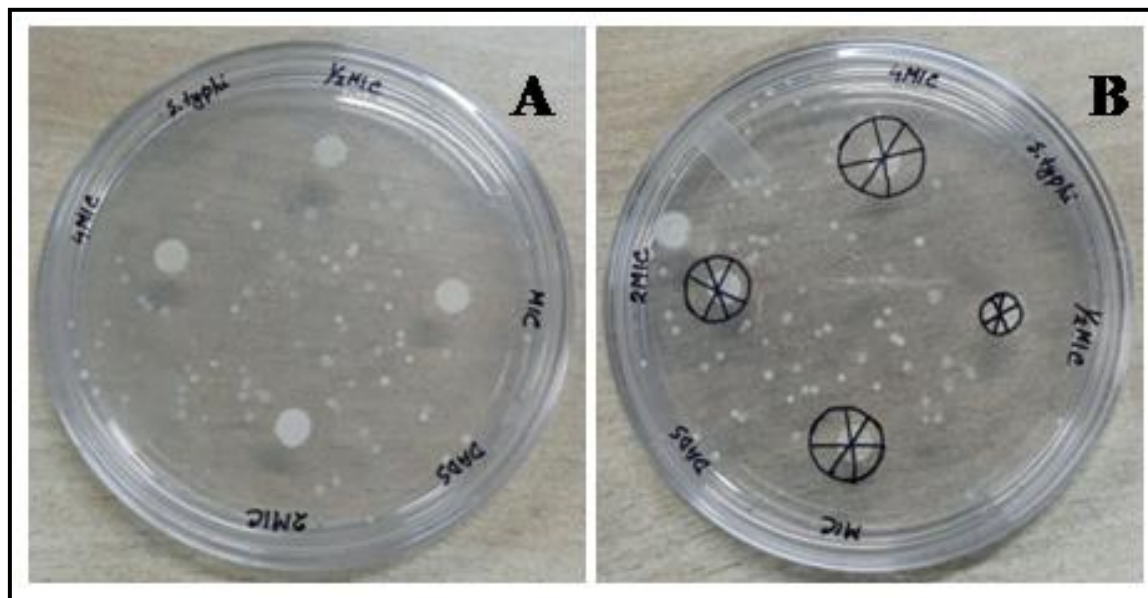
Fig 5.30: Nutrient agar plate of zone of inhibition study of DADS over *S. typhi*

These test results conclude the effect of DADS on the inhibition of *S. typhi*. The test results are plotted in fig 5.29 in a bar diagram. As shown in the image, the measurement is always taken three times, and the mean data are shown on the bar graph above. The MIC value is high enough to stop bacteria from growing. The maximum inhibition of bacterial growth is observed when the drug concentration is 4MIC. The zone of inhibition is measured as 1.35cm.

5.9.4 Growth Curve Analysis:

In order to conduct studies on the growth of bacterial populations, viable cells must be inoculated into a sterile broth medium and the culture must be incubated at the ideal temperature, pH, and gaseous conditions. A population growth curve, which is constructed by plotting the increase in cell numbers versus the time of incubation, can be used to chart the dynamics of microbial growth under these conditions. Here, the increased cell number reflects absorbance, and the time is fixed i.e., 6 hours and the variable thing is the concentration of the drug. Measurement of cellular mass can be calculated using spectrophotometers at 600 nm to determine developing turbidity.
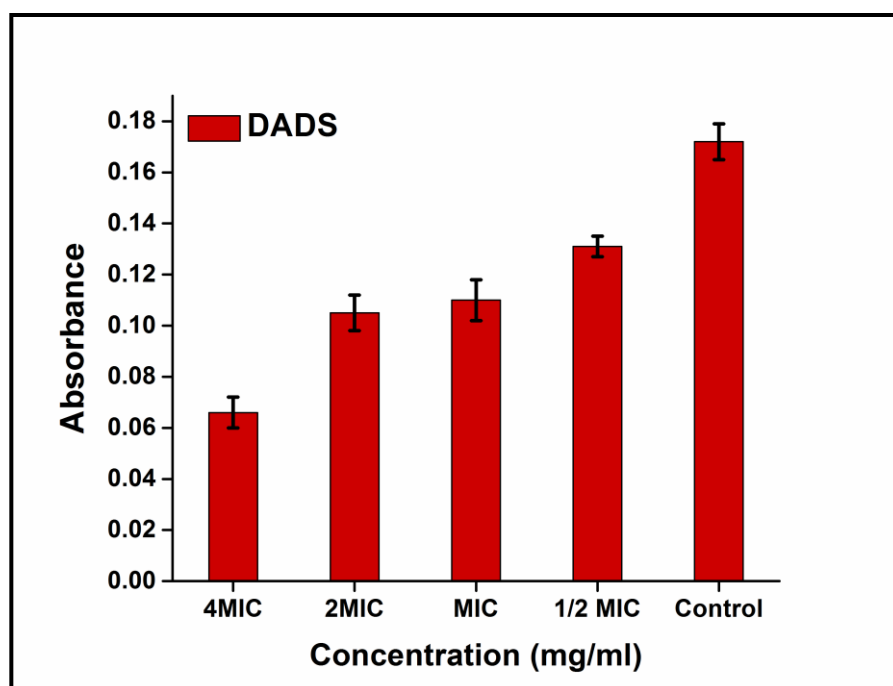
Fig 5.31: Growth curve of *S. typhi* after treatment with DADS

Compared to the controlled growth of the different concentrations of the drug DADS inhibits microbial growth. With the increasing concentration absorbance is reduced means bacterial growth is also inhibited. There is a very small difference in the growth between MIC and 2MIC of the DADS drug released from SiO_2 nanoparticles.

On the other hand, the population of the bacterial cell decreases with an increase in the concentration of the drug DADS as shown in Fig 5.31. Minimum absorbance of 0.065 is observed for a 4MIC concentration of DADS.

5.9.5 CFU Count Study:

Following the growth curve analysis assay, 10 µL of aliquots containing DADS drug and microorganism concentrations are spread on agar media using a spreader from each container. Ethanol is used to sterilize the spreader prior to use. For 24 hours, these agar plates are incubated at 37°C. The colonies are counted on the plates the following day. The entire procedure is repeated three times, and the mean value is considered final. Table 5.31 summarizes the CFU count study after treatment with the DADS drug released in SiO_2 nanoparticles at different concentrations.

Table 5.31: Number of colonies of *S. typhi* bacteria after treatment with DADS drug at their respective concentration

Conc	DSS2G	4MIC	2MIC	MIC	½ MIC	Control
CFU	68	6	35	57	153	226

As concentration increases from the MIC value of the drug, inhibition power also increases. If compared with control growth, almost 25% growth is seen in MIC concentration which is good enough. The 4MIC concentration is high enough for any microorganism and may have some toxic effect, so almost no growth is observed.

5.9.6 Microscopic analysis:

Before doing the microscopic analysis of the bacterial sample, a series of steps are required to follow to get a proper view of the microorganism. The detailed procedure is mentioned in chapter 4 (section 4.9.6). Fig 5.32 & 5.33 are the FESEM images of *S. typhi* and treated *S.typhi* with DADS are shown.
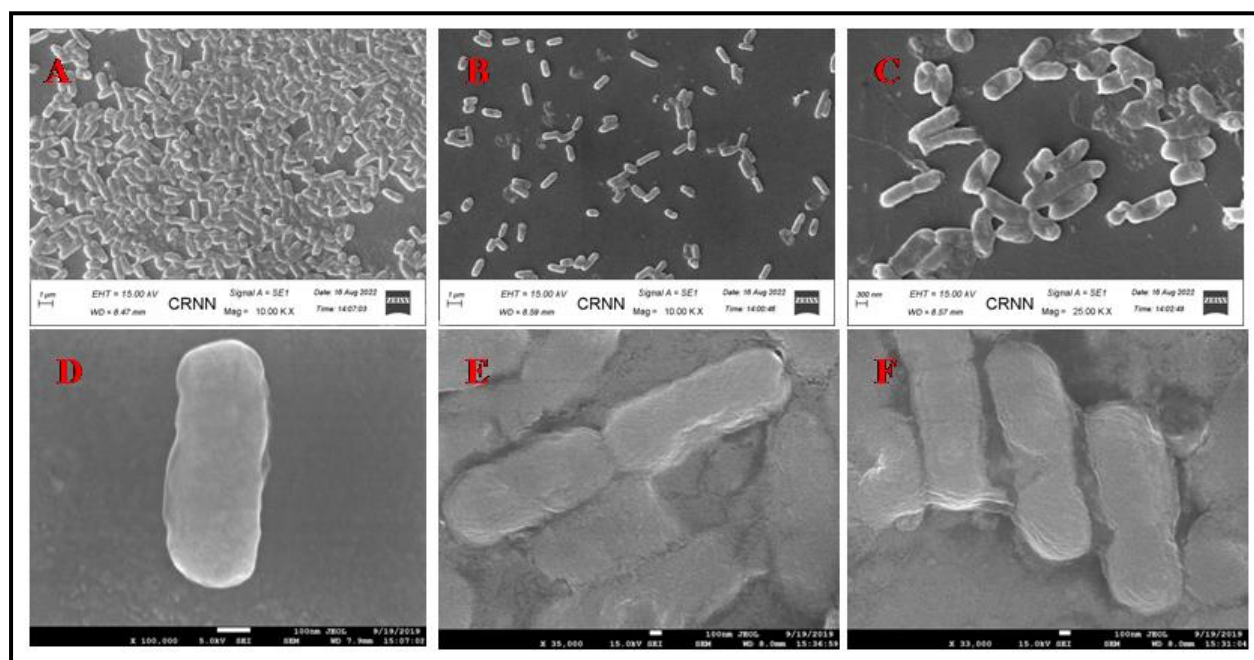
Fig 5.32: Microscopic view of control *S. typhi* bacteria (A-F)
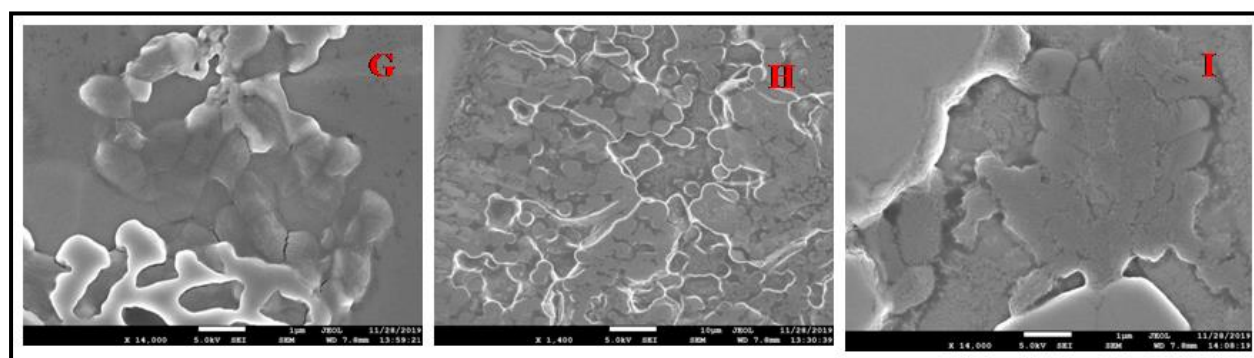
Fig 5.33: Microscopic view of treated *S. typhi* with DADS (G-I)

Microscopic analysis revealed the structure of bacteria treated withreleased drug from drug entrapped nanocarrier. Here the cell wall of all the bacteria was deformed; they became smaller in size, mostly fused together, and appeared almost like the cell wall deficient L forms. The drug i.e, garlic especially the active component Diallyl disulfide could damage the cell structure and function as already reported.

5.10 Anticancer assay:
To see the effectiveness of DADS two different anticancer assays are done over the HepG2 cell line. They are the MTT assay and MB assay.

5.10.1 MTT assay:
The details procedure of this assay is mentioned in chapter 4 (section 4.10.1)
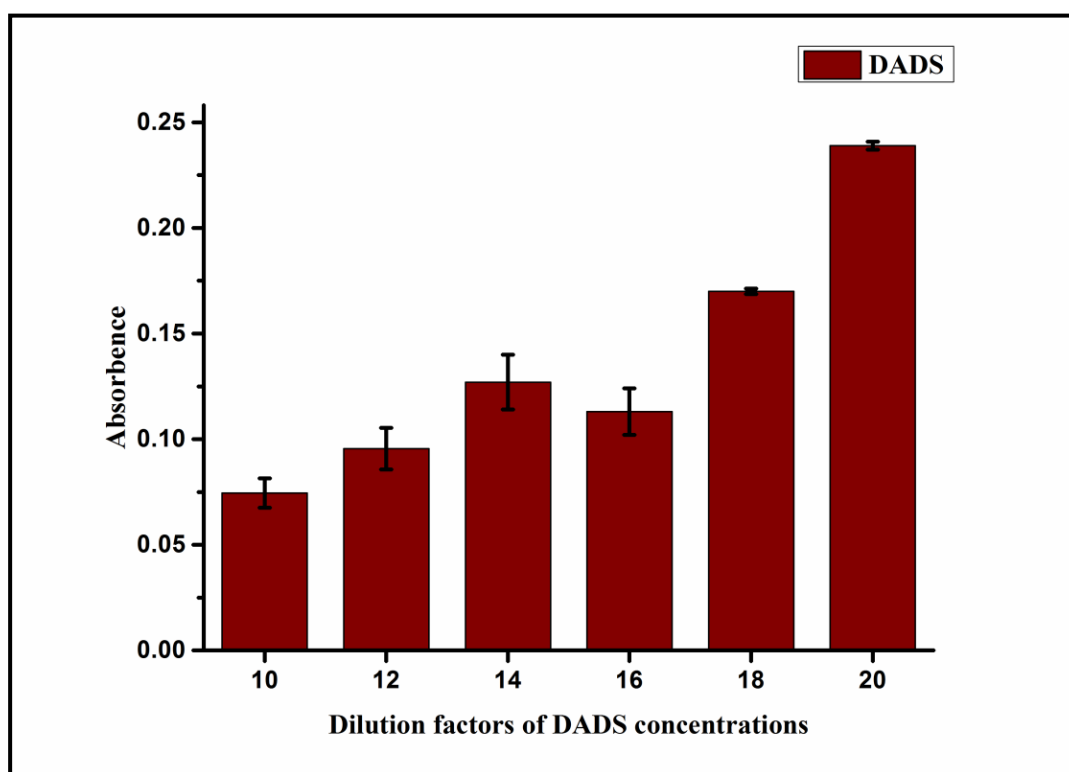
Fig 5.34: Graphical representation of absorbance with concentrations of DADS is shown in figure 5.34. DADS has diluted 10 to 20 times the stock concentration. Absorbance is directly proportional to the living cells present in the respective wells

The number of living cells in each well automatically increases as the concentration of the drug decreases. Thus a minimum living cell can be observed when the drug concentration is maximum. Spectophotometric analysis yields this information. The IC_{50} value is the 14th dilution of DADS. However, this data may be misinterpreted for the chemical and sample colors. Methylene blue assay is also used to verify the experimental results.

5.10.2 Methylene blue assay:

HepG2 cells are cultured in 12 well plates at 37 degrees celsius for 48 to 72 hours in DMEM (Dulbecco's minimal Essential Medium), which is supplemented with antibiotics like penicillin, streptomycin, and amphotericin B and 10% heat-inactivated FBS (fetal bovine serum).

In order to carry out the methylene blue staining assay, the cells are separated, seeded into six-well plates, and kept in an incubator at 37°C and 5% CO2 for 48 hours. Here, the drug concentrations are taken into account at IC50 values. Utilizing inverted microscopic observations, this assay is examined. Microscopic pictures of methylene blue assay are given in Fig 5.35 & 5.36.
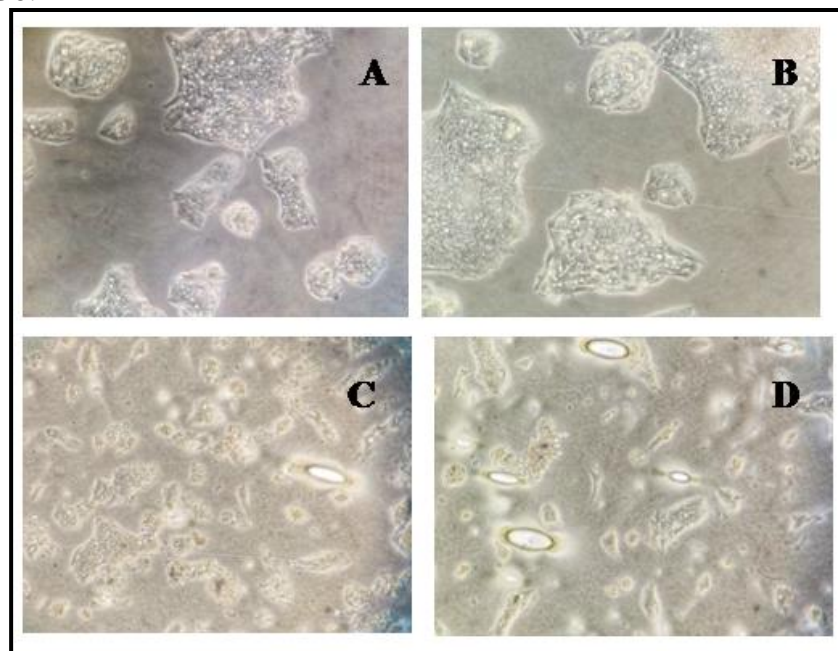
Fig 5.35: Microscopic analysis of HepG2 cell lines in set of methylene blue assay. For control sample freshly cultured and 24 hr incubated bare HepG2 cells are considered. HepG2 cells of 0 hr and 24 hr incubation (A) and (B) respectively for control sample. 1 hr and 24 hr incubation of HepG2 cells with DADS treatment (C) and (D) respectively
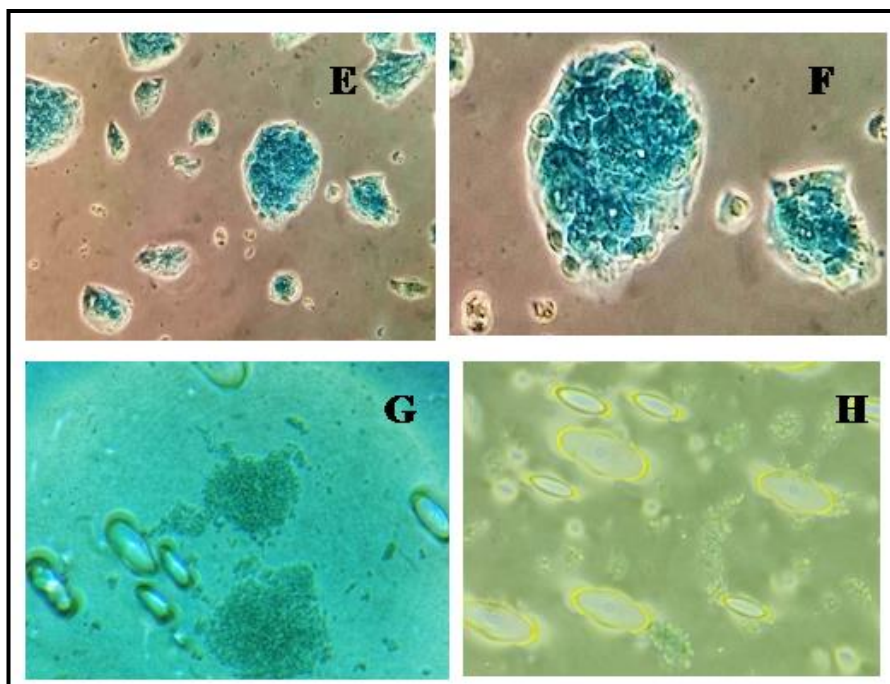
Fig 5.36: Figure E &F represent the control cells with methylene blue staining and G&H represent DADS treated HepG2 cells of methylene blue staining

Result:

DADS is very effective against this HepG2 cell line. After 24 hours of incubation, the cells are not alive. Dead cells are in the medium which becomes cell debris. Methylene blue cannot stain debris, as there are no specific cell clumps seen it stains the medium, and the whole picture came blue.

5.11 Antiviral assay:

Delta SARS-CoV-2 spike RBD protein was chosen as the viral agent for the antiviral assay. The entire experiment is conducted with eggs from *Gallus gallus domesticus*.

For experimental analysis, 13-day old embryonated eggs are procured from Government State Poultry Farm in Kolkata, India. After surface sterilization with rectified spirit, the eggs are candled for embryo viability.

A region is set apart around 1/4 inch beneath and parallel to the base of the air cell and sanitized. In order to avoid damaging the shell membrane, a hole is drilled at this location. With the hole facing upward, the embryo is positioned horizontally. The eggshell is punctured with a sterilized

1/8-inch fine-gauge needle and 0.1 milliliters of inoculum is injected. In an egg incubator, the inoculated eggs are incubated at 37°C and sealed. After 48 hours (on the 16th day) of incubation, 5–10 mL of allantoic fluids are collected in sterile vials and stored at 80 °C for further analysis. Before that, every egg is exposed for two hours at 2–8 °C. In addition, the physical conditions of each embryo are observed.

Table 5.32: Sample name of DADS set for the antiviral experiment

Sl no	Sample name	Sample code
1	DADS raw	DR
2	DADS released in SBF	DRS
3	Ag challenged by DADS raw	DDR
4	Ag challenged by DADS released in SBF	DDRS
5	SBF Control	SC
6	Ag challenged by SBF control	DSC
7	Antigen	Ag

To conduct comparative gene expression studies real-time PCR with dNTPs, Taq polymerase, $MgCl_2$, buffer, and SYBR Green-tagged primers are used. The changes in expression are compared to the housekeeping gene ß actin and calculated as a fold increase or decrease from the value of the normal control.

Table 5.33: Increase in cytokines (fold increase in comparison with normal control) in different experimental sets after 48 hours

SET	IFNα	IFNß	IL-6	IL-8	IL-1B	IL-10
DR	2.46	44.07	13.78	13.07	0.45	2.89
DRS	11.46	8.41	11.20	7.97	7.75	4.38
DDR	4.82	16.96	8.89	41.50	11.35	47.87
DDRS	2.77	1.82	8.03	14.57	8.26	16.07
SC	0.27	7.05	0.00	0.00	0.29	0.88
DSC	4.00	2.89	15.08	7.97	12.51	13.64
AG	1692.57	149.09	7.285	3.02	2.02	2.948

This is the mean fold expression of all genes over the set of samples or material injected within the embryonated eggs. These gene expressions are the results of the effectiveness of the set of samples.
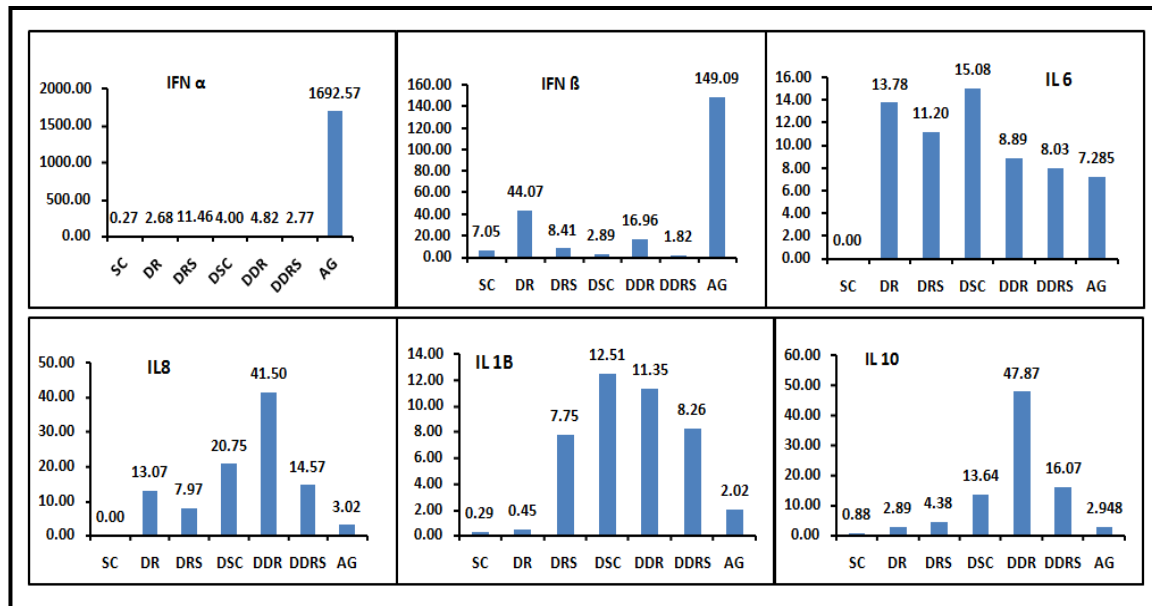
Fig 5.37: Relative fold change in expression of selected gene in respect of housekeeping gene ß actin
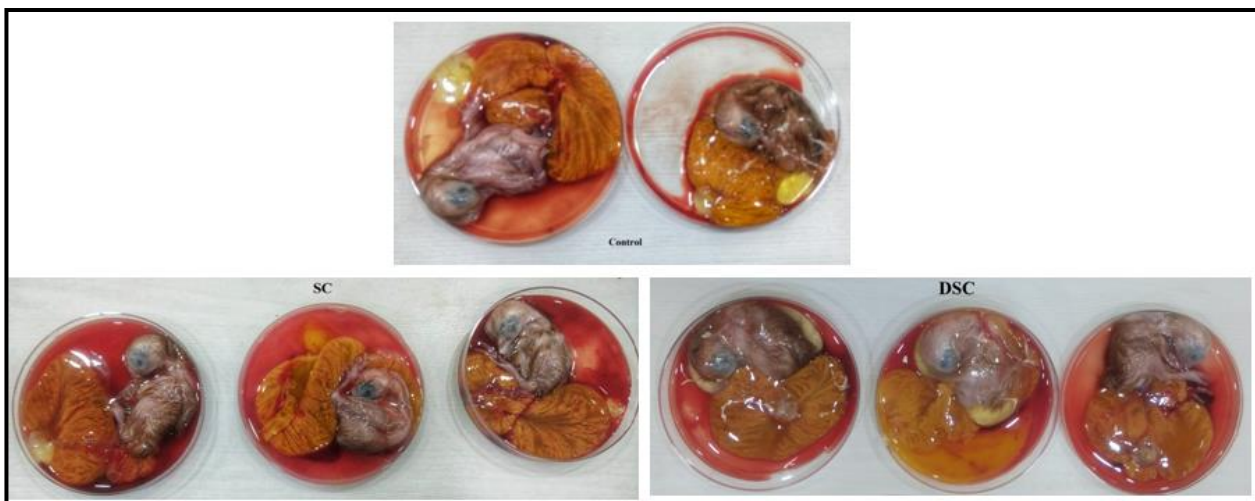
Fig 5.38: Pictures of egg embryo of controls after 48 hours of incubation
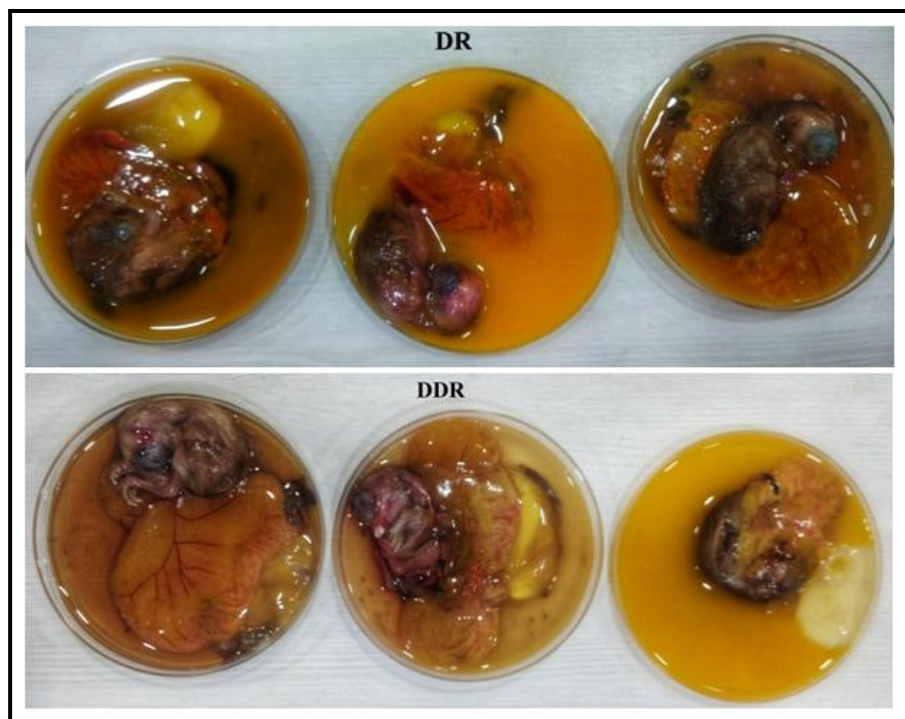
Fig 5.39: Pictures of egg embryo treated with raw garlic and antigen challenged by raw garlic
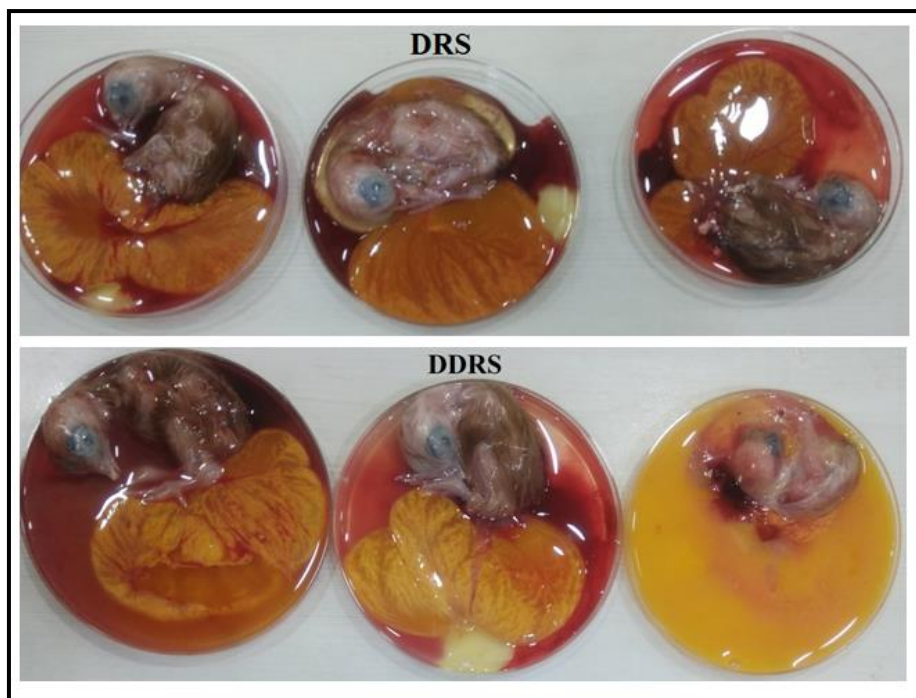
Fig 5.40: Pictures of treated embryo with released garlic and Ag challenged by released garlic from nano particles

Results and interpretation:

IFN alpha: Although the antigen markedly increases IFN-ALPHA gene expression (1692.57 times than the control) the SBF markedly decreases the gene expression to almost zero level other than DADS released from nanocarrier (11.46 times). DADS Raw in other experimental sets mild insignificant upregulation was noted. The result indicates that DADS release is capable of upregulating IFN- alpha gene significantly.

IFN-ß-In this experiment although the vehicle SBF markedly decrease IFN-ß gene expression but a significant recovery was noted with DADS Raw. However, DADS release was not capable of upregulating IFN-ß gene expression.

IL-6- The results show that DADS Raw& DADS Rel. are capable of increasing IL-6 gene expression but when the antigen was challenged with SBF then also IL-6 gene expression is increased. This may indicate that when DADS raw & DADS rel. are applied directly they are capable of increasing IL-6 on the other hand the electrolytes present in SBF may also effectively increase this gene expression only when challenged after administration of antigen.

IL-8- The results indicated almost similar changes to IL-6. One must note that both IL-6 & IL-8 are responsible for producing cytokine storms when infected with SARS-Cov-2 thus a tendency of increasing IL-6 & IL-8 gene expression is not apparently beneficial to the healthy body system.

IL-1ß- The expression of IL-1 ß is almost the same as IL-6. This gene expression is also not beneficial to the normal body system.

IL-10- IL-10 gene expression is markedly increased with DADS Raw and DADS Release after their challenge following Ag administration. And this change is much more expressed than the proinflammatory genes IL-6,IL-8, and IL-1ß are increased and may be detrimental to the health system but DADS Raw and DADS Release are capable of counteracting those detrimental changes by markedly increasing anti inflamatory cytokine gene IL-10 and thus it appears that both DADS Raw and DADS release will give overall beneficial effect in SARS-CoV -2 pathological changesand appears to be an excellent agent in the management of corona virus

infection. In the future, an imbalance and markedly increase in proinflamatory cytokines are the main cause of mortality in Covid 19 disease.

5.12. Conclusion:

DADS is extracted in ethanol medium and entrapped in both type of SiO_2 nanocarriers. The entrapment of DADS in SiO_2 nanopaticles is confirmed by FTIR analysis. Presence of 900-1100 cm^{-1} is for the C-S bond and 400-700 cm^{-1} is assigned to S-S stretching in FTIR plot of DADS entrapped SiO_2 nanopaticles confirms the presence of DADS phytochemicals in SiO_2 nanopaticles.

DADS is released from the SiO_2 nanocarriers into SBF & SGF and the cumulative dissolution percentage is calculated using UV-Vis spectrophotometer. It is observed that 57% DADS is released in SGF and 39% DADS is released in SBF for irregular shaped SiO2 whereas, dissolution percentage of DADS is increased in both media in case of sphere shaped SiO_2 nanoparticles. In this case 81% and 70% DADS is released in SGF and SBF media respectively.

Release kinetics study (both burst and sustained release) of DADS in SBF & SGF for irregular shaped and sphere shaped SiO_2 is carried out. In each case using regression coefficient values the best fitted kinetic model is identified.

Release kinetic study of DADS in SBF from three different irregular shaped silica nano carriers (Sample S2, S4 and S6) reveals that burst release of DADS from samples S2 & S6 best fit to Higuchi model & sample S4 fit to first order model. Sustained release of DADS from S4 & S6 samples in SBF follows koresmeyer peppas model and S2 follows higuchi model. Burst & sustain release of DADS in SGF from S2 fits on first order model. Burst & sustained release of DADS from S4 match with koresmeyer peppas model & higuchi model respectively. DADS release from S6 follows higuchi model and zero order model for burst and sustained release respectively. In every model 'n' value is greater than 0.89 that means all release mechanisms are super case II transport except burst release from S4 in SBF and from S2 in SGF, where n< 0.89 implying release mechanisms are anomalous (non-fickian) diffusion.

In the kinetic study of release of DADS from three different sphere samples of silica nano carriers (SS2, SS4 & SS6) in both SBF and SGF, for burst release match to Higuchi model. For

sustained release from SS2, SS4 & SS6 in SBF, match with koresmeyer peppas model, higuchi model and first order kinetic model respectively. For sustained release of DADS in SGF, from SS4 & SS6 kinetic model fits to Higuchi model and SS2 fits to Koresmeyerpeppas model respectively. In every model 'n' value is greater than 0.89 indicating all release mechanisms are super case II transport.

In the application part, released DADS from irregular and sphere shaped are compared and highest percentage of released DADS is considered for the applications. The highest DADS release is found to the very effective as an antimicrobial agent for *Salmonella typhi* bacteria. The MIC value calculated is 0.941 mg/ml. The zone of inhibition is 1.1 mm for MIC concentration. The CFU count is 68 for the released DADS. Microscopic view shows the deformation of bacterial sample comparing to the control sample after treatment with released DADS.

In anticancer study, at first IC_{50} value of pure drug is determined. For this DADS is diluted from 10 to 20 times from a stock concentration of 1mg/ml. From spectrophotometric analysis IC_{50} value is obtained as 14th for DADS. This IC_{50} value of pure DADS is considered for methylene blue assay as it is regarded as effective concentration for hepatocellular carcinoma cell line. In the methylene blue assay most of the cancer cells are present with debries as there are no specific cell clumps seen after treatment with IC_{50} concentration of DADS which means it is very effective for HCC cancer cell line.

In the antiviral assay it is observed from all cytokines expression it appears that both DADS raw and DADS release will give overall beneficial effect in SARS-CoV -2 pathological change sand appears to be an excellent agent in the management of coronavirus infection. In the future, an imbalance and markedly increase in proinflamatory cytokines are the main cause of mortality in Covid-19 disease.

References:

1. Pal, P., Dey, R., Das, S., & Chaudhuri, M. G., 2018. Nanomaterials in Relation To Their Drug Delivery and Release Mechanisms: a Review Exemplified With Some Herbal Drugs, World Journal of Pharmaceutical Research, *7*(9), pp. 1782–1804.

2. Tao Z. Mesoporous silica-based nanodevices for biological applications. RSC Advances. 2014;4(36):18961.

3. Somade OT, Ugbaja RN, Alli AA, Odubote OT, Yusuf TS, Busari BT. Diallyl disulfide, an organo-sulfur compound in garlic and onion attenuates trichloromethane-induced hepatic oxidative stress, activation of NFkB and apoptosis in rats. Journal of Nutrition & Intermediary Metabolism. 2018;13:10-9.

4. Tepe B, Sokmen M, Akpulat H, Sokmen A. In vitro antioxidant activities of the methanol extracts of five species from Turkey. Food Chemistry. 2005;92(1):89-92.

5. Lanzotti V. The analysis of onion and garlic. Journal of Chromatography A. 2006;1112(1-2):3-22.

6. Corzomartinez M, Corzo N, Villamiel M. Biological properties of onions and garlic. Trends in Food Science & Technology. 2007;18(12):609-25.

7. Leuschner RGK, Ielsch V. Antimicrobial effects of garlic, clove and red hot chilli onListeria monocytogenesin broth model systems and soft cheese. International Journal of Food Sciences and Nutrition. 2003;54(2):127-33.

8. Mostafa MG, Mima T, Ohnishi ST, Mori K. S-Allylcysteine Ameliorates Doxorubicin Toxicity in the Heart and Liver in Mice. Planta Medica. 2000;66(2):148-51.

9. Yin M-c, Cheng W-s. Antioxidant and antimicrobial effects of four garlic-derived organosulfur compounds in ground beef. Meat Science. 2003;63(1):23-8.

10. Yin M-c, Cheng W-s. Antioxidant Activity of Several AlliumMembers. Journal of Agricultural and Food Chemistry. 1998;46(10):4097-101.

11. Iranshahi M. A review of volatile sulfur-containing compounds from terrestrial plants: biosynthesis, distribution and analytical methods. Journal of Essential Oil Research. 2012;24(4):393-434.

12. Haina Wang XJ. Drug Metabolism and Pharmacokinetics of Organosulfur Compounds from Garlic. Journal of Drug Metabolism & Toxicology. 2013;04(05).

13. Mnayer D, Fabiano-Tixier A-S, Petitcolas E, Hamieh T, Nehme N, Ferrant C, et al. Chemical Composition, Antibacterial and Antioxidant Activities of Six Essentials Oils from the Alliaceae Family. Molecules. 2014;19(12):20034-53.

14. O'Gara EA, Hill DJ, Maslin DJ. Activities of Garlic Oil, Garlic Powder, and Their Diallyl Constituents against Helicobacter pylori. Applied and Environmental Microbiology. 2000;66(5):2269-73.

15. Lampe JW. Health effects of vegetables and fruit: assessing mechanisms of action in human experimental studies. The American Journal of Clinical Nutrition. 1999;70(3):475s-90s.

16. Fukushima, S., Takada, N., Wanibuchi, H., Hori, T., Min,W., & Ogawa, M.,. Recent Advances on the Nutritional Effects Associated with the Use of Garlic as a Supplement Suppression of Chemical Carcinogenesis by Water-Soluble Organosulfur, (1988), pp. 1049–1053.

17. Dutta D, Paul B, Mukherjee B , Mondal L, Sen S, Chowdhur C & Chatterjee Debnath M., 2019 . Nanoencapsulated betulinic acid analogue distinctively improves colorectal carcinoma in vitro and in vivo, 2019, *9:11506.*

18. Compounds, O., 1964. C-S Stretching Frequency. *Science*, *42*, pp. 36–42.

19. Tasci B, Kutuk H, Koca I. Determination of alliin and allicin in the plant of Allium scorodoprasum L. subsp. Rotundum by using the infrared spectroscopy technique. Acta Horticulturae. 2016(1143):133-8.

20.Pukkela P, Borra S. Machine Learning Based Plant Leaf Disease Detection and Severity Assessment Techniques: Stateof- the-Art. Lecture Notes in Computational Vision and Biomechanics: Springer International Publishing; 2017. p. 199-226.

CHAPTER 6

Release kinetics study of Aloin& DADS from nano clay carrier and its applications

6.1 Introduction:

Nanocomposite technology has the potential to enhance a wide range of polymer properties, including mechanical, thermal, barrier, durability, chemical stability, flame retardancy, scratch/wear resistance, biodegradability, and optical, magnetic, and electrical properties. [1,2,3,4] The final property of nanocomposites are influenced by the interfacial interactions, component properties, microstructure and their composition. However, the dimensions and microstructure of the filler phase have been shown to have a significant impact on the properties of nanocomposites.[5] To put it another way, the final morphology and properties of the polymer nanocomposite are primarily influenced by the nature of the filler. Clays belong to the category of nanofillers that have been extensively utilized in the process of making polymer nanocomposites. Due to their dramatically improved properties in comparison to conventional filled polymers in a very low fraction of filler addition, the development of polymer/clay nanocomposites has recently garnered a growing amount of interest. [6,7] Due to their unique properties, polymer/clay nanocomposites have received a lot of attention and research interest. These properties are impossible to achieve with microfillers or other nanofillers. Clays are becoming increasingly important in the contemporary polymer industry due to their improved value-added properties, mechanical properties, and light weight without sacrificing pure polymer processability. Layered silicates, the main class of silicates with layered structures, include clay minerals. Natural or synthetic minerals known as layered silicates are made up of regular stacks of alumino silicate layers that have a high aspect ratio and a large surface area. Layered silicates are inexpensive and readily available. Clays are currently the most widely used layered silicates for the production of polymer nanocomposites. A portion of the soil fraction with a particle size of less than 2 µm is referred to as clay. The nanoscale thickness of the clay layers is approximately 1 nm. Clays are made up of many different unique formulas, structure, and properties, like swelling and exfoliation. Polymer nanocomposites can be made from members that can be exfoliated by polymer chains or monomers and distributed as individual clay layers within a polymer matrix. Clays are made up of layers. Tetrahedral sheets, in which a silicon atom is surrounded by four oxygen atoms, and octahedral sheets, in which an aluminum or magnesium metal is surrounded by eight oxygen atoms, are used to construct the layers. By sharing oxygen atoms, the tetrahedral (T) and octahedral (O) sheets fuse together. With a regular gap in between, the layers remain close together. The void is referred to as a gallery or interlayer. D-spacing

(d001) or basal spacing is the thickness of repeated units in a regular multilayer structure with one layer and one inter layer space. Clays' X-ray diffraction patterns can be used to measure or calculate their basal spacing. The nature of the clay as well as the degree of swelling or hydration of the interlayer cations affects the dimension of the layers. For montmorillonite, the distance between the layers is about 1 nm. The interlayer distance varies based on the charge density of the layers, the interlayer cation radius, and its degree of hydration. The electrostatic and van der Waals forces that hold the layers together are relatively weak. Cations in the spaces between layers can be hydrated in aqueous solutions, a process known as "clay swelling," due to the thin forces between layers. The increased interlayer space is caused by swelling.[8]

Clays are frequently utilized in the pharmaceutical industry, either as net ingredients or as activated ingredients. It has been observed that when administered concurrently, they may interact with drugs, thereby reducing their absorption. Swelling clay minerals like montmorillonites (MMT), which produce a homogeneous dispersion of hydrated nanocrystals in pure water, are included in this category and can be used to achieve technological and biopharmaceutical advantages regarding the control of release. Electrostatic interaction stabilizes bioactive molecules in the interlayer spaces, allowing for controlled release by exchanging bioactive molecules with other ions if there are enough in the biological environment. In a diluted solution, the net effect of the attractive and repulsive forces (DLVO) between two clay particles is attractive. [9] The clay layers tend to move away when some parameters, like pH and electrolyte concentration are controlled, which affect the attractive force.

In this chapter, aloin and DADS are entrapped within nano clay carrier and they are released in SBF and SGF. The release kinetics of the two herbal extractions in both media is studied. Released samples are considered for application in antimicrobial and anticancer agent.

6.2 Methodology:

6.2.1 Synthesis of NaMMT clay:

Na modification is done at room temperature with 0.1 N NaCl. 5 gm MMT clay is dispersed within a beaker having 100 ml of deionized water. Then it is allowed to stir for 5-10 hours on a magnetic stirrer. After that, 0.1N NaCl with required quantity is added and allowed to mix properly with clay. After proper mixing, the total clay solution is transferred to centrifuged tubes. Then it is centrifuged at 4000 rpm for 5- 10 minutes. After centrifugation, supernatant is discarded and sediment is washed with deionized water until all chlorine goes out. Then sediment is collected and oven dried at 105˚C to make water free. Then the dry sample is ground in morter and powder of NaMMT is obtained. This NaMMT powder is used for all characterization and experiment purpose.
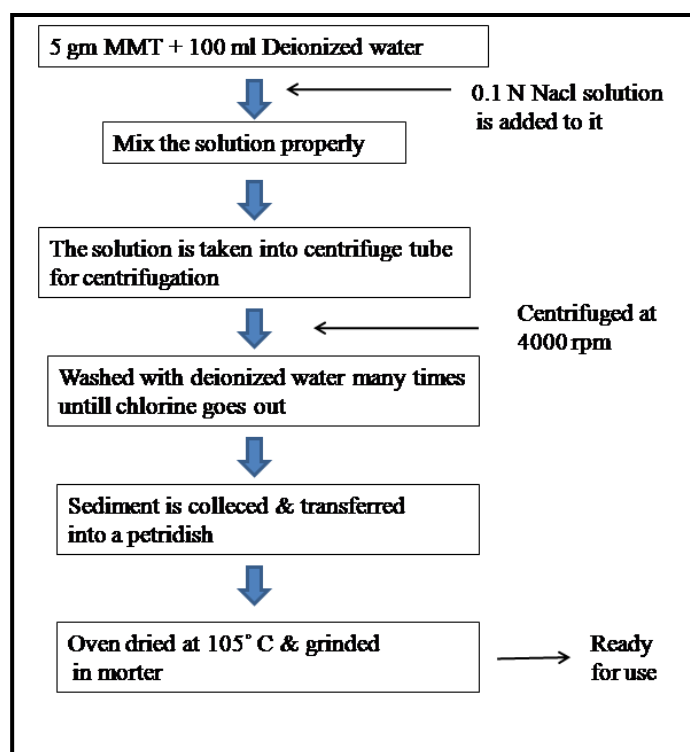
Fig 6.1: Overall process of synthesis of sodium modified MMT clay

6.2.2 Characterization of nanoclay:

Characterization of nano clay is done with X-ray diffraction (XRD) patterns, analyzed with Rigaku, Ultima IV, Japan and microscopic analysis through scanning electron microscope and transmission electron microscope.

6.3 Result and discussion:

6.3.1 XRD analysis:
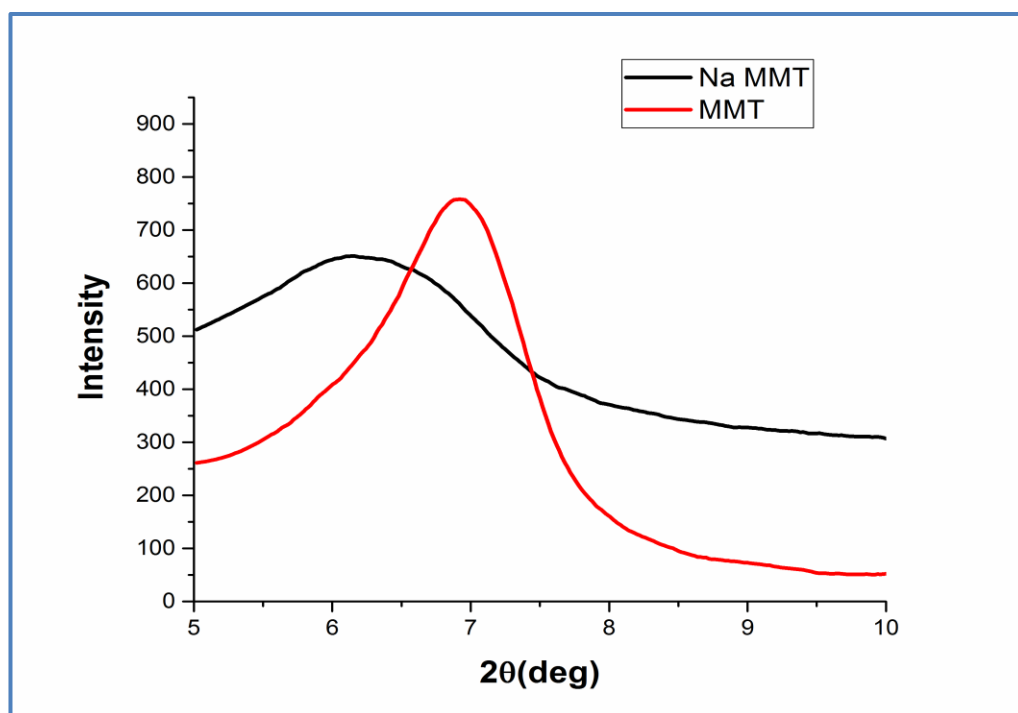
Fig6.2: XRD graph of MMT (red) Na MMT (black)

Fig. 6.2 represents the XRD plots of MMT clay and NaMMT clay. It is observed from the XRD data, the plot of surfactant modified MMT i.e. NaMMT clay is shifted in left side indicating blue shifting. This blue shifting means interlayer space is increased which is good for more drug entrapment. More drug entrapment will result in more drug delivery. Thus NaMMT is a better drug carrier compared to ordinary MMT and thus all experiments are done with Na MMT clay.

6.3.2 SEM analysis:
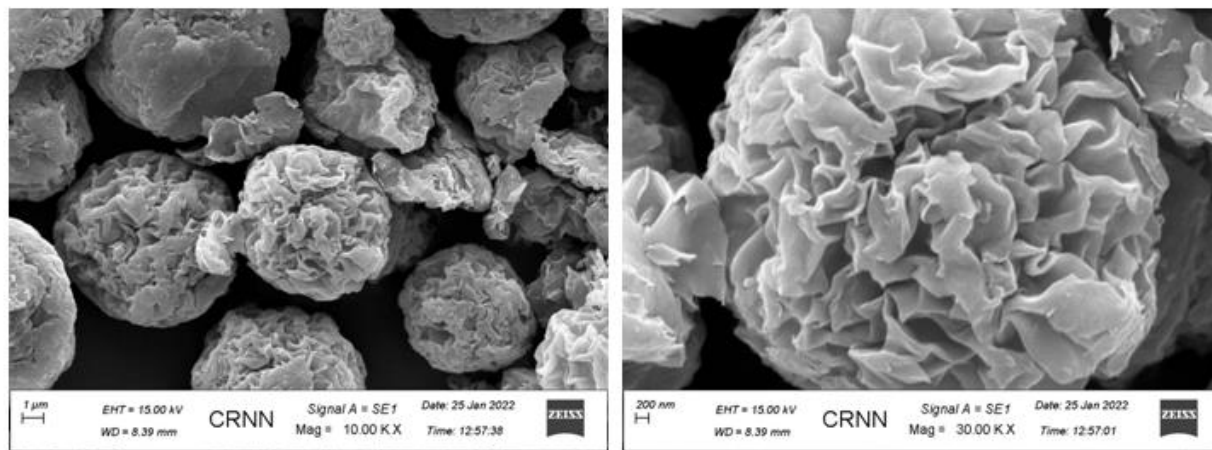
Fig 6.3: SEM analysis of Na MMT clay

Layered clay material has flecks like structure which is prominently seen in SEM micrograph. Highest magnification shows the orientation in flecks properly. These flecks are the layers which make this substance more surface opening nanomaterial.

6.3.3 TEM analysis:
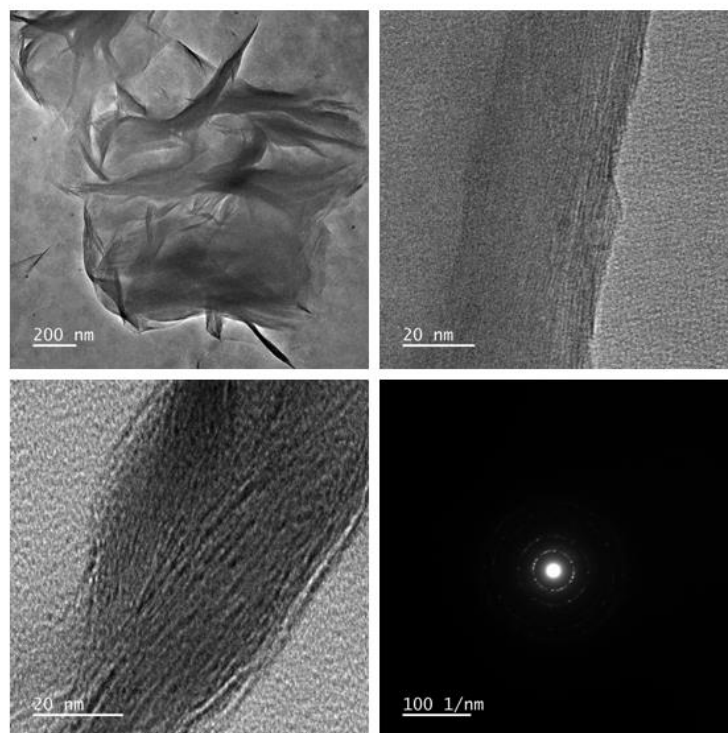
Fig 6.4: TEM analysis of Na MMT clay

TEM analysis shows the interlayer spacing of the material. The flecks structure is more magnified here also. Interlayer spacing is found to be 2.5 nm to 1 nm.

6.4 Drug loading determination:

Aloin powder is dispersed in 2% methanol solution with continuous stirring where 2 mg silica particles are added and allow this mixture for stirring at least 24 hours at 37 ˚C at 250 rpm. The concentration of drug is calculated through UV-Vis spectrophotometer at 298 nm. The loading percentage of a drug within any matrix or vehicle is determined through this equation (1)

$$\text{Drug loading \% (Actual)} = \frac{Amount of drug in nanoparticles}{Amount of nanoparticles} \times 100 \tag{1}$$

Drug loading within the delivering carrier is an important parameter to evaluate the therapeutic efficacy of the particular drug delivery because it determines the administered formulation.

Encapsulation efficiency is determined through the equation (2)

$$\text{Encapsulation efficiency (\%)} = \frac{Drug loading \% (Actual)}{Drug loading \% (Theoritical)} \times 100 \tag{2}$$

Table 6.1: Sample name with drug loading and encapsulation efficiency

Sl no	Sample name	Drug loading (%)	Encapsulation efficiency (%)
1	Aloin entrapped NaMMT clay	0.43	87.17
2	DADS entrapped NaMMT clay	0.39	78.82

6.5 Characterization of drug entrapped clay:

6.5.1 FTIR analysis:
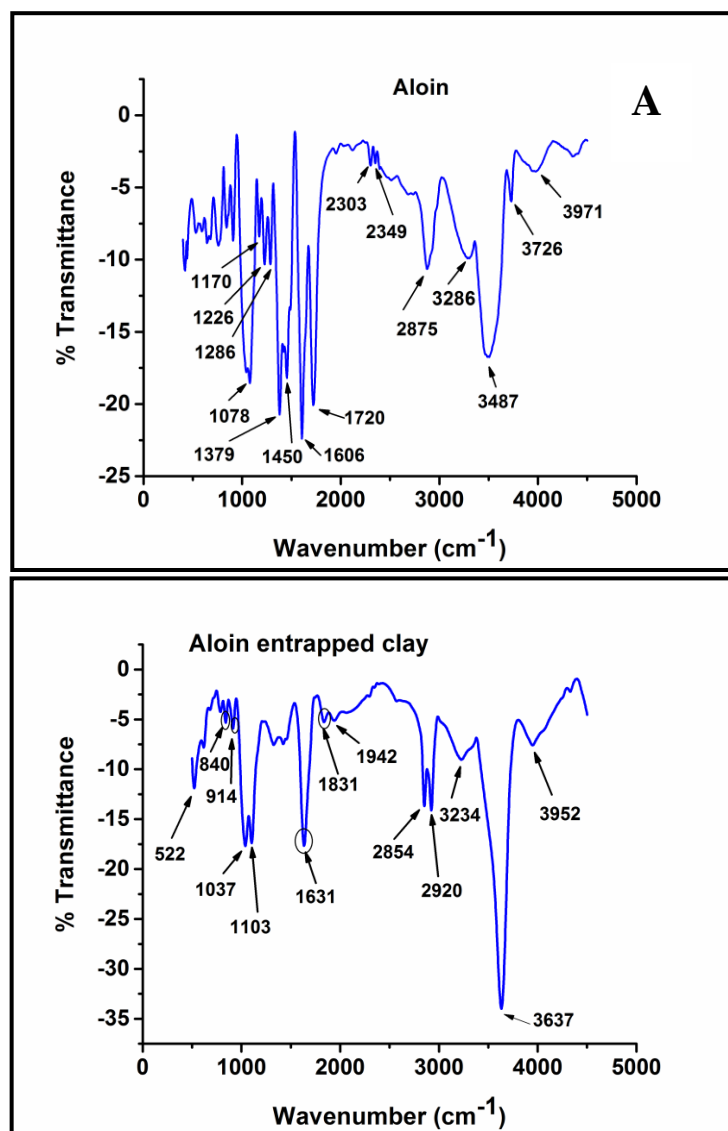
Fig 6.5: FTIR analysis of Aloin (A) and Aloin entrapped within clay (B)

790-850 cm-1 vibration is denoted for C=C bond. 900-1300 cm-1 vibration is for C-O & 1600-1680 cm-1 for C=C and 1650 -1850 cm-1 is for C=O. 844 cm-1, 908 cm-1, 1606 cm-1, 1720 cm-1 vibrations are seen in in Fig 6.5A which is denoted for C=C, C-O, C=C & C=O respectively. In the Fig 6.5B 844 cm-1 is red shifted to 840 cm-1. 908 cm-1, 1606 cm-1 & 1720 cm-1 is blue shifted to 914 cm-1, 1631 cm-1 & 1831 cm-1 respectively . Comparing the

vibrations with Fig 6.5A, it is concluded that aloin is entrapped within the clay as reflected in Fig 6.5B.
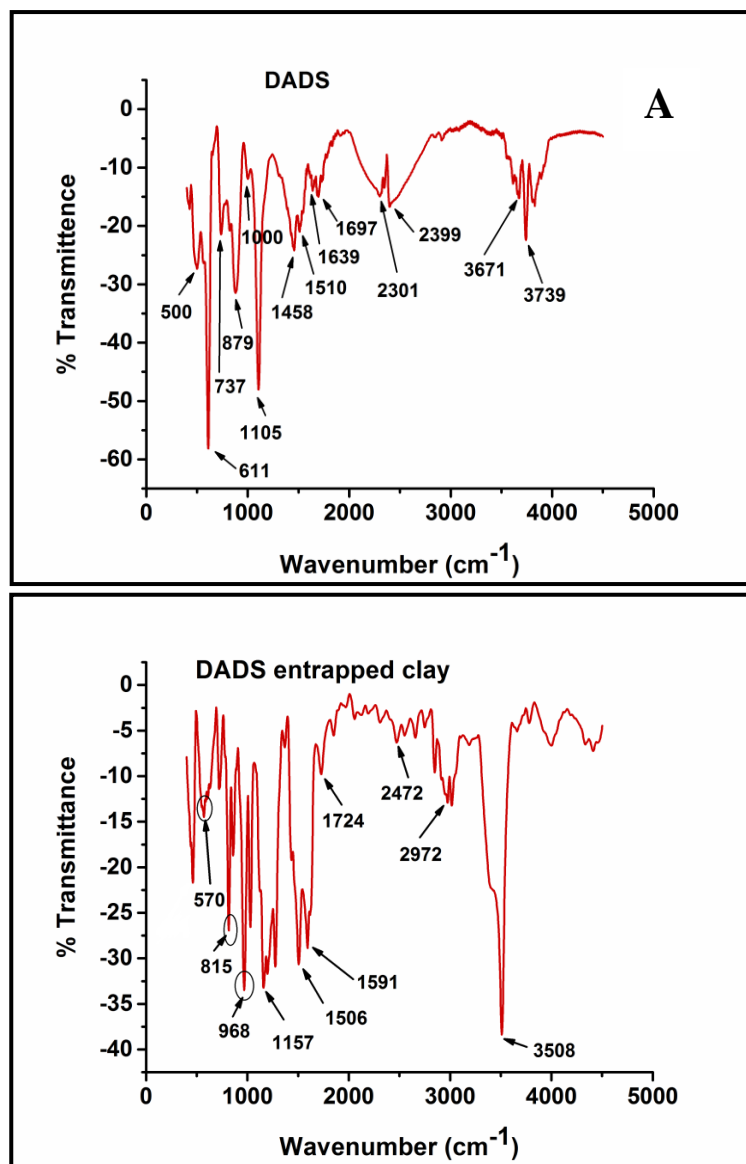
Fig 6.6: FTIR analysis of DADS (A) and DADS entrapped clay (B)

Comparing with two graphs 6.6A & 6.6B there are many new absorptions found in the spectrum of dialyl disulphide entrapped irregular shaped silica which is the result of DADS entrapment. 900-1100 cm^{-1} is for C-S bond. 400-700 cm^{-1}is assigned to S-S stretching and 790 -840 cm^{-1} is for C=C vibration. In the graph 6.6A 426 cm^{-1}is found for the bond vibration of S-S stretching which come from Diallyl disulphide compound which is red shifted to 460 cm^{-1}in graph 6.6B.

1000 cm^{-1} in graph 6.6A is responsible for C-S bond which is increased to 968 cm^{-1} in graph 6.6B due to the entrapment of drug within it.

6.6 Drug release studies:

Clay entrapped drug molecules are released in two different pH medium SBF and SGF for predetermined time duration. This release study is done in a BOD shaker at room temperature. At every time interval 3 ml of medium is collected and replaced with fresh medium to maintain the concentration of the medium. The collected samples are measured at uvvis spectrophotometer and collected data is used to do kinetic models.
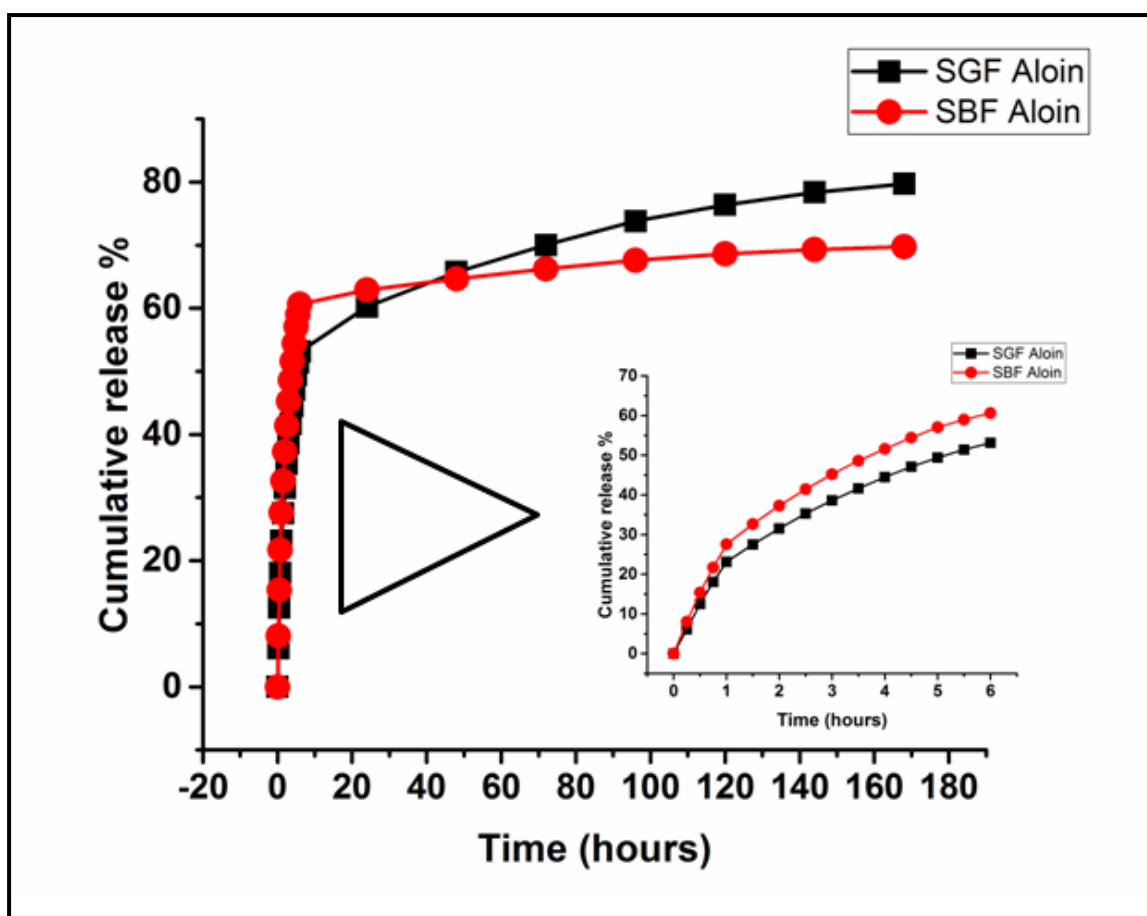
Fig 6.7: Drug dissolution profile of Aloin from Na MMT clay
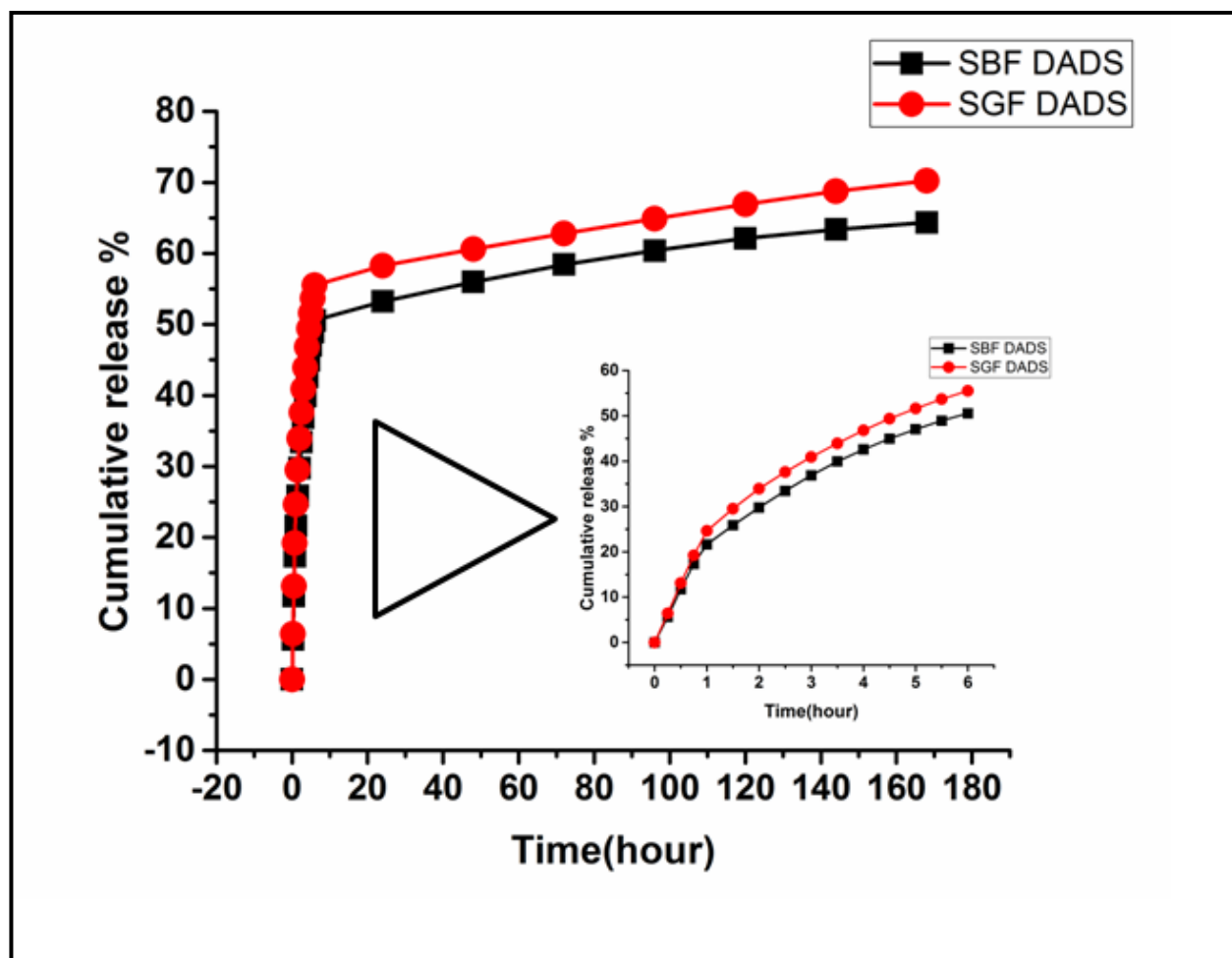
Fig 6.8: Dissolution profile of DADS from Na MMT clay

6.7 Drug release profile and kinetic behavior study of Aloin& DADS sample in two different medium:

Table6.2: Cumulative release of drugs in SBF and SGF from nano clay

Sl no	Sample name	%Cumulative release
1	ACB (Aloin entrapped nanoclay released in SBF)	69
2	ACG (Aloin entrapped nanoclay released in SGF)	79
3	DCB (DADS entrapped nanoclay released in SBF)	64
4	DCG (DADS entrapped nanoclay released in SGF)	70
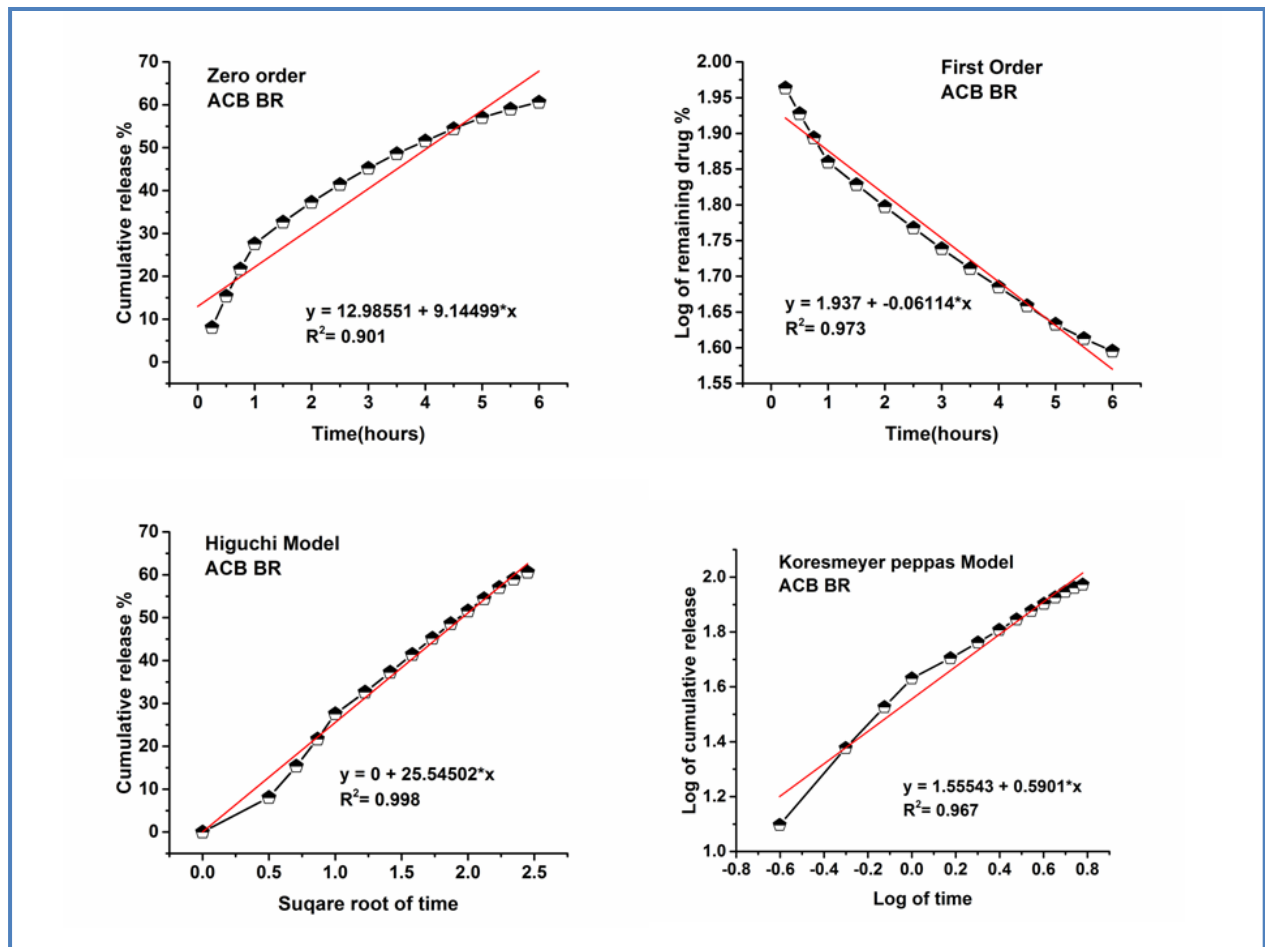
Fig 6.9: Release kinetic models of Aloin in SBF for first 6 hours
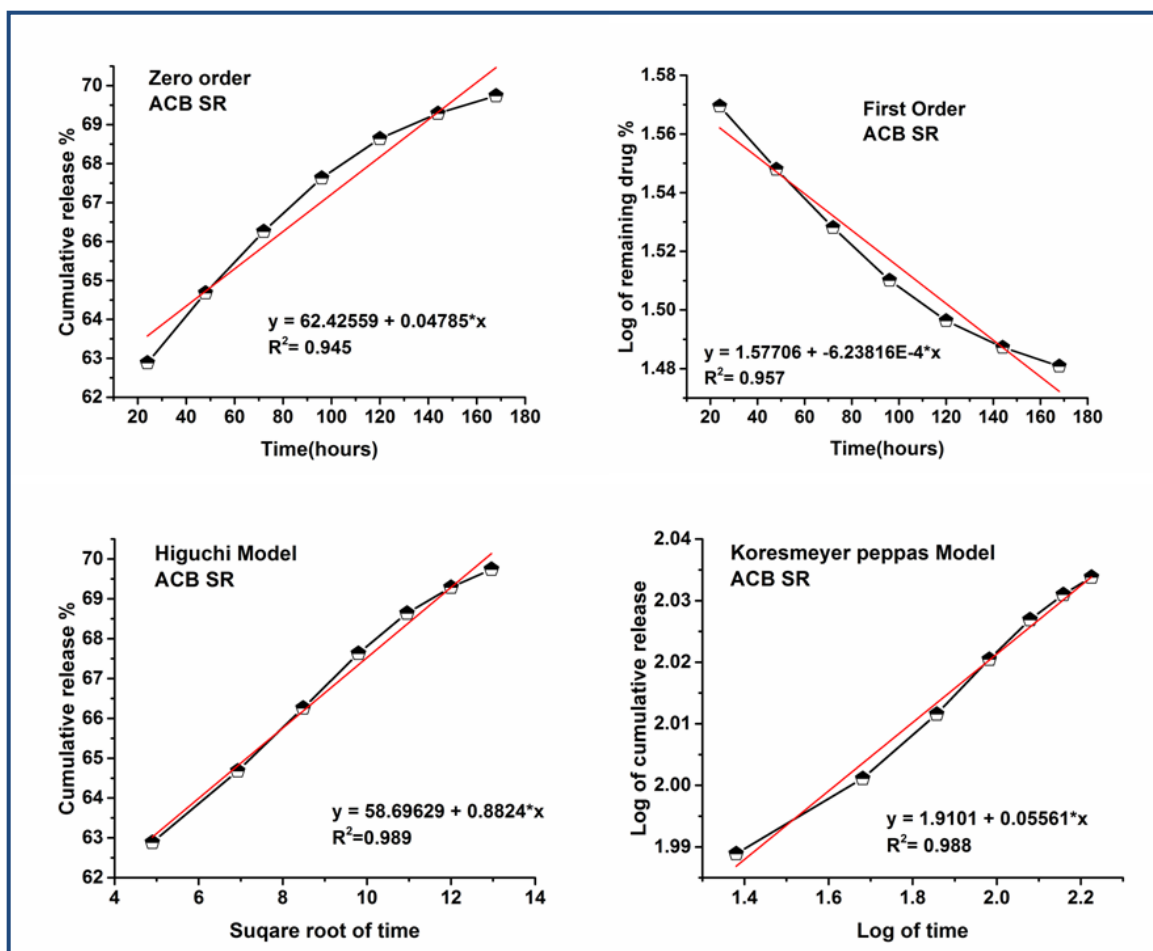
Fig 6.10: Release kinetic models of Aloin from nano clay for 24-168 hours in SBF

Table 6.3: Kinetic data of Aloin obtained from nano clay in SBF medium

Sample name	Zero order (R^2 value)		First order (R^2 value)		Higuchi model (R^2 value)		Korsmeyer-peppas (R^2 value)		Korsmeyer-peppas n=release exponent	
Aloin released	BR	SR	BR	SR	BR	SR	BR	SR	BR	SR
SBF	0.901	0.945	0.973	0.957	**0.998**	0.934	0.967	**0.988**	1.55	1.91

For burst release and sustained release of aloin from nano clay in SBF, the best fitted model Higuchi model and Koresmeyer peppas model respectively. And for every model 'n' value is greater than 0.89 that means all release mechanism is super case II transport.
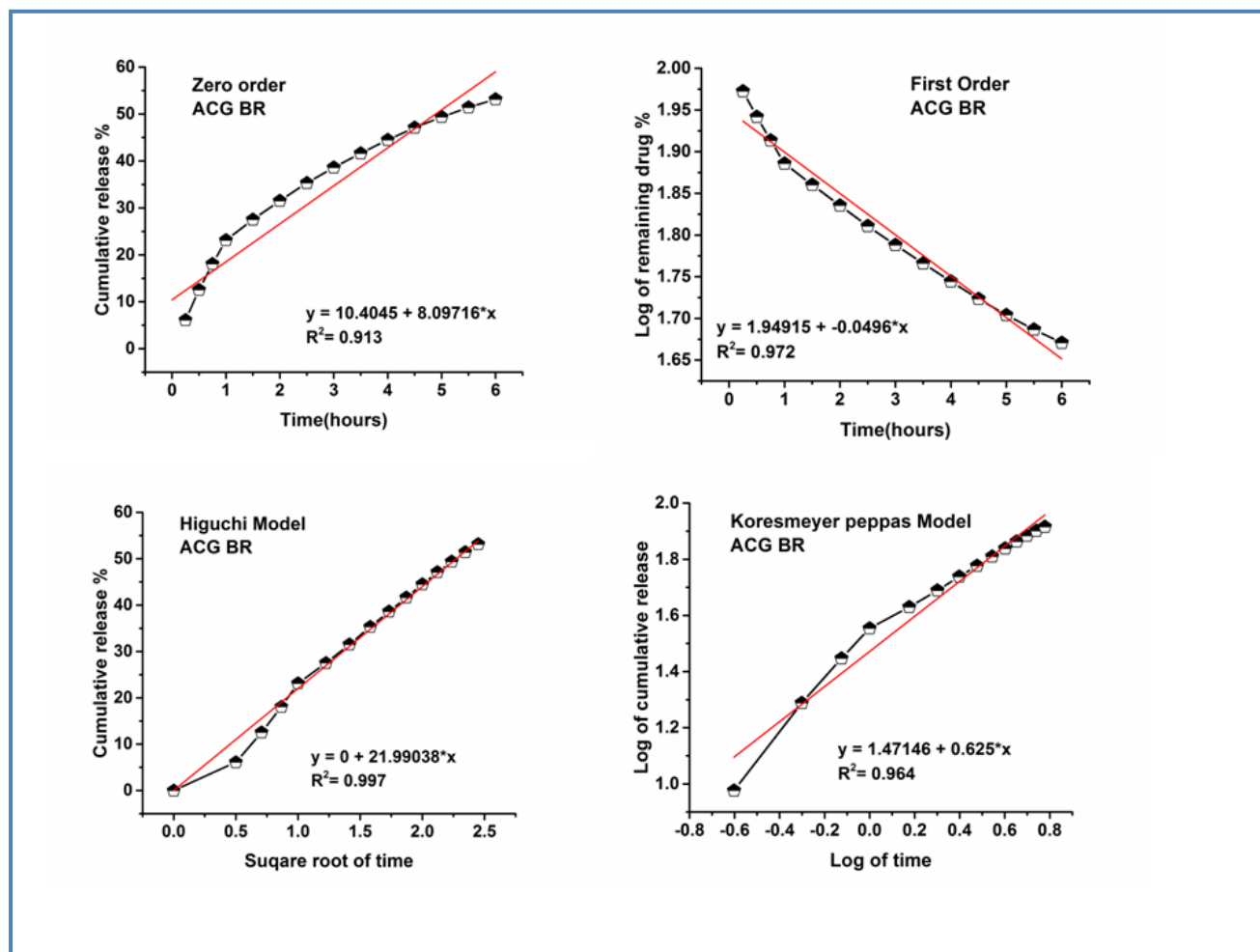
Fig 6.11: Release kinetic models of Aloin from nano clay for first 6 hours in SGF
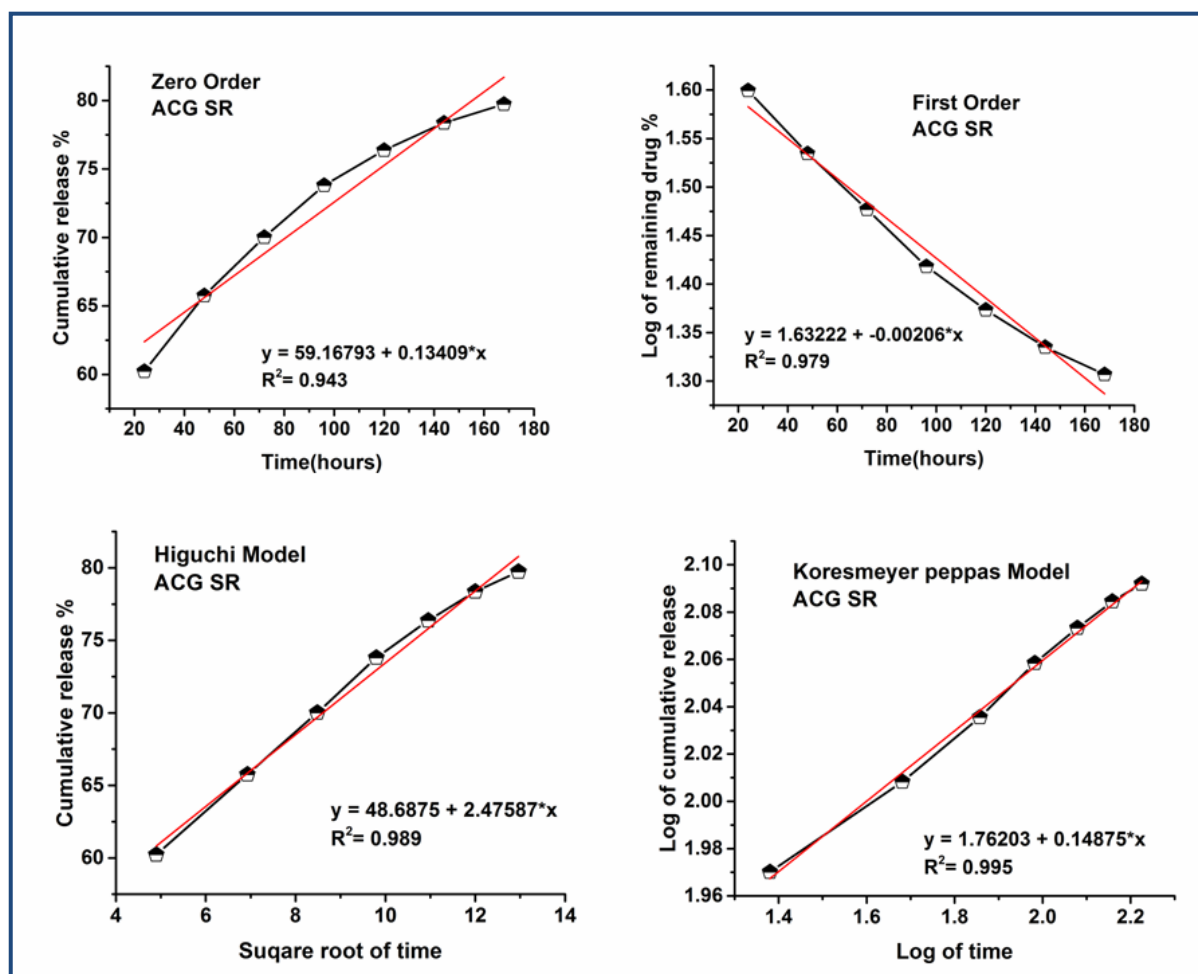
Fig 6.12: Kinetic models of Aloin from nano clay for 24-168 hours in SGF

Table 6.4: Kinetic data of Aloin obtained from nano clay in SGF medium

Sample name	Zero order (R^2 value)		First order (R^2 value)		Higuchi model (R^2 value)		Korsmeyer-peppas (R^2 value)		Korsmeyer-peppas n=release exponent	
Aloin released	BR	SR	BR	SR	BR	SR	BR	SR	BR	SR
SGF	0.913	0.943	0.972	0.979	**0.997**	0.989	0.964	**0.995**	1.47	1.76

For burst release and sustained release of aloin from nano clay in SGF, the best fitted model is Higuchi model and Koresmeyer peppas model respectively. And for every model 'n' value is greater than 0.89 that means all release mechanism is super case II transport.
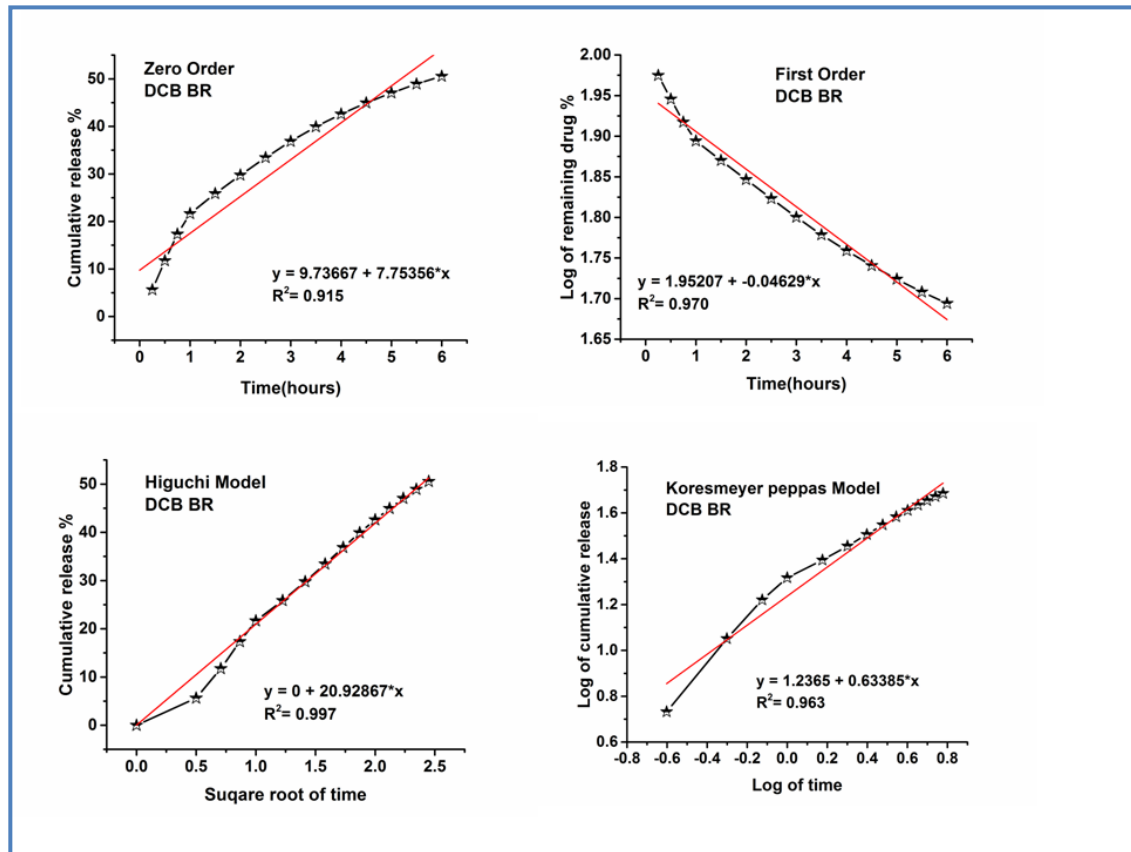
Fig 6.13:Release kinetic models of DADS in SBF for first 6 hours
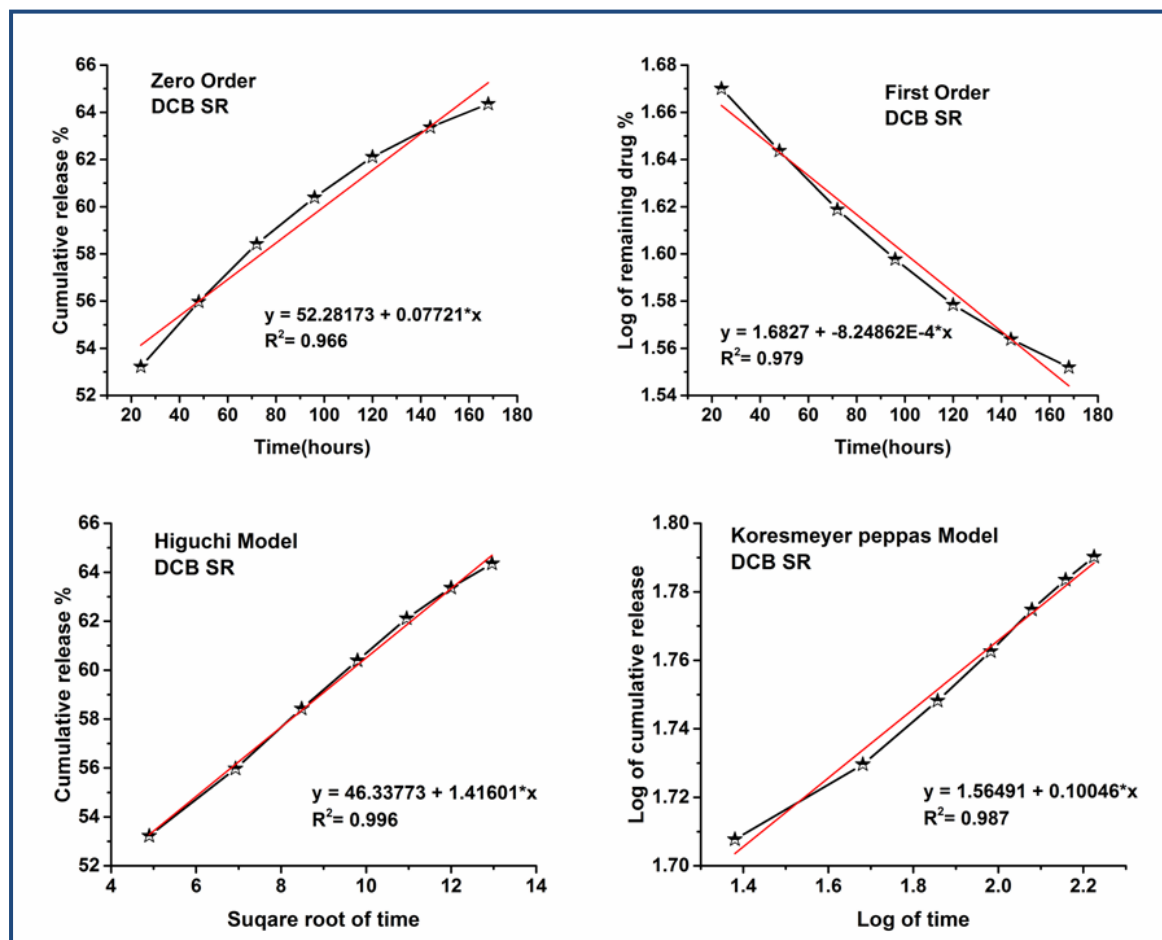
Fig 6.14: Release kinetic models of DADS in SBF for 24-168 hours

Table 6.5: Kinetic data of DADS obtained from nano clay in SBF medium

Sample name	Zero order (R^2 value)		First order (R^2 value)		Higuchi model (R^2 value)		Korsmeyer-peppas (R^2 value)		Korsmeyer-peppas n=release exponent	
DADS released	BR	SR	BR	SR	BR	SR	BR	SR	BR	SR
SBF	0.915	0.966	0.970	0.979	**0.997**	**0.996**	0.963	0.987	1.23	1.56

For burst release and sustained release of DADS from nano clay in SBF, the best fitted model is Higuchi model. And for every model 'n' value is greater than 0.89 that means all release mechanism is super case II transport.
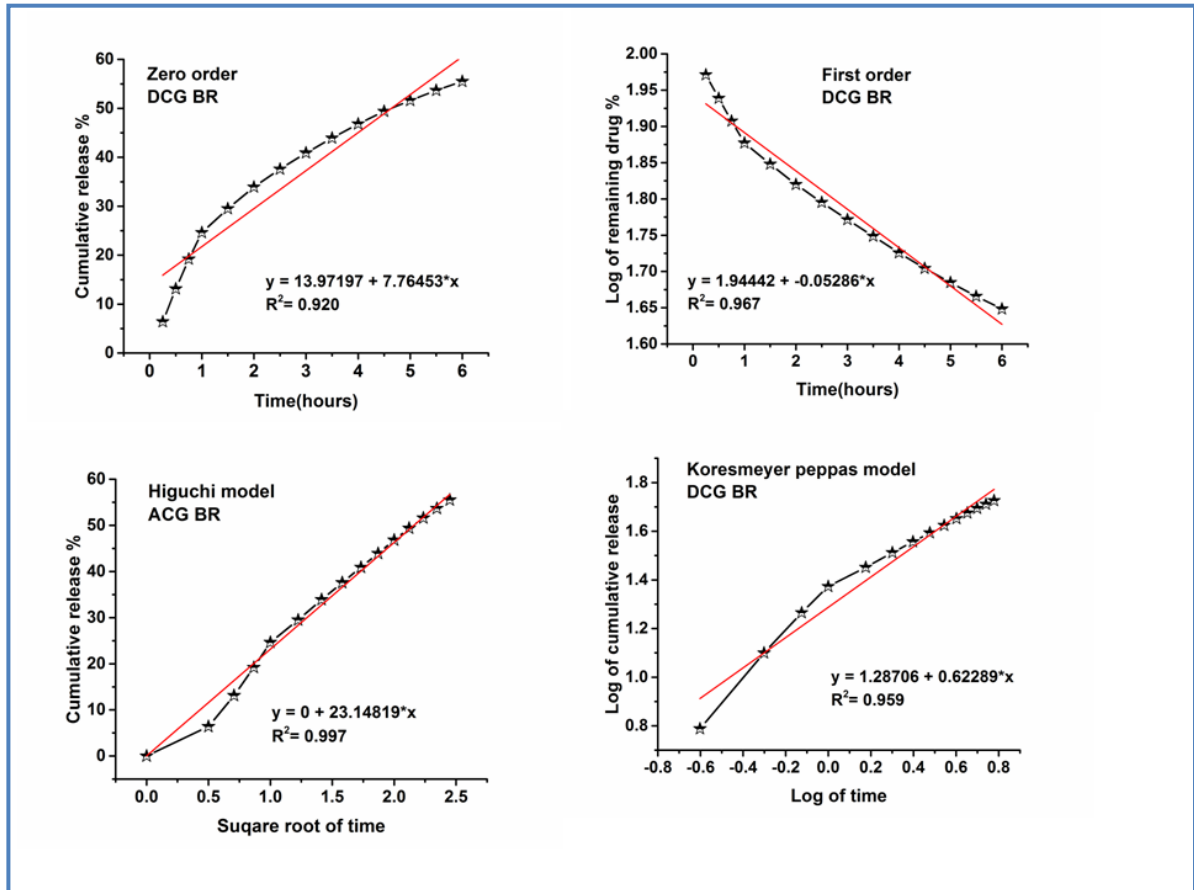
Fig 6.15: Release kinetic models of DADS in SGF for first 6 hours
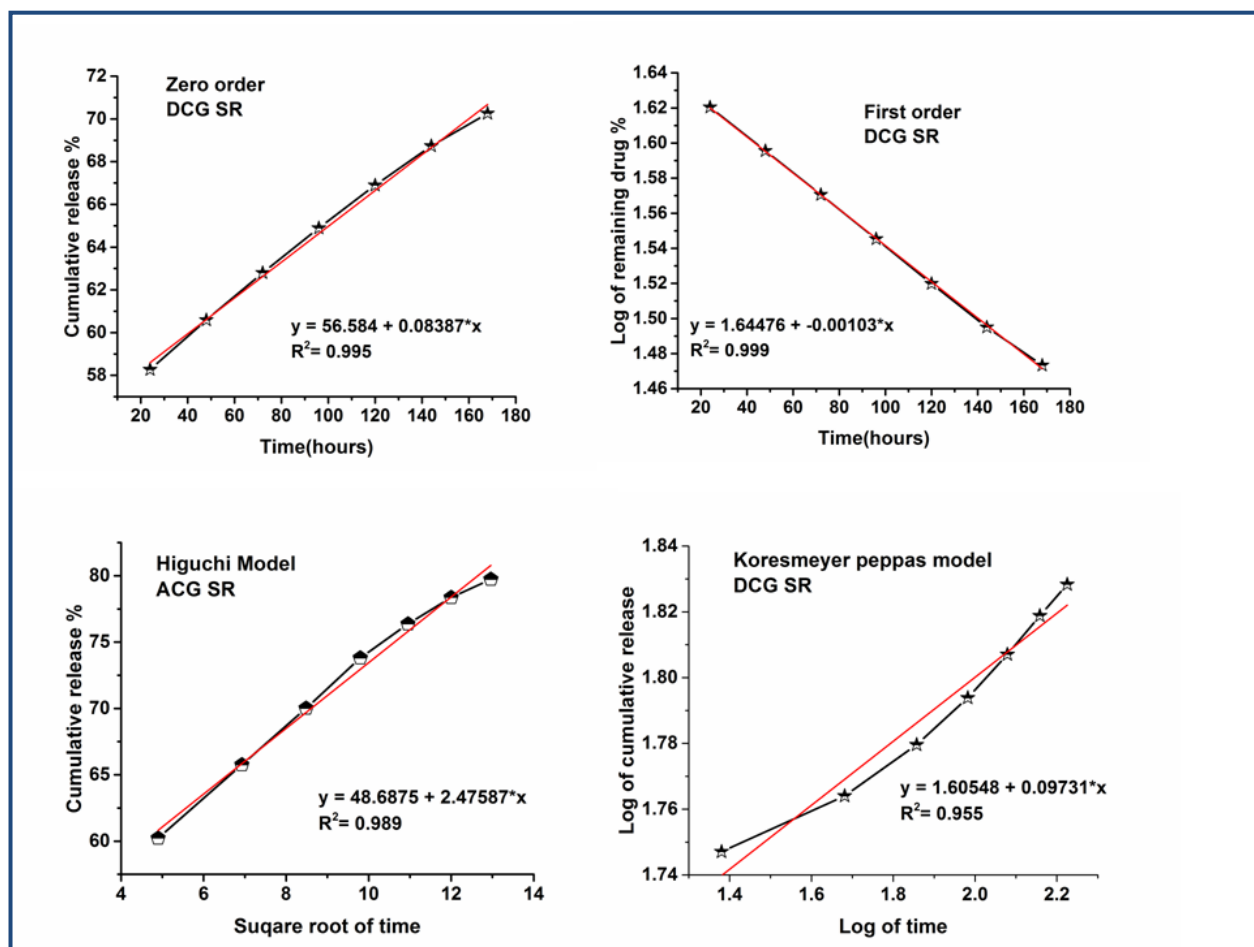
Fig 6.16: Release kinetic models of DADS in SGF for 24- 168 hours

Table 6.6: Kinetic data of DADS obtained from nano clay in SGF medium.

Sample name	Zero order (R^2 value)		First order (R^2 value)		Higuchi model (R^2 value)		Korsmeyer-peppas (R^2 value)		Korsmeyer-peppas n=release exponent	
DADS released	BR	SR	BR	SR	BR	SR	BR	SR	BR	SR
SGF	0.967	0.995	0.920	**0.999**	**0.997**	0.989	0.959	0.955	1.28	1.60

For burst release and sustained release of DADS from nano clay in SGF, the best fitted model is Higuchi model and First order model respectively. And for every model 'n' value is greater than 0.89 that means all release mechanism is super case II transport.

6.8 Antimicrobial activity assay:

Antimicrobial activity of pure drug aloin & DADS are studied thoroughly in chapter 4 & 5. Aloin released and DADS released from nanoclay is considered as experimental sample here. All the 4 concentrations are given here along with this sample. For antimicrobial activity assay MIC study, ZOI study and growth curve analysis is done with the pure drug aloin & DADS. All the experimental details and results with discussions are given in chapter & 4(section 4.9) & 5 (section 5.9) for aloin and DADS respectively. Here, sustained release sample is used to test the CFU count study. As both aloin & DADS are more soluble in lower pH, so more drug percentage is available in SGF release medium than SBF medium. Both this samples are used for the CFU count experiment.

CFU Count Study: Aloin released from clay is considered as sample ACB and ACG in released medium in SBF and SGF respectively. DADS released from clay is considered as sample DCB and DCG in released medium in SBF and SGF respectively. ACB, ACG, DCB & DCG samples with the microorganism *S. typhi* are kept in beakers at BOD shaker for 4-5 hours. 10 μL of aliquots from each beaker having different concentrations of drug with microorganism is taken and spread on agar media with a spreader. Before spreading the spreader is either sterilized with ethanol or autoclaved. These agar plates are incubated at 37 ˚C for 24 hours. Next day the plates are taken and colonies are counted. The whole procedures are done in triplicate and mean value is considered as final.

Table 6.7: Number of colonies of drug Aloin and DADS at the respective concentration along with released from nano clay

Drug	Released in SBF	Released in SGF	4MIC	2MIC	MIC	½ MIC	Control
Aloin	65	57	5	29	39	112	
DADS	79	62	6	35	57	153	226

Release percentage of aloin & DADS are more in SGF than in SBF. Percentage of drug affects the growth of microorganism as reported in CFU count. Higher the drug percentage, lower the count. According to this, CFU count changes with percentage of release of drug. Comparing with the control and known concentrations of drug, CFU count of *S. typhi* when treated with released drug is in the middle state between MIC and ½ MIC concentrations.

6.9 Anticancer study:

6.9.A: Anticancer study Aloin:

MTT assay is done with the pure drug aloin to see the anticancer effect of this drug. There is such differences find in different known concentrations of aloin already given in the chapter 4.

As more aloin is released in SGF medium, this ACG sample is used to do the MB assay. Details procedure of MB assay is mentioned in chapter 4 (section 4.10).
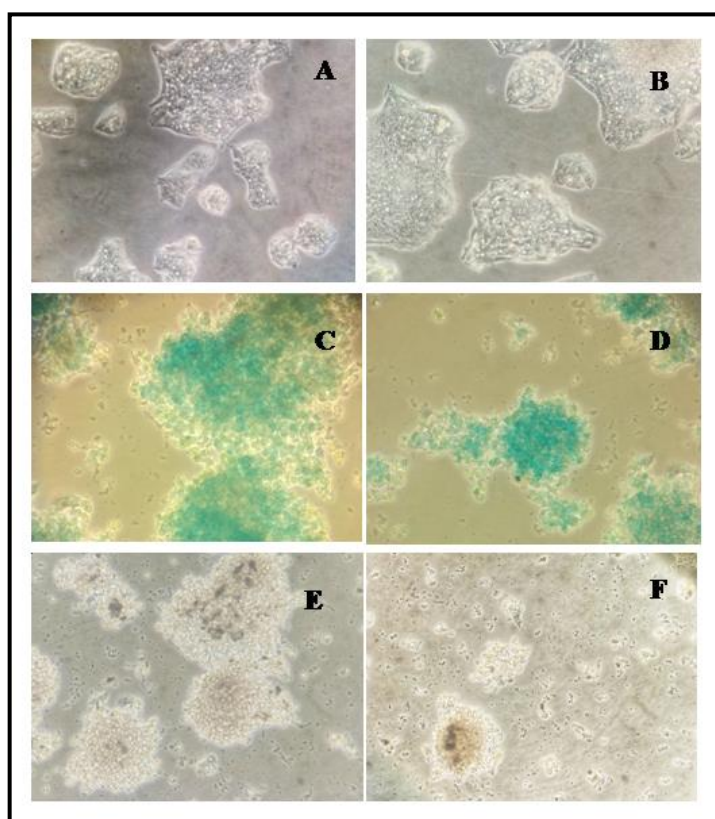
Fig 6.17: Microscopic analysis of HepG2 cell lines in set of methylene blue assay. For control sample freshly cultured and 24 hr incubated bare HepG2 cells are considered. HepG2 cells of 0 hr and 24 hr incubation (A) and (B) respectively for control sample. After methylene blue saining of 24 hr incubation of HepG2 cells with aloin treatment (C) and (D). After PBS wash of these cells (E) & (F)

This MB assay revealed that aloin released from nanoclay is also capable of killing the cancer cell line. The percentage of killing can enhance with the entrapment of more aloin within clay which will release more aloin in the medium. If the percentage of drug aloin is increased then killing rate will increase.

6.9.B Anticancer study of DADS:

MTT assay is done with the pure drug DADS to see the anticancer effect of this drug. There is such differences find in different known concentrations of DADS. All the experimental details and results are already given in the chapter 5 (section 5.10). As more DADS is released in SGF medium, this DCG sample is used to do the MB assay. Details procedure of MB assay is mentioned in chapter 5 (section 5.10).
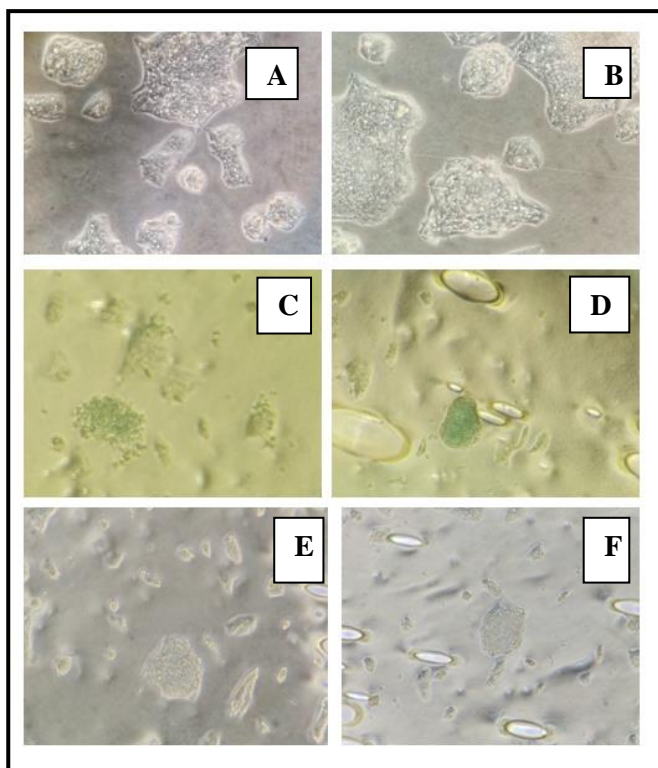
Fig 6.18: Microscopic analysis of HepG2 cell lines in set of methylene blue assay. For control sample freshly cultured and 24 hr incubated bare HepG2 cells are considered. HepG2 cells of 0 hr and 24 hr incubation (A) and (B) respectively for control sample. After methylene blue saining of 24 hr incubation of HepG2 cells with DADS treatment (C) and (D). After PBS wash of these cells (E) & (F)

Nanoclay released DADS is applied as anti cancer agent in this assay to see the effect of the released drug. Comparing with the control sample, released DADS is effective against HepG2 cell line which is clear in stained and PBS washed samples.

6.10 Antiviral assay:

Antiviral assay is done in the egg model means in in-vivo model. For this experiment the highest percentage of released aloin and DADS samples are considered as 'nano carrier released drug'. Aloin and DADS released from one specific silica nanocarrier is considered for antiviral assay.

6.11 Conclusion:

1. Modification of clay with Na gives the opportunity for more drug entrapment within clay as this modification increase the interlayer gapping. This is confirmed by blue shifting of the XRD plot of clay. Scanning electron microscopic view reveals the flecks like structure of nanoclay. Interlayer spacing of modified clay is found to be 1 – 2.5 nm as observed HRTEM. FTIR analysis confirms the entrapment of both drugs aloin and DADS within clay layers. 900-1300 cm-1 vibration is for C-O & 1600-1680 cm-1 for C=C and 1650 -1850 cm-1 is for C=O in aloin entrapped clay FTIR graph represents the presence of aloin phytochemical within clay. 900-1100 cm^{-1} is for C-S bond. 400-700 cm^{-1} is assigned to S-S stretching in DADS entrapped clay FTIR graph proves the presence of DADS within clay layers.

2. 69% and 79% aloin loaded drugs is released from nanoclay in SBF and SGF medium respectively where more percentage of release in acidic medium. 64% and 70% DADS is released from nanoclay in SBF and SGF medium respectively where more percentage of release is seen in acidic medium like aloin drug. Release kinetics study (both burst and sustained release) of aloin and DADS in SBF & SGF for nanoclay is carried out. In each case using regression coefficient model the best fitted kinetic model is identified.

3. For clay carrier, burst release and sustained release of aloin in SBF and SGF medium follow Higuchi and Koresmeyer peppas model respectively. In case of DADS, burst release and sustained release in SBF medium match with Higuchi model and in SGF medium burst release fits to Higuchi model and sustained release fits to First order kinetic model. And in every model 'n' value is greater than 0.89 that means all release mechanisms are super case II transport.

4. In case of antibacterial study, CFU count of *S. typhi* is 65 and 57 after treatment with released aloin in SBF and SGF. As in SGF medium percentage of drug release is higher than SBF which results more inhibition of bacterial growth followed by less CFU count. As well as in DADS the CFU count is 79 & 62 for DADS released in SBF and SGF. Here is also, highest percentage of release gives lower CFU count as it inhibits more.

5. In case of anticancer study, methylene blue staining assay confirms the ability to destroy the HCC cell lines for both of the drugs. The affectivity of DADS is much higher than aloin over this

cell line as depicted in the pictures (6.17 & 6.18). Most of the cells are destroyed resulting cell debries present in the medium after treatment with DADS.

References:

1. L. Armentano, M. Dottori, E. Fortunati, S. Mattioli, & J. M. Kenny, Biodegradable polymer matrix nanocomposites for tissue engineering: A review. Polymer Degradation and Stability. 2010; 95(11):2126-2146

2. P. Cosoli, G. Scocchi, S. Pricl, & M. Fermaglia, Many-scale molecular simulation for ABS-MMT nanocomposites: Upgrading of industrial scraps. Microporous and Mesoporous Materials, 2008; 107, 169-179.

3. H. Ma, Z. Xu, L. Tong, A. Gu, & Z. Fang, Studies of ABS-graft-maleicanhydride/clay nanocomposites: Morphologies, thermal stability and flammabilityproperties. Polymer Degradation and Stability., 2006; 91, 2951-2959.

4. J. K. Pandey, K. R. Reddy, A. P. Kumar & R. P. Singh, An overview on the degradability of polymer nanocomposites. Polymer Degradation and Stability, 2005; 88,234-250.

5. N. Sheng, M.C Boyce, D. M. Parks, G.C. Rutledge, J.I. Abes, &R. E. Cohen, Multiscale micromechanical modeling of polymer/clay nanocomposites and theeffective clay particle.Polymer, 2004; 45, 487-506.

6. P. C. LeBaron, Z. Wang,&T. J. Pinnavaia, Polymer-layered silicate nanocomposites: an overview. Applied Clay Science., 1999; 15, 11-29.

7. E. T. Thostenson, C. Li, & T. W. Chou, Nanocomposites in context. Compos. Science Technology, 2005; 65, 491-516.

8. V. Mittal, Polymer Layered Silicate Nanocomposites: A Review. Materials, 2009; 2, 992-1057.

9. A. Rehab, N. Salahuddin, N. Nanocomposite Materials Based on Polyurethane Intercalated into Montmorillonite Clay.Mater.Sci. Eng. A, 2005; 399, 368–376.

CHAPTER 7

Overall Conclusion

In this research work, efficacy of sustained released herbal drugs (*Aloe vera* and garlic) for cure and control of typhoid (bacterial disease), Covid - 19 (Viral disease) and liver cancer are evaluated. To achieve sustain release of drugs, both the drugs are extracted and entrapped with in bio compatible porous silica nano particles of different morphology and within nanoclay. Entrapment of the herbal extracts within nanoparticles is confirmed by FTIR plot. Presence of C=C bond and C=O bond of aloin which is the active component of *Aloe vera*and C-S and S-S bonds of DADS which is the active component of garlic in the FTIR plot of both drug entrapped silica nanoparticles and nano clay indicates the successful entrapment of the drugs in the nano carriers. Silica nano particles have two different types of morphology - irregular shape and spherical shape.In each type of silica nano particles, the molar ratio of the precursors i.e., TEOS, ethyl alcohol and water control porosity of the silica nano particles. Spherical shaped silica nano particles are more porous as revealed from BET analysis with higher surface area. It is also inferred from BET study that with increase in ethyl alcohol percentage the gel porosity increases in case of acid catalyzed irregular shaped silica nano particle with maximum surface area is achieved at the molar ratio of TEOS: ethyl alcohol: water = 1: 6: 1. Whereas, in case of base catalyzed sphere shaped silica gel samples maximum surface is achieved at the molar ratio of 1: 2: 1 of TEOS: ethyl alcohol: water. It is observed drug loading efficiency of nano carrier increases with increase in the surface area of the nano carriers. Thus, drug loading efficiency of spherical shaped nano particles (maximum 90.53% for aloin and 95.75% for DADS) is higher compared to irregular shaped nanoparticles (81.58% for aloin and 91.62% for DADS). Entrapped drug is released in two media- simulated body fluid (SBF, pH 7.4) and simulated gastric fluid (SGF, pH 1.2).Rate of drug release in the media depends upon factors like the nature of the drugs, pH of the medium and porosity of the nano carriers. Due to higher porosity, dissolution rate of both drugs are more from spherical shaped silica nano particles (81% for bothaloinand DADS) compared to irregular shapesilica nano particles (68% for aloin and 57% for DADS). Moreover, it is also observed that cumulative release rate of aloin is higher in SGF (68% from irregular shaped and 81% from spherical silica nano particles) as compared to SBF (52% for irregular shaped and 60% for spherical silica nano particles) due to acidic nature of SGF.So, the process parameters for the synthesis of silica nano carrier as a porous substrate for use in drug delivery is optimized at 1: 2: 1 of TEOS: ethyl alcohol: water with CTAB surfactant in basic medium.

Nano clay is also found to be a very good substrate for entrapment of bothaloin and DADS with entrapment efficiency 87.17% for aloin and 78.82 % for DADS. Drug release from nano clay follows the same pattern as silica nano particles with higher release in SGF (79% aloin and 70% DADS) compared to release in SBF (69% aloin and64% DADS).

Release kinetics study for both burst and sustained release of aloin and DADS from all types of silica nano carrier and clay is carried out to find the best fitted kinetic model.

Release kinetic study of aloin in SBF from three different irregular shaped silica nano carriers reveals that burst release of aloin from samples S2 & S4 fit to first order model and S6 best fit to Higuchi model. Sustained release of aloin from sample S2, S4 & S6 of the same set of silica samples in SBF follows koresmeyerpeppas model. Burst & sustain release aloin in SGF from S2 & S4 follow first order kinetic model, whereas, release from S6 set is found to match zero order and higuchi model for burst and sustained release respectively. In every model 'n' value is greater than 0.89 that means all release mechanisms are super case II transport.

In the kinetic study of release of aloin from three different sphere samples of silica nano carriers in SBF, burst release from SS2, SS4 & SS6 fit to Higuchi model whereas, sustained release from SS2, SS4 & SS6 follows Higuchi model, first order model and Koresmeyer peppas model respectively. For release of aloin in SGF, burst release from all three types of silica samples match to Higuchi model. Sustained release from SS2 and SS4 fit to Higuchi model and release from SS6 samples follows Zero order model. In every model 'n' value is greater than 0.89 indicating all release mechanisms are super case II transport.

Release kinetic study of DADS in SBF from three different irregular shaped silica nano carriers (Sample S2, S4 and S6) reveals that burst release of DADS from samples S2 & S6 best fit to Higuchi model & sample S4 fits to first order model. Sustained release of DADS from S4 & S6 samples in SBF follows Koresmeyer peppas model and S2 follows Higuchi model. Burst & sustain release of DADS in SGF from S2 fits on first order model. Burst & sustained release of DADS from S4 match with Koresmeyer peppas model & Higuchi model respectively. DADS release from S6 follows Higuchi model and Zero order models for burst and sustained release respectively. In every model 'n' value is greater than 0.89 that means all release mechanisms are

super case II transport except burst release from S4 in SBF and from S2 in SGF, where n< 0.89 implying release mechanisms are anomalous (non-fickian) diffusion.

In the kinetic study of release of DADS from three different sphere samples of silica nano carriers (SS2, SS4 & SS6) in both SBF and SGF, for burst release match to Higuchi model. For sustained release from SS2, SS4 & SS6 in SBF, match with Koresmeyer peppas model, Higuchi model and first order kinetic model respectively. For sustained release of DADS in SGF, from SS4 & SS6 kinetic model fits to Higuchi model and SS2 fits to Koresmeyer peppas model respectively. In every model 'n' value is greater than 0.89 indicating all release mechanisms are super case II transport.

For clay carrier, burst release and sustained release of aloin in SBF and SGF medium follow Higuchi and Koresmeyer peppas model respectively. In case of DADS, burst release and sustained release in SBF medium match with Higuchi model and in SGF medium burst release fits to Higuchi model and sustained release fits to First order kinetic model. And in every model 'n' value is greater than 0.89 that means all release mechanisms are super case II transport.

Antibacterial study of released aloin and DADS against *S. typhi* proves the efficiency of the herbs as an antibacterial agent. MIC values estimated 2.5 mg / ml and 0.0941 mg / ml for aloin and DADS respectively. MIC values indicate, DADS as an antibacterial agent is more efficient compared to aloin. CFU count of released aloin and DADS are found to be 56 (from aloin entrapped spherical silica, released in SGF) and 68 (from DADS entrapped spherical shaped silica, released in SGF) respectively whereas, the control CFU is found to be 226. Although DADS is more effective compared to aloin as per MIC value, lower CFU count of *S. typhi* colonies by aloin is due to higher cumulative release percentage of aloin in SGF than DADS indicating better control of bacterial growth by released aloin. Thus, released aloin is found to be more efficient in controlling *S. typhi* growth compared to release DADS and the best media for aloin release is found to be gastric fluid. CFU count for aloin and DADS released from clay are 57 and 62 respectively. Thus, clay can be considered as an efficient bio compatible substrate for drug delivery. Microscopic images reveal the deformation of the bacterial cells in presence of the released drugs. The cells are fused together in presence of both aloin and DADS.

Aloin in the preventive experimental sets in the chicken egg model could counteract and prevent damaging action of pro-inflammatory cytokines IL-6, IL-8 and IL-1β by increasing more gene expression of anti-inflammatory cytokine IL-10. It indicates that aloin could prevent the damage of different organs in cytokine storm, which is the main pathogenic factor in morbidity and mortality in SARS-CoV-2 infections, mediated mainly by the S-protein of the virus. IFNα and IFNβ are also mildly increased indicating a beneficial role in this condition. IL-1ß is increased and may be detrimental to healthy system but DADS Raw and DADS Release are capable of counteracting those detrimental changes by markedly increasing anti inflamatory cytokine gene IL-10 and thus it appears that both DADS Raw and DADS Release will give overall beneficial effect in SARS-CoV -2 pathological changes and appears to be an excellent agent in the management of corona virus infection.

In anticancer study, at first IC_{50} value of pure drugs is determined. For this both the drugs are diluted from 10 to 20 times from a stock concentration of 1mg/ml. From spectrophotometric analysis IC_{50} value is obtained as 12th dilution for aloin and 14th for DADS. This concentration is considered for methylene blue assay as it is regarded as the effective concentration against the hepatocellular carcinoma cell line. But for the chemical and sample colours, this data may misinterpret sometimes. To confirm this experimental datas methylene blue assay is also done. Methylene blue stains both nuclei and cytoplasm of the both living and dead cells. If methylene blue is applied to live cells, enzymes present within live cell reduce the dye and become colourless which dead cells cannot. So, dead cells remain blue in colour and live cell become white after PBS wash. In case of aloin treatment this is prominent that 80-90% of cells are dead. Methylene blue cannot stain debries, as there is no specific cell clumps are seen in DADS treated medium so, it stains the medium and the whole picture came blue.

Future scope of work

- Study of pharmacokinetic behavior of pure drugs as well as drug entrapped nanocarriers of both silica and clay and compare their pharmacokinetic profile.
- Study of in vivo model of antimicrobial assay as well as anticancer assay with best results depending upon in vitro study.
- Study of histopathology after Covid-19 treatment with both drugs and observe the tissue damage after this viral infection.

PhD Thesis

8%
SIMILARITY INDEX

PRIMARY SOURCES

1	getjson.sid.ir Internet	1410 words — 4%
2	www.ijpbs.com Internet	750 words — 2%
3	philippineculturaleducation.com.ph Internet	380 words — 1%
4	www.tandfonline.com Internet	193 words — 1%

Pritha Pal
03/05/2023

Mahua Ghosh Chaudhuri
2/5/23.

Dr. (Ms) Mahua Ghosh Chaudhuri
Associate Professor
School of Materials Science and Nano Technology
Jadavpur University
Kolkata-700 032, India

04/05/2023

Dr. Satadal Das
MBBS, MD, DCP, DBMS.